THE MODELLING AND CONTROL OF REMOTELY OPERATED UNDERWATER VEHICLES

by

Kevin R. Goheen, B.Sc.

A Thesis Submitted for the Degree of
DOCTOR OF PHILOSOPHY
in the
FACULTY OF ENGINEERING
UNIVERSITY OF LONDON
July 1986

Department of Mechanical Engineering
University College London
Torrington Place
London WC1E 7JE

ABSTRACT

This thesis considers the design and evaluation of autopilots for Remotely Operated Underwater Vehicles (ROVs), unmanned submarines used in offshore oil, salvage and military applications.

A very comprehensive hydrodynamic model of a ROV produced by the National Maritime Institute, Feltham, Middlesex, is subjected to an extensive verification study. It is concluded that conventional hydrodynamic modelling techniques are very expensive and uncertain and hence any ROV autopilot must be, in some manner, adaptive; that is, independent of 'a priori' knowledge of the vehicle.

The theory, implementation and simulated performance of three different adaptive autopilots is presented, based on the NMI model. Two of these systems use multivariable recursive system identification techniques to estimate the performance of the vehicle on-line. These methods are also discussed as an alternative route to ROV models.

A summary of the thesis is given along with recommendations for areas which require further study.

An appendix is included which describes a series of tank trials at Admiralty Research Establishment (Haslar); one of the goals of these tests was to validate this simulation study.

ACKNOWLEDGEMENTS

I would like to express my appreciation to members of the Department of Mechanical Engineering, UCL, especially the Automatic Control Group, who were generous with their support and advice during the course of this project. The contribution of my supervisor, Dr. E.R. Jefferys, who combined technical expertise with moral encouragement, deserves particular mention. Special thanks also to Dr. D.R. Broome for providing such an excellent working environment.

The financial support of the Association of Commonwealth Universities made this research possible and is gratefully acknowledged.

TABLE OF CONTENTS

Chapter 3: Validation of the ROV Model

Chapter 4: Control System Design

Chapter 5: Self-Testing Controller Analysis and Performance

Chapter 6: Modelling ROV Dynamics by System Identification

LIST OF TABLES

LIST OF FIGURES

Chapter 1

Introduction

1.1 A Brief History of Manned and Unmanned Ventures Under the Sea

Legend has it that Alexander of Macedon "piloted" the first manned underwater vehicle when he was lowered in a glass barrel into shallow water to observe marine life [1]. If this is true, Alexander was the first in a long line to venture into the sea. In his case, it was for the sake of scientific observation and, more than likely, "to boldly go where no man has gone before". In the years since then, military and commercial use of the world's oceans has superceded these more noble objectives. Man has learned that 70 percent of the world's surface is ocean and has recently been exploiting the continental shelf areas for their resources, mainly petroleum and natural gas. The continental shelves are only 8 percent of the ocean, so simple-minded logic suggests that perhaps 92 percent of the wealth the sea has to offer remains untapped [2], though hydrocarbons tend to accumulate in areas of crustal thinning. To date, ambient or hyperbaric (saturation) diving has dominated subsea work but physiological obstacles limit the use of divers in deeper water; in practice, 330m is usually the maximum depth for useful work. Man has tried to circumvent this limit by developing a series of craft to carry him deeper than diving permits, but even so the danger remains. Cervo (1831), whose spherical chamber was crushed by the pressure, was the last recorded victim of an attempt to dive in pressure resistant wooden chambers. Busby [3] gives accounts of 39 emergency incidents involving manned submersibles which directly endangered or resulted in loss of life. Increased concern for safety has resulted in regulations requiring redundant back-up systems which have increased the capital and operating costs of manned vehicles. All of these, naturally enough, are factors which have helped the development and proliferation of Remotely Operated (Underwater) Vehicles (ROVs).

Probably the first ROV was developed by Dimitri Rebikoff in 1953, who modified a Diver Propulsion Unit to act as a tethered ROV. He named it "Poodle" and on its first set of trials found shipwrecks at

160m and 210m, a successful debut by any standard. The United States Navy's CURV (Cable Controlled Underwater Research Vehicle) family were the next representative class of ROVs. They were designed to retrieve unexploded torpedoes, but became notable for their involvement in a pair of incidents involving the salvage of other objects. CURV was used in 1966 to recover a H-bomb which was lost in the sea off Palomeres, Spain. The vehicle was originally dispatched to attach lift lines to the bomb but became entangled in the bomb's parachute; the whole mess was subsequently dragged to the surface by the vehicle's umbilical cable! In 1973, CURV III attached a rescue line to the PISCES III manned submersible which was stranded at 480m off Ireland with two pilots trapped inside.

Nevertheless, by the mid 1970s, manned submersibles and divers still commanded the majority of subsea work. These systems had the advantage of placing human brain and eyes at the work point and divers had the further advantage of greater dexterity than manipulator arms. A 1971 study [4] showed divers were on the average 4 times faster than manned or unmanned teleoperator systems when working on subsea tasks. However, by the late 1970s, improvements in manipulators, computing devices and sensors had reduced the advantages of a man in the sea and large numbers of manned vehicles remained idle or were scrapped. The ROV market underwent a boom in the same period. In 1974, 20 systems were in existence, all dedicated to military or scientific endeavours. Fueled by the North Sea oil activity, 500 ROVs had been added to the world's inventory by 1980, 90 percent of the non-military market occupied by vehicles which support offshore oil activities. On the military side, mine neutralization was the major application. ECA of France had sold 230 PAP 104 ROVs (roughly translated to "Self-Propelled Fish") to NATO navies by the same date. The most recent publicised use of ROVs was in 1985 when two French-built SCARAB (Submersible Craft Assisting (Cable) Repair and Burial) vehicles, deployed from the Canadian Coast Guard Ship John Cabot, discovered and then helped recover parts of the Air India Boeing 747 which went down off Cork in June of that year.

1.2 A Typical ROV Mission

Features of the vehicle and problems encountered during its operation can be described conveniently by outlining a typical ROV mission. ROVs are of two basic types: "eyeball" vehicles, designed for observation only such as the small, spherical Hydro Products RCV 225 or larger "worker" vehicles such as the aforementioned SCARAB, which is designed, owned and operated by a consortium of telecommunications companies. Vehicles in the latter class are usually of an open-frame construction, chosen for its cheapness and the ease with which extra tools, manipulator arms and instruments may be attached to the vessel according to the requirements of the job. It will be shown later that this design which ignores hydrodynamic efficiency and the day to day modifications add to the control system designer's difficulties.

Suppose a worker vehicle is to be deployed from its support ship in an attempt to carry out Non-Destructive Evaluation (NDE) of welds on an oil rig. The first problem the crew will encounter is launching the vehicle. Most ROVs have 'A'-frame launchers which extend over the side of the ship to aid the operation, but the relative motion of sea and ship can lead to collisions between the ROV and hull and 'slamming' of the ROV onto the sea surface. This tends to make launch and recovery impossible in any weather above a sea state 3. Assuming the launch is successful , the pilot then guides the vehicle to the worksite. The navigation aids he will use are either vision, acoustics, dead reckoning or a combination of these. Navigation systems will be described more extensively in the next section. Suffice it to say that finding the workstation in turbid water can be time consuming and difficult.

The vast majority of ROVs are attached to their support vessel by tethers. Control signals and power for propulsion, tooling and instrumentation are sent down the umbilical cable while data from the vehicle's various sensors is transmitted back to the surface. The first ROVs and manned submersibles used the umbilical for communications and emergency retrieval only, with power supplied by on-board batteries. The 'Guppy' (1970), a two man submersible, put

power down the cable for the first time, allowing for essentially unlimited operation. Though this was a major improvement, the umbilical, paradoxically, can also cause the most difficulties during the mission. In strong currents after a certain length has been deployed, the drag on the cable dominates the vehicle drag and limits the vehicle's "footprint", the area or volume the vehicle can work in given the position of its support ship. The greatest danger though is the umbilical becoming entangled in a subsea structure. Pilots, through necessity, become expert at knowing the location of the umbilical at all times, though most current ROVs employ umbilical 'turn' indicators which assist somewhat with cable management.

The pilot is now near the worksite. The next task is to take up and hold station so that NDE tools may carry out the weld inspection. The vast majority of ROVs do not have any automatic feedback control. Instead, the pilot is faced with a battery of controls, one for each thruster. In the worst case, thrusters operate in the bang-bang mode though most are constant blade pitch angle, variable speed (constantly adjustable) or fixed speed, variable pitch. If equipped only like this, station holding in a varying current such as found around most subsea structures can be a mentally exhausting process.

The UK Department of Energy recently sponsored a trial in Loch Linnhe which set a number of different vehicles to work on typical subsea tasks [5]. Conclusions were drawn about the present capability and shortcomings of tethered ROVs and recommendations made for areas of future research. Station holding merits particular attention, since during the trials, it was shown to occupy up to 35 percent of the total work time. It can be achieved by various methods, including controlled free hover, use of grab manipulators or specialised fixtures on the vehicle or the use of a support provided at the worksite. The first method is the most versatile, but in tests it was noticed that the vessel could not maintain a fine accuracy of position. The limitations were:

"1) the inability of the vehicle to counter the side-acting currents at the site.

2) the pilot workload needed to maintain the vehicle on station, in addition to the demands of the task.

3) the inability of the pilot to hold a position in the horizontal plane within the required limits."

The report states further:

> ...observations were unable to identify where in the control loop the limitations arose i.e. whether there was insufficient:
>
> information supplied to the pilot
>
> speed and correctness of the pilot's response
>
> response time of the thrusters
>
> restoring acceleration produced by the thrusters

The Department of Energy concludes:

> ...the ultimate improvement would be an automatic positioning system that would leave him free to concentrate on the actual task. It was noted that when auto-heading and auto-depth systems were used they controlled these parameters within limits that the pilot could not have consistently maintained, and the overall performance was improved as a result. An auto-position system requires a more advanced form of control... but, if this can be developed, the facility would be a major step forward in ROV technology.

As the DoEn report stated, the auto-positioning problem is a combination of insufficient information for the pilot and his inability to form thruster commands quickly and accurately. Should a sufficiently complete navigation system be available however, manual control would no longer be suitable because a human pilot could not handle the increased level of information. This thesis is concerned with addressing this second problem. Features and disadvantages of existing ROV navigation and control systems will be examined in the next two sections before the present work is outlined.

1.3 Navigation Systems

Though the main subject of this report concerns the control of ROVs, control in any context cannot be discussed without a mention of sensors. Any closed-loop control system is only as good as the quality of the feedback signals.

Marine systems which operate on the sea have access to a number of navigation methods of varying cost and accuracy. These include DECCA, LORAN, satellite navigation, radar or celestial (sextant), all of which require the transmission of electromagnetic radiation. Sea water causes a prohibitively high attenuation of these signals ,100 dB/m at 300 kHz increasing to 1000 dB/m at 30 MHz, which makes them unsuitable for ROV navigation although visual information is of limited use near objects of interest. However, in the North Sea, visibility of 5m is considered very good.

This leaves two families of systems applicable to ROV navigation: acoustics and dead reckoning. A good review of these techniques is found in [6] and only brief descriptions will be given here.

Acoustic techniques include sector-scan sonar, directional hydrophones, doppler sonar, long-baseline, short-baseline and supershort-baseline. Acoustic signals suffer little attenuation in sea water, though it does increase with frequency (typically .001 dB/m at 10 kHz rising to 10 dB/m at 10MHz [7]). The disadvantages include multipath propagation, though a possible solution to this is to use coded pulses, shadow zones, signal drop-outs caused by interference with air bubbles from thrusters, long time delays due to sound's relatively low velocity of propagation (typically 1.5 km/s) and low bandwidth (30 kbits/s compared with 300 kbits/s for coaxial cable and 3 Mbits/s for fibre optics [8]).

The most important acoustic systems are the baseline technologies. Long-baseline navigation uses three or more transponders, piezo-electric pingers which transmit only when interrogated by another acoustic source, set out on the sea bed in a large array. The ROV carries a master unit which interrogates the array. The time

between querying each transponder and its reply being received determines its range. The knowledge of three or more ranges determines the global position of the master unit. Short-baseline navigation places the transducers on widely spaced points on the support ship's hull and the operation is the same as with long-baseline except that the global position and attitude of the ship must be known to fix the ROV's position. Supershort-baseline uses a very precise 3 element hydrophone on the ship's hull. Measurements of time and phase difference from the ROV's signal gives slant angle, azimuth angle and range. Of these systems, long-baseline is the most accurate, but it is expensive and the deployment and retrieval of the transducer array takes time.

Another study of ROV control [9] reported that most acoustic navigation systems have relatively low update rates (1 Hz or slower) and high noise (typically a large fraction of a metre) which implies that only a low bandwidth control system can be implemented. Fortunately, high bandwidth control is only needed in small areas, for manipulator tasks, say, and therefore high frequency systems can be used which have lower noise and higher update rates because echoes die more quickly. The authors of [9] report that Applied Sonics Corporation of Gloucester, Virginia, USA has built an 800 kHz positioning system with a maximum range of 30m, resolution of 2 mm and an update rate in excess of 20 Hz. The University of Edinburgh's Wave Power Group also indicates success with a high accuracy device. The prototype delivers 0.1 mm accuracy at a 10m range and 50 Hz update.

Dead Reckoning systems include taut wire, trailing wheel, current meter log combined with yaw gyro, doppler log/yaw e.g. Krupp Atlas and Inertial Navigation Systems (INS) e.g. Ferranti. The taut wire method is simply a known length of wire stretched between a datum and the point of interest; it is still much used for ship dynamic positioning and diver searches. Only vehicles which travel directly on the seabed can navigate by trailing wheel. Displacement is calculated by counting the wheel's rotations as the vehicle moves. This combined with heading will give the instantaneous position. Current meter logs and doppler logs use, respectively, small propellers and acoustics to measure the relative velocity between the

vessel and the water. Again, the heading angle, measured by a yaw gyro or compass, also has to be known to calculate global displacement. Of course, these two methods can only measure position relative to the water, a serious problem when trying to manoeuver in a current. INSs have three linear accelerometers and three rate gyros mounted at mutual right angles which measure acceleration in each degree of freedom. The last three methods are the most versatile, but suffer from drift from the true position because velocity (and in the case of INS, acceleration) must be integrated to derive displacement; therefore it is necessary to stop occasionally at datum positions to return errors to zero.

Honeywell Corporation [10] reports that work is proceeding with range measurement by Green Laser, whose frequency content is in the low region of the spectrum and hence attenuated less than other electromagnetic signals. Ranges up to 100m were mentioned with the possibility of 330m by 1990.

The problems of navigation within a steel or concrete structure have received much attention but to this date no system which allows tracking of a ROV in this situation has been developed. The authors of [6] point out the need for a solution:

> ...The problems of navigation in and around such things as steel production platforms cannot be overstated and in concrete structures the navigational problem has been likened to a man equipped only with a flashlight searching the runways of Heathrow airport on a very dark night for a 10cm crack in the concrete.

Approaches to developing a structural navigation system will probably involve scanning sonar for obstacle avoidance and tracking plus inertial navigation for use when acoustics fail.

1.4 Existing ROV Control Systems and Previous Studies

Because the work described here is of a rather specialised nature, previous studies into ROV control systems are not numerous although studies on problems such as ship and submarine autopilots and

aerospace applications, especially helicopters, is often relevant.

In section 1.2, it was shown that a pilot would need to be adjusting thruster levels constantly to hold station in a turbulent current because most ROVs do not have any autopilot capability. However, some vehicles incorporate automatic depth and heading features. An example is the Hydro Products RCV 225. A ROV which had this feature was used in the Loch Linnhe trials [5] and the Department of Energy reports that even this limited control capacity was an enormous improvement over a human pilot. However, this author and others [9] state that the problems of extending such control to translational position and velocity are formidable.

Kazerooni and Sheridan of MIT carried out a simulation study of ROVs under closed-loop control [11]. Hydrodynamic effects were modelled as only an added mass and a square-law drag term in each degree of freedom; the model was assumed to contain no hydrodynamic coupling. The only other nonlinearities accounted for in the simulation and control law design were the rigid-body kinematic terms. Their controller is implemented in digital form; at each sampling step, the instantaneous linear model is calculated. This is then considered to be a series of single input/single output (SISO) systems relating forces and moments to acceleration in that degree of freedom. The control law is based on a pole placement method and the output from the controller is six forces and moments; these are assumed to be available from the thrusters. In simulation, the authors demonstrate separate attitude and position controllers with good step responses and deterministic disturbance rejection.

There are three major shortcomings with this method. First of all, too much 'a priori' knowledge of the vehicle is required; it will be shown in chapter 3 that an accurate model of the ROV and its thrusters is difficult and expensive to derive. Secondly, [11] has an excessively naive view of the hydrodynamic forces and thruster characteristics. Finally, no indication is made in the report of effects of measurement noise on the closed-loop response.

Work on ROV control has also been carried out for a number of

years in Heriot-Watt University's Department of Electrical Engineering. Fyfe and Russell describe the position control system which is the basis of a hierarchical scheme involving artificial intelligence at the highest level [12]. Heriot-Watt's research is now directed at these higher level control functions and their implementation in an autonomous ROV [13].

For the low level control, their approach was to identify enough linear hydrodynamics in tank tests to be able to design a system which is stable in closed-loop feedback and robust to vehicle changes. The model simulated included nonlinear kinematic terms and more complicated hydrodynamics than [11], in that it included coupling, but these were still linear. A series of SISO controllers at the local velocity level were implemented. These produced forces and moments which were the input for a thruster allocation module. It was reported that the resultant closed-loop system was decoupled enough for the higher levels to be successful, though they note that the success of the scheme deteriorates with the amount of open-loop coupling. The navigation system they simulate has a very slow update rate of 0.125 Hz and high levels of noise (typically, standard deviations in the X and Y directions of between 1.0m and 1.2m); the position controller uses an observer based on a reduced order model of the dynamics to counteract these problems. Reference [12] reports that the observer has an adaptive gain for the measurement error term.

Both this work and the MIT project require 'a priori' knowledge of the vehicle's hydrodynamics and thruster characteristics and, as noted above, control degrades with increased hydrodynamic coupling.

Fung and Grimble of the University of Strathclyde have also dealt with control problems in a noisy marine environment. They were concerned with dynamic positioning of drill ships and semi-submersible oil rigs [14]. Filtering of the measurements is required in order to remove the high frequency (greater than 0.3 rad/s) first-order wave induced motions; an attempt to counteract them would cause thrust devices to experience excessive wear and waste energy. A fixed-gain Kalman Filter is used to estimate the low frequency motion, caused by wind, current and second-order wave drift forces. The Kalman Filter

requires knowledge of the ship's low frequency equations of motion and the covariances of the measurement noise and the noise driving the internal model of the waves. This is coupled with a self-tuning filter which estimates the parameters of the wave model and adapts to changing weather conditions or direction of the prevailing sea.

The most recent ROV controller project noted here was inspired by the Deep Submergence Laboratory at the Woods Hole Oceanographic Institute who are building a ROV called JASON for deep ocean scientific tasks. The vessel will be able to descend to 2000m and will feature a supervisory control system to coordinate the movements of the vehicle and manipulator. The lowest level is global position control. JASON, at the time, was under construction so the position controller was simulated and then implemented on a Benthos RPV-430 vehicle [9]. The authors point out that a ROV's equations of motion are nonlinear, coupled and difficult to model and identify as did this author [15, 16]. Their approach is to employ a sliding mode nonlinear control method called "suction control" which can be described as a model reference technique which rationally takes into account uncertainties in the model. The theory of this method is more completely described in [17].

The authors show very good results in simulation and demonstrate that the closed-loop system can cope with modelling errors and sensor noise. This controller however, like the previous two described, uses a thruster allocation module; again, this suffers from the need to know thruster characteristics.

1.5 Present Study

This chapter has attempted to show that there is a need for a system to automatically control the translational and rotational velocities and positions of a ROV and, indeed, a few possible solutions have been suggested and implemented. All proposed solutions must take account of the navigation problem and also that ROVs are "multivariable, interacting dynamic systems containing nonlinearities due to rigid-body coupling, hydrodynamic forces on the vehicle and its

umbilical and advance coefficient and momentum drag effects in the thrusters" [15]. Vehicle dynamics can also be time varying in two senses. In the very short term, manipulator position and load can radically change the kinematics and hydrodynamics and on a day-to-day basis, operators often add pieces of equipment to the vessel as the job requires.

The design of a conventional multivariable controller requires a good model of the ROV and its thrusters. It will be shown later that expensive laboratory facilities are needed to identify the model and that the possibility of modelling errors forces either the hydrodynamic analyst or the control engineer to verify that it is sufficiently accurate for design purposes.

This study will consider controller designs which minimize the amount of 'a priori' knowledge required: the so-called "Adaptive" and "Self-Tuning" controllers. It will also describe the problems of conventional modelling techniques; not only do these difficulties suggest the need for a controller which would identify plant parameters on-line, but they also encouraged an investigation into the suitability of "Recursive System Identification" (SI) techniques as an alternative modelling method.

Chapter 2 considers the equations of motion that are customarily used to describe the ROV, its umbilical and the environment.

The model of the UMEL "Seapup" which was used for the controller design studies is introduced in chapter 3; an account is given of the extensive verification procedure. The behaviour of the umbilical model is also included, as is the stochastic current model. The chapter considers a typical configuration change that an operator might make to a ROV; this will be used later for controller robustness studies.

A hierarchical structure is chosen for the ROV autopilot. In chapter 4, reasons for this choice are given and the different levels described. The rest of the chapter is devoted to the theory and implementation of a "Self-Testing" velocity controller.

The performance of this controller is examined in chapter 5; frequency-domain and time-domain methods are used in the evaluation.

Recursive System Identification is considered as an alternative modelling technique in chapter 6. Some results of using the output of the nonlinear simulation, complete with sensor models, as inputs to SI algorithms are given.

Chapter 7 describes two multivariable adaptive control schemes and their performance. The first is an explicit method which identifies a simplified open-loop model and then uses the control law of chapter 4 while the second is an implicit generalised minimum variance law.

The main body of the thesis is concluded by reviewing the results of the study and discussing the suitability of these modelling and control techniques as well as making recommendations for areas of further study.

Appendix A describes a series of tank trials designed to gather data for system identification and to test all three controllers under sheltered conditions. Hardware and software requirements are discussed.

Chapter 2

ROV Equations of Motion

2.1 Introduction

The equations of motion of a ROV have many similarities with the more familiar models of aircraft or conventional submarines, both of which have been well documented [18, 19]. There are important differences, however, which contribute to the difficulties of designing a control system.

Aircraft and submarines have an operating velocity along one axis which is much greater than the other two components and it is convenient to linearise their nonlinear dynamics about this condition. Yoerger and Newman [9] point out that a procedure for designing an aircraft or submarine autopilot could use this property. Linear controllers can be designed at each operating point and the gains expressed as polynomial functions; during operation, speed can be monitored and the gains adjusted accordingly. ROVs, however, may have comparable velocities along all three axes which would make this kind of velocity scheduling unwieldy, if not unmanageable.

The nature of the forces between the water and the vehicle sets submarines and ROVs apart from aircraft. Hydrodynamic interaction is more difficult to analyse than aerodynamics firstly because water is more dense than air and will have larger effects roughly in proportion and also because more engineering effort in the past has gone into aircraft research than into maritime problems. Naval architecture research has shown however that these forces have dynamic and static components, are difficult to measure and highly nonlinear [20].

A fuller appreciation of the inherent difficulties of ROV autopilot design and the choice of controller methods, described in chapters 4 and 7, should be possible after this chapter's discussion of the components included in the model of a ROV, its umbilical cable and the environment.

2.2 Coordinate Systems

A ROV, if considered to be a rigid body, has six degrees of freedom corresponding to translation along three axes and rotation about these axes. The equations of motion are best represented in axes fixed to the vehicle so that properties that depend on vehicle geometry, e.g. kinematics and hydrodynamics, remain constant when vehicle orientation relative to the global coordinate frame changes. Figure 2.1 shows a typical ROV and the axis set used to describe it. Translational motion in the local x, y and z axes are usually called surge, sway and heave while rotations about the same three axes are roll, pitch and yaw.

The orientation of the body coordinate frame with respect to the global axes set is described by its Euler Angles: yaw (ψ), pitch (θ) and roll (ϕ). These angles are not vector quantities and in order to avoid ambiguity must be applied in this order to rotate an axis set from an initial orientation parallel to the global frame into line with the body-fixed axes.

For simulation purposes, it is important to note that the rates of change of the global displacements and orientation (X,Y,Z,ϕ,θ,ψ) are not equivalent to the local velocities (u,v,w,p,q,r), but instead, related through functions of the Euler Angles. The linear velocity transformations are derived by applying, successively (since they are not vector quantities) the rotations ϕ , θ and ψ to the local velocity vector. The matrix transformation is:

$$\begin{Bmatrix} \dot{X} \\ \dot{Y} \\ \dot{Z} \end{Bmatrix} = \begin{vmatrix} \cos\psi\cos\theta & \cos\psi\sin\theta\sin\phi - \sin\psi\cos\phi & \cos\psi\sin\theta\cos\phi + \sin\psi\sin\phi \\ \sin\psi\cos\theta & \sin\psi\sin\theta\sin\phi + \cos\psi\cos\phi & \sin\psi\sin\theta\cos\phi - \cos\psi\sin\phi \\ -\sin\theta & \cos\theta\sin\phi & \cos\theta\cos\phi \end{vmatrix} \begin{Bmatrix} u \\ v \\ w \end{Bmatrix} \quad \ldots.(2.1)$$

Local angular velocities are transformed in a different manner because rotation in global coordinates is the vector sum of local

angular velocities and the rotational velocity of the local frame with respect to the global coordinates. The required relationship is:

$$\begin{Bmatrix} \dot{\phi} \\ \dot{\theta} \\ \dot{\psi} \end{Bmatrix} = \begin{vmatrix} 1 & \sin\phi \tan\theta & \cos\phi \tan\theta \\ 0 & \cos\phi & -\sin\phi \\ 0 & \sin\phi \sec\theta & \cos\phi \sec\theta \end{vmatrix} \begin{Bmatrix} p \\ q \\ r \end{Bmatrix} \quad \ldots.(2.2)$$

2.3 Equations of Motion

The following development expands upon the work in [15]. The equations which describe the motion of the ROV in the local coordinate axes are:

$$\begin{aligned} \hat{[M]}\ \dot{(Q)} = & \quad F_d(u, v, w, p, q, r) \\ & + \hat{H}\ (u_r, v_r, w_r, p_r, q_r, r_r) \\ & + G(\phi, \theta, \psi) + T + U \end{aligned} \quad \ldots(2.3)$$

where $\hat{M}$ = mass matrix including hydrodynamic added mass

$Q = (\ u\ v\ w\ p\ q\ r\ )^T$, the velocity vector

F_d = vector of rigid-body kinematic forces

$\hat{H}$ = vector of hydrodynamic forces

G = vector of hydrostatic forces

T = vector of forces due to thrusters

U = vector of forces due to umbilical cable

The subscript 'r' denotes a relative motion between vehicle and water. The best way to understand these equations is first to consider an alternative formulation:

$$[M]\ \dot{(Q)} = F_d + \Sigma(\text{all external forces}) \quad \ldots.(2.4)$$

In these equations, [M] does not contain added mass terms. Along with the terms in F_d, it forms the standard equations of motion for any rigid body with axes origin at an arbitrary point. These equations are developed fully in [19]; the same derivation will be discussed briefly here.

Let the velocity of the centre of mass of a rigid body of mass 'm' be:

$$\underline{U} = u\underline{i} + v\underline{j} + w\underline{k} + \underline{\Omega} \times \underline{R} \qquad \ldots.(2.5)$$

where $\underline{\Omega} = p\underline{i} + q\underline{j} + r\underline{k}$, the rotational velocity about the axis centre which has a linear velocity $u\underline{i} + v\underline{j} + w\underline{k}$ and $\underline{R} = x\underline{i} + y\underline{j} + z\underline{k}$ is the vector locating the centre of mass with respect to the axes origin.

Newton said:

$$F = \frac{d(m\underline{U})}{dt} = m\frac{d}{dt}[\, u\underline{i} + v\underline{j} + w\underline{k} + \underline{\Omega} \times \underline{R}\,]$$

$$= m\frac{d}{dt}[(u + qz - ry)\underline{i} + (v - pz + rx)\underline{j} + (w + py - qx)\underline{k}\,]$$

$$= m[\,(\dot{u} + \dot{q}z + q\dot{z} - \dot{r}y - r\dot{y})\underline{i} + (\dot{v} - \dot{p}z - p\dot{z} + \dot{r}x + r\dot{x})\underline{j} + (\dot{w} + \dot{p}y + p\dot{y} - \dot{q}x - q\dot{x})\underline{k}$$

$$+ (u + qz - ry)\dot{\underline{i}} + (v - pz + rx)\dot{\underline{j}} + (w + py - qx)\dot{\underline{k}}\,] \qquad \ldots.(2.6)$$

For a rigid body:

$$\dot{\underline{i}} = \underline{\Omega} \times \underline{i} = -q\underline{k} + r\underline{j}$$

$$\dot{\underline{j}} = \underline{\Omega} \times \underline{j} = p\underline{k} - r\underline{i} \qquad \ldots.(2.7)$$

$$\dot{\underline{k}} = \underline{\Omega} \times \underline{k} = -p\underline{j} + q\underline{i}$$

By substituting (2.7) into (2.6) and gathering components, the three linear force balances become, finally:

$$F = m\{\,[\,(\dot{u} + qw - rv) - x(r^2 + q^2) + p(qy + rz) + (\dot{q}z - \dot{r}y)\,]\,\underline{i}$$
$$+ [\,(\dot{v} + ru - pw) - y(p^2 + r^2) + q(px + rz) + (\dot{r}x - \dot{p}z)\,]\,\underline{j}$$
$$+ [\,(\dot{w} + pv - qu) - z(p^2 + q^2) + r(px + qy) + (\dot{p}y - \dot{q}x)\,]\,\underline{k}\,\} \qquad \ldots.(2.8)$$

Three moment balances are also required. The moment about A of the momentum relative to A is:

$$\begin{aligned}\underline{h}_A &= \sum \underline{r}_i \times \delta m_i \dot{\underline{r}}_i \\ &= \sum (\underline{r}_{iG} + \underline{R}) \times \delta m_i (\dot{\underline{r}}_{iG} + \dot{\underline{R}}) \\ &= (\underline{R} \times \dot{\underline{R}}) \sum \delta m_i + \sum \underline{r}_{iG} \times \delta m_i \dot{\underline{r}}_{iG} \\ &= m (\underline{R} \times \dot{\underline{R}}) + \underline{h}\end{aligned} \qquad \ldots.(2.9)$$

The moment of external forces about A is:

$$\begin{aligned}\underline{G}_A &= \sum \underline{r}_i \times \underline{F}_i = \sum (\underline{r}_{iG} + \underline{R}) \times \underline{F} \\ &= \underline{R} \times \underline{F} + \underline{G}\end{aligned} \qquad \ldots.(2.10)$$

As well, since:

$$\underline{G} = \dot{\underline{h}} \qquad \ldots.(2.11)$$

then:

$$\underline{G}_A = \underline{R} \times m\dot{\underline{U}} + \dot{\underline{h}} \qquad \ldots.(2.12)$$

where $\underline{U}$ is the velocity of the mass centre.

Equation (2.9) is used to eliminate $\underline{h}$ from (2.12):

$$\begin{aligned}G &= \underline{R} \times m\dot{\underline{U}} + \dot{\underline{h}}_A - m (\underline{R} \times \ddot{\underline{R}}) \\ &= \dot{\underline{h}}_A + \underline{R} \times m (\dot{\underline{U}} - \ddot{\underline{R}}) \\ &= \dot{\underline{h}}_A + \underline{R} \times m \dot{\underline{U}}_A\end{aligned} \qquad \ldots.(2.13)$$

Consider the first term in (2.13). This is the conventional expression for the moment of momentum about a nonaccelerating point or the centre of mass:

$$\underline{h} = \begin{Bmatrix} h_x \\ h_y \\ h_z \end{Bmatrix} = \begin{vmatrix} I_{xx} & -I_{xy} & -I_{xz} \\ -I_{yx} & I_{yy} & -I_{yz} \\ -I_{zx} & -I_{zy} & I_{zz} \end{vmatrix} \begin{Bmatrix} p \\ q \\ r \end{Bmatrix} \qquad \ldots.(2.14)$$

Here, however, x, y and z are measured from the point A. The derivation of this result is illustrated for the first component h_x and uses the following expression for a triple vector product:

$$\underline{r} \times (\underline{\Omega} \times \underline{r}) = (\underline{r} \cdot \underline{r}) \underline{\Omega} - (\underline{r} \cdot \underline{\Omega}) \underline{r} \qquad \ldots.(2.15)$$

It follows:

$$h_x = \Sigma \delta m_i [\ (x^2 + y^2 + z^2)\ p\ -\ (xp + yq + zr)\ x\ ]$$
$$= [\ \Sigma \delta m_i (y^2 + z^2)\ ,\ -\Sigma \delta m_i xy\ ,\ -\Sigma \delta m_i xz\ ]\ [p\ \ q\ \ r]^T \qquad .....(2.16)$$

where
$$I_{xx} = \Sigma\ (y^2 + z^2)\,\delta m_i$$
$$I_{xy} = \Sigma\ xy\,\delta m_i$$
$$I_{xz} = \Sigma\ xz\,\delta m_i$$

Equation (2.13) is now written in the form:

$$\underline{G}_A = (\dot{h}_x \underline{i} + \dot{h}_y \underline{j} + \dot{h}_z \underline{k}) + \underline{\Omega} \times \underline{h}$$
$$+ m \underline{R} \times (\dot{u}\underline{i} + \dot{v}\underline{j} + \dot{w}\underline{k}) + m \underline{R} \times (\underline{\Omega} \times \underline{U}) \qquad ....(2.17)$$

In component form, this simplifies to:

$$L = (\dot{h}_x + qh_z - rh_y) + m\ [\ (y\dot{w} - z\dot{v}) + y(pv - qu) - z(ru - pw)\ ]$$
$$M = (\dot{h}_y + ph_z - rh_x) + m\ [\ (z\dot{u} - x\dot{w}) + z(qw - rv) - x(pv - qu)\ ]$$
$$N = (\dot{h}_z + ph_y - qh_x) + m\ [\ (x\dot{v} - y\dot{u}) + x(ru - pw) - y(qw - rv)\ ]$$
$$....(2.17a)$$

The six relations (2.8) and (2.17a) are the equations of motion for a rigid body with axis centre at an arbitrary point.

Attention is now returned to equation (2.4). The summation term is conveniently broken into:

$$\Sigma(\text{all external forces}) = \hat{H}\ (\dot{u}_r, \dot{v}_r, \dot{w}_r, \dot{p}_r, \dot{q}_r, \dot{r}_r, u_r, v_r, w_r, p_r, q_r, r_r\ )$$
$$+ G\ (\phi, \theta, \psi) + T + U \qquad ....(2.4a)$$

These four terms may be considered in turn.

2.3.1 Hydrodynamic Forces and Moments

The hydrodynamic forces along the surge, sway and heave axes, X,Y,Z and the moments about the same three, L,M,N, are functions of the instantaneous motion, the previous motion of the vehicle and the ROV's geometry. These forces are conventionally represented in terms of 'slow motion derivatives'. As an example, the moment about the yaw axis caused by acceleration in the x direction is expressed as $N_{\dot{u}}\dot{u}$, where $N_{\dot{u}} = \partial N / \partial \dot{u}$. These hydrodynamic derivatives are measured experimentally and can lead to very complicated expressions. The method of slow motion derivatives uses a Taylor Series expansion of the function to show that the effects of the past velocities are accounted for by the instantaneous higher derivatives. The infinite series is curtailed at the accelerations, a step which can be justified if the departure from the reference motion is 'slow'.

The values of the hydrodynamic derivatives can be determined by the methods of oscillatory coefficients, impulse response functions or regression analysis. The first involves forcing a model vessel (or the actual ROV, if it is small enough) through sinusoidal motion at a series of frequencies in a test tank equipped with a planar motion mechanism and measuring the forces in-phase and in quadrature with the imposed displacement. The derivatives are the limit of the frequency dependent forces as the frequency approaches zero. Impulse response methods are more appropriate for taking into account the time history effects of the vehicle's motion. A velocity which consists of only one degree of freedom, but of arbitrary form, is imposed on the vehicle and the resulting force measured. The ratio of Fourier transforms of the force and velocity is the frequency response of the hydrodynamic derivative. The Inverse Fourier transform of this quantity is the impulse response function, which, when convoluted with a velocity time series, yields the force corresponding to this velocity.

Unfortunately, these two methods cannot model nonlinear effects and can only measure a pair of coefficients with each series of tests. This is a serious problem in the case of the ROV because a linear model of the hydrodynamics will not be sufficiently accurate and even

if nonlinearities could be handled, the number of terms needed would require excessively many tests. Regression analysis is best suited for these requirements. A model structure can be chosen which incorporates whatever linear or nonlinear terms the analyst feels are suitable. Constrained model tests are executed and all forces and motions recorded. A numerical optimisation routine uses this data to determine simultaneously the best values of all the hydrodynamic derivatives; statistical tests can determine if the inclusion of specific terms is justified.

This latter approach was used by the National Maritime Institute of Feltham, Middlesex (now British Maritime Technology) in their study of ROV hydrodynamics, sponsored by the UK Department of Energy's Advisory Group for Underwater Technology [20]. The UMEL 'Seapup' was tested and the resulting model was made available to University College London for use in the present study. Details of this model and the verification study which it was subjected to are given in chapter 3. Suffice it to say for the moment that the optimisation algorithm can choose inappropriate values for the hydrodynamic derivatives if it converges to a local, instead of a global minimum, or if the assumed form of the model is incorrect.

The NMI report also reached some qualitative conclusions about ROV hydrodynamics. The common space-frame structure of ROVs, engineered with "little regard to the usual strictures of hydrodynamic design", is best characterised as a "bluff-body". The flow about such a shape has large areas of separation; the result is an eddying, disturbed region which gives rise to forces generally larger than would have occurred if the flow had remained attached. The eddying effects can also cause oscillatory forces to "lock on" to the vehicle's motions if the frequency of the eddy shedding is close to one of the ROV's natural frequencies. This is a very important factor in the umbilical cable's behaviour, discussed in section 2.3.4.

Separation, however, can cause reductions in hydrodynamic forces if the vehicle or some of its body parts has a spherical or cylindrical shape and if the vehicle is operating in the critical regime where the transition from laminar to turbulent flow occurs.

This is often the case with ROVs because of their low operational speed.

These factors make a nonlinear ROV hydrodynamic model necessary and raises doubts about those previous studies which only incorporate linear models in their simulations. NMI included in the 'Seapup' model 84 hydrodynamic terms to describe the six forces and moments; 71 were nonlinear, the only linear terms being those involving acceleration, i.e. added mass.

All of the velocities and accelerations used in hydrodynamic force calculations are in terms of relative motion between the water and vehicle. The present study assumes that the fluid accelerations and angular velocities are negligible which leaves only u, v and w as relative quantities. Terms involving acceleration, such as $N_{\dot{u}}$, are included on the left hand side of (2.4) in order to solve for accelerations; this leaves the equations in the form of (2.3), with hydrodynamic effects included in the mass matrix.

2.3.2 Hydrostatic Forces and Moments

The determination of the G term in (2.3) is a much simpler matter than the hydrodynamic forces. The buoyancy forces act vertically at the centre of buoyancy, by definition, while the weight is applied in the opposite direction through the centre of gravity. The relative position of these two points and the attitude of the vehicle, defined by its Euler Angles, determines the hydrostatic moments.

2.3.3 Thruster Forces

The ROV's thrusters, used for both propulsion and directional control, are strongly nonlinear actuators. The axial thrust produced is dependent on blade pitch angle, angular speed and inflow conditions, the latter two which are combined in the advance coefficient:

$$J_o = V/nD \qquad \ldots.(2.18)$$

where V is the axial speed of the thruster, n is the shaft angular speed and D is the propeller diameter. For a fixed speed propeller operating in open water conditions, a typical relationship between thrust, advance coefficient and blade pitch angle is shown in figure 2.2. However, when installed on a ROV, thrusters often behave differently because of interactions between thrusters and between thrusters and vehicle. When operating at low speeds, 50 percent of the effectiveness of a ducted thruster comes from the duct itself, an annular aerofoil [20]. If the flow to and from the duct is impeded by other parts of the vehicles structures, severe losses of effectiveness can occur. For example, in the present study the measured contribution the vectored thrusters to the yaw moment is only 15 percent of their theoretical open-water value.

Momentum drag effects occur when an operating thruster is moved perpendicular to its axial direction. Water which is to be moved through the blades must first be accelerated up to the normal speed of the thruster which causes an apparent drag force opposing the normal velocity. Momentum drag is a major component of the drag for hovercraft, where it is necessary to pass large volumes of air down through the lift fan to maintain clearance. An expression for momentum drag, R, is given by Dand and Every [21]:

$$R = \frac{\pi}{2} p n D^3 V \sqrt{\frac{K_0}{\pi}} \qquad \ldots.(2.19)$$

where p is the water density, n the rotational speed of the propeller, D the propeller diameter, V the normal velocity of the thruster and K_0 the thrust coefficient at zero advance coefficient.

Another interaction between thruster and vehicle which can occur is the so-called 'jet effect'. Suppose a thruster discharges in front of a large flat portion of the vehicle. If the ROV is moving normal to the thruster's axial direction, it is possible for the jet to be turned to flow over the ROV. This can cause regions of low pressure and hence unbalanced forces and moments.

2.3.4 Umbilical Cable

Other maritime applications of cables include towed vehicles and sonar arrays and for moored ships and structures. The aeronautical engineer is interested in their behaviour when analysing glider tows and in-flight refueling. When researching the modelling of the ROV's umbilical cable, it was found that previous works, though motivated by different applications such as these, all came to the conclusion that analytical solution is possible only for certain simple cases, numerical solutions necessary for realistic cases prohibitively expensive and the hydrodynamic loading very uncertain.

The umbilical cable is simultaneously a help and a hindrance to ROV operations. It allows missions of essentially unlimited duration by dispensing with the need to carry batteries or other power sources onboard, but at the same time, cable entanglement and severance are the most common causes of vehicle loss. Additionally, cable drag at modest depths can consume most of the vehicle's propulsive power, limiting the ROV's "footprint". Increasing the available power to the ROV might not be a solution either; more electrical current requires a thicker cable whose drag will possibly be larger than the increased thrust.

The mechanics of the cable itself, without external loading, are developed by Jefferys and Patel [22], Ferriss [23] and other authors and follows from straightforward application of Newton's Laws to a flexible beam, or string, if bending resistance is ignored. These may be solved by a number of techniques. Reference [22] discusses the suitability of 'transmission line' models, modal analysis and finite element techniques for examining the resulting dynamics. Hydrodynamic loading, however, defies analysis and empirical results must be considered; a good review is given in [21]. Most analysis techniques start by assuming that the normal, tangential and lift (lateral) forces are all independent, which is dubious when the cable becomes steeply inclined to the flow. At this point, the normal force becomes strongly correlated with the tangential. However, it is assumed for convenience that this can be ignored and the force components examined

separately. Normal force calculations can be based on experimental data for infinite rigid cylinders in a flow, modified to take into account cable roughness, flexibility, incidence to the flow, turbulent oncoming flow and strumming; low amplitude, relatively high frequency lateral vibrations caused by vortex shedding. More will be said of this important effect later. All of these real considerations tend to increase the drag coefficient over the experimentally derived value.

Tangential drag is generally ignored as little data is available, and that which exists shows much scatter. Fortunately, this component is very much smaller than the normal and lateral forces. Lift forces act normal to both the cable direction and the flow and cause a two dimensional velocity flow field to yield a three dimensional cable shape. Large lateral deflections, known as "kiting", are a result of lift forces and are not the same as strumming, as they are a steady state effect. Again, since there is no easy analysis technique available, experimental values of the lift coefficient must be used.

Strumming can increase the drag of an umbilical by up to three times that of a rigid cylinder and therefore, overwhelms all other uncertainties. Experiment and real experience have shown that cables will oscillate in this manner in nearly any flow. Lateral motion is caused by the periodic forces arising from the Karmen vortex street downstream of the umbilical. The frequency of the vortex shedding is given by the Strouhal relationship:

$$S = f_s D / V \qquad \ldots.(2.20)$$

where f_s is the frequency of vortex shedding, D is the cable diameter, V is the velocity of the flow and S, the Strouhal number, approximately 0.2 for Reynolds numbers of concern. Skop, et al [24] assembled published results of the increase in normal drag coefficient and related them to a "wake stability parameter" by the relations:

$$W_r = (1 + 2y/D)\, f_s / f_c \qquad \ldots.(2.21)$$

$$C_D/C_{DO} = 1.0 + 1.16(W_r - 1)^{0.65} \qquad \ldots.(2.22)$$

where W_r is the wake stability parameter, y the amplitude of lateral vibration, D the umbilical diameter, f_s and f_c the frequencies of vortex shedding and cable vibration respectively, C_{DO} the drag coefficient for the nonstrumming case and C_D, the modified drag coefficient. Equation (2.22) yields C_D in the range of 1.0 C_{DO} to 3.0 C_{DO} for relevant W_r values. These relations indicate that drag due to strumming may be reduced by decreasing D (as this lowers the cable area and more than compensates for increasing W_r and hence C_D) or decreasing the amplitude of vibration. A variety of strumming supressors have been suggested by ROV manufacturers; these consist of cable attachments which interfere with vortex formulation and take the form of aerofoil fairings, trailing flags, ribbons, fringes or helical strakes. Operators have indicated an unwillingness to use strumming suppressors because they are expensive, can cause handling problems when the cable is being deployed or retrieved and can actually increase normal drag because of increased effective diameter.

Jefferys and Patel [22] used a finite element model in their work on taut mooring systems; Kapsenberg [25] also employs this method for simulating umbilical dynamics in the ROV simulator of TNO-IWECO, Delft, Holland. While good results were obtained, it was at the cost of excessive computational effort. A suitable real-time model was obtained by simulating a series of quasi-static situations, where the instantaneous cable loading is determined by the endpoints of the umbilical and the relative velocity of the cable through the fluid. The cable is assumed to take up a parabolic shape.

A similar quasi-static approach was chosen for the present study because of a number of reasons. The increased complication and computational resources needed for a dynamic analysis were thought to be of questionable value when all that was really necessary for evaluation of the ROV's autopilot was a good approximation of the disturbance forces. As well, work at the National Physical Laboratory in Teddington, Middlesex has produced a static umbilical computer model suitable for inclusion in the simulation used in this study [23]. The NPL investigation was sponsored by the Department of Energy as yet another part of their ROV initiative.

NPL actually produced a series of reports on umbilical cable calculations. In [26], Ferriss discusses the numerical solution of the differential equations describing the three-dimensional equilibrium of an inelastic, flexible umbilical subjected to hydrodynamic and gravity loading. This was extended in [27] to produce time varying solutions for an umbilical attached to a mass driven by known forces. The static solution was represented by a finite sum of Chebyshev polynomials. Ad hoc methods were required to extend the Chebyshev technique so it would converge to the proper solution in the dynamic case. Unfortunately, both cases required large amounts of computer storage and time and the need was identified from talks with the ROV industry for a cheap, approximate solution. Reference [23] describes an analytical static solution that can be achieved by making certain simplifying assumptions. The first is that tangential hydrodynamic loading can be neglected when compared with the tangential component of gravity; in contrast, the normal hydrodynamic drag is considered to be much larger than normally directed gravity. Finally, it is assumed that the current vector is in the horizontal plane with no vertical component.

The cable is described by six nonlinear ordinary differential equations; three represent the force balance in the tangential, normal and lateral directions while the others give the geometric gradients in terms of the local inclination ϕ_u and azimuth θ_u. Hydrodynamic loading in the normal and lateral directions is represented by modified square law damping:

$$G = K\, U_G \sqrt{(U_G^2 + U_H^2)} \qquad \ldots.(2.23)$$

$$H = K\, U_H \sqrt{(U_G^2 + U_H^2)} \qquad \ldots.(2.24)$$

where $K = p\, t\, C_D / 2$

Here, G and H are the normal and lateral hydrodynamic forces, U_H and U_G the normal and lateral relative velocities through the fluid, p the fluid density , t the cable diameter and C_D the drag coefficient as in (2.22). In the present work, strumming is taken into account by (2.21) and (2.22); these relations yield an upper value of C_D of 3.

C_{DO} for wake stability parameters of interest. It was decided to use $C_D = 2.5\ C_{DO}$ in order to be reasonably pessimistic about the effects of umbilical drag. The boundary conditions for the six differential equations assume that both ends are fixed at known coordinates; the velocity of the vehicle is allowed for by modifying U_G and U_H in (2.23) and (2.24).

The analytical integration of the umbilical's simplified static equations is developed fully in [23]. The result is a single transcendental equation which must be solved numerically to yield the attitude and tension at each end of the cable. Ferriss determined that a linear Newton Raphson iterative technique converges quickly enough and is simple to implement. For each intermediate point where these quantities plus the coordinates are required, another nonlinear equation must be solved numerically. The NPL report describes the situations where the assumptions made cause solutions to be far removed from the exact case. Ignoring tangential drag is of primary importance when the cable length is relatively long. In all cases, the simplified solution will only be useful when the ratio of gravitational to hydrodynamic loading is less than 0.1, otherwise, the assumptions about gravity loading will not be valid. Fortunately, for a near-neutrally buoyant cable, which most vehicles employ, the above situation occurs whenever the vehicle is moving relative to the water.

The NPL FORTRAN code was inserted into the present study's simulation with minimal modifications, though a 'buffer' routine was necessary to convert between the two different coordinate conventions. An allowance was made for bypassing the umbilical calculations if the hydrodynamic loading was too low.

2.4 Stochastic Current Model

The principle disturbances acting on a ROV are the forces and moments caused by current and turbulence. Given the instantaneous current speed and direction and the hydrodynamic properties of the vehicle, these forces and moments can be calculated. By ignoring the effects of the water's acceleration, the force becomes a function of only the relative velocity between vehicle and water. A standard

current model is assumed with current direction zero degrees when flowing along the positive X-axis and ninety degrees when along the positive Y-axis. The component in the global Z-direction is assumed to be always zero. Figure 2.3 shows the relationship between global-axes, body-axes and current direction.

The simulation first determines the instantaneous current speed and direction from a pair of discrete stochastic models. The components in the global X and Y coordinates are determined. By using the vehicle's Euler angle, these are converted to body-fixed x, y, z coordinates and the relative velocity between vehicle and water is calculated. It is these relative velocities that are used to determine the hydrodynamic forces acting on the ROV, through the previously defined (H) vector.

The stochastic nature of the current can be modelled by a pair of first order Gauss-Markov functions:

$$c(k+1) = a_c + b_c c(k) + d_c w_c(k) \qquad \ldots.(2.25)$$

and

$$\alpha(k+1) = a_\alpha + b_\alpha \alpha(k) + d_\alpha w_\alpha(k) \qquad \ldots.(2.26)$$

to describe current speed and direction respectively, where:

$c(k)$ = current speed at time k

$\alpha(k)$ = current direction at time k

and $w_c(k)$ and $w_\alpha(k)$ are gaussian white noise processes [28]. The current is modelled as a coloured noise process with significant power up to 0.1 $\frac{rad}{s}$. This corresponds to a break time, T_c = 10 s. If T_s is the sampling time of the process, then:

$$b_c = b_\alpha = \exp(-T_s/T_c) \qquad \ldots.(2.27)$$

$$d_c = d_\alpha = 1 - \exp(-T_s/T_c) \qquad \ldots.(2.28)$$

The process is assumed to have a mean level ($\bar{c}, \bar{\alpha}$) and a variance (σ_c, σ_α). The mean can be modelled by choosing:

$$a_c = \bar{c}\,(1 - b_c) \qquad \ldots.(2.29)$$

$$a_\alpha = \bar{\alpha}\,(1 - b_\alpha) \qquad \ldots.(2.30)$$

Note that [28] gives an incorrect expression for the mean values.

The power of the white noise processes, $w_c(k)$, $w_\alpha(k)$ are given by:

$$\sigma^2_{w_c} = \frac{(1 - b_c^2)(\sigma_c^2 + \bar{c}^2) - 2\,a_c b_c \bar{c} - a_c^2}{d_c^2} \qquad \ldots.(2.31)$$

$$\sigma^2_{w_\alpha} = \frac{(1 - b_\alpha^2)(\sigma_\alpha^2 + \bar{\alpha}^2) - 2\,a_\alpha b_\alpha \bar{\alpha} - a_\alpha^2}{d_\alpha^2} \qquad \ldots.(2.32)$$

and since $\alpha(k)$ and $c(k)$ should be strongly correlated, we choose:

$$w_\alpha(k) = (\sigma_\alpha / \sigma_c)\, w_c(k) \qquad \ldots.(2.33)$$

2.5 Summary

This chapter has reviewed the choices that were made for each of the components that made up the open-loop ROV simulation; the vehicle, its umbilical cable and the environment. The ROV itself involves rigid-body gyroscopic forces, hydrostatics, hydrodynamics and thruster models. This study was fortunate to have access to a very comprehensive ROV model developed by British Maritime Technology. The effects of the cable and stochastic current help make the ROV autopilot a unique control design problem and so it is very important that representative simulations be used; in each case a compromise was made between complication and accuracy such that it was believed more analysis and computational effort would yield diminishing returns.

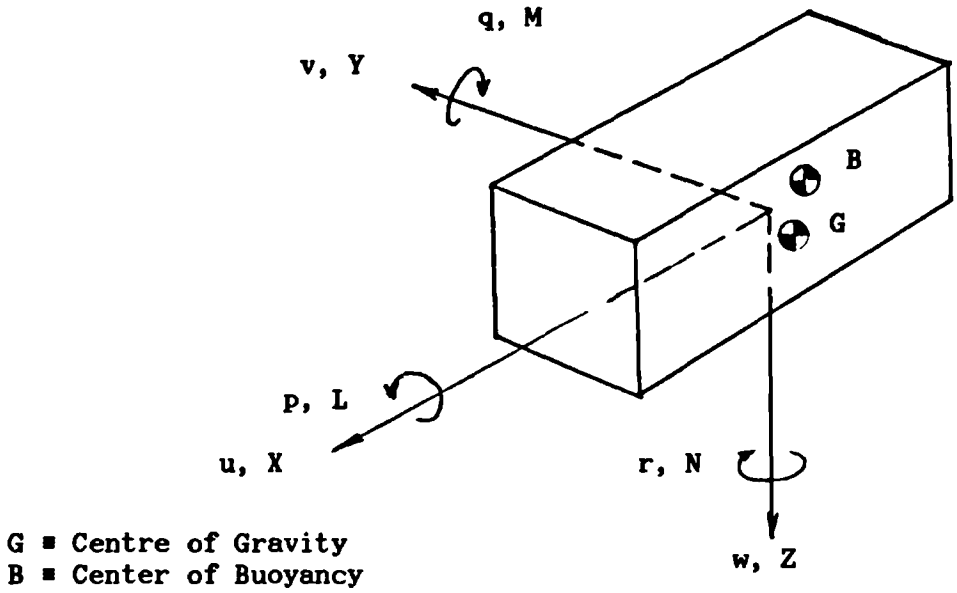

Figure 2.1 : The ROV axis set

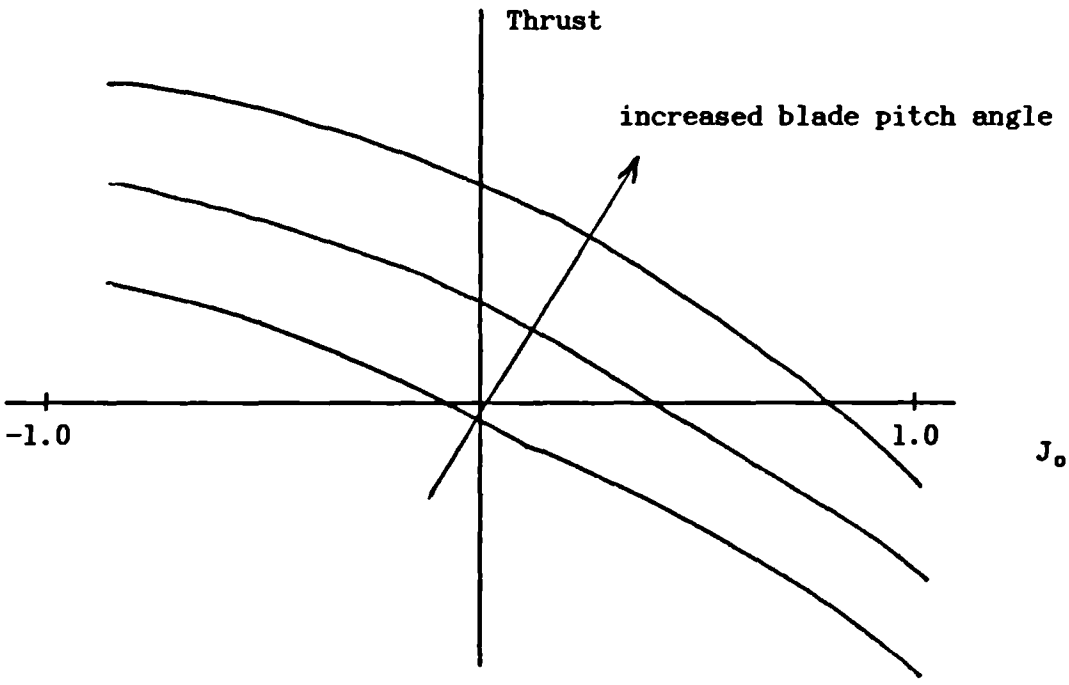

Figure 2.2 : The relationship between axial thrust, blade pitch angle and advance coefficient for a typical thruster

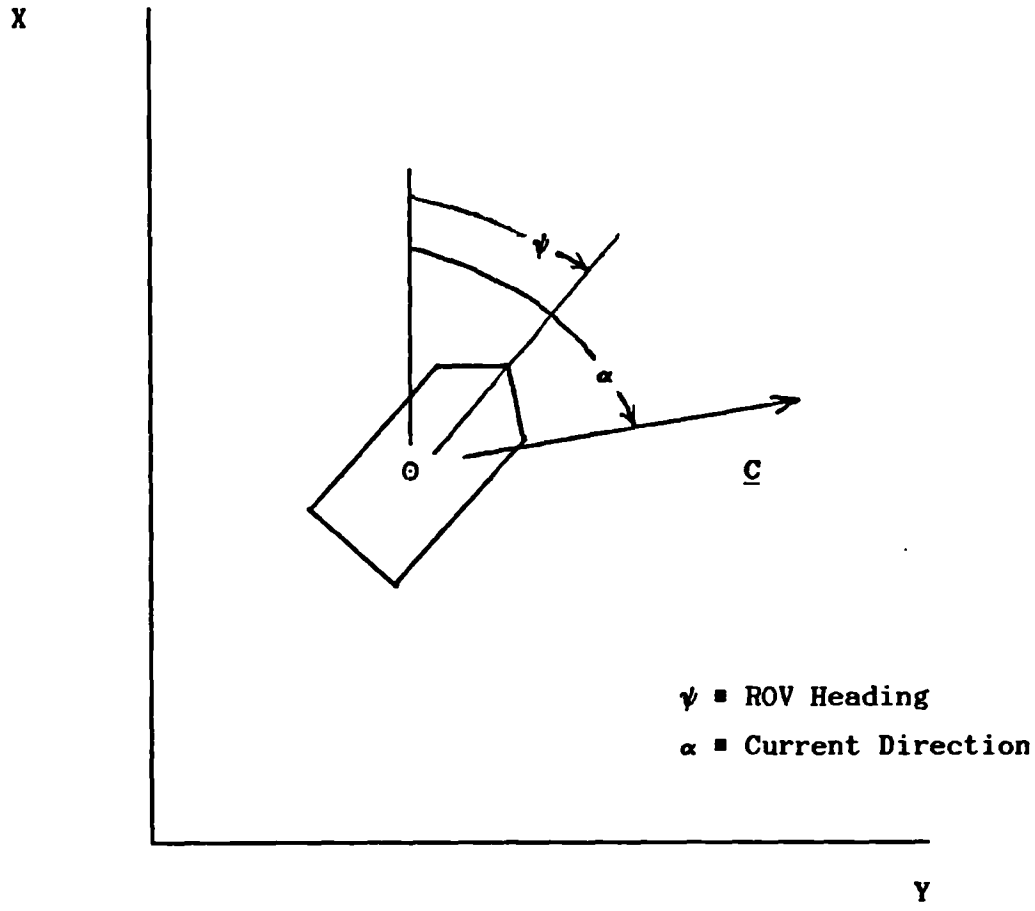

Figure 2.3 : Sign convention for the current model

Chapter 3

Validation of the ROV Model

3.1 Introduction

The first activity in the investigation of the control of ROVs was to evaluate the open-loop vehicle model of the UMEL 'Seapup', supplied to University College London by the UK Department of Energy's Advisory Group for Underwater Technology . As stated in section 2.3.1, the model was developed by the National Maritime Institute, now British Maritime Technology (BMT). The first stage of their study had two objectives: the parameters of a comprehensive vehicle and umbilical model were to be used in a ROV simulator and general conclusions were to be reached about the form of ROV hydrodynamics. The Department of Aeronautics at the Cranfield Institute of Technology is developing the software for the simulator [29], which the DoEn hopes will be used for pilot training. YARD Limited of Glasgow is implementing the software on special purpose simulation and graphics computers. BMT hopes to extend their results so that hydrodynamic parameters for a vehicle can be estimated from vehicle geometry alone, allowing performance to be assessed before a new vehicle is built.

The UMEL Seapup is an observation craft equipped with four constant speed, controllable pitch thrusters. It is 0.82m long by 0.31m wide by 0.43m high and has a mass of 115 kg. The thrusters are shaft driven from a single motor. Two are mounted at the rear of the craft directed in the longitudinal direction, on the port and starboard sides. These are called the main thrusters and provide much of the force and moment which control surge and yaw. The vectored thrusters are fixed at angles of 45 degrees to the vertical and are mounted on the longitudinal centreline. Use of these thrusters together will tend to cause the vehicle to move in heave whereas differential thrust will move the vehicle in sway.

The Seapup's upper surface is covered by a smooth cowling which contains the buoyancy material and electronic components while the lower half of the vessel is of an open-frame construction and contains

the motor, gearbox and instrument payloads. These features strongly affect the behaviour of the vehicle. Studies [20] have shown that the flow over the upper part of the craft is smooth with well defined streamlines while it is separated and turbulent in the open lower area and behind the vehicle. This will lead to pressure differences which will cause the vehicle to rise while moving in surge or sway. Another effect is that flow entering the main thrusters will be disturbed and nonuniform.

The Seapup simulation was considered to be the most comprehensive ROV model yet developed, certainly much more realistic than those used in most previous ROV autopilot studies [11, 12, 13] and therefore, very much suitable for the evaluation of different control schemes. However, before control system design could proceed, it was necessary to confirm that the "plant" model for which the controller was to be designed accurately reflected the real behaviour of the ROV.

The model verification study is the subject of this chapter. The simulation was implemented in FORTRAN IV (later FORTRAN 77) on a DEC PDP 11 computer; this simulation software has also been installed on a VAX 11/780 at JH Division, Admiralty Research Establishment Portland, Dorset. A series of free response tests to initial conditions and thruster blade pitch step response tests were used to test the model. The position and velocity histories of the vehicle were examined and compared with the results of free-running experiments carried out at BMT. Simulation results were also compared with qualitative ideas of how a symmetrical ROV should behave.

This chapter will also consider the umbilical cable and environment models developed in chapter 2. Drag for typical cable configurations and the effects on the vehicle's performance at varying depths will be examined. Suitable choices for the parameters in the current/ turbulence model will be discussed and a typical time series and resulting spectral content presented.

3.2 Initial Eigenvalue Analysis

Before the verification procedure simulations were run, the full nonlinear set of equations of motion were linearised about the quiescent state and the eigenvalues of the system extracted. With this information, it could be determined what integration time step would ensure that the integration technique (fourth-order Runge-Kutta) would remain stable.

The linearisation procedure approximated the nonlinear equations of motion:

$$\dot{q} = H(q,u) \qquad \ldots.(3.1)$$

by the general linear state space form:

$$\dot{q} = A(\bar{q},\bar{u})\, q + B(\bar{q},\bar{u})\, u \qquad \ldots.(3.2)$$

As a reminder to the reader, the state vector consists of the ROV's six displacements and six velocities while the four thruster blade pitch angles make up the input vector. Fourth-order Taylor Series approximations of $\partial H/\partial q$ and $\partial H/\partial u$ were used for A and B [30]. The (ij)th element of A is given by:

$$A_{ij} = [\, -H_{ij}(\bar{q}+2h_i,\bar{u}) + 8H_{ij}(\bar{q}+h_i,\bar{u}) - 8H_{ij}(\bar{q}-h_i,\bar{u}) + H_{ij}(\bar{q}-2h_i,\bar{u})\,] \,/\, [12\, h_i] \qquad \ldots.(3.3)$$

where $\bar{q}$ and $\bar{u}$ are the values of the state and input about which the linearisation is to take place and h is the vector of finite spacings of the state values. A similar expression exists for B_{ij}.

The eigenvalues are listed in table 3.1a. The eigenvalue routine used, the IMSL's (International Mathematics and Science Library) QR algorithm, yielded four poles at $s = 0.0$ which represent the approximately pure integration of u, v, w and r to X, Y, Z and ψ. The fastest oscillatory pole was at 0.4011 Hz and the fastest real part of any pole was (-)2.0098 1/s i.e. a time constant of -0.498 seconds. A rule of thumb is that for a simple Euler integration method, gradients should be calculated at twenty times the fastest oscillatory pole. In this case, that is 0.1247s. A fourth-order Runge-Kutta uses a gradient

calculated four times during the time step, which makes it far more stable and accurate than Euler's method, where numerical errors are proportional to the time step, dt, squared. In a fourth-order Runge-Kutta, errors are proportional to dt raised to the power five. The Runge-Kutta algorithm also had the advantage of being self-starting, like all single-step methods which only use values obtained in the previous time instant.

The simulations were first run at an integration step of 0.1s; results at 0.05s and 0.025s were compared with these to demonstrate that 0.1s was numerically stable and accurate. Finally, because the more accurate Runge-Kutta, rather than the Euler method was being used, 0.2s trials were compared to those at 0.1s and found to be nearly identical; therefore, it was decided to use the larger time step. The linear model that was derived for this analysis could also be used in time domain simulations. It was useful to employ it rather than the nonlinear equations when trying to determine whether unexpected effects observed on a closed-loop system, described in chapters 4 and 7, were due to the controller or the nonlinear open-loop vehicle. It also ran much more quickly than the nonlinear model, suggesting that this may be a possible way of quickening a time domain simulator. However, system identification techniques, the subject of chapter 6, will be shown to be more suitable for this purpose.

3.3 Description of Verification Tests and Initial Performance

Table 3.2 lists the simulations that were carried out, the inputs (thruster blade pitch angles), initial conditions and the quantities that the simulation was intended to evaluate. Simulations 1 and 2 were designed to demonstrate the transient autonomous behaviour of the Seapup when released from initial roll and pitch angles, respectively. The influence of the thrusters was totally removed from these simulations. Note that this cannot be done by simply putting the blade pitch angles to zero since offsets and momentum drag will cause the thrusters to produce forces at this setting. In both cases, damped second order behaviour of the pitch and roll angles was expected, because the separation of the centre of mass and the centre of buoyancy

acts as a position restoring spring when either a pitch or roll angle exist and the hydrodynamic drag forces act as damping elements.

The roll angle simulation, no. 1, used as its initial condition a roll angle of 24 degrees, the value that was reported in the free-running tests to be the maximum forced roll angle at zero forward speed. Instead of the expected behaviour, the solution became unstable with large negative values for pitch rate and vertical velocity. In the pitch simulation, from an initial pitch angle of 22 degrees bow up, the solution was again unstable, with large negative pitch rate and heave velocity.

For a correct model, simulation 3 should show that the top forward speed is 1.13 m/s and the maximum transient pitch angle and pitch rate in an impulsive start are 22 degrees bow up and 18 deg/s respectively. The simulation yielded a maximum pitch angle of 41.2 degrees bow up and a maximum pitch rate of 50.0 deg/s, well above the values obtained in the NMI tests. The forward speed seemed to be converging to approximately 0.9 m/s when the equations became unstable. They indicated that the pitch rate became increasingly large in the negative sense and finally unbounded.

The maximum roll angle in a forced roll at zero forward speed and the maximum velocity in pure lateral translation should both occur when the vectored thrusters are set one at the positive limit, one at the negative i.e. one pushing, one pulling. Also, one should expect symmetric behaviour when the simulation is run with the signs of the thruster blade pitch angles reversed, since the Seapup is left-right symmetric. Simulations 4a and 4b both became unstable (unbounded negative pitch rate), 4a after 0.40s and 4b after 1.60s. The experiments showed that the maximum roll angle achieved is 24 degrees and the maximum roll rate was 34 deg/s. The simulations indicated that the maximum roll angle and roll rate were 233 degrees and 205 degrees/s, respectively. Furthermore, the simulations did not show the expected symmetric behaviour.

Pure vertical translation was meant to be achieved with the vectored thrusters set so that they both push or pull at the same time.

The free-running tests showed that the maximum vertical velocity was 0.33 m/s down and 0.02 m/s up. Simulation 5b was unstable, as the pitch rate became unbounded at a slow rate, and gave a maximum velocity of 0.38 m/s up. Simulation 5a went unstable at 4.6s, but before that occurred, the vertical velocity was beginning to converge to approximately 0.9 m/s.

These unstable simulations were unexpected after the eigenvalue analysis which indicated that the system's poles were all in the right-half complex plane. However, these results are only valid for the operating point about which the vehicle's dynamics were linearised. The analysis was repeated at u = 0.70 m/s, w = 0.30 m/s (i.e. roughly where instability set in during simulation); the eigenvalues at this point are listed in Table 3.1 b. The two unstable oscillatory poles relate to the pitch (0.185 $\pm$ 1.26j rad/s) and roll (0.564 $\pm$ 2.97j rad/s) modes.

3.4 Destabilisation Due to Errors in Hydrodynamic Analysis

From all of these simulations, it can be concluded that the model in its original form does not correctly reflect the characteristics of the vehicle. It was suspected that the hydrodynamic parts of the equations were most likely to be at fault, since the individual terms that make up the hydrodynamic forces are the result of curve-fitting to the results of planar motion mechanism (PMM) tests and there are no fixed rules about which terms should be included in the hydrodynamic model. It is possible to add terms to curves which, simultaneously, improve the fit to PMM data and destabilise the model. Consider the following example, illustrated in figure 3.1. The characteristics of a nonlinear damper are to be measured. The relationship between damping force and velocity is:

$$F(u) = u - 0.2 \sin(u) \qquad \ldots.(3.4)$$

An experiment is done and the damping force at five velocities in the range -1 to +1 is recorded. Not knowing the sinusoidal relationship of this particular damper and having only five data points, the analyst

fits the polynomial curve:

$$F(u) = u - 0.25\,u^3 \qquad \ldots.(3.5)$$

This expression relates the damping force and velocity very nearly exactly in the range considered during the experiment. If this expression for damping force is used in a simulation where larger velocities occur than in the experiment, an unstable solution emerges. This is because when the damping force is extrapolated above a certain velocity, it becomes negative because of the cubic term. This instability would not occur if the correct damping relationship had been obtained. This example is, admittedly, contrived, but it does illustrate the problems that can occur when analysing experimental hydrodynamic data.

The plan of action was to examine the details of each of the five simulations and determine the mechanism in the equations that leads to these incorrect answers. If a specific slow motion derivative (SMD) was suspected of being incorrect, it was set to zero and the simulation run again to check the assumption. Hopefully, a set of stable equations which roughly characterise the vehicle would result.

Before this work began, there were already some doubts about the mass matrix. Newman shows that for a rigid body in an ideal fluid, the mass matrix should be symmetric i.e. $m_{ij} = m_{ji}$ [31]. The Seapup's mass matrix was far more asymmetric than expected, even considering that the vehicle is in a real, viscous fluid. As an example of the problems that can occur with this formulation, consider the nonlinear equations linearised about the quiescent state and put into the form:

$$\dot{q} = Aq + Bu \qquad \ldots.(3.2)$$

where q = 12x1 vector of vehicle displacements and velocities

u = 4x1 vector of thruster blade pitch angles

Examination of B showed that the left-right symmetry that was expected (eg. the main port thruster causing the same forward

acceleration as the main starboard thruster) does not always occur. This problem was traced back to the asymmetric mass matrix, though it will be shown in the next section that some hydrodynamic terms involving velocity also contribute to this effect. The matrix was symmetrised by comparing each m_{ij} to m_{ji} and setting them both equal to the one with the smallest magnitude. Though there is no theoretical basis for this method, it is a starting point.

3.5 Hydrodynamic Modifications

Simulations 1 through 5 were run again with this new mass matrix. Results in many cases were much improved. The forward speed simulation this time resulted in a stable solution. The maximum forward speed was 0.91 m/s, the maximum transient pitch rate was 25.1 deg/s and the maximum pitch angle was 37.5 degrees bow up. The vehicle very quickly settled to a steady-state, travelling along an upward pointing path with the bow 32.6 degrees up.

The vertical translation simulations were also improved. The vehicle was less unstable while moving vertically than with the original mass matrix. However, in both simulations 5a and 5b, the solution did eventually become unstable, with an ever increasing "hunting" motion of the ROV as it pitched back and forth in the X-Z plane. This hunting motion was more pronounced while moving downwards. The maximum heave velocity was 0.6 m/s down and 0.3 m/s up, both above the values observed in the free-running tests.

The symmetric mass matrix improved the pitch and roll angle simulations. In simulation 1 (initial roll angle, 24 degrees), the simulation was less unstable than when the original data was used. There was still divergent instability of pitch rate. Simulation 2 yielded second order type of behaviour for the pitch angle, but it was still slightly unstable instead of displaying the positively damped motion which was expected.

When the vectored thrusters were set to move the ROV laterally, again the simulation results were improved, but still not correct. Both

simulations 4a and 4b gave no reasonable value of maximum sway velocity, since the vehicle was able to roll completely over. Simulation 4a went unstable in pitch rate and vertical velocity at 6.2s. These simulations still did not yield the symmetric behaviour that would be expected and the maximum roll rate was much too high (over 225 deg/s).

It was concluded from this set of simulations that the symmetric mass matrix improves the behaviour, but that two problems still exist; unstable pitching motion and unstable roll motion. The unstable pitch mode was examined first. All the terms which contribute to the total hydrodynamic pitch moment were inspected to see whether they could lead to instability. A term with large magnitude was $M_{|w|q}$, which was also positive. Since, by definition, the absolute value of heave velocity is always positive, this term had the effect of a negative damper, taken by itself. The damping force arising from this term might possibly be cancelled out by the other fifteen pitch moment terms, so $M_{|w|q}$ was set equal to zero and the simulations were run again to see if this term was the cause of the instability.

The simulations in which there were pitch instabilities were much improved. Simulations 5a and 5b (pure heave motion) now had a hunting motion which decreased in magnitude on each cycle. The maximum heave velocities were 0.64 m/s down and 0.32 m/s up, still larger than experimentally observed values. The forward velocity test was nearly unchanged. The maximum forward speed was 0.91 m/s at steady-state pitch angle of 32.6 degrees bow up. The maximum pitch rate during the impulsive start was 24.3 deg/s.

The transient behaviour in the pitch and roll simulations was now stable. The pitch test yielded damped second order behaviour. The roll test was also stable, though there remained inconsistent behaviour of the vehicle yawing to starboard when released from both positive and negative roll angles, a result not expected with a left-right symmetric vessel. The hydrodynamic terms were examined for properties which would cause this inconsistent behaviour. It can be shown that for symmetric behaviour to occur, the symmetric forces, X, Z and M, must not contain terms which are multiples of an odd number of asymmetric

degrees of freedom. Similarly, the asymmetric forces, Y, L and N, must not have terms which are multiples of even numbers of asymmetric degrees of freedom. Using this criteria, the following hydrodynamic terms were set to zero:

X: X_r, X_{vrr}, X_{vpp}, X_{pq}, X_{qr}
Y: Y_{vp}
Z: Z_{ur}, Z_{vrr}, Z_{pq}
L: L_{vvw}, L_{vp}
M: M_{ur}, M_{vvr}, M_{vrr}, M_p, M_{qr}
N: N_{vp}

All the simulations were rerun and in the appropriate cases, perfectly symmetric behaviour occurred. The autonomous pitch and roll angle simulations were stable and simulations 1a and 1b were symmetric; the behaviour of the relevant degrees of freedom are illustrated in figures 3.2 (roll) and 3.3 (pitch). The maximum ahead speed was now 0.98 m/s, still less than the experimental result, 1.13 m/s. Simulation no. 3 also yielded a maximum pitch angle during an impulsive start of 32.5 degrees and a maximum pitch rate of 23.2 degrees/s, which compare with the observed values of 22 degrees and 18 degrees/s. These quantities are shown in figure 3.4. The heave velocity simulations gave the result of 0.33 m/s down and 0.17 m/s up (figures 3.5 a) and b), respectively), again with stable solutions. The vehicle trials indicated that these values were 0.33 m/s down and 0.02 m/s up.

The lateral velocity simulations did not show any improvement, except that they were now symmetric with each other.The vehicle still did complete barrel-rolls when the vectored thrusters were put in a push-pull configuration. All of the hydrodynamic roll moment terms were examined and none, on first inspection, were thought to lead to unstable behaviour, so attention was turned to the thruster equations. In these equations, the contribution of each thruster to resultant forces and moments is modified by an "installation coefficient", which supposedly models the effects of interaction between thrusters and interaction with the vehicle itself. There are four thrusters and six forces or moments, so there are twenty-four installation coefficients. Most of these are between the values of zero and one, reflecting the

fact that the thruster unit contributes less force when installed on the vehicle than when operating in open water. The exceptions to this were the ones associated with roll moment, which had the values of 2.55 for the main thrusters and 3.99 for the vectored thrusters. These values seemed very high, and they suggest either typographical errors or problems with the theoretical modelling of the system.

The lateral motion simulations were repeated with lower values of the roll installation coefficients (b_{4j}, j=1,4) until the maximum roll angle achieved during the simulation corresponded with that obtained during the free-running test. The ratio b_{43}/b_{41} was kept at 3.99/2.55. When b_{41} and b_{42} were set to 0.22 and b_{43} and b_{44} were set to 0.34, simulations 4a and 4b yielded a maximum roll angle of with magnitude 24.8 degrees. This value was very close to the experimental value of 24 degrees, and so it was concluded that these installation coefficients more correctly modelled the true behaviour. This conclusion was given further support when the maximum roll rate of 32.7 deg/s was compared to 34 deg/s obtained during the free-running tests. Furthermore, the maximum sway velocity achieved was 0.34 m/s, which agreed very closely with 0.33 m/s measured experimentally. Figure 3.6 depicts the behaviour of the sway velocity, roll angle and roll rate during the sway test.

With these changes to the mass matrix, hydrodynamic coefficients and thruster installation coefficients, the simulated vehicle has performance close to that observed during the vehicle trials. This model will be used throughout the rest of this work.

3.6 Vehicle Modifications and Their Effect on Performance

It was mentioned previously that many ROVs are of an open-frame construction. Besides being inexpensive and relatively strong, this structure has another advantage that is particularly appealing to operators. Different cameras, instruments and tools are easily attached or removed as the task requires; this feature is looked upon very favourably because it enables one vehicle to operate in a number of roles. One recent ROV, the OSEL/GEC 'Dragonfly', has been designed

as a modular structure so that entire work 'packs' may be changed very rapidly. While this is very convenient when expensive offshore operations are taking place, the change in vehicle configuration is yet another difficulty the designer of the ROV autopilot must overcome. A closed-loop system which performs well for the baseline vehicle will not be useful if the performance degrades excessively when a configuration change is made to the ROV. Therefore, it is essential to evaluate the 'robustness' of any controller i.e. the closed-loop sensitivity to changes in open-loop dynamics, if a design study is to be considered complete.

The present work will consider the addition of a 15kg object on the lower edge of the Seapup's bow, exactly on the y-centreline. This represents over 13 percent of the baseline vehicle's mass and so, should be a pessimistic estimate of an operator's modification. The size of the object is such that it may represent a television camera/ lighting set or a small manipulator arm.

A number of assumptions were made about this object in order to calculate the effects on the baseline vehicle parameters. It was considered to be spherical, with a specific gravity of 0.9. Hydrodynamic effects are limited to added mass only, with no attempt being made to estimate the drag. The values of added mass are calculated from inviscid flow theory for a sphere of known radius in a fluid of known density. This increases the value of the diagonal terms of the total mass matrix as well as $N_{\dot{p}}$ and $L_{\dot{r}}$ because $\bar{I}_{xz}$, the added mass counterpart of I_{xz}, becomes nonzero. The centre of gravity is moved forward 4.6 cm and down 1.4 cm while the centre of buoyancy moves 4.3 cm forward and 1.9 cm down. These shifts cause the vehicle to take a more bow-down position at rest; the pitch angle changes from 0.0 degrees to -6.3 degrees.

A selection of the verification tests listed in table 3.2 were run again to evaluate the changes in open-loop performance caused by the addition of the object. Figure 3.7 illustrates the typical changes that occur; here, the results of the surge velocity test are shown. The vehicle is slower to respond because of its increased inertia; 95 percent rise times have increased to 2.8 seconds from 2.2 seconds in

the surge test. The eigenvalue analysis, described in the next section, also shows this trend for slower dynamics. It is interesting to note that the maximum surge speed has actually increased to 1.13 m/s from 0.98 m/s for the baseline vehicle. This occurs because the object serves to force the bow of the vessel down to 20.8 degrees from 27.4 degrees; there is less net buoyancy opposing surge motion despite the buoyancy becoming more negative.

The heave tests showed the maximum heave velocity had changed to 0.35 m/s downwards from 0.33 m/s for the baseline vehicle and 0.14 m/s upwards as compared to 0.17 m/s. Both of these results were caused by the increased negative buoyancy. Minimal changes were noted during the sway test. The maximum sway speed became 0.35 m/s (baseline, 0.34 m/s), while the maximum roll angle and roll rate decreased to 22.6 degrees and 29.4 degrees/s (baseline: 24.8 degrees and 32.7 degrees/s).

3.7 Open-Loop Poles and Zeros

Though time-domain simulation is very useful for evaluating a system's behaviour and is one of the few methods available for analysing nonlinear processes exactly, frequency-domain results can be important when designing controllers or analysing the effects of applying a particular controller. The positions of the open-loop eigenvalues were also useful when determining the time step for the numerical integration scheme.

For a nonlinear system, eigenvalue decompositions can be done at all points in the state-space that the system can reach; numerical methods, described in section 3.2, are used to linearise the equations of motion about the state under investigation. For a ROV, there are eight degrees of freedom that could effect the poles and zeros (u, v, w, p, q, r, ϕ and θ; changes in global X, Y, Z and ψ will make no difference). A complete investigation should consider all points in the 8-dimensional space. However, this scheme is unmanageable and so only changes in surge speed will be considered. This is justified on the grounds that the vehicle will have a greater variation in this degree of freedom than any other.

The first step in this study was to determine the linearisation points. At each forward speed, the pitch angle and the commands to all four thrusters are required. All other states were known to be zero, for the vehicle is moving in purely longitudinal motion. At zero surge speed, it was possible to calculate the thruster levels by analytical methods, since only thruster forces and buoyancy have to be balanced. However, hydrodynamic and kinematic forces affect the other equilibria; these were determined once the velocity controller, described in chapter 4, was implemented. Consider for example a surge speed of 0.7 m/s; the vehicle takes up a pitch angle of 10.0 degrees with main thrusters set to 14.6 degrees and vectored thrusters at -5.9 degrees. The equations of motion are then expressed in the standard state-space form:

$$\dot{q} = A\,q + B\,u \qquad \ldots.(3.2)$$

$$y = C\,q + D\,u \qquad \ldots.(3.6)$$

Here, A and B are determined from the Taylor Series approximation described in section 3.2. The matrix D is null and C, of dimension 4x12, selects u, v, w and r as outputs from the twelve states.

The open-loop poles satisfy the system's characteristic polynomial:

$$| sI - A | = 0 \qquad \ldots.(3.7)$$

The six modes of the baseline and modified vehicles are shown in figures 3.8 and 3.9, respectively. The surge and sway modes have real stable poles which become greater in the negative sense with increasing surge speed. The roll and pitch modes are, of course, oscillatory and also become more damped as speed increases. There are two combined sway-yaw modes which, at low speeds, are real, then become oscillatory and finally, real once again. The modified vehicle poles are all slightly slower than their baseline counterparts. This is caused by the increased inertia of the vehicle; the time domain simulations of section 3.6 also indicated this change in dynamics. Both vehicles, after the model verification described earlier, are now stable at all surge speeds. The migration of the poles is quite dramatic, indicating

that the system nonlinearities are very important, a factor which will affect the control system design.

There are many definitions of the zeros of a system. This study is interested in the transmission zeros, a subset of the system zeros as defined in [32]. The system zeros are the solutions of:

$$\begin{vmatrix} sI-A & B \\ C & D \end{vmatrix} = 0 \qquad \ldots.(3.8)$$

The NAG (Numerical Algorithms Group) routine F02BJF, an implementation of the QZ algorithm, was used to solve this generalised eigenvalue problem, which is of the form:

$$[M]\ w = s\ [N]\ w \qquad \ldots.(3.9)$$

The system zeros are made up of the subsets of transmission, input-decoupling, output-decoupling and input/output-decoupling zeros [33]. The solution of (3.8) at each linearisation point yielded 16 zeros; 2 pairs of complex conjugates, 4 at zero and 8 at infinity. The test for an input-decoupling zero is:

$$v^*\ [\ sI-A,\ B\ ] = 0 \qquad \ldots.(3.10)$$

i.e. the left eigenvector associated with the zero lies in the null space of the 'input' matrix. Output-decoupling zeros have right eigenvectors which are in the null space of the 'output' matrix:

$$[\ sI-A,\ C\ ]\ w = 0 \qquad \ldots.(3.11)$$

A zero and associated pair of eigenvectors which simultaneously satisfy (3.10) and (3.11) is said to be an input/output decoupling zero. The set of system zeros is defined as:

$$\begin{aligned} \{\text{ system zeros }\} = {} & \{\text{ transmission zeros }\} \\ & - \{\text{ input decoupling zeros }\} \\ & - \{\text{ output decoupling zeros }\} \\ & + \{\text{ input/output decoupling zeros }\} \end{aligned} \qquad \ldots.(3.12)$$

By using these definitions, it was found the four solutions of value 0.0 were output-decoupling zeros, leaving the two pairs of complex conjugate solutions as transmission zeros. The output-decoupling zeros are related to the four displacements, X, Y, Z and Ψ, which do not couple with the dynamics. The migration of the transmission zeros with surge speed is shown in figure 3.10; the loci for the both baseline and modified vehicles are plotted. Notice that both systems become nonminimum phase at increasing velocity, the baseline vehicle at 0.7 m/s and the modified ROV at 0.5 m/s. This property can effect the choice of controller.

3.8 Umbilical Model Performance

The decision to use a static cable model, updating the configuration and drag at each time step, proved to be justified. The disadvantage of a fully dynamic cable model is that it consumes far too many computer resources. Even the static model slowed down the ROV simulation by approximately 30 percent and dynamic methods were reported to require many more computations than the static case [23].

Still, the chosen method provided a good approximation to the real cable disturbance loads, again according to [23]. The computer programme, written by the National Physical Laboratory, can be altered to give the position, attitude and internal forces at any intermediate point on the cable, though in the ROV simulation, only those values at the lower end were required. Figure 3.11 shows a typical configuration for the conditions noted on the diagram. Here, as in the simulation, the top end is assumed to be fixed to the support ship, the bottom is attached to the ROV and the flow across the cable is determined by the relative velocity between ROV and current.

Another illustration of the umbilical model's performance is a representative effect on the vehicle. To illustrate this, the vehicle is put through the surge velocity test at varying depths. The support ship is assumed to be directly above the ROV at the start of the simulation and the cable is always 40 percent longer than the straight line between ship and vehicle. The Seapup has a cable of diameter

2.5 cm and negligible weight in water. The normal drag coefficient, increased due to the strumming effects noted in section 2.3.4, was set to 2.5. The results at depths of 50m, 100m and 200m were as follows (recalling that the maximum speed of the vehicle without cable drag was 0.980 m/s)

Depth (m)	Maximum Speed (m/s)	F_x (N)	F_z (N)
50	0.474	-148.	-104.
100	0.354	-163.	-112.
200	0.259	-172.	-119.

These simulation results show the same trends as real ROV operations, where pilots have noted that cable drag radically affects the performance of their vehicles, limiting speeds and operational range.

3.9 Choice of Environmental Parameters

Representative values for the statistical parameters of a disturbing current were evaluated in a Department of Energy study into underwater vehicle performance [5]. At their test site in Loche Linnhe, a sea loche with tides, the current was measured between 0 and 1 knot at the surface and between 0 and 0.5 knots at the workframe with extreme cases of up to 1.0 knot. There was no indication in this reference of variance or frequency content.

For simulation purposes, it is assumed that the mean speed of the current is 0.5 knots or 0.26 m/s and that the 1.0 knot extreme which is reported is at the 3σ limits. This implies:

$$\sigma_c = (1.0 - 0.5)/3 = 0.167 \text{ kt}$$
$$= 0.086 \text{ m/s}$$

It is also assumed that the standard deviation of the direction of the current is given as in [28] as σ_α = 20 degrees. With $\bar{\alpha}$ of zero degrees, a break frequency of 0.0159 Hz or 0.1 rad/s and a sampling time of 0.2 s and using equations 2.27 through 2.33, the current model becomes:

$$c(k+1) = 0.0051483 + 0.9801987\, c(k) + 0.0198013\, w_c(k) \quad ....(3.13)$$

$$\alpha(k+1) = 0.9801987\,\alpha(k) + 0.0198013\, w_\alpha(k) \quad ....(3.14)$$

$$\text{and} \quad E\{ w_c(k)\, w_c(k) \} = 0.739269$$

$$w_\alpha(k) = 232.546\, w_c(k)$$

A realisation of this process is shown in figure 3.12a. Only the speed history of the process for 40 seconds is depicted; of course, the direction history is merely a scaled version of the speed. For this test case of 201 samples:

$$\bar{c} = 0.2717 \text{ m/s}$$
$$\sigma_c = 0.0690 \text{ m/s}$$
$$\bar{\alpha} = 2.491 \text{ degrees}$$
$$\sigma_\alpha = 15.91 \text{ degrees}$$

Thirty realisations of 256 samples were processed by a discrete FFT algorithm and the average level at each frequency calculated. The results are shown as a linear-log plot in figure 3.12b. On this graph, the square root of the zero frequency component (here, 0.277 m/s) should be equal to the mean value of the process (0.260 m/s) and the frequency content should only be significant between 0 and 0.1 rad/s. Despite the use of only a first order model, the results are reasonably close to the desired frequency content.

3.10 Summary

A physically plausible model of Seapup has been obtained after changes in the mass matrix, the removal of a number of hydrodynamic terms and the reduction in the roll moment thruster installation coefficients. The mass matrix has, however, been arbitrarily symmetrised. BMT should perhaps reanalyse their data for a model which assumes a left-right symmetric vehicle. It is interesting to note that all parties in the DoEn ROV initiative have taken the present study into account and modified their model along similar lines [34].

There still remain some inconsistencies, such as maximum speeds in the X, Y and Z directions which do not correspond with the free-running test data. This is not surprising since the hydrodynamic terms might

not have been calculated at top speeds. To further improve the model, the 'drag' terms in the X, Y and Z force equations could be modified to match simulation maximum velocities with experimental results.

Approximations were made to derive linear models of the ROV at different operating points; these were used to calculate the system's poles and zeros. Examination of these indicated that the vehicle is open-loop stable at all surge speeds, becomes nonminimum phase at high speeds and has widely varying dynamics over its operation range.

The models of the umbilical cable and the stochastic current were shown to approximate the behaviour of their real counterparts sufficiently well to justify their inclusion in the ROV simulation.

Table 3.1

a) Eigenvalues at the Quiescent State		b) Eigenvalues at an Unstable Operating Point : u = 0.70 m/s, w = 0.3 m/s	
Real	Imaginary	Real	Imaginary
0.0	0.0	0.0	0.0
0.0	0.0	0.0	0.0
0.0	0.0	0.0	0.0
0.0	0.0	0.0	0.0
-0.08541	0.0	-0.58612	0.0
-0.38472	0.0	-0.98149	0.0
-0.60135	0.0	-1.9557	0.0
-2.0098	0.0	-6.2043	0.0
-0.20376	±1.3586	0.18544	±1.2568
-0.21943	±2.5202	0.56402	±2.9652

Note: All values in (radians/s).

Table 3.2

Open-Loop Simulations for Model Verification

Simulation No.	Inputs	Outputs
1	Thrusters Disabled Roll Angle(t=0) = 24 deg	-Transient behaviour
2	Thrusters Disabled Pitch Angle(t=0) = 22 deg	-Transient behaviour
3	Angle(1)=Angle(2)= 35 deg Angle(3)=Angle(4)= 0 deg	-Top forward speed -Maximum transient pitch angle in an impulsive start
4a	Angle(3)= 35 deg Angle(4)= -35 deg Angle(1)=Angle(2) = 0 deg	-Maximum roll angle in forced roll,zero forward speed -Maximum velocity in pure lateral translation
4b	As 4a except Angle(3)= -35 deg Angle(4)= 35 deg	-As 4a
5a	Angle(3)=Angle(4)= 35 deg Angle(1)=Angle(2)= 0 deg	-Maximum velocity in pure vertical translation (down)
5b	Angle(3)=Angle(4)=-35 deg Angle(1)=Angle(2)= 0 deg	-Maximum velocity in pure vertical translation (up)

Notes: Thruster No.1: Main Port
Thruster No.2: Main Starboard
Thruster No.3: Vectored Starboard
Thruster no.4: Vectored Port

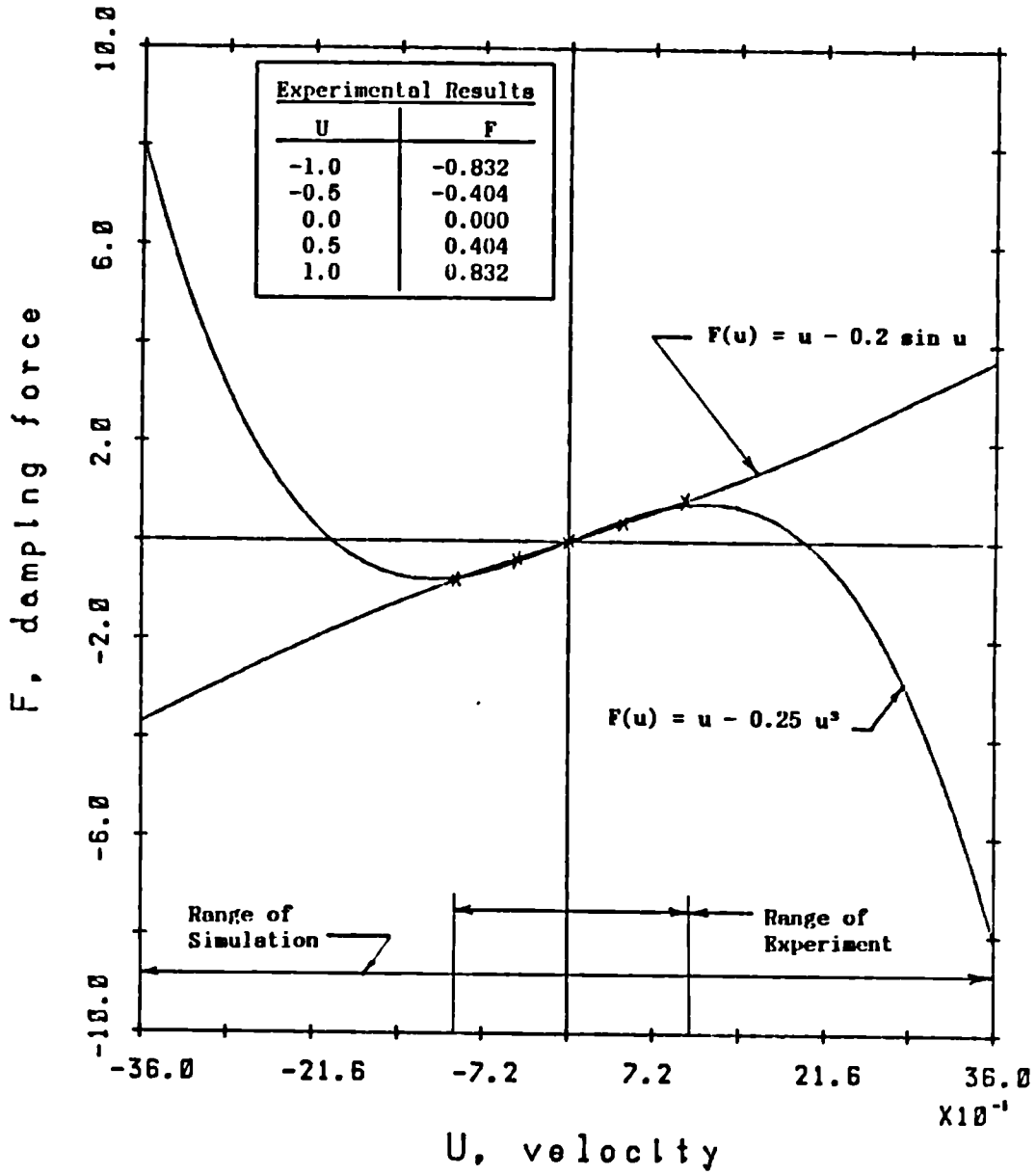

Figure 3.1 : Analysis of Experimentally Derived Damping Characteristics

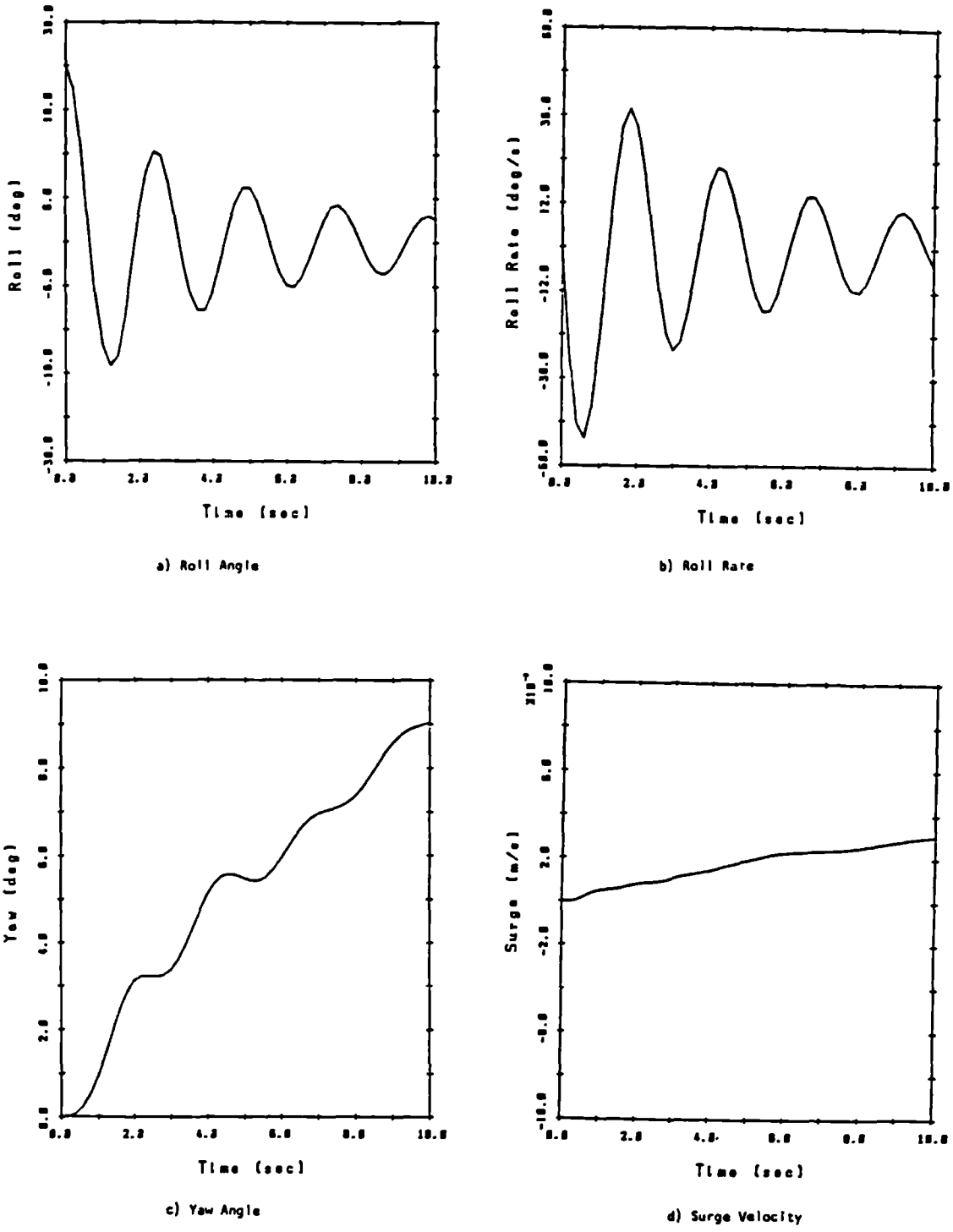

Figure 3.2 : Seapup Response; Autonomous Roll Test

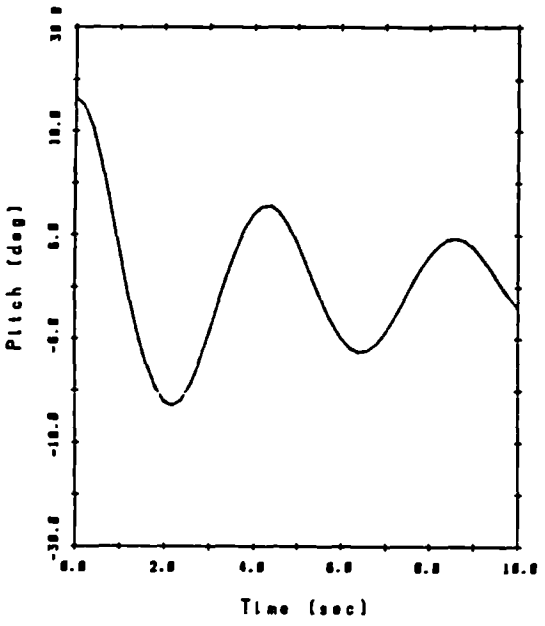

a) Pitch Angle

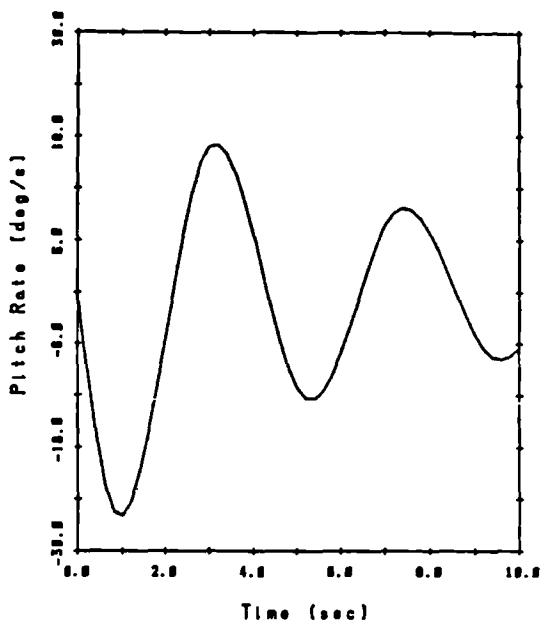

b) Pitch Rate

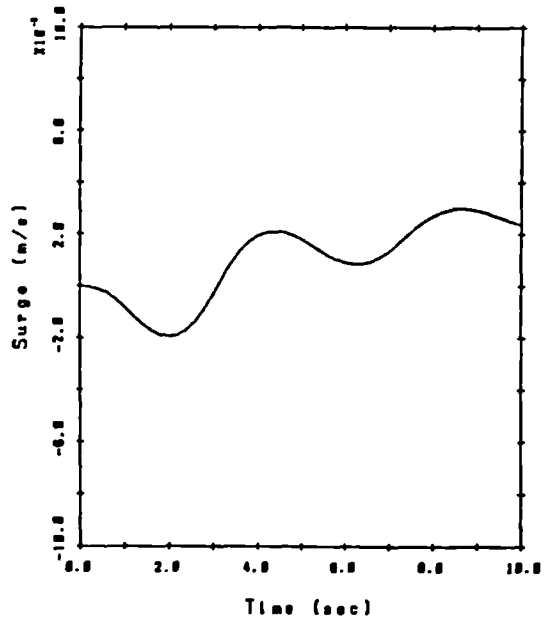

c) Surge Velocity

Figure 3.3 : Seapup Response; Autonomous Pitch Test

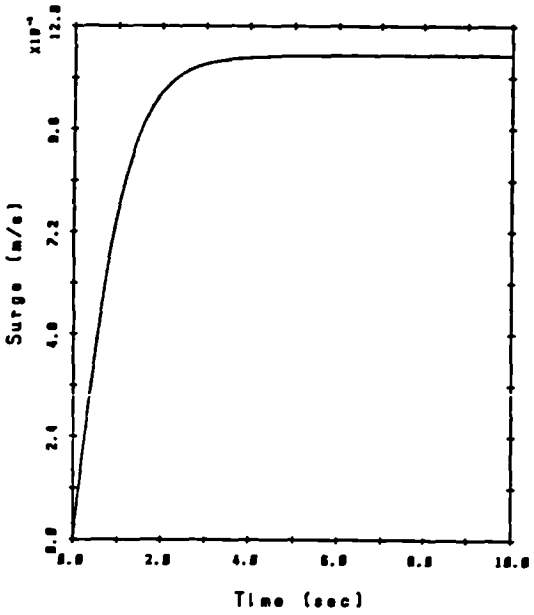

a) Surge Velocity

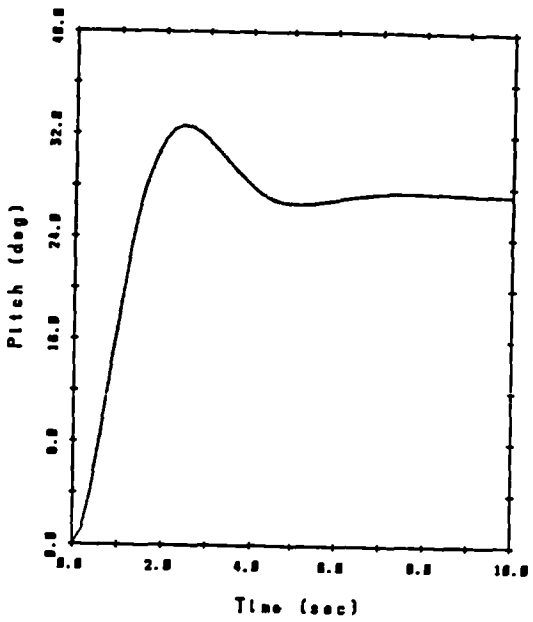

b) Pitch Angle

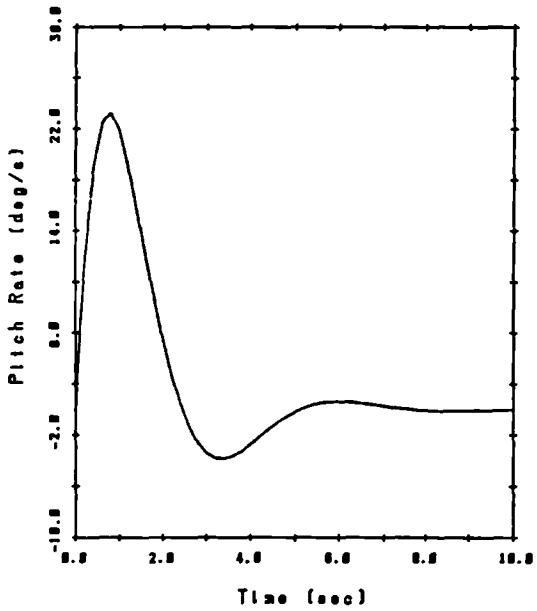

c) Pitch Rate

Figure 3.4 : Seapup Response; Surge Test

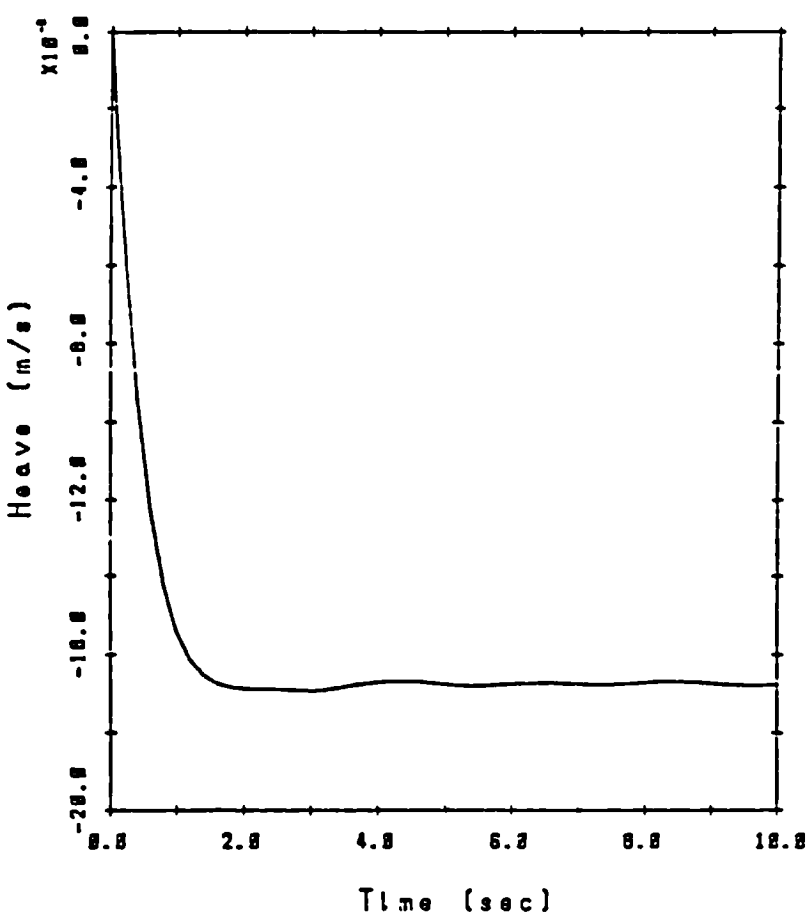

a) Heave Velocity (Up)

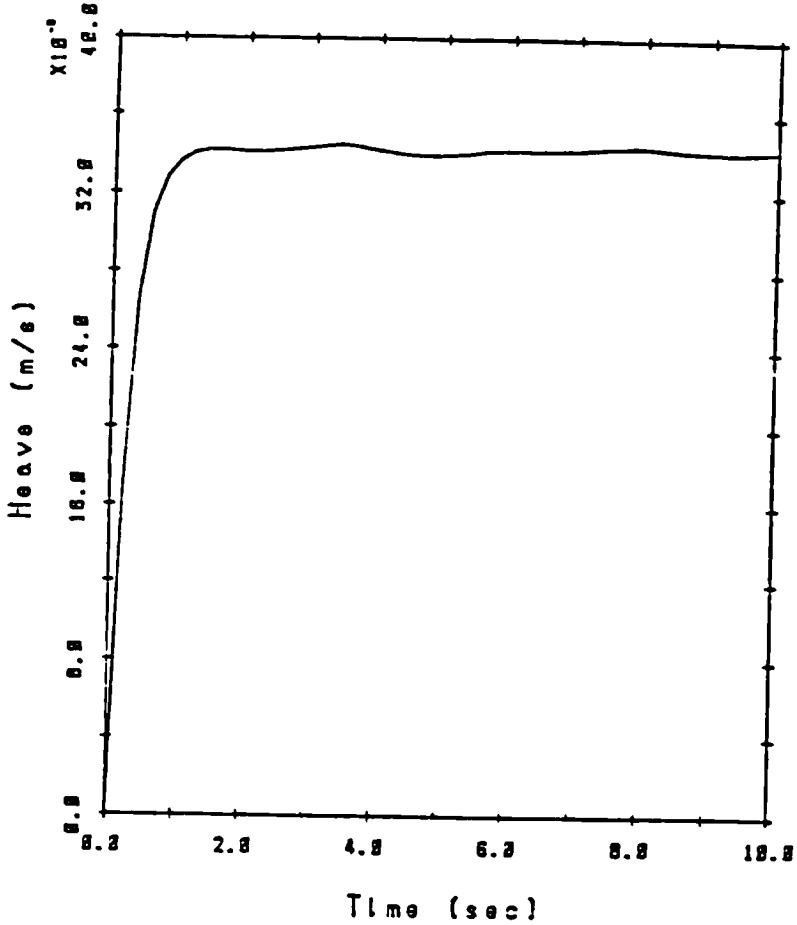

b) Heave Velocity (Down)

Figure 3.5 : Seapup Response; Heave Test

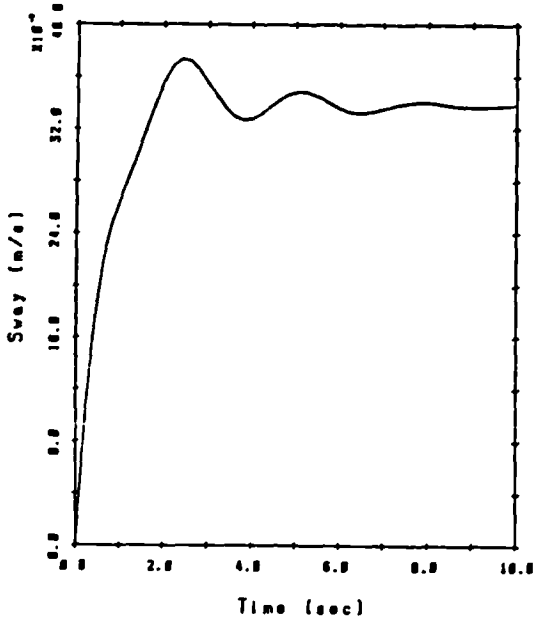

a) Sway Velocity

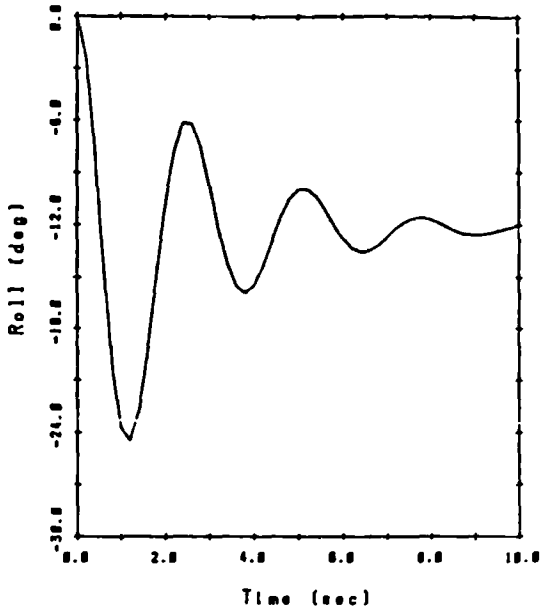

b) Roll Angle

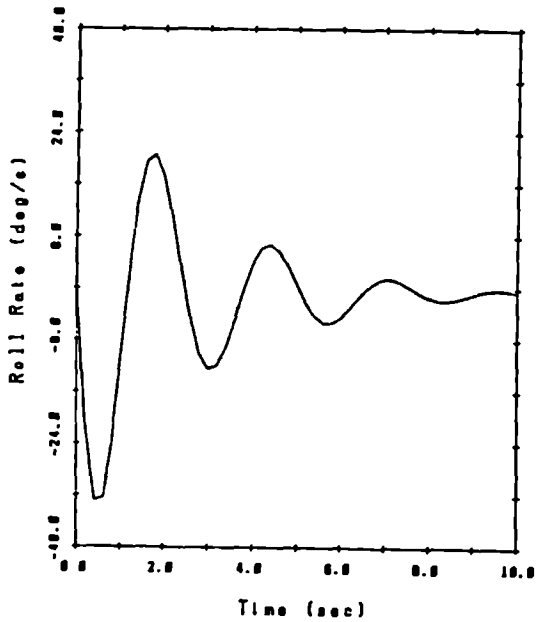

c) Roll Rate

Figure 3.6 : Seapup Response; Sway Test

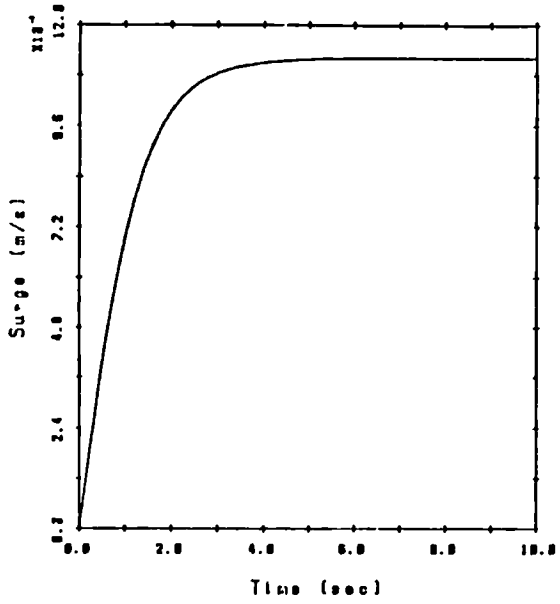

a) Surge Velocity

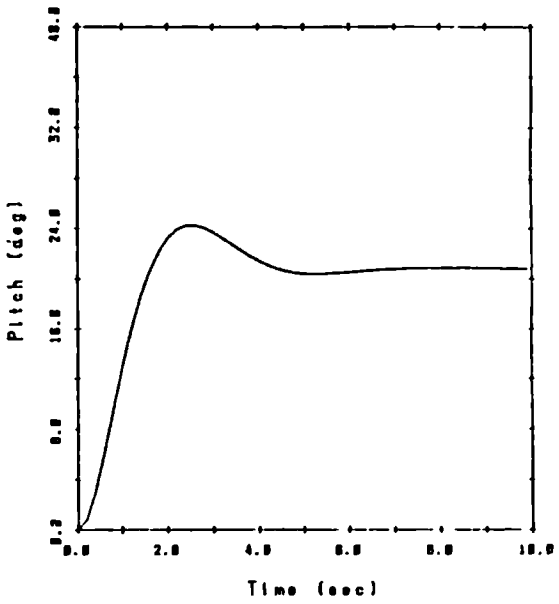

b) Pitch Angle

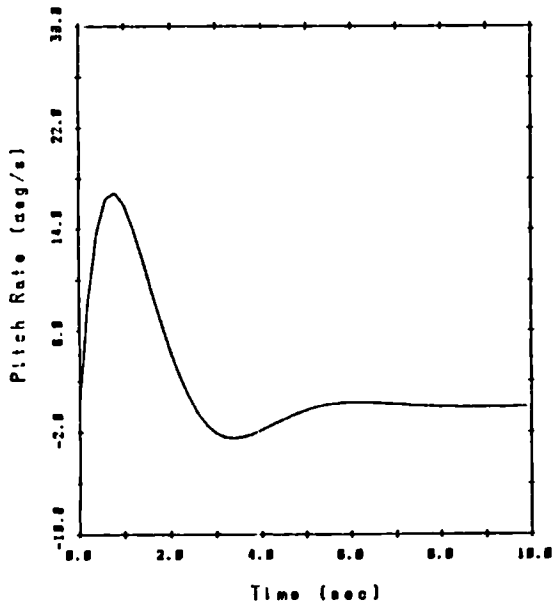

c) Pitch Rate

Figure 3.7 : Modified Seapup Response; Surge Test

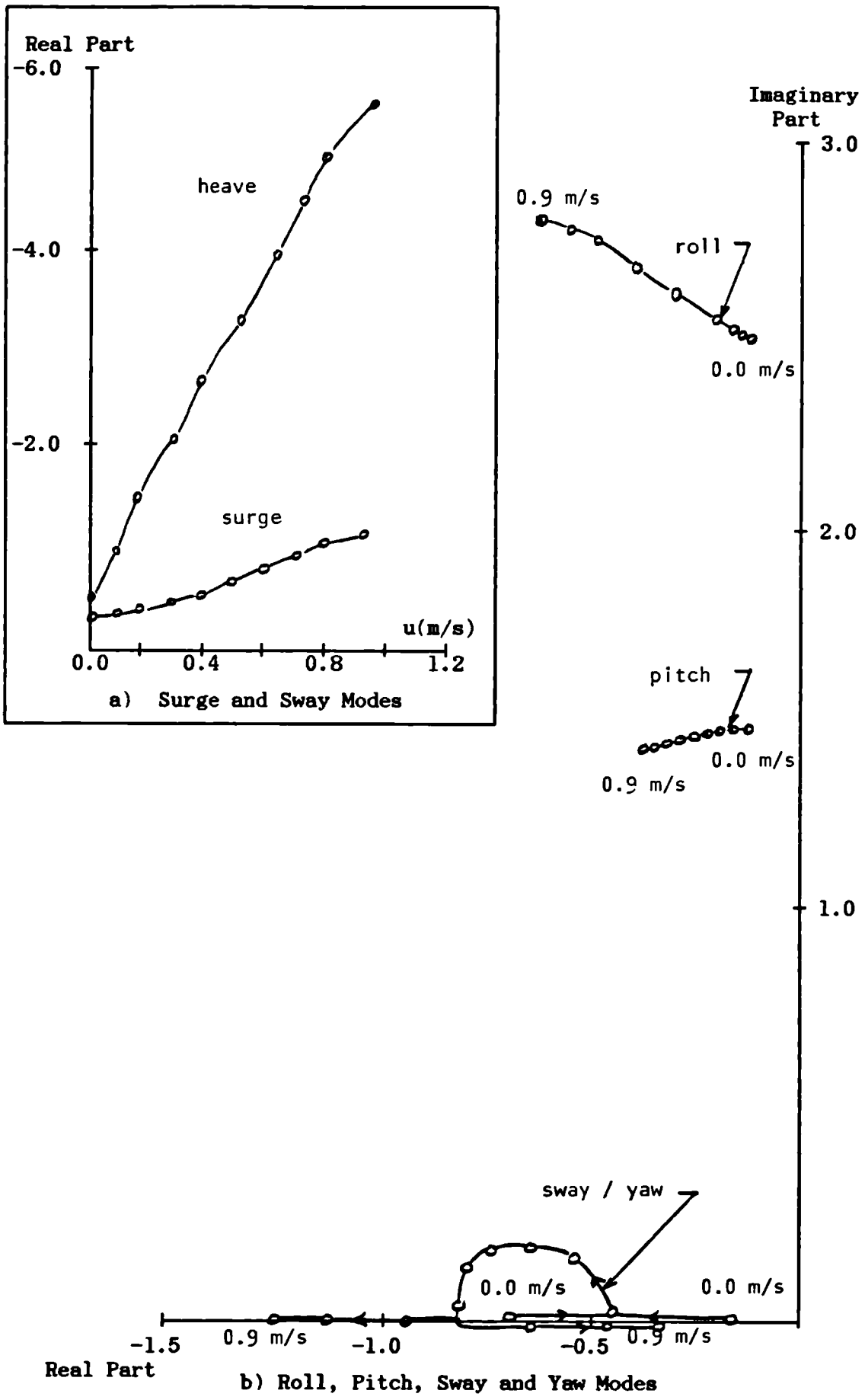

Figure 3.8 : Seapup Open-Loop Eigenvalues

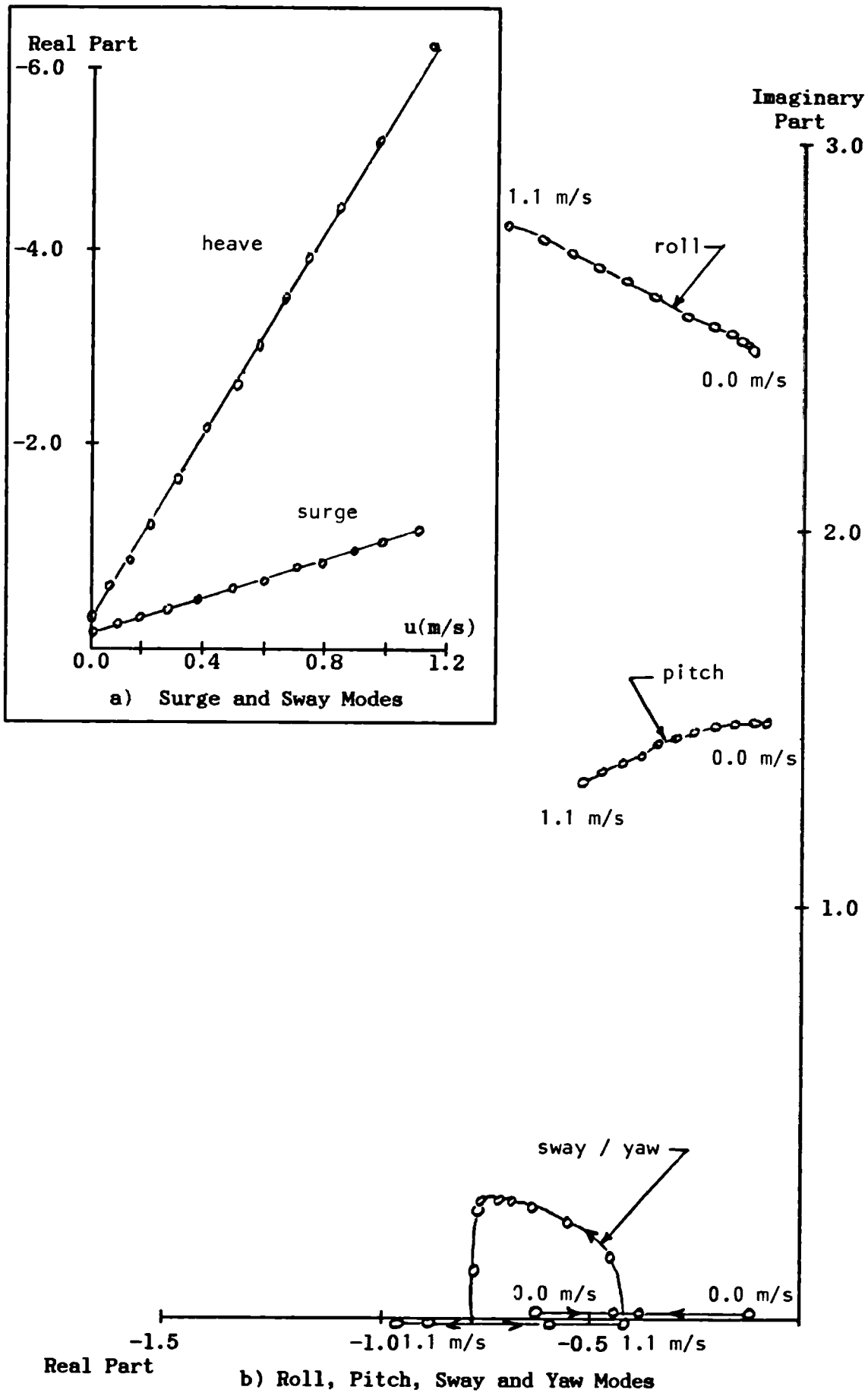

Figure 3.9 : Modified Seapup Open-Loop Eigenvalues

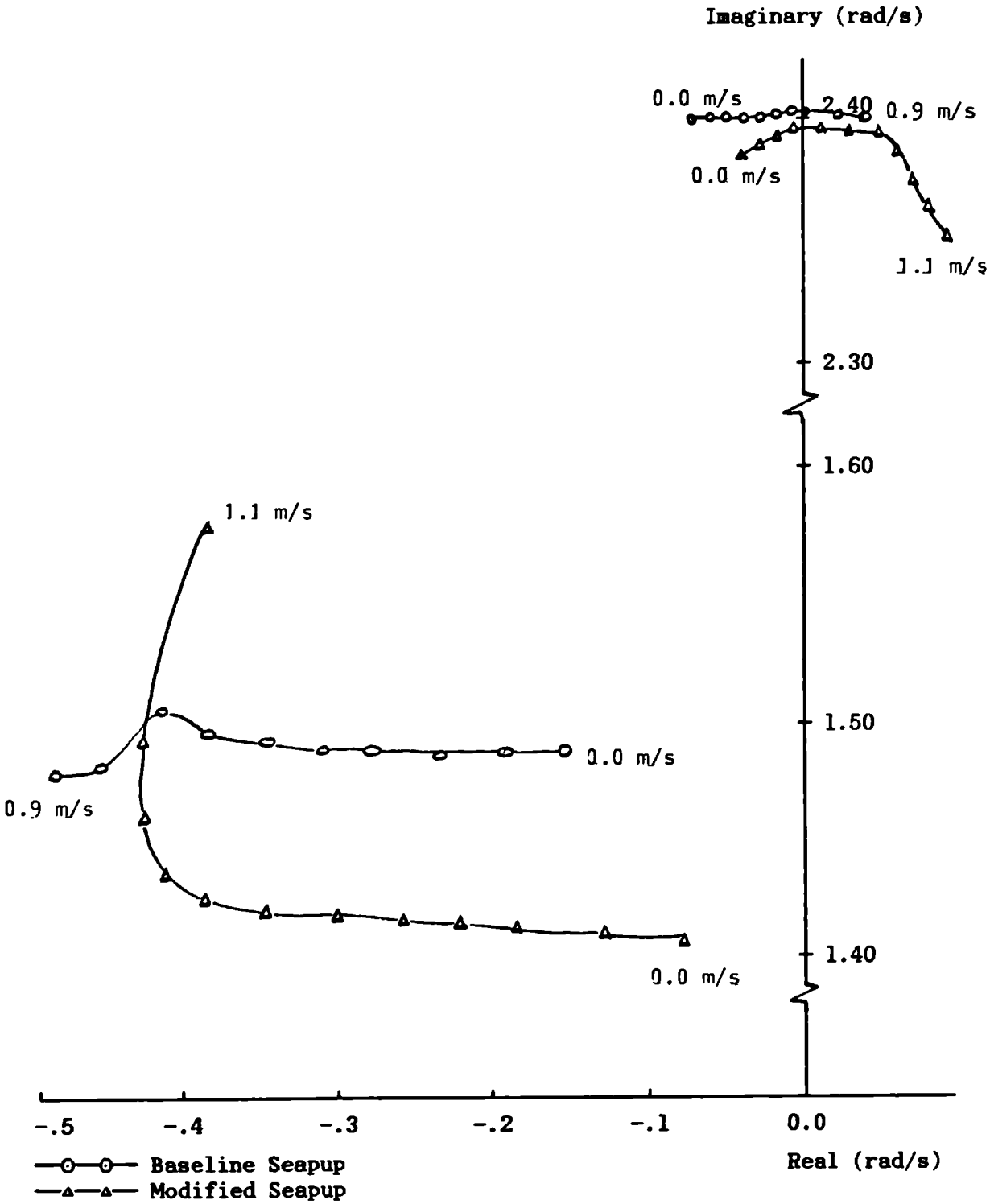

Figure 3.10 : Baseline and Modified Seapup Open-Loop Systems Zeros

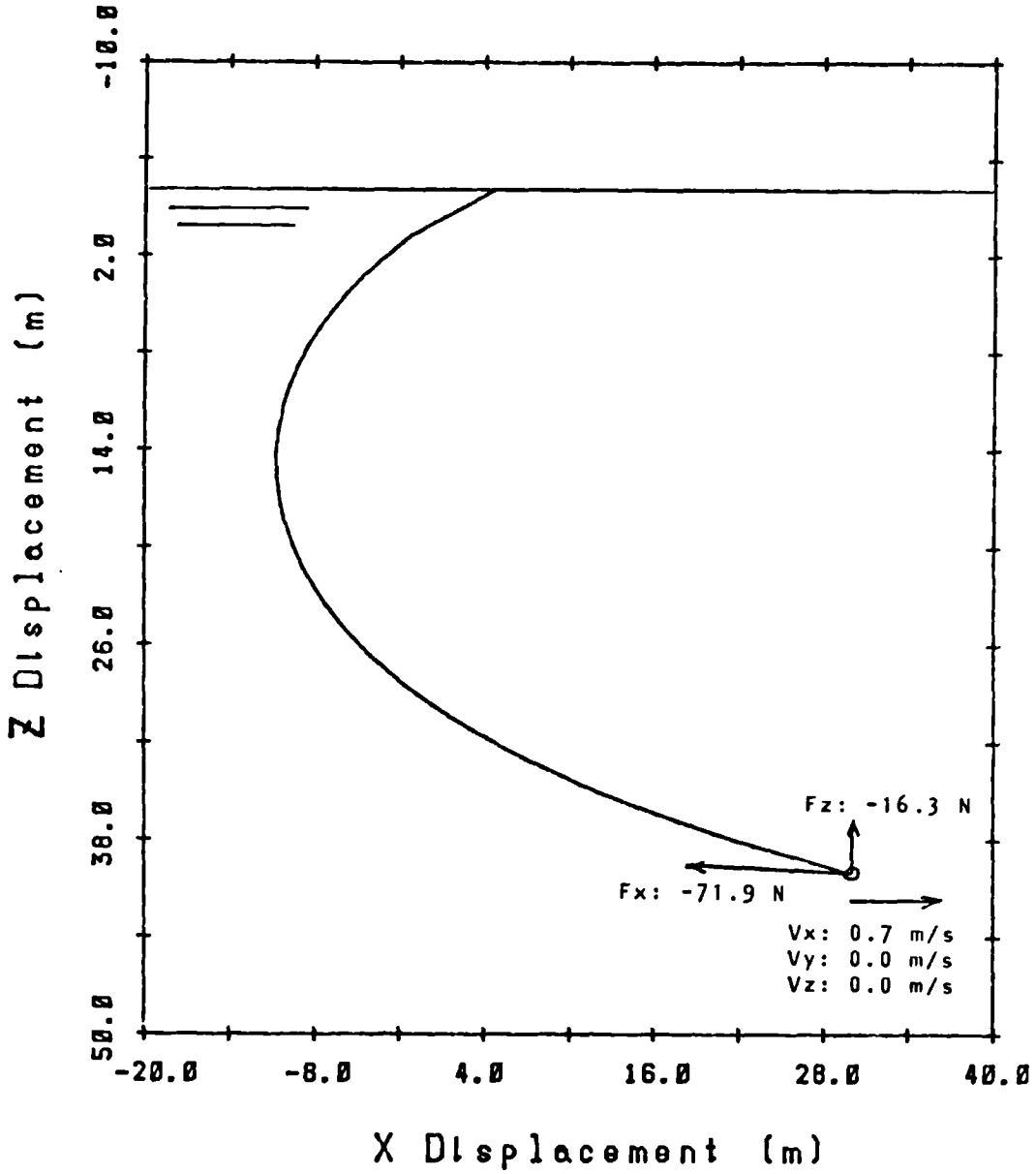

Figure 3.11 : Performance of Umbilical Cable Model

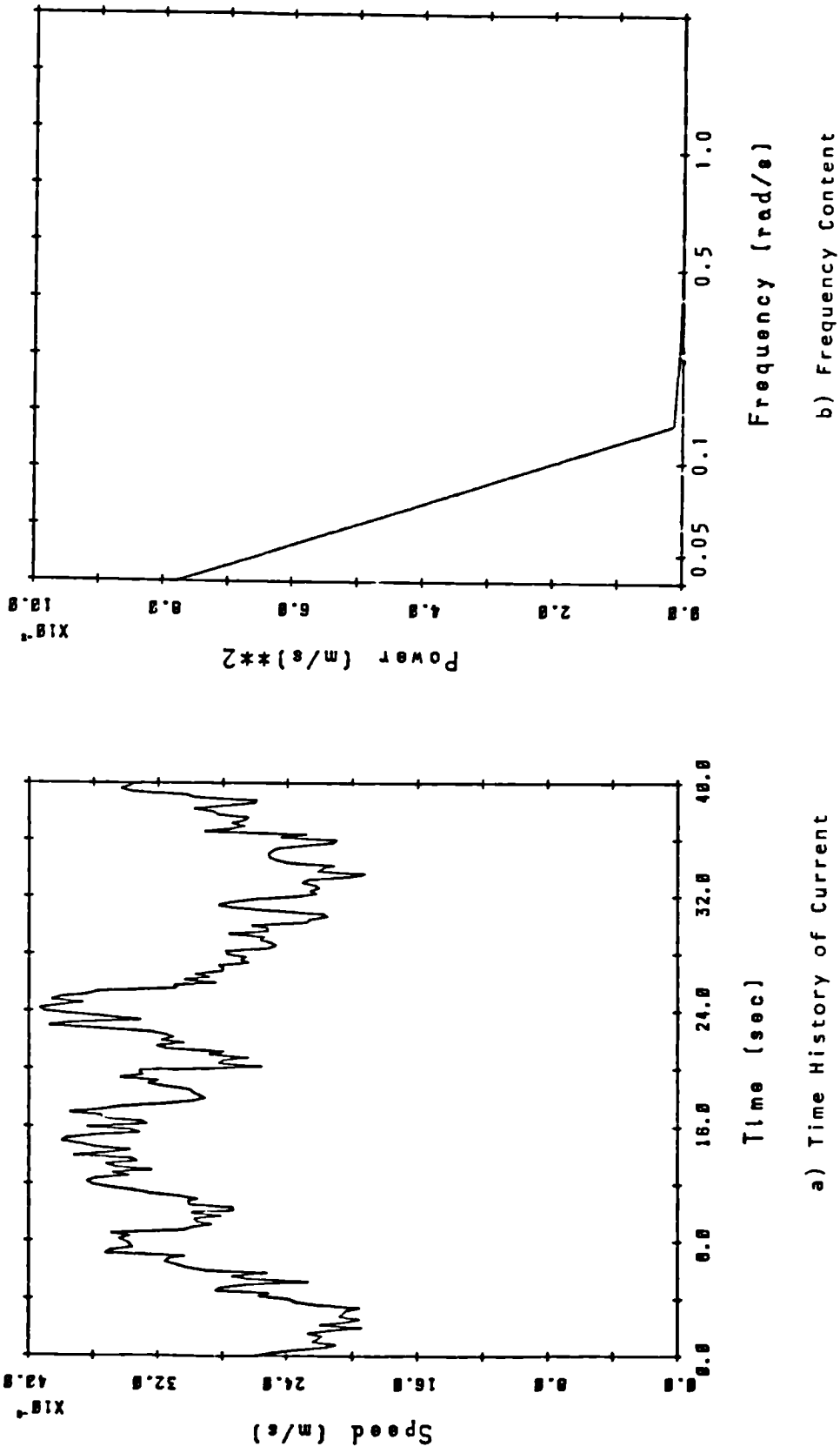

Figure 3.12 : Performance of Stochastic Current Model

Chapter 4

Control System Design

4.1 Introduction

The previous two chapters contained descriptions of the components which make up a ROV simulation and a study which verified that the simulation performs adequately; the design of the control system may now be addressed. The aims of this exercise are:

a) to develop a structural philosophy and define in general the functional blocks in the structure,

b) to examine the ROV system and determine the factors which have made autopilot design prohibitively difficult in the past, and

c) to develop the velocity controller functional block with a system which would overcome the problems of (b).

4.2 Structural Philosophy; Hierarchical and Supervisory Control

The control of an ROV is best implemented as a type of hierarchical scheme known as supervisory control. There will be a number of levels, each varying in function and complexity. Singh [35] defines four characteristics of a hierarchy:

a) There are a number of decision making units arranged in a pyramid.

b) The entire system has an overall goal and the goals of the individual decision makers are in harmony.

c) There is an iterative information exchange between levels with commands going down and information being passed up.

d) The time horizon increases the higher one goes in the pyramid i.e. the decisions at a higher level are based on farther reaching considerations.

Hierarchies in dynamic systems either naturally occur or can be formed by the control system designer. The advantages of hierarchical control can be numerous. It is useful to implement such a system when the job of controlling the entire system to reach its goal becomes too complex for one decision maker. Many jobs can be run in parallel leading to more useful work being accomplished. Lastly, a system which has only a few centralised task coordinators minimises the number of communications links between decision makers. A three level hierarchy is depicted in figure 4.1.

A variation of hierarchical control known as supervisory control has been proposed by Ferrel and Sheridan for the control of deep space probes in order to deal with the problem of time delays [36]. Supervisory systems have only one 'leg' of the hierarchical pyramid (see figure 4.2). Under supervisory control, higher levels direct the action of subordinates by planning the actions they should take, monitoring the performance and trusting them to accomplish the task without continuous assistance. This approach to control system design was again chosen by Sheridan and Verplank in their recent work on undersea teleoperators, their term for an ROV equipped with manipulator arms [8]. Though they were more concerned with control of the manipulator arms, the points they raise are equally valid for the ROV control problem. They present a number of arguments which favour a multilevel control system. Communications rates are limited for a truly autonomous unmanned submarine by the sonic link with the operator. In order to carry out tasks, it is necessary that a certain amount of "intelligence" be onboard the ROV and that control from the surface consist of commands such as "follow the pipeline at a set height above it" rather than "now set the aft starboard thruster to half speed ahead". Even when the communication bandwidth is not limited, as is the case here where it is assumed there is a umbilical cable linking the surface and the ROV, supervisory control may be applied advantageously to achieve faster or better control, to control

more degrees of freedom simultaneously than the operator could manage directly and to relieve the operator of tedium. The hierarchical scheme is also attractive because it separates the control problem into a number of levels, each much easier to design and analyse on an individual basis.

The control system for the ROV autopilot will have three levels. A series of task controllers will be next to the operator. He will be able to choose to execute such functions as hovering, following the seabed at a set height and heading or moving to a point. The task controller will generate a series of reference signals for a global position controller which will ask the body-coordinate velocity controller to calculate the thruster levels.

The advantages of the hierarchical scheme are easily illustrated using this example of a three-level controller, illustrated in figure 4.3 . The design of the high-level task controllers becomes manageable if it can be assumed that the vehicle it sees has decoupled, well-behaved dynamics and that body-global coordinate transformations can be ignored. Ideally, the task controller will want to issue commands such as "move 2 metres north-west" and to run in an open-loop mode with, at the most, minimal feedback. Given the nature of ROV motion, this goal is unattainable unless some form of compensation, most likely involving feedback, is placed between the vehicle and the task controller. The global position controller, using the ROV's Euler angles as a feedback signal, will convert a global position error into a body coordinate position error and demand local velocities to reduce this error. Again, the design and structure of this controller is made much simpler if the vehicle it controls has "nice" dynamics. At the lowest level, this quality can be achieved reasonably simply by a multivariable decoupling controller which either wholly or partially compensates for the nonlinearities of the vehicle. The rest of this chapter and the next will be concerned with the design of the velocity controller and the resulting performance of the closed-loop system.

4.3 Velocity Controller Design

The design of a multivariable controller to achieve the decoupled, well-behaved dynamics governing local velocities is a relatively straightforward procedure if a reliable model of the open-loop system is available and if the open-loop process has reasonably constant dynamics over its range, i.e. it is approximately linear. With the advent of computers, many design packages have become available which greatly simplify this procedure [37]. Output or state feedback compensators can be designed and analysed using various methods. Pole-assignment moves the open-loop eigenvalues so that an unstable system is stabilised or a sluggish plant is made to respond more quickly. The original work on the pole-assignment problem was done by Wonham [38] and there are connections between this and the multivariable generalisation of the root locus method described by Postlethwaite and MacFarlane [39]. Multivariable frequency response techniques include generalisations of Nyquist stability results (MacFarlane [40]) and the Inverse Nyquist Array method, developed by Rosenbrock [41], a graphical method of calculating forward loop controllers to achieve simultaneously stability and output decoupling. Optimal control techniques formulate the control problem in terms of a performance index which is minimised by the choice of controller. When the performance index is a weighted sum of the squares of the output errors and inputs and when stochastic disturbances act on the system, the problem is said to be Linear-Quadratic-Gaussian (LQG). Deterministic optimal feedback control was originally described by Kalman [42], based on Pontryagin's maximum principle [43] and the dynamic programming method of Bellman [44]; the extension of the method to handle stochastic disturbances was introduced by Astrom [45].

If the nonlinearities have been correctly identified, linear design techniques can be used at a variety of operating points and the gains in the various compensators scheduled to change with components of the system state, such as forward speed or position of the manipulator arm. However, whether the system is linear or nonlinear, the property that all these techniques have in common is that they require a fairly accurate plant model in order to proceed with design,

yet as shown in chapter 3, this is precisely what is not available in this application. An accurate model of the ROV and its thrusters requires expensive, specialised laboratory facilities. The model derived is likely to be affected by experimental errors, so before design of a conventional decoupling controller can begin, the engineer must verify that the model is sufficiently accurate for design purposes, a time consuming and expensive process.

However, not all of the nonlinearities affecting the system can be identified prior to the controller design. Operators of ROVs tend to add and remove different pieces of equipment such as arms and television cameras as the individual job requires. These changes can radically alter the kinematic and hydrodynamic properties of the vehicle and perhaps make the conventional controller worthless. These unpredictable changes must be dealt with by other techniques. One such method is adaptive control. An adaptive control system perform two functions; while controlling the process, it learns about it and optimises its own performance. Initially, this approach to the velocity control system appeared ideal; it would be unaffected by inaccuracies in any model since it would identify plant parameters on-line. Adaptive control can work for some nonlinear plants since they are represented by the "best" instantaneous linear model, but the dynamics of the plant must not change too quickly if the controller is to adapt as fast as the plant is evolving. However, as shown in section 3.7, the open-loop poles and zeros of a ROV are strong functions of its operating point and it was feared that an attempt to implement an adaptive control system would fail. In addition, the computational burden, and hence, cost, of a fully adaptive control scheme could make it impractical for offshore operators. The mathematical complexity was also seen to be a drawback; operators would prefer a simple fixed-gain controller which would be less expensive and easier to understand. However, the advantages of fully adaptive control could outweigh these drawbacks in many applications and chapter 7 considers two such systems.

The second class of control system design methods that can be used when a reliable plant model is not available are the robust techniques. A robust control system is one which has fixed gains and

maintains acceptable performance when the parameters characterising the plant change within certain bounds. Postlethwaite, et al. have generalised the concept of stability margins so that from a Bode-type plot, multivariable gain and phase margins may be determined [46]. Another approach to multivariable gain and phase margins and bandwidth for combined control and estimator designs has been developed by Safanov as a result of his general stability theorem [47]. The disadvantage with these methods is that specialised software is required to carry out the complicated calculations involved during design and these calculations must be repeated for each new vehicle, adding a large amount to the development cost of a new ROV. Though a totally accurate model is not required if a robust controller is to be implemented, a nominal model and its range of variation is, which will add complications and cost to the design. Of course, this is equally true for conventional linear design techniques; they, too, must be repeated for each new vehicle.

Ideally, what is required is a control method which could be developed once and then applied with minimal modifications (and expense) to any ROV. Such a method needs to combine the ideas of adaptive and robust control in that it would automatically adapt a fixed gain controller to any ROV and the design of this controller would be such that it would be immune to changes in the dynamics of that particular vehicle.

4.4 Robust Controllers for Unknown Multivariable Systems

Owens and Chotai have developed a proportional plus integral controller based on a low order representation of the process which is to be controlled [48]. This scheme has numerous advantages. Firstly, it is a design method for plants so complicated that the only tool available is time domain simulation and for plants that have much uncertainty in their modelling. Additionally, the calculations involved require only "back of the envelope" computing facilities. The closed-loop system produces decoupling with the required second order behaviour in each loop. There are restrictions on the type of plant for which closed-loop stability is guaranteed however; these will be

noted later.

This section summarises reference [48] which should be consulted for the full presentation but the essential parts of the development of this controller are included here.

The design technique is based upon the idea of modelling all of the unknown or complicated dynamics of the open-loop plant by the multivariable equivalent of the first order lag. It is useful in circumstances where quantitative information is not available, but some structural information is, say, from the underlying physical laws. This is the case with the ROV, where it is known that the velocity degrees of freedom u, v, w and r will behave approximately like first order systems unlike pitch and roll which are second order. Since there is no position restoring force in these degrees of freedom, given a step input the velocity in these degrees of freedom will approximately approach a steady-state value in a monotonic fashion.

The intuitive ideas of this control method are best illustrated using the single input - single output (SISO) example. The problem is illustrated in figure 4.4. A PI controller, K(s), is to be designed for the real plant G(s) with unity negative feedback and for reasons cited previously, G(s) is not known. G(s) can be described by the linear time invariant state-space form:

$$\begin{aligned} \dot{x}(t) &= A\,x(t) + B\,u(t) \\ y(t) &= C\,x(t) \end{aligned} \qquad \ldots.(4.1)$$

Clearly, the transfer function is:

$$G(s) = C\,(sI - A)^{-1}B \qquad \ldots.(4.2)$$

The only quantitative information available is the system response y(t) to a step input. The real plant's transfer function can be approximated roughly by a first order lag:

$$G_A(s) = a\,/(1 + sJ) \qquad \ldots.(4.3)$$

where a and J are constructed from the real response y(t) as shown in figure 4.5.

Alternatively, (4.3) becomes:

$$G_A^{-1}(s) = sA_0 + A_1,\ A_0 \neq 0 \qquad \ldots.(4.4)$$

$$\text{where} \quad A_0^{-1} = dy/dt\Big|_{t=0} = a/J = \lim_{s\to\infty} sG(s) = CB \qquad \ldots.(4.5)$$

$$\text{and} \quad A_1^{-1} = y_A(+\infty) = y(+\infty) = a = \lim_{s\to 0} G(s) \qquad \ldots.(4.6)$$

The relations (4.5) and (4.6) are a result of applying the initial and final value theorems, respectively. From (4.4) and (4.5), it is worth noting that $CB \neq 0$ and that the system transfer function must be of rank unity.

A PI controller:

$$K(s) = pJ/a\ (1 + 1/sT) \qquad \ldots.(4.7)$$

can be put in the forward path and p and T adjusted so that the desired characteristics of the approximate feedback system are obtained. In order to make a prediction about the behaviour of the real feedback system, it is necessary to assume that all the open-loop zeros of G(s) are in the open left-half plane or that G(s) is minimum phase. Since it has also been assumed that G(s) has rank unity, a root locus of the closed-loop system will have one first order asymptote at high gains while the other loci approach the open-loop zeros (figure 4.6). This would indicate that for the real feedback system it can be said that for high enough controller gains, the closed-loop system will be stable.

This result can be applied to the sampled data, discrete time case. For a zero-order hold applied to the inputs and referring again to figure 4.5, the first order model becomes:

$$G_A(z) = a\ /(1 + (z-1)(a/b)) \qquad ....(4.8)$$

where h is the sampling interval. The problem of designing a two term controller for a digital implementation can be intuitively compared to the continuous case by noting that fast samplings rates correspond to the use of high continuous gains [49]. Therefore, again intuitively, the discrete, closed-loop system will be stable if the sampling rate, h^{-1} , is reasonably high and the underlying continuous system is minimum phase with rank one transfer function.

This control method can be generalised to the multi-input / multi-output (MIMO) case by defining the discrete multivariable first order lag (MFOL):

$$G_A^{-1}(z) = (z-1)\ B_0 + B_1\ ,\ |B_0| \neq 0 \qquad ....(4.9)$$

In this system there are m inputs and outputs and so both B_0 and B_1 are mxm matrices.

The two term controller for this system is:

$$K(z) = B_0 \mathrm{diag}\{1 - k_j\ c_j + (1-k_j)(1-c_j)z/(z-1)\} - B_1 \qquad ....(4.10)$$

which is a discrete proportional plus integral form. This can be realised by the state space model:

$$\begin{aligned} q_{k+1} &= q_k + e_k \\ u_k &= B_0\{\mathrm{diag}(1-k_j)(1-c_j)\}\ q_k \\ &\quad + (B_0 \mathrm{diag}\{2-k_j-c_j\} - B_1)\ e_k \\ &\qquad\qquad 1 \leqslant j \leqslant m \end{aligned} \qquad ....(4.11)$$

The closed-loop transfer function is:

$$H_c(z) = (I + G(z)K(z))^{-1} G(z)K(z) \qquad ....(4.12)$$

which, after manipulation, becomes:

$$H_c(z) = \text{diag}\{1/((1-k_j)(1-c_j))\}(z(\text{diag}\{2-k_j-c_j\} - B_0^{-1}B_1) + (B_0^{-1}B_1 - \text{diag}\{1 - k_jc_j\})) \quad 1 \leqslant j \leqslant m \quad \ldots.(4.13)$$

Owens and Chotai show that the condition $B_0^{-1}B_1 \simeq 0$ can always be achieved for fast sampling rates [50]. For this condition, the closed-loop transfer function is:

$$H_c(z) = \text{diag}\{(z(2-k_j-c_j) - (1-k_jc_j)) / ((z-k_j)(z-c_j))\} \quad 1 \leqslant j \leqslant m \quad \ldots.(4.14)$$

and $$H_c(1) = I_m \quad \ldots.(4.15)$$

Equation (4.13) indicates that when $B_0^{-1}B_1 \simeq 0$, the resultant closed-loop system will be stable for:

$$|k_j| < 1, \ |c_j| < 1, \quad 1 \leqslant j \leqslant m \quad \ldots.(4.16)$$

The values of k_j and c_j will define the closed-loop poles for the jth loop. In addition, the system will have low levels of interaction and (4.15) shows that reference signals will be tracked with zero steady-state error.

The problem remains of estimating B_0^{-1} and B_1^{-1}. If the state space discrete model of the real system is:

$$x_{k+1} = \phi\, x_k + \Delta\, u_k \quad \ldots.(4.17)$$
$$y_k = C\, x_k$$

then (4.5) and (4.6) can be generalised to the multivariable case:

$$B_0^{-1} = \lim_{|z| \to \infty} z\, G(z) = C\Delta \quad \ldots.(4.18)$$

$$B_1^{-1} = \lim_{z \to 1} G(z) = C(I - \phi)^{-1}\Delta \quad \ldots.(4.19)$$

If the real plant is open-loop stable then these quantities can be derived from m open-loop step tests, with input vectors $\underline{u}_1 \ldots \underline{u}_m$. The vectors u_j must be chosen to span the m dimensional input space. Two pieces of output data are collected from the jth test; the vector of

responses at the first sampling period, $\underline{y}_j^1$, and the vector of steady-state values, $\underline{y}_j^\infty$. The required approximate model becomes:

$$B_0^{-1} = [\underline{y}_1^1 \ldots . \underline{y}_m^1][\underline{u}_1 \ldots . \underline{u}_m]^{-1} \qquad \ldots .(4.20)$$

$$B_1^{-1} = [\underline{y}_1^\infty \ldots . \underline{y}_m^\infty][\underline{u}_1 \ldots . \underline{u}_m]^{-1} \qquad \ldots .(4.21)$$

If G is open-loop unstable, then (4.21) fails and B_1^{-1} must be calculated by using (4.19) which will need the state space representation of the system.

Here, again, in the multivariable case, some conclusions can be reached about the behaviour of the real plant under the control of (4.10) with unity negative feedback. If the unknown continuous multivariable plant is minimum phase and of full rank (CB nonsingular), then it will be stable so long as the approximate plant has been constructed as per (4.18) through (4.21), the tuning parameters have been chosen to satisfy (4.16) and the sampling rate is "sufficiently fast". Unfortunately, this minimum sampling rate required to guarantee stability is not computable. Owens has, however, developed frequency and time domain methods which can prove stability and put bounds on the real response when the real plant is linear [51]. It is also worth noting that the condition of the real plant being non-minimum phase does not necessarily imply that the closed-loop system will be unstable. If the nonminimum phase zeros are sufficiently close to the unit circle, then the closed-loop eigenvalues are less likely to have migrated to the unstable area for medium gains ($|k_j| < 1$, $|c_j| < 1$, and h^{-1} not "too fast").

4.5 ROV Controller Design Based on Approximate Models

Owens and Chotai's method of approximating the complicated transfer function by a first order system is now applied to the specific problem of designing a control system for a ROV. Once the step data has been generated and B_0 and B_1 identified from it, calculating and incorporating the derived controller into the closed-loop system is a reasonably simple matter. The ROV Seapup has,

as previously mentioned in chapter 3, four independently controllable thrusters and at the velocity level, there are six outputs to be manipulated: surge, sway, heave, roll, pitch and yaw velocities. It is obvious that two of the velocities cannot be controlled if the other four are to be independently adjusted; fortunately, roll and pitch are buoyancy stabilised and so, if necessary, can be left to regulate themselves. Therefore, the four outputs which must be sensed and fed back are the three linear velocities and yaw rate. It is important to again note that it is these four degrees of freedom which have a response most resembling a first order lag and the choice of these output variables for the control system will lead to a design with the greatest chance of success. Roll and pitch velocities demonstrate a second order response which might have to be controlled by other methods. In this chapter, it is assumed that perfect output feedback is available for the purpose of concentrating solely on the behaviour of the controller. The nature and behaviour of output sensing will be examined in a subsequent chapter and the effects on the overall control system will be discussed.

4.5.1 System Identification

Before the ROV can be piloted through its controller, four input step tests must be executed and the approximate model, the multivariable first order lag (MFOL), identified from the data. This test is to be executed off-line and so a batch method of identification can be used. If the vector of inputs for each separate test is a scalar multiple of a unit vector, then each test can be analysed independently. For example, in the case of Seapup, the approximate model will take the form:

$$\begin{Bmatrix} y_1 \\ y_2 \\ y_3 \\ y_4 \end{Bmatrix} = \begin{vmatrix} G_{11} G_{12} \cdots & G_{14} \\ G_{21} \cdots & \\ \cdot & \\ G_{41} & \cdots G_{44} \end{vmatrix} \begin{Bmatrix} u_1 \\ u_2 \\ u_3 \\ u_4 \end{Bmatrix} \qquad \ldots.(4.22)$$

where $(y_1 y_2 y_3 y_4)^T = (u \; v \; w \; r)^T$

$$\text{and} \quad \begin{Bmatrix} u_1 \\ u_2 \\ u_3 \\ u_4 \end{Bmatrix} - \begin{Bmatrix} \text{blade pitch angle of main port thruster} \\ " \quad " \quad " \quad " \quad " \quad \text{stbd} \quad " \\ " \quad " \quad " \quad " \quad \text{vectored port} \quad " \\ " \quad " \quad " \quad " \quad " \quad \text{stbd} \quad " \end{Bmatrix}$$

For inputs of the form, $(0,.. \lambda_j,..0)$, j=1,4, the individual elements of the transfer function, G_{ij}, i=1,4, can be identified. Since the entire system is to be approximated by a MFOL, each element of [G] is a first order lag. The controller is to be implemented as a digital system and so each element, G_{ij}, will be of the form:

$$G_{ij}(z) = b_{ij} / (z - a_{ij}) \qquad ....(4.23a)$$

or equivalently:

$$y_{ij}(t+1) = a_{ij}y\ (t) + b_{ij}u\ (t),$$
$$u_k(t) = 0,\ t > 0,\ 1 \leqslant k \leqslant 4,\ k \neq j \qquad ....(4.23b)$$

Owens and Chotai's controller requires information about the time constant and steady-state gain for each input-output channel, in the form of the response at $t = 1$ to a unit step at $t = 0$ and the steady-state response. This information is stored in the matrices B_0^{-1} and B_1^{-1}, respectively. Clearly, from the identified model (4.23) we can obtain the required values:

$$[B_0^{-1}]_{ij} = b_{ij} \qquad ....(4.24a)$$

$$[B_1^{-1}]_{ij} = b_{ij}/(1 - a_{ij}) \qquad ....(4.24b)$$

Two methods of batch identification of first order lags were investigated. The first was Prony's method [52] which is used to determine approximate models of the form:

$$f(t) \cong C_1 e^{d_1 t} + C_2 e^{d_2 t} + \ldots \quad \ldots + C_n e^{d_n t} \qquad ....(4.25)$$

Prony's method fits a continuous function to a set of equally distributed points. By knowing the sampling time of the controller, the derived function can easily be used to generate the required discrete-time information. Prony's method can be modified to satisfy some constraints exactly, such as in the case of the first order lag

when $d_1 = 0$, $n = 2$ and $C_2 = -C_1$. The technique involves splitting the problem into two parts. In the first, a transformation is made to equation (4.25) to make it linear in a function of the d_i coefficients. This set of coefficients is then solved approximately by the method of least squares. Another set of linear equations in the C_i coefficients are now able to be produced by knowing the time constants and these can be solved, again by least squares. This method was checked for its suitability in this application by generating a batch of fifty, then one hundred samples from a known first order differential equation of the form:

$$dy/dt = a\, y(t) + b\, u(t) \qquad \ldots.(4.26)$$
$$y(0) = 0,\ u(t) = 1,\ t > 0$$

The time constant and final value of this system are given by:

$$T_c = 1 / a \qquad \ldots.(4.27a)$$
$$y_\infty = -b / a \qquad \ldots.(4.27b)$$

This data and the sampling time was put through Prony's algorithm which identified a model:

$$y(t) = C(1 - e^{dt}) \qquad \ldots.(4.28)$$

This model was compared to the original by noting that:

$$T_c = 1 / d \qquad \ldots.(4.29a)$$
$$y_\infty = C \qquad \ldots.(4.29b)$$

if the identification is exact.

Results in the case of both sample sizes were excellent in that expressions (4.29a) and (4.29b) held exactly. The test was then made more realistic by adding a noise term to the system (4.26). This term took the form of a normally distributed white noise signal with a specified power. This was meant to simulate the differences between the response of the real system which can be attributed to higher order linear or nonlinear behaviour and to stochastic disturbances such as operating the vehicle in turbulence and the dynamics of the

measurement sensors. It will be important that the identification routine used in the ROV controller design be robust in the presence of such disturbances. Unfortunately, though Prony's method gave exact results in the case of zero noise, it was very intolerant to noise on the signal, giving totally erroneous time constants for even moderate noise power, though the identified final output value was not affected as much. This result is not surprising since Prony's method relies on the difference between subsequent samples which are affected substantially by noise on the signal.

The second identification algorithm tested was a standard batch least squares (BLS). Data was fitted to a first order discrete model of the form:

$$y(t+1) = f\, y(t) + g\, u(t) \qquad \ldots.(4.30)$$

BLS is easily extended to the general form, a nth order ARMA (auto-regressive moving-average) model:

$$\begin{aligned} y(t) - a_1 y(t-1) - \ldots - a_n y(t-n) \\ - b_1 u(t-1) - \ldots - b_n u(t-n) = e(t;\theta) \end{aligned} \qquad \ldots.(4.31)$$

The objective of the curve fitting is minimisation of the sum of the squared errors. The function is given by:

$$J(0) = \sum_{t=0}^{N} e^2(t;\theta) \qquad \ldots.(4.32)$$

$$\text{where} \quad \theta = \{ a_1, \ldots a_n, b_1, \ldots b_n \}$$

The full development of this algorithm is given in [53].

This algorithm was tested using the same benchmarks as Prony's method and unlike Prony's, did not fit as an exact model in the case of no noise, but conversely, it was very robust when noise was added to the output signal. Comparisons were made here by noting the relationships comparing the value of y after one sampling time and the final value of y from (4.27) and (4.30):

$$T_c = dt \,/\, \ln(\, f \,) \qquad \ldots.(4.33a)$$

$$y_\infty = g \,/(\, 1 - f \,) \qquad \ldots.(4.33b)$$

Table 4.1 summarises the results of testing these two algorithms. Measurement noise, as noted in chapter 1, is a major problem in ROV applications, so the batch least squares method was considered most suitable. Other advantages of BLS included easily being able to account for general input signals and modelling higher order systems. This is of interest because future work might include making a higher order approximation to the real vehicle, with or without time delays, in an effort to produce better control.

4.5.2 The Self-Test Algorithm

The control system for the ROV will consist of a digital proportional plus integral control law designed using an approximation of the full order, nonlinear vehicle. The control law and identification algorithm have been described in preceeding sections and the algorithm which supervises the self-test routine is the subject of this section.

Before operations begin or after an ROV has undergone a configuration change, the vehicle is manually piloted away from the support ship where the self-test can be executed autonomously under computer control. The self-test consists of a step input to each thruster in turn, for a preset time, each followed by a period which allows the vehicle to return to quiescence. Velocity data is logged while the thruster is operating and the batch least squares algorithm is used to derive a first order approximation for each input-output pair. This may be done at the end of each individual thruster test since the inputs have been chosen to be scalar multiples of the unit vectors.

The self-test actually consists of two complete cycles through all the thrusters. During the first set, no information is known about the the system, and therefore, a controller cannot exist. Quiescence between thruster tests is achieved by setting all the thrusters to their zero level (zero speed or zero blade pitch angle)

though this is not necessarily the level required for hovering. The reasons for this are that the vehicle may not be neutrally buoyant as is the case with Seapup, or for controllable blade pitch thrusters, zero thrust might actually be obtained only at a nonzero setting. After each individual step test is finished and the thruster returned to the zero level, the total speed of the vehicle is calculated at each sampling time and when it falls beneath a preset level, the next thruster is incremented. When this has been done with all of the thrusters, a first attempt at the controller can be calculated. All the step tests are then run again, but with two differences. The quiescence period now takes place under the influence of the controller with all reference velocities set to zero and the level of the thrusters required for quiescence can now be offset from the zero setting. Because the system is now being controlled, a much smaller value for the total vehicle speed which characterises quiescence can be set. Simulation shows that the results of the second test are very much improved over the first, primarily because each step test begins closer to zero initial conditions.

4.6 Gain Scheduling

Though the fixed gain controller is meant to be robust with respect to changes in the vehicle dynamics, this property only guarantees stability of the closed-loop system. It is unreasonable to expect the system to show the same degree of performance when operating around a state other than the nominal one at which the self-test took place. In particular, one would expect the closed-loop poles to migrate from their assigned values and the amount of output decoupling to decrease. Control systems for aerospace applications are usually designed for systems which have radically changing dynamics with respect to the operation point and gain scheduling is used to compensate. The control laws are adapted to flight conditions by scheduling the gains as functions of the system state. For ROVs, the most dominant factor changing the dynamics is the forward speed, u, since all the hydrodynamic derivatives are functions of the total vehicle speed and the forward speed range is usually larger than the sway or heave speed range. It therefore makes sense to schedule the gains of the ROV's control law with changes in the surge velocity.

Gain scheduling is easily incorporated into the self-test and control algorithms. After the second iteration of the thruster step tests at zero surge speed, a fixed gain PI plus offset controller has been calculated. This controller can then be used by the algorithm to bring the vehicle up to a steady forward speed; say, half of full speed. The thruster perturbations then take place about this steady operating point and another fixed gain controller can be designed for changes about this new operating point. The test can be repeated again and again at different forward speeds and at each speed three pieces of information are determined: the matrix of proportional gains, the matrix of integral gains and the vector of inputs required for steady operation at that speed, i.e. the offset. These quantities are then expressed as functions of the surge speed so that during operation, speed can be monitored and the control law adjusted accordingly.

4.7 Comparison to Helicopter Controller Design

As noted in chapter 1, existing ROV control systems are reasonably primitive. Most vehicles are either entirely manually driven or only have limited automatic guidance systems, such as heading or depth control. This is a difficulty for those attempting to embark on an exercise such has been described in this chapter since the designer cannot draw on previous work. Fortunately, there are parallels between the problems of designing control systems for ROVs and for helicopters. It is illuminating to look at the results of a helicopter autopilot design study [54] and note the similarities and differences with the ROV controller described here.

ROVs and helicopters are remarkably alike. They both cannot be adequately modelled as linear time-invariant systems because their point of operation in their 'flight' envelope can change quickly. The nonlinearities in the two systems are caused by the same three phenomena; rigid-body coupling, the fluid forces acting on the vehicle and the actuators, which in both cases are screw propellers. The variance of ROV dynamics with time was shown to be caused by operators adding or removing auxiliary equipment; similarily the payload,

position of the centre of gravity and pressure altitude cause variations in the helicopter's behaviour. Lastly, both control systems will face the difficulty of noisy state or output feedback signals from dissimilar sensors.

The authors of [54] begin by considering the problem to be separable into control system design and estimator design. With four inputs (differential collective, gang collective, gang cyclic and differential cyclic rotor deflections) only four state variables can be independently controlled. Two different controllers are implemented; a velocity-command law ($y = (\dot{X}, \dot{Y}, \dot{Z}, \dot{\Psi})$) and an attitude control law ($y = (\phi, \theta, \Psi, \dot{Z})$). Each law was designed using a linearised model of the helicopter at 28 different points in the flight envelope and the gains were scheduled with the true airspeed, the heave velocity and the yaw velocity. The control laws are of a PI structure and are derived using an optimal quadratic formulation. A bank of reduced order Kalman Filters is implemented to estimate the system state.

This approach is in some ways similar to the method followed here, but there are significant differences. The nonlinear nature of both systems is addressed by scheduling the gains derived by using locally linearised models. The structure of both controllers is PI but they are derived using fundamentally different techniques. The helicopter's were calculated from a quadratic criteria while the ROV's controller is based on output decoupling and pole-placement.

However, the fundamental difference in the methods is that the helicopter design is accomplished by assuming that the open-loop model, derived from a combination of physical modelling and aerodynamic tests, was correct. This assumption is not necessarily correct for the ROV design exercise and necessitated the robust self-design method.

4.8 Summary

In this chapter, the structure of the ROV controller was described in terms of a hierarchical scheme with three levels: task, global displacement and local velocity. A number of multivariable control schemes for the local velocity level were described and rejected because they all require a reliable plant model. Adaptive and robust control were rejected as well for other reasons, at least temporarily, but the ideas of both of these were used as the basis of a decoupling multivariable controller based on an approximate model of the ROV. This approximate model can be identified off-line by a "self-test" executed by the ROV. The system identification technique, the control law synthesis and the supervisory algorithm have been described. A method of incorporating gain scheduling as a function of surge speed has been presented.

Table 4.1

Performance of the Batch Identification Algorithms

System : $y(t) = -y(t) + u(t) + w(t)$

$y(0) = 0; \quad u(t) = 1, \; t \geq 0$

$y_\infty = 1.0$

$\tau_c = -1.0$

Sampling Rate : 5 Hz

$E\{w(t)w(t)\}$		Prony's Method		Batch Least Squares	
		50 Samples	100 Samples	50 Samples	100 Samples
0.0	$\bar{y}_\infty$	1.00000 (1)	1.00000	1.00000	1.00000
	σ_{y_∞}	0.4882×10^{-3}	0.0	0.3453×10^{-3}	0.0
	$\bar{\tau}_c$	-1.00000	-1.00000	-1.00000	-.99997
	σ_{τ_c}	0.0	0.0	0.0	0.0
0.001	$\bar{y}_\infty$	0.91366	0.95350	0.98930	0.99218
	σ_{y_∞}	0.6783×10^{-3}	0.3814×10^{-1}	0.7029×10^{-2}	0.8301×10^{-2}
	$\bar{\tau}_c$	-0.12498	$-.5088 \times 10^{-1}$	-0.90502	-.92202
	σ_{τ_c}	0.4047×10^{-1} (2)	0.1747×10^{-1} (3)	0.5268×10^{-1}	0.7966×10^{-1}
0.005	$\bar{y}_\infty$	0.90646	—	0.97014	0.97086
	σ_{y_∞}	—	—	0.1482×10^{-2}	0.1896×10^{-1}
	$\bar{\tau}_c$	$-.5983 \times 10^{-1}$	—	-0.71222	-0.69015
	σ_{τ_c}	— (4)	— (5)	0.10946	0.10321
0.01	$\bar{y}_\infty$	—	—	0.95278	0.95738
	σ_{y_∞}	—	—	0.2261×10^{-1}	0.2702×10^{-1}
	$\bar{\tau}_c$	—	—	-0.52652	-0.53589
	σ_{τ_c}	— (5)	— (5)	0.9296×10^{-1}	0.13856

Notes : 1) Parameters calculated for 20 realisations of the process

2) 1 failure of algorithm

3) 14 failures

4) 19 failures

5) 20 failures

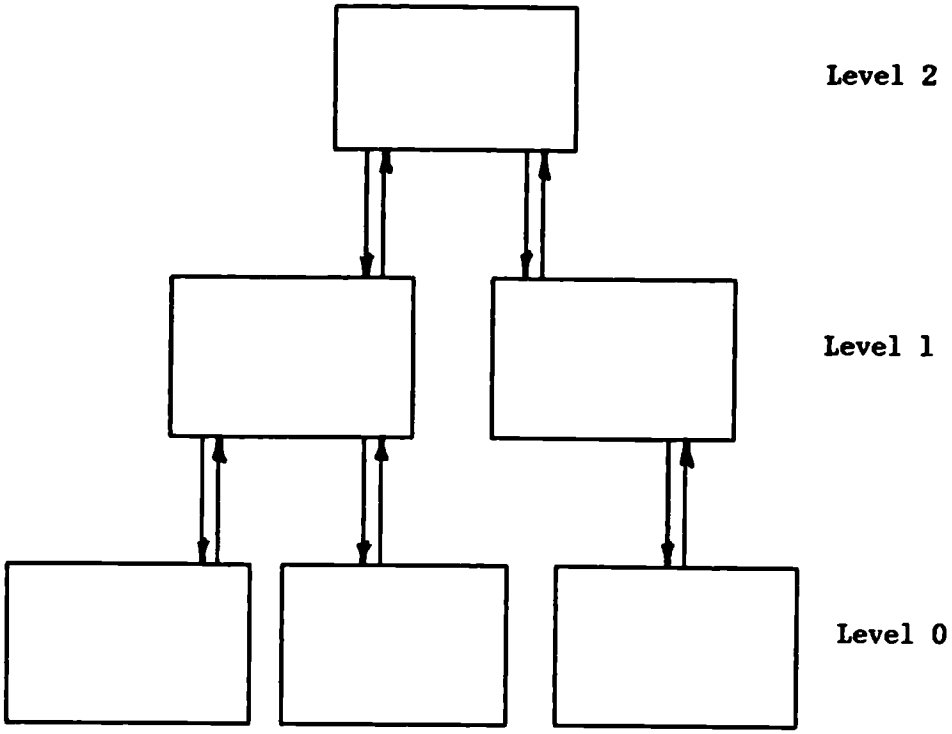

Figure 4.1: A Three-Level Hierarchy

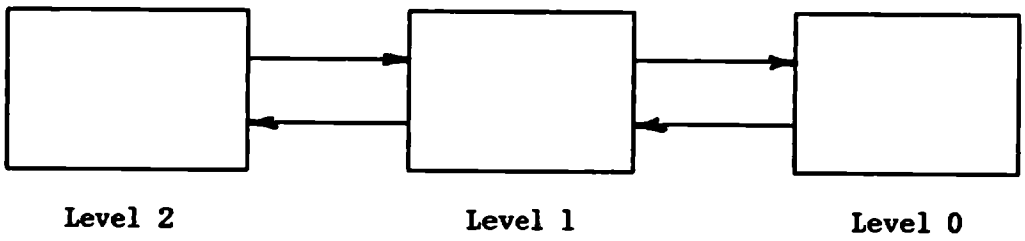

Figure 4.2: A Three-Level Supervisory System

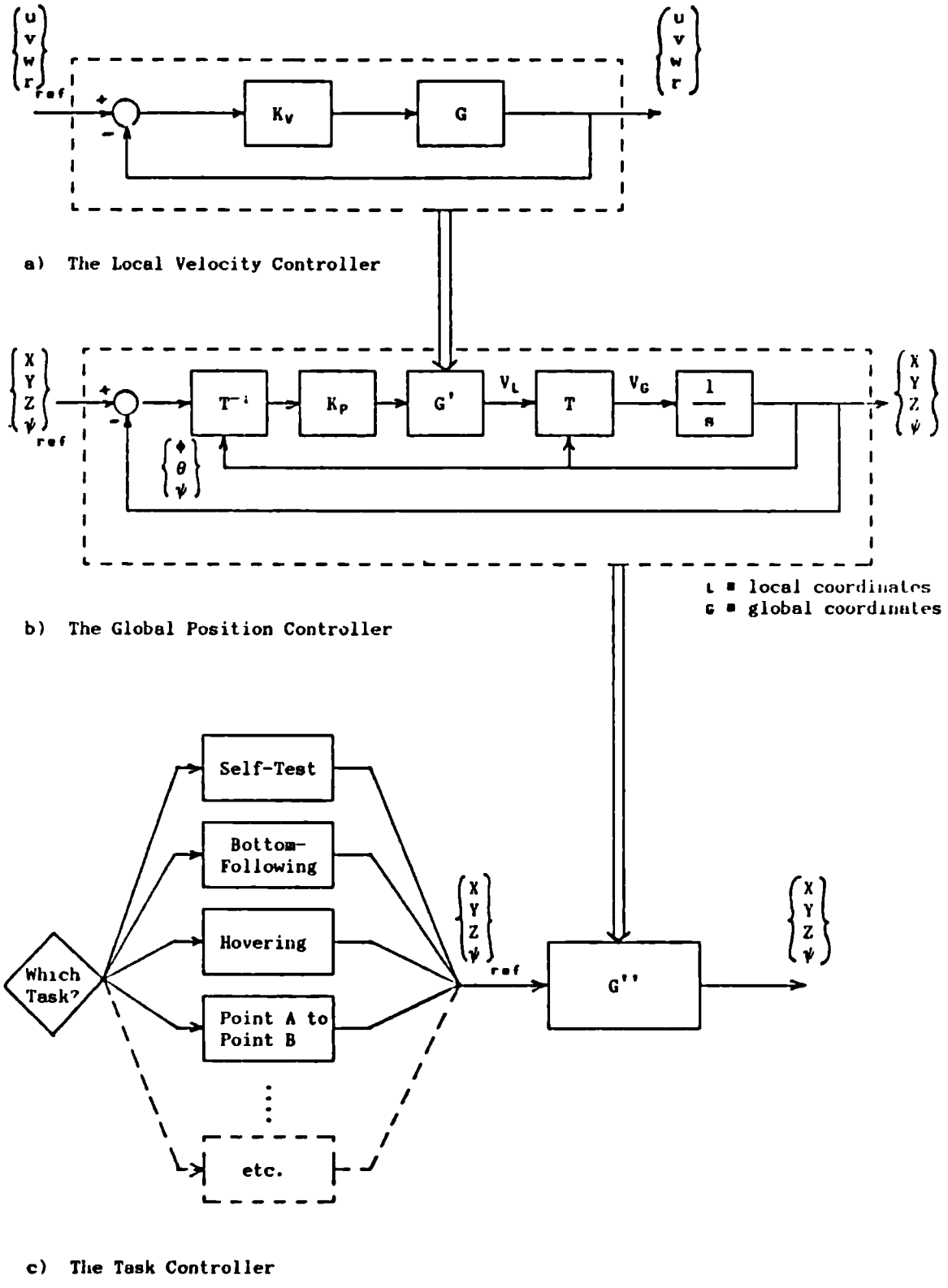

Figure 4.3 : The Proposed ROV Supervisory Control System

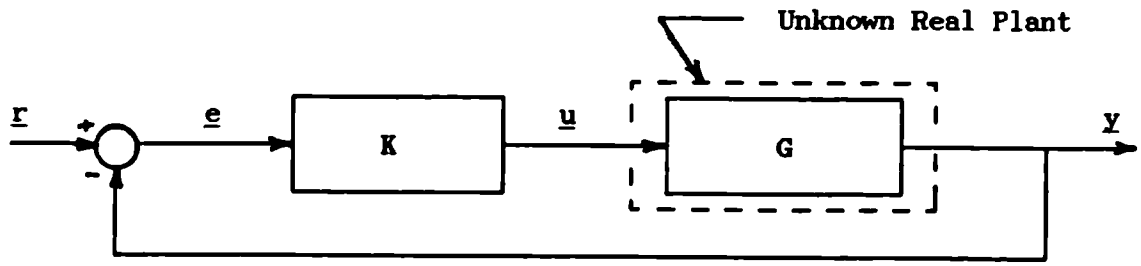

Figure 4.4 : Real Feedback Control System

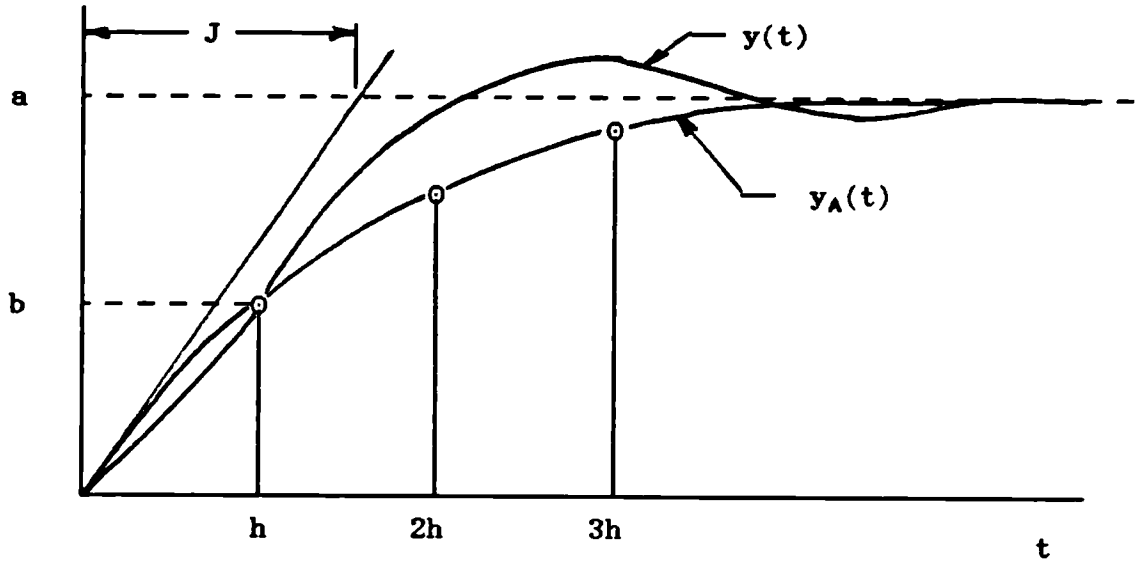

Figure 4.5 : Construction of the Approximate Plant, G_A

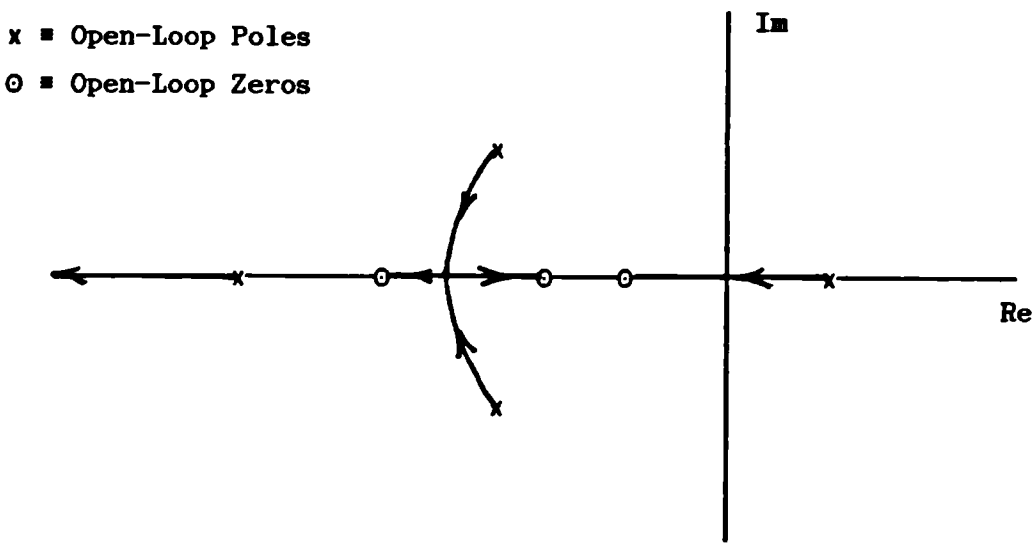

Figure 4.6 : A Representative Root Locus Plot

Chapter 5

Self-Testing Controller Analysis and Performance

5.1 Introduction

In this chapter, the various figures of merit which characterise a control system are presented for the ROV Seapup linked with the robust PI controller. An appraisal of a closed-loop system considers a number of features. Those presented here are:

a) the migration of the closed-loop eigenvalues as the mean forward speed changes.

b) the response of the system to step changes in reference velocities. Both individual changes and combination reference steps are considered.

c) the ability of the system to reject deterministic and stochastic load disturbances.

d) the robustness of the closed-loop system to changes in the vehicle's physical configuration.

These features are presented for different sampling rates and for scheduled and fixed gain controllers.

The algorithm for identifying the first order model from the step test data is also evaluated. The success of the self-test is characterised by its accuracy and to a lesser extent, the time and space that it uses.

5.2 A Note on the Choice of the Closed-Loop Poles

The results of the analysis reported in this chapter all depend on the choice of desired discrete-time closed-loop poles; the k_j and c_j of equation 4.11. Unless otherwise noted, all of the results

reported are for the closed-loop system with the poles chosen as follows:

T_s = 0.2 s	j	k_j	c_j
	1	0.8	0.8
	2	0.85	0.85
	3	0.75	0.75
	4	0.65	0.65

T_s = 0.05 s	j	k_j	c_j
	1	0.94574	0.94574
	2	0.96018	0.96018
	3	0.93060	0.93060
	4	0.89790	0.89790

The poles were chosen by observing the performance of the closed-loop simulation being sampled at 5 Hz and varying the pole positions until the response of certain step tests was considered adequate. The factors that were considered were the speed of the response, the magnitude of the control signals and the occurrence of the limit cycles. The limit cycle behaviour will be addressed more extensively in section 5.4.2.

In an ideal autopilot, there would be a mechanism for automatically choosing these closed-loop poles. Optimal control methods are good in this respect because the placement of the poles, an abstract procedure for someone not trained in control engineering, is replaced by a cost function in which the opposing goals, usually output tracking and actuator effort, are represented as an explicit compromise. However, current opinion is that all controllers, even those designed by optimal methods, require a 'performance oriented knob', a way of manually choosing the behaviour of the system.

When the sampling time was changed to see the effect on the system, the k_j and c_j were modified such that they corresponded to the same continuous-time eigenvalues as in the case of the 5 Hz sampling rate. This was done by using the following relationship between the s- and z-planes. If the continuous signal is sampled at a rate T_s, then:

$$z = \exp(s\, T_s) \qquad \ldots.(5.1)$$

5.3 Performance of the Self-Test Algorithm

Though the structure of the self-test algorithm, described in section 4.5.2, is fixed, there are still parameters in the algorithm which must be specified by the designer. These are the sampling rate, which is also the rate used by the controller, the number of samples to collect in each test and the speeds which are to be the quiescence limits prior to each test.

The sampling rate used as a baseline was the fastest rate that was thought to be achievable for output feedback from sonar-type devices [6]. This limit was 5 Hz, though it is worth noting Owens and Chotai show that, when using their scheme, faster sampling rates will lead to better control [48].

Specifying the number of samples to collect for each self-test is a compromise. Many samples will lead to a more accurate approximation, but it will also require more memory space in the vehicle's control computer and the test will require larger amounts of time and space to execute for a given sampling rate. Fifty-one samples was chosen; with this number adequate approximations were being made and the time for a entire cycle of tests was only about one minute.

The choice of quiescence speeds is also a compromise. Smaller levels will lead to more accurate results in the self-test, but will also require more time to be taken up by testing. In fact, during the first testing cycle when zero initial conditions are being sought by setting the thrusters to zero blade pitch angle, the Seapup reaches finite forward and downward velocities because it is negatively buoyant and because the thrusters produce a finite thrust at this setting. In this case, the quiescence speed must be chosen to be greater than this steady-state speed or the test for zero speed will never be satisfied. This quiescent speed is chosen by letting the ROV drift before the start of the test. However, with the controller in place after the first cycle, this level can be reduced to less than ten percent of the original value.

As an illustration of the performance of the self-test algorithm, a set of simulated test results for Seapup will be presented. These will be compared to the the same values that a human observer would choose, given a log of the velocities achieved during the test.

5.3.1 Time Constants and Steady-State Gains Chosen by a Human Observer

To generate the benchmark B_0^{-1} and B_1^{-1} matrices, defined in equations (4.18) and (4.19), the Seapup was simulated in open-loop mode. The setting for the thruster blade pitch angles to achieve quiescence was calculated to be:

$$u_0^T = \{ -3.383, -3.383, -13.098, -13.098 \} \quad ....(5.2)$$

Each open-loop simulation, test 'i', consisted of initialising the vehicle to $q_0 = (0)$ and $u = u_0$ and then incrementing thruster 'i' by eight degrees. This value was chosen because it caused significant velocities that were less likely to be lost in either the process or the measurement noise, though neither of these were added to this simulation.

B_0^{-1} is the matrix of the responses at $t = 1 * T_s$ to a unit step input at $t = 0$. The sampling rate here is 5 Hz ($T_s = 0.2s$). B_0^{-1} ij is the initial response of output i to input j. Similarly, B_1^{-1} contains the collection of steady-state responses of outputs i to step inputs j. For the conditions given above, the Seapup simulation yielded:

$$B_0^{-1} = \begin{bmatrix} .0026 & .0026 & .000125 & .000125 \\ -.0001 & .0001 & -.0004265 & .0004265 \\ .0000625 & .0000625 & .000525 & .000525 \\ .2629 & -.2629 & .001588 & -.001588 \end{bmatrix} \quad ....(5.3a)$$

$$B_1^{-1} = \begin{bmatrix} .0246 & .0246 & .00064 & .00064 \\ -.00409 & .00409 & -.00766 & .00766 \\ -.0006 & -.0006 & .004875 & .004875 \\ 1.9612 & 1.9612 & -.04990 & .04990 \end{bmatrix} \quad ....(5.3b)$$

Here, the output corresponds to $\{ u, v, w, r \}^T$ where the linear

velocities are measured in metres per second and the yaw rate in degrees per second.

As mentioned in section 4.6, gain scheduling can be used to partially compensate for changing dynamics with forward speed. In this chapter, a simple scheme of gain scheduling will be investigated. The time constant and steady-state gain matrices will be calculated at two speeds (0.0 m/s and 0.7 m/s), the controller calculated at each condition and linear interpolation used during operation at other speeds.

When performing the identification at speeds other than zero it is important that the correct formulation is used. The approximate model is given by (4.9) :

$$G_A^{-1}(z) = (z - 1)\, B_0 + B_1 \qquad \ldots.(4.9)$$

This is easily transformed into:

$$y(t) = B_0^{-1}(B_0 - B_1)\, y(t-1) + B_0^{-1}\, u(t-1) \qquad \ldots.(5.4)$$

Consider the problem of identifying B_0^{-1} and B_1^{-1} from a system linearised about a point other than zero, say y_0 which corresponds to a non-zero input u_0. Equation (5.4) can be reformulated in terms of changes from steady-state values:

$$y'(t) = B_0^{-1}(B_0' - B_1')\, y'(t-1) + B_0^{-1}\, u'(t-1) \qquad \ldots.(5.5)$$

$$\text{where } y'(t) = y(t) - y_0$$
$$u'(t) = u(t) - u_0$$

Clearly B_0' and B_1' can be identified by the least squares method if the inputs to the algorithm are y' and u'. For a non-zero linearisation point, the control law (4.11) becomes:

$$\begin{aligned} e_k &= (r_k - y_0) - (y_k - y_0) = r_k - y_k \\ q_{k+1} &= q_k + e_k \\ u_k &= B_0 \{ \text{diag}(1 - k_j)(1 - c_j) \}\, q_k \qquad \ldots.(5.6) \\ &\quad + B_0 \{ \text{diag}(2 - k_j - c_j) \}\, e_k + u_0(r) \end{aligned}$$

The self-test information was calculated for y_0^T= (0.7, 0, 0, 0) and u_0^T = (14.589°, 14.589°, -5.929°, -5.929°) in order to have a benchmark for the gain-scheduled controller. The values recorded from the velocity log were:

$$B_0^{-1} = \begin{bmatrix} .00325 & .00325 & -.001125 & -.001125 \\ -.00025 & .00025 & -.001300 & .001300 \\ .000375 & .000375 & .01200 & .01200 \\ .361725 & .361725 & -.009825 & .009825 \end{bmatrix} \quad \ldots.(5.7a)$$

$$B_1^{-1} = \begin{bmatrix} .01514 & .01514 & -.00565 & -.00565 \\ -.00700 & .00700 & -.00490 & .00490 \\ -.00060 & -.00060 & .00209 & .00209 \\ 1.3419 & -1.3419 & -.13100 & .13100 \end{bmatrix} \quad \ldots.(5.7b)$$

5.3.2 Time Constants and Steady-State Gains Chosen by the Self-Test Algorithm

In this section, two cases were examined. In both runs, individual thruster tests were run for 10 seconds at a sampling rate of 5 Hz and turbulence disturbances and measurement noise were not included. In the first simulation, which may be described as quasi-ideal, at the beginning of each individual thruster test the state was set to q = (0) and u = u_0. This simulation was also run for a mean forward speed of 0.7 m/s. The second self-test was made more realistic by having the vehicle attempt to reach the quiescence level automatically as described in section 4.5.2. The results of these simulations are compared to the results of (5.3) in tables 5.1 and 5.2.

5.3.3 Discussion

The automatic self-test identifies the characteristics of the ROV reasonably well, especially when artificial quiescence is imposed. There do exist identification errors however. These can be attributed to the vehicle not starting the test at the desired initial conditions, not to the identification routine failing. This was checked for cases in which the approximations generated from the velocity logs and the realistic self-tests were extremely different.

The initial conditions for the test in question were set up in the open-loop simulation and the appropriate thruster incremented. Invariably the log would show that the least-squares algorithm had worked properly and the errors between the two methods had been caused by the errors in initial conditions. This is another source of modelling error which, along with the errors produced by lumping all of the vehicle dynamics into a first order lag, might cause control to be degraded.

Other important characteristics of the self-test are the amount of time required and the space of ocean that is used during its execution. It is crucial to keep the amount of time required for testing as low as possible since, as previously shown in section 1.2, offshore operations are very expensive and there is a strong incentive with ROV operators to reduce operation time.

For a self-test executed at a single speed, 0.0 m/s, the time required to carry out the two cycles was 119.2 seconds. The time included 8 subcycles at 10 seconds each and the remainder was consumed by waiting for quiescence to be achieved. Assuming that the vehicle was at the global X, Y, Z zero point at the beginning of the test with its bow pointing in the X direction ($\psi = 0$ degrees), the vehicle required a space of 9.4 m (X) by 5.2 m (Y) by 5.7 m (Z). When the test was continued to include another velocity schedule point at 0.70 m/s, another 60.2 seconds was required. The space of water used increased to 33.4 m (X) by 33.0 m (Y) by 12.0 m (Z). The Z value ranged from 5.7 m below the initial value to 6.3 m above it.

5.4 Performance of the Closed-Loop System

5.4.1 Closed-Loop Eigenvalues

As was the situation with the open-loop model, the stability of a closed-loop system is described by its eigenvalues. In sections 3.2 and 3.7, the eigenvalues of the open-loop system were given by:

$$| sI - A | = 0 \qquad \ldots.(3.7)$$

where the open-loop state-space model was:

$$\dot{x} = A\,x + B\,u \qquad \text{....(3.2)}$$
$$y = C\,x$$

Recall that A and B were derived from the nonlinear model:

$$\dot{x} = H(\,x,\,u\,) \qquad \text{.....(3.1)}$$
$$y = C\,x$$

by a fourth-order Taylor series expansion about the operating point of interest.

The closed-loop system sampled at 5.0 Hz and 20.0 Hz is to be compared. Since the underlying continuous system does not change, it is important that the desired discrete-time closed-loop poles that the designer chooses (equation 4.10) should map to the same continuous-time poles, independent of the sampling rate. Failure to do this will cause the system to respond faster as the sampling rate increases, leading to actuator saturation and degraded controller performance.

The eigenvalue analysis of the composite system consisting of open-loop plant, forward loop controller and unity negative feedback loop will be done in the discrete-time domain for reasons which will be made apparent. Figure 5.1 shows the configuration of the closed-loop system. Notice that the digital controller is interfaced to the continuous system by samplers on the reference and output feedback signals and by a zero order hold (ZOH) on the output of the controller. The ZOH would consist of a digital to analogue converter in the real system. Discrete outputs from the controller are latched and held at a constant level till the next output from the controller appears, as in figure 5.2. The samplers behave in a similar manner. A continuous signal is latched over a very short period of time and an analogue to digital converter creates an input from this for the control computer.

On first inspection, it seems that the eigenvalue analysis of the closed-loop system can be attempted in the s-domain or the z-domain. Assume for the moment that it is to be carried out in continuous time. The dynamic controller has the governing state-space equation, derived in the previous chapter:

$$q_{k+1} = I\ q_k + I\ e_k \qquad \ldots.(4.11)$$
$$u_k = K_{int} q_k + K_{err} e_k$$

This can be converted to a zero order hold, followed by a continuous state-space model by using the relations:

$$\dot{q} = A_c\ q + B_c\ e \qquad \ldots.(5.7)$$
$$u = C_c\ q + D_c\ e$$

where $A_c = \ln(\ I\ )\ /\ T_s$

$$I = \int_0^{T_s} \exp(A_c(T_s - t))\ B_c dt$$

$$K_{int} = C_c \text{ and } K_{err} = D_c$$

Clearly, $A_c = [0]$ and $B_c = (1.0/T_s)\ I$

The resulting closed-loop system is depicted in figure 5.3 where the ZOHs have been replaced by their Laplace transforms, $(1-\exp(-sT_s))/s$ and it is assumed that the reference and output feedback samplers are working synchronously, enabling them to be combined into a single ZOH in the forward loop.

Because of the pure time delay, the closed-loop characteristic polynomial will be transcendental, foiling any conventional attempt to solve for the eigenvalues. Fortunately, this problem does not appear in the discrete formulation. The open-loop plant transfer function, preceded by the ZOH, can be discretised into the model:

$$x_{k+1} = \bar{\Phi}\ x_k + \Delta\ u_k \qquad \ldots.(5.8)$$
$$y_k = C\ x_k$$

where $\bar{\Phi} = \exp(\ A\ T_s)$

and $$\Delta = \int_0^{T_s} \exp(A (T_s - t)) B \, dt$$

The closed-loop discrete system is of finite order in z and can be solved by standard eigenvalue techniques.

Calculating the z-plane characteristic values requires a number of steps. After the linear state space model of the open-loop process has been obtained from the nonlinear model, it must be converted to the equivalent discrete equation (5.8).

$\bar{\Phi}$ can be approximated by the evaluation of the series representation of the matrix exponential to a suitably large number of terms:

$$\bar{\Phi} = I + AT_s + A^2T_s^2 / 2! + \ldots + A^nT_s^n / n! + \ldots \qquad \ldots.(5.9)$$

which can also be written:

$$\bar{\Phi} = I + A\,Ts\,\Psi \qquad \ldots.(5.10)$$

where $$\Psi = I + A\,T_s / 2! + A^2T_s^2 / 3! + \ldots.$$

Δ can be evaluated by noting that:

$$\begin{aligned} \Delta &= \exp(A\,T_s) \int_0^{T_s} \exp(-A\,t)\,dt \;\; B \\ &= -A^{-1}(I - \exp(A\,T_s))\,B \\ &= -A^{-1}(I - (I + A\,T_s\Psi))\,B \qquad \text{(from (5.10))} \\ &= T_s\,\Psi\,B \qquad \ldots.(5.11) \end{aligned}$$

Equations (5.10) and (5.11) lead to a particularly convenient method for numerically evaluating the discrete time model.

The discrete open-loop model can be augmented to take into account the dynamics of the forward loop controller and the negative unity feedback loop. Define an augmented state vector $x_s = (x \;\; q)^T$. From (5.7) and (5.8), the augmented system equations become:

$$\begin{Bmatrix} x \\ q \end{Bmatrix}_{k+1} = \begin{bmatrix} \Phi & \Delta K_{int} \\ 0 & I \end{bmatrix} \begin{Bmatrix} x \\ q \end{Bmatrix}_k + \begin{bmatrix} \Delta K_{err} \\ I \end{bmatrix} e_k \qquad \ldots.(5.12)$$

$$y_k = [\, C \;\; 0 \,] \begin{Bmatrix} x \\ q \end{Bmatrix}_k$$

or:

$$x_{s_{k+1}} = \Phi_s x_{s_k} + \Delta_s e_k$$

$$y_k = C_s x_{s_k}$$

Now define the negative unity feedback loop:

$$e_k = r_k - y_k \qquad \ldots.(5.13)$$

$$= r_k - C_s x_{s_k}$$

The closed-loop augmented system becomes:

$$x_{s_{k+1}} = (\Phi_s - \Delta_s C_s)\, x_{s_k} + \Delta_s r_k \qquad \ldots.(5.14)$$

$$y_r = C_s x_{s_k}$$

Clearly, the closed-loop characteristic polynomial is:

$$| zI - \Phi_s + \Delta_s C_s | = 0 \qquad \ldots.(5.15)$$

Reiterating, the steps required to generate the system's closed-loop poles are:

i) Linearise the state-space equations of the ROV using a Taylor series. A linear continuous time state-space model is obtained.

ii) Given the sampling rate, convert these equations to a discrete time representation, using a finite number of terms in the series expression of the matrix exponential.

iii) Augment the system states with the dynamics of the forward loop controller, taking into account velocity scheduling if it is being used.

iv) Solve the eigenvalue problem, $| zI - \bar{\Phi}_s + \Delta_s C_s | = 0$. Here, the QR algorithm is used.

v) Convert the discrete time eigenvalues to continuous time so that a comparison may be made between the performance of the closed-loop system at different sampling rates.

Equation 5.15 produces 16 eigenvalues; four from the pure integration from velocities to displacements X, Y, Z and Ψ and twelve from combined vehicle and controller dynamic states. These are in the discrete time domain. It is worth noting that the underlying continuous system can have an infinite number of s-plane eigenvalues. These arise because of the sampling process which introduces $\exp(-sT_s)$ terms into the closed-loop characteristic polynomial. If a pole turns out to be on the the negative real z-axis, it maps onto an infinite number of points on the s-plane, at multiples of the Nyquist frequency, $1 / (2*T_s)$.

Figures 5.4 through 5.9 show how the eigenvalues associated with the different modes (surge, sway, heave, yaw, roll and pitch, respectively) change with mean forward velocity. In each diagram, part (a) depicts the loci at a sampling rate of 5 Hz, with and without linear gain-scheduling. Part (b) shows the same two loci for a controller sampling rate of 20 Hz. The initial and steady-state vehicle response values for the calculation of both controllers were taken from the realistic self-test. Some of the more interesting features of this analysis are now described.

i) Surge Modes - This mode was the most favourably affected by the addition of gain scheduling, not surprisingly. With scheduled gains, the loci move very little with changing speed. The gain scheduled branch at 5 Hz becomes more stable with increased u but at 20 Hz it becomes less stable. The fixed gain loci show the same trends for both sampling rates

ii) Sway Modes - Except in the case of fixed gains at the 20 Hz sampling frequency, there was very little pole migration here. Notice here, as well as on the branches of other modes, a large migration

when the forward speed changes from 0.7 m/s to 0.8 m/s. In section 3.7, this is shown to be the point where the open-loop system becomes nonminimum phase. Recall also that according to Owens and Chotai [48], the underlying multivariable system must be minimum phase to guarantee closed-loop stability with their controller.

iii) Heave Modes - Though all the heave loci start off near their desired values, they move rapidly away with increased forward speed. A poor choice of controller has lead to an instability on the 5 Hz scheduled gain branch at high speed. Again, the largest movement occurred when the system's open-loop zeros crossed into the right-half plane.

Another interesting feature is the portion of the 5 Hz, fixed gain locus at 15.708 rad/s. This, of course, is the Nyquist frequency for this system. At this point the 16 degree of freedom augmented system has an infinite number of poles because of the transcendental features introduced by the sampling process.

iv) Yaw Modes - These remain stable in all four configurations over the entire speed range. At zero forward speed, the poles are very close to their desired values. The largest change in the loci again occurs between 0.7 m/s and 0.8 m/s.

v) Roll Modes - Though pitch and roll are not direct output variables to the controller, these modes are affected by the controller's actions. The roll mode shows the most dramatic effect of the right-half plane zeros with a sudden shift to instability at the transition speed. Up to this point, the fixed gain controller was holding the locus very steady at both sampling rates.

vi) Pitch Mode - Stability is achieved throughout the speed range with all of the controller configurations. Here again, most of the movement takes place at 0.8 m/s.

This analysis shows that the desired closed-loop eigenvalues can be achieved if the self-test algorithm has identified the open-loop model with sufficient accuracy. It is also evident that the

nonminimum phase behaviour of this particular ROV system adversely affects the stability of the controlled system. No real improvement is noted when the sampling rate is increased to 20 Hz, but scheduling can sometimes help. Here, it did cause the loci of the surge poles to remain closer to their desired value.

5.4.2 Response to Step Changes in Reference Velocities

Fixed Gains, 5 Hz Sampling Rate

A control system can be evaluated in the time domain by its response to step changes in the reference quantities. The step response can be characterised by its rise time, settling time, overshoot and steady-state error. Multivariable systems must also be evaluated for the degree of output decoupling.

The first cases that were considered were individual changes to each of the four reference velocities from an initial zero state. The magnitude of the steps was taken to be seventy-five percent of the maximum velocity available in that degree of freedom achieved while running under open-loop control. These values were:

u = 0.85 m/s : test a)
v = 0.29 m/s : test b)
w = 0.25 m/s : test c)
r = 31.5 deg/s : test d)

In all tests, the data from the realistic self-test (see table 5.1) was used to generate the controller gains. Figures 5.10 through 5.16 show the response of the system to step changes in u, v, w and r. In each figure, the time history of the linear velocities, the yaw rate, the roll and pitch angles and the thruster blade pitch angles are depicted. The desired poles selected are as noted in section 5.2, the sampling rate is 5 Hz and the constant gain controller is used for each simulation. Selected results of step tests with the sampling rate increased to 20 Hz and gain scheduling utilised will also be presented.

a: Surge (figure 5.10)

As can be seen from the figure, the response to this reference input is very good. The vehicle reaches its desired velocity in about 5.0 s with only a 1.7 percent overshoot. Interaction effects are very low, especially in sway and heave. The roll angle remains between ± 5.0 degrees. The pitch angle rises to approximately 26.2 degrees at 1.8 s then settles to a steady value of 14.3 degrees, bow up. Control effort is characterised by the thruster blade pitch angles; here, the main thrusters saturate for 0.8 seconds then quickly drop back to their steady-state value, 20 degrees.

b: Sway (figure 5.11)

Here, the control objective was reached less successfully. The closed-loop poles in this loop were made to be relatively slow ($z = 0.85$) because it was found that if they were faster they could cause small limit cycles to appear in other situations. This will be discussed later.

The ROV only attains the steady-state sway velocity of 0.277 m/s, short of the 0.29 m/s reference value. The maximum velocities under closed-loop control may be less than those reported in chapter 3 because the controller must consider all four output variables. Consider the thruster blade pitch angles in figure 5.11. Notice that the vectored starboard thruster is saturated and that the vectored port thruster is not being increased despite the improvement in lateral velocity that would occur; to do so would move u, w and/or r away from their references.

Another sway velocity test is shown in figure 5.12. Here, the reference velocity has been decreased to 0.25 m/s. The vehicle is able to achieve this velocity; ninety-five percent rise time is 1.8 s and the overshoot is 5.2 percent. Interaction effects are larger here than in the surge test, but they are quickly eliminated. As expected, the roll angle at first becomes quite large (-15.2 degrees), but quickly reaches its more acceptable value of -4.7 degrees. The pitch angle remains between 1.7 and -2.0 degrees throughout the simulation.

The starboard vectored thruster saturates for much of the 10 s but eventually comes off its limit.

c: Heave (figure 5.13)

In this test, the heave velocity rose to its 95 percent level within four sampling time units (0.8 s) and the surge, sway and yaw velocities remained very small. The pitch angle stays between ± 5 degrees and the roll angle is insignificant.

At first there were some problems in this test. Originally, k_2 and c_2, the factors governing the sway poles, were set to 0.8 and during the heave simulation, a small roll-sway limit cycle was set up with the vectored thrusters alternating at each sampling time between +26 degrees and +2 degrees. Moving these poles back to 0.85 solved this problem, but at the expense of making the sway response more sluggish.

d: Yaw (figure 5.14)

The response was initially very good, with the yaw velocity rising to 95 percent levels within 2.6 seconds. Up to 9.0 s, interaction velocities decreased continuously but at this time, a small sway-roll limit cycle with a period of 6.2 s began. Despite this, the yaw velocity remained within 7 percent of its reference value. Some experimentation was done with this test. The test was simulated for 40 s rather than the usual 10 s to ensure that the behaviour was a limit cycle and not the onset of instability. Notice that 40 s is the time scale on all the graphs of figures 5.14, 5.15 and 5.16. The values of k_2 and c_2 were varied in an effort to eliminate the limit cycle. As they approached 1.0, the onset of the limit cycle was delayed and eventually eliminated within the 40 s window. Figure 5.15 depicts the results when k_2 and c_2 were set to 0.95. Of course, for these poles, responses to changes in the reference sway velocity became very slow.

Further evidence that this was indeed a limit cycle and not an instability was gathered by substituting a full order, linearised

(about zero speed) version for the nonlinear model of the vehicle. This model was obtained by using the same Taylor series expansion as was used in the eigenvalue analysis. The result is shown in figure 5.16. The offending behaviour does not appear, suggesting that it was a limit cycle caused by the system nonlinearities, not an instability caused by the second-order system being controlled by a controller designed for a first-order system.

It is important that the system be evaluated for reference demands which are more likely to be encountered in operations. The first combination command considered is:

$$r^T = \{\ 0.2\ \text{m/s},\ 0.1\ \text{m/s},\ 0.1\ \text{m/s},\ 0.0\ \text{deg/s}\ \}$$

moving ahead slowly while at the same time edging sideways and downwards. Such a manoeuver might take place when examining a sloping section of an oil rig. The result of this simulation is given in figure 5.17; very good response in all outputs is achieved simultaneously.

A medium speed turn is examined next. In this case:

$$r^T = \{\ 0.3\ \text{m/s},\ 0.0\ \text{m/s},\ 0.0\ \text{m/s},\ 15\ \text{deg/s}\ \}$$

and figure 5.18 contains the results. Again the controller has performed well.

Effects of Gain Scheduling and Sampling Rates

In this section, the effect on the performance of the closed-loop system in the time domain caused by implementing gain scheduling and an increased sampling rate is evaluated by considering a selection of the test cases of the previous section. Those chosen for examination are the surge velocity and yaw rate step demands. Simulations included a linearly scheduled gain controller operating at the baseline rate of 5 Hz, a fixed gain controller operating at 20 Hz and a gain scheduled controller operating at 20 Hz.

The interesting feature about the addition of gain scheduling to the surge test, shown in figure 5.19, is that a steady-state error is present in the surge velocity, despite none of the thrusters being saturated. At first, this seems impossible because of the integration in the forward loop. Examination of the controller derived at 0.7 m/s shows that the terms which relate the error and the integral of the error of the surge velocity to the main thrusters' blade pitch angles are negative. This can only be so because of errors in the identification of the model at this speed. Human generated observations indicate that, at this speed, increased forward velocity is achieved by increasing the setting of the main thrusters. The mechanism of the steady-state error is as the forward speed increases, the gain matrices are turned farther away from their more accurate values obtained at zero speed until some gains are actually of the incorrect sign. A steady-state error is reached since any further increase in speed will lead to the main thrusters being decreased because of the increasingly negative gain matrices.

This feature also helps explain some of the less than ideal results of the eigenvalue analysis. It would not be expected that the closed-loop system would have poles very near the desired values if the approximate model has such gross errors in it.

Though not shown here, the addition of gain scheduling has not radically changed the yaw test since the forward speed remains smaller throughout this simulation than in the surge test.

Modifying the fixed gain controller to operate at 20 Hz has a much more beneficial effect on the ROV. Figure 5.20 shows that, in the surge test, the rise time to achieve the demanded forward speed has decreased and the overshoot is down to only 0.35 percent. In the yaw test (figure 5.21), the limit cycle still occurs. Its period has decreased to 2.0 s and the fluctuations in the state variables are much smaller. The yaw rate remains within 4.4 percent of the set point throughout the limit cycle.

When gain scheduling is added to the 20 Hz controller, the problems which appeared at 5 Hz during the surge test reoccur in a

similar manner indicating that the identification procedure at the higher speed has also failed at the faster sampling rate.

5.4.3 Disturbance Rejection

ROVs operate in a noisy environment. Two of the factors which cause difficulty are currents and turbulence. In strong currents, if a vehicle is operating under manual control, taking up and holding station can be time consuming and mentally exhausting as the operator must continuously adjust thruster levels. An automatic closed-loop control system can only be successful if it can compensate for these type of disturbances and relieve the operator of much of this tedious portion of his workload.

Both deterministic and stochastic current disturbances are considered here. Deterministic disturbances consist of step changes in current velocity and direction. Consider the following example, illustrated in figure 5.22. The controller is based upon the realistic self-test; it is in the constant gain configuration and the sampling rate is 5 Hz. Initially quiescent, the system is given a step change in reference velocities:

$$r^T = (\ 0.2\ \text{m/s},\ 0.1\ \text{m/s},\ 0.1\ \text{m/s},\ 0.0\ \text{deg/s}\ )$$

This is the inspection manoeuver presented in the previous section, except that at 10 s, a current of 0.26 m/s flowing at zero degrees (along the positive X axis) is created. As shown in the diagram, the forward velocity temporarily increases to 0.2574 m/s. As well, there is a small increase in the heave velocity. Both of these errors are quickly eliminated as the thrusters reach their new steady-state levels. The forward speed is back to within five percent of the set point within 5.8 s.

The first-order Gauss-Markov turbulence model described in section 2.4 is used to determine the system response to stochastic disturbances. The situation considered is hovering at the global zero position at a zero heading. The vehicle is left to drift for 10 s in

a current with a mean speed of 0.26 m/s and standard deviation 0.086 m/s. The average current direction is zero degrees with a standard deviation of 20 degrees. Figure 5.23 shows the results of activating the 5 Hz controller at 10 s. Despite two of the thrusters becoming saturated, the drift velocity is quickly eliminated. The yaw velocity temporarily increases and then is brought back closer to zero. The linear positions and heading angle are of interest here. After the controller is connected, the position is held to within 0.60 m in X, 0.06 m in Y and 0.06 m in Z. The heading angle remains within 5 degrees. These figures would be smaller in operation where the controller would be operating continuously and no large drift velocities had been allowed to build up. The same situation is illustrated in figure 5.24, except that the controller is operating at 20 Hz. One advantage of the faster sampling rate is apparent; since the system effectively runs open-loop between samples, disturbances will have a greater effect at slower sampling rates causing the output variables to stray farther from their reference values.

5.5 Robustness to Physical Configuration Changes

One of the figures of merit to be considered in this chapter was the robustness of the closed-loop system. Robustness is defined by the maximum variation in plant open-loop dynamics that can be tolerated before a particular feedback scheme becomes unstable. These changes can arise because of parameter variations, unmodelled dynamics or nonlinearities, all of which are present in this application.

A measure of the robustness of the self-designing controller can be evaluated by considering a typical physical configuration change which a ROV operator might carry out; the addition of an extra television camera to the bow of the vessel. The effects on the open-loop poles and zeros and open-loop time response, as well as a full description of the changes caused by the camera to the vehicle parameters was presented in sections 3.6 and 3.7. In summary, a 15 kg mass, assumed to be spherical, is attached to the 115 kg Seapup at the lower edge of the bow on the longitudinal centreline. This changes the mass matrix significantly because of its physical and hydrodynamic

added mass. The drag force vector is also likely to change but since these effects cannot be calculated from inviscid flow theory, they were assumed to be zero.

All six branches of the modified ROV's open-loop root locus have roughly the same shape as the baseline vehicle's, but with slightly differing values. The zero loci also have the same shape but an important point to note here is that the nonminimum phase branch crosses into the right half plane at a surge speed of approximately 0.4 m/s. For the unmodified vehicle, this occurred at 0.75 m/s. An interesting point is that the maximum open-loop forward speed of the ROV has increased from 0.97 m/s to 1.1 m/s with the addition of the bow-mounted camera. This occurs because the baseline vehicle tends to take up a bow-up attitude when moving forward; u is decreased because of the portion of the gravity vector (for this ROV, greater than the buoyancy vector) which points in the negative X direction. The negatively buoyant bow camera acts to limit the pitch angle and so, increases the top speed.

5.5.1 Closed-Loop Eigenvalues

The loci of the closed-loop eigenvalues are shown in figures 5.25 through 5.30 as a function of forward speed. These poles are calculated for a sampling rate of 5 Hz, originally in discrete time, though here they are converted and presented in the s-domain. The controller in place is that one calculated from the self-test of the baseline Seapup.

The surge modes, shown in figure 5.25, have approximately the same values as were calculated for the unmodified vehicle (figure 5.4a). At zero speed, they are slightly oscillatory and as u increases, become overdamped.

Comparing figures 5.6a and 5.27 shows that the heave modes again have a portion of their locus at the Nyquist frequency. This mode remains stable and overdamped at all speeds.

Though the sway and yaw modes have loci which migrate very much with forward speed, an undesirable quality, fortunately they remain well damped (figures 5.26 and 5.28). There are no obvious similarities between these loci and those in figures 5.5a and 5.7a for the unmodified vehicle.

Lastly, the roll and pitch modes can be seen to be well behaved from figures 5.29 and 5.30. The pitch locus is similar to that of the baseline vehicle. It is oscillatory and becomes more damped with increasing velocity. The roll mode also has this quality, in contrast to its counterpart for the unmodified ROV, which becomes unstable for speeds greater than 0.8 m/s (figure 5.8a).

This section is concluded by noting that the open-loop nonminimum phase crossover point is not as evident from the closed-loop poles as it was with the unmodified ROV. Here, in general, pole migration is more distributed over the entire range of speeds, rather than being associated with this critical surge velocity.

5.5.2 Response to Step Changes in Reference Values

The step responses that are to be compared here to those of the baseline vehicle are the surge test, the medium speed turn and the inspection manoeuver. Each of these will be considered in turn.

a: Surge Test (figure 5.31)

As expected, the extra mass caused the 95 percent rise time to increase slightly from 1.4s to 1.6s. However, other factors have improved. The overshoot in surge velocity is down from 1.7 percent to 0.8 percent and the interaction effects on sway, heave and yaw velocities have also decreased. Of course, the initial peak value in pitch angle is less than when the baseline vehicle was simulated as is the final value of pitch angle (10.9 degrees as compared with 14.3 degrees). The action of the thrusters goes through a similar transient and then quickly settles to a different steady-state.

b: Medium Speed Turn (figure 5.32)

The system has responded well here. Again, the only notable changes have been the slight increase in rise times and a different steady-state pitch angle.

c: Inspection Manoeuver (figure 5.33)

This simulation is also very similar to its baseline counterpart. The response of the system is very good, with fast rise times, zero steady-state errors and little interaction.

5.5.3 Discussion

The control system has been shown to be tolerant to a change in physical configuration of a fairly large magnitude. Though some of the closed-loop poles have migrated a large amount with increased forward speed, these modes have turned out to be well damped. This is confirmed by examining the responses of the vehicle to the different reference velocity changes, all of which are good.

5.6 Summary

The success of the self-test algorithm and velocity controller has been evaluated by considering a number of features. The self-test algorithm performed well at zero forward speed since the values of time constant and steady-state gain it calculated were similar to those chosen manually from a log of velocities achieved during a series of step tests. This could not be said of the self-test executed at 0.7 m/s because steady-state errors were observed during step response simulations when linear gain scheduling was utilised. The self-test at this speed failed because of the non-quiescent initial conditions. Otherwise, these simulations showed that the vehicle responds very well to a variety of reference inputs. While gain scheduling did not prove to be beneficial, an increased sampling rate of 20 Hz did shorten response times. The faster sampling also

helped limit the effects of current and turbulence. Even when operating at 5 Hz, the system was found to partially reject such disturbances, holding the vehicle within centimeters in linear displacement.

A method of calculating the closed-loop poles for the combined continuous-time vehicle and discrete-time controller was described and the root loci of the various modes plotted as functions of ahead speed. It was shown that the controller can achieve the desired closed-loop poles if the self-test has identified the open-loop model with sufficient accuracy and that nonminimum phase behaviour can adversely effect the system.

The robustness of the controller was evaluated by considering the addition of an object, about the size of a television camera, to the bow of the vehicle. The closed-loop system still yielded excellent responses to reference inputs.

Table 5.1

Comparison of Identified Approximate Models at u_o = 0.0 m/s

Output	Input	Initial Values			Final Values		
		Velocity Log	Artificial Quiescence	Realistic Quiescence	Velocity Log	Artificial Quiescence	Realistic Quiescence
u	1	.00226	.002199	.002575	.0246	.02658	.02605
u	2	.00226	.002199	.002455	.0246	.02658	.02600
u	3	.000125	.0000050	.0001045	.00064	-.0001568	.002520
u	4	.000125	.0000050	-.00003116	.00064	-.0001568	.001034
v	1	-.0001	-.00004576	-.00008308	-.00409	.005354	-.01515
v	2	.0001	.00004576	.00006323	.00409	-.005354	-.1780
v	3	-.0004265	-.0004329	-.0004354	-.00766	-.007970	-.006480
v	4	.0004265	-.0004329	.0004922	.00766	.007970	.007750
w	1	.0000625	-.000008689	-.00004197	-.0006	-.0004368	-.0004332
w	2	.0000625	-.000008689	-.00002950	-.0006	-.0004368	-.0005488
w	3	.000525	.0006522	.0005101	.004875	.006392	.004799
w	4	.000525	.0006522	.0005715	.004875	.006392	.004458
r	1	.2629	.2794	.3091	1.9612	2.440	2.015
r	2	-.2629	-.2794	-.2963	-1.9612	-2.440	-1.937
r	3	.001588	-.002356	-.004264	-.0499	.1257	1.537
r	4	-.001588	.002356	.003690	.0499	-.1257	-0.3942

Table 5.2

Comparison of Identified Approximate Models at u_o = 0.7 m/s

Output	Input	Initial Values			Final Values		
		Velocity Log	Artificial Quiescence	Realistic Quiescence	Velocity Log	Artificial Quiescence	Realistic Quiescence
u	1	.00325	.03201	.02538	.01514	.1531	.1050
u	2	.00325	.03201	.02462	.01514	.1531	.1054
u	3	-.001125	.03242	.01840	-.00565	-.00565	.09559
u	4	-.001125	.03242	.01770	-.00565	-.00565	.09189
v	1	-.00025	-.0005997	-.0008928	-.0070	-.006661	-.008324
v	2	.00025	.0005997	.001190	.0070	.00661	.008707
v	3	-.0013	-.0008753	-.0003327	-.0049	-.004026	-.001728
v	4	.0013	.0008753	.0004845	.0049	.004026	.001747
w	1	.000375	-.00002044	-.0002060	-.0006	-.0002020	-.001905
w	2	.000375	-.00002044	-.0003528	-.0006	-.0002020	-.001390
w	3	.0120	.001236	.00009995	.00209	.001965	.0001234
w	4	.0120	.001236	.0003195	.00209	.001965	.0004066
r	1	.3617	.2808	.4114	1.3419	1.2070	1.609
r	2	-.3617	-.2808	-.5212	-1.3419	-1.2070	-1.635
r	3	-.009825	-.03030	-.01185	-0.1310	-0.1681	-0.2438
r	4	.009825	.03030	.02909	0.1310	0.1681	0.2116

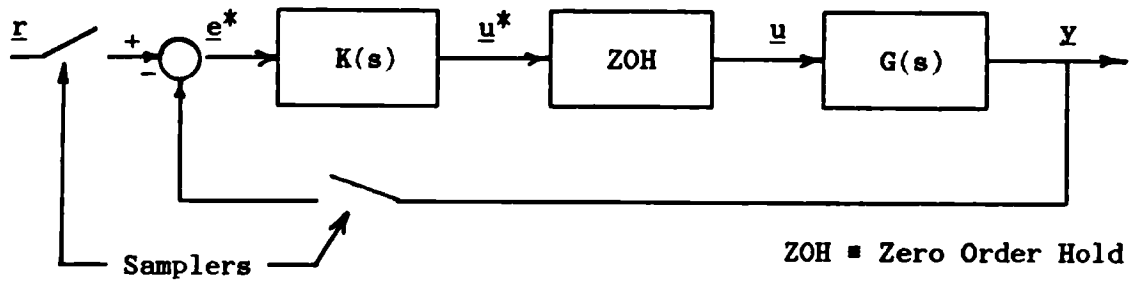

Figure 5.1 : Closed-Loop Control System

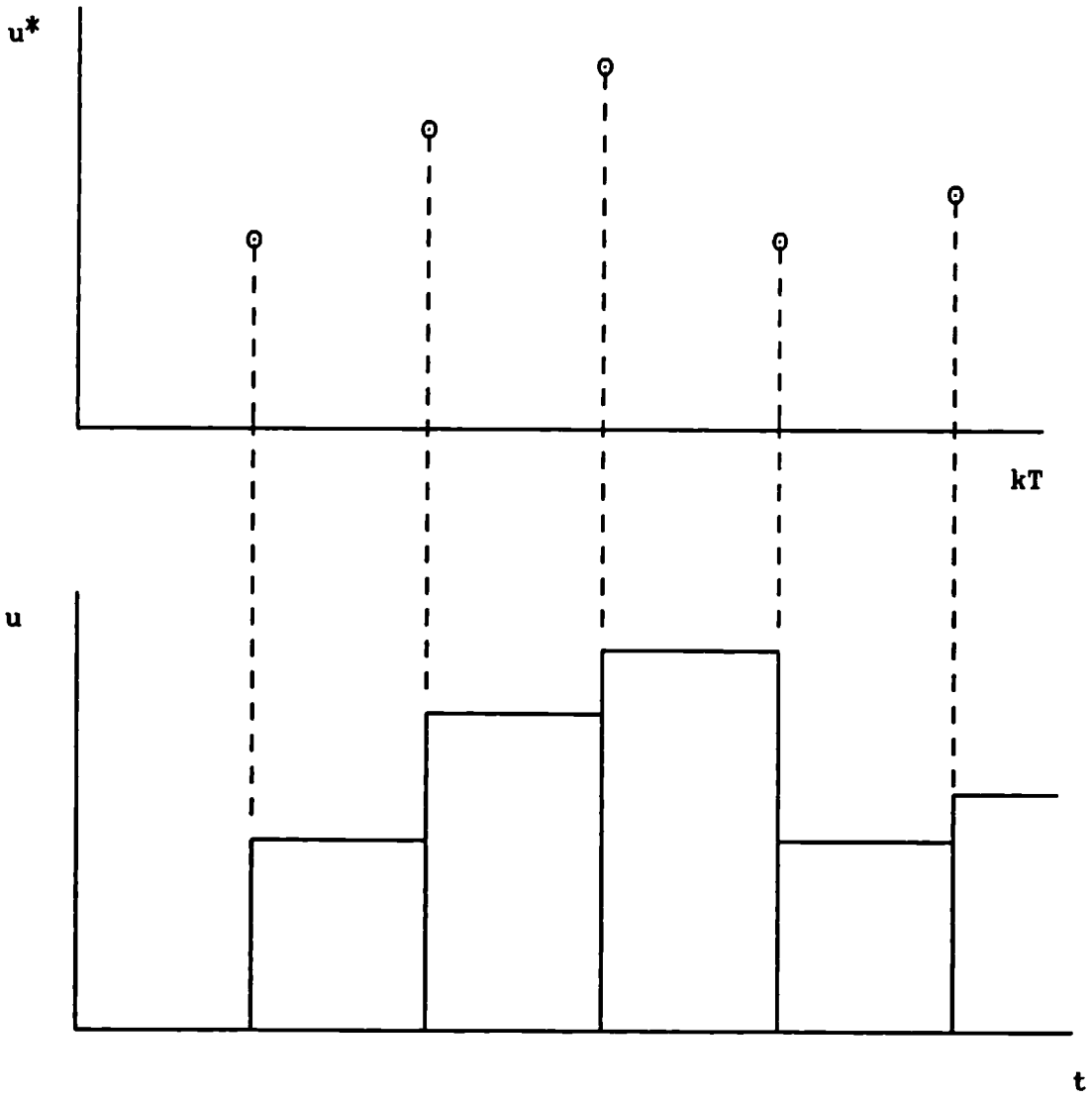

Figure 5.2 : The Zero Order Hold Model

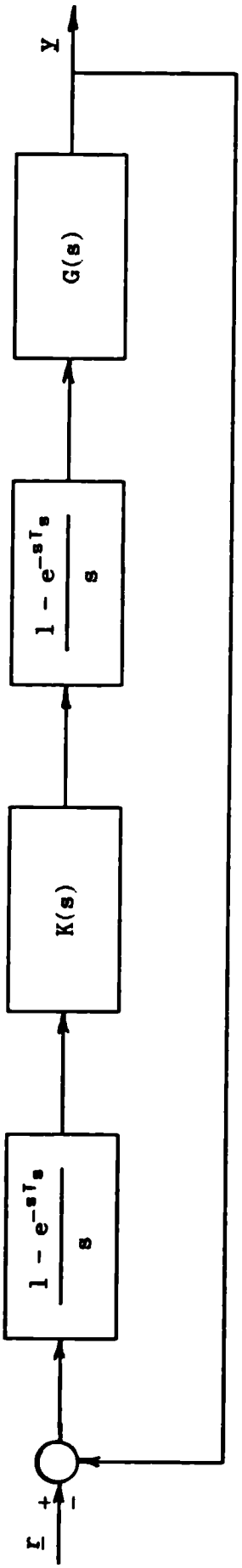

Figure 5.3 : The Equivalent Continuous System

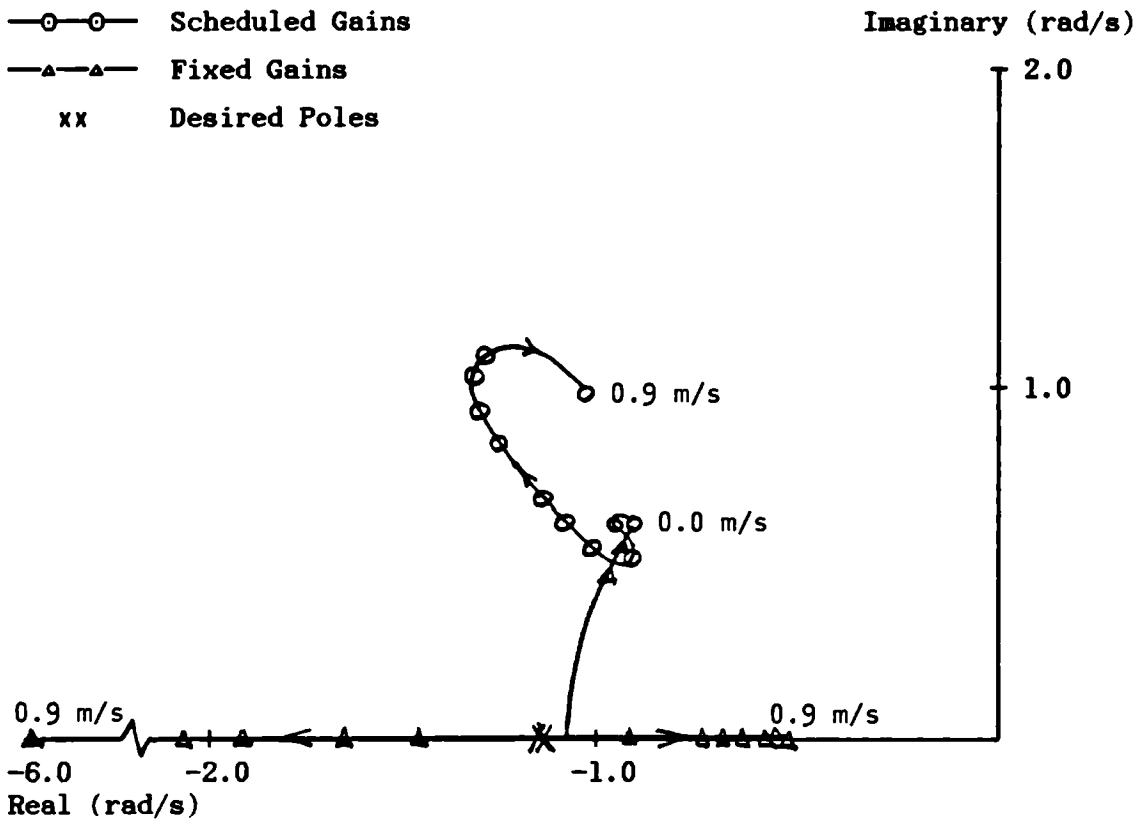

a) Sampling Frequency = 5 Hz

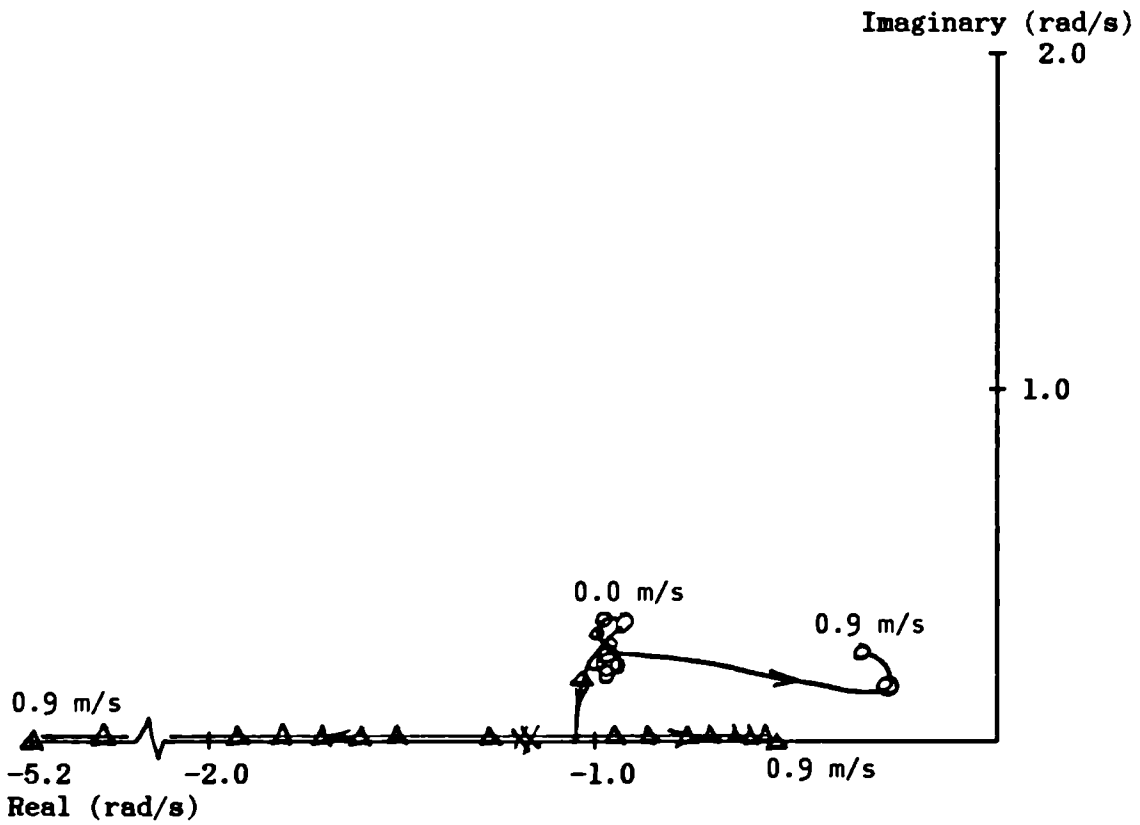

b) Sampling Frequency = 20 Hz

Figure 5.4 : Locus of Surge Mode Eigenvalues

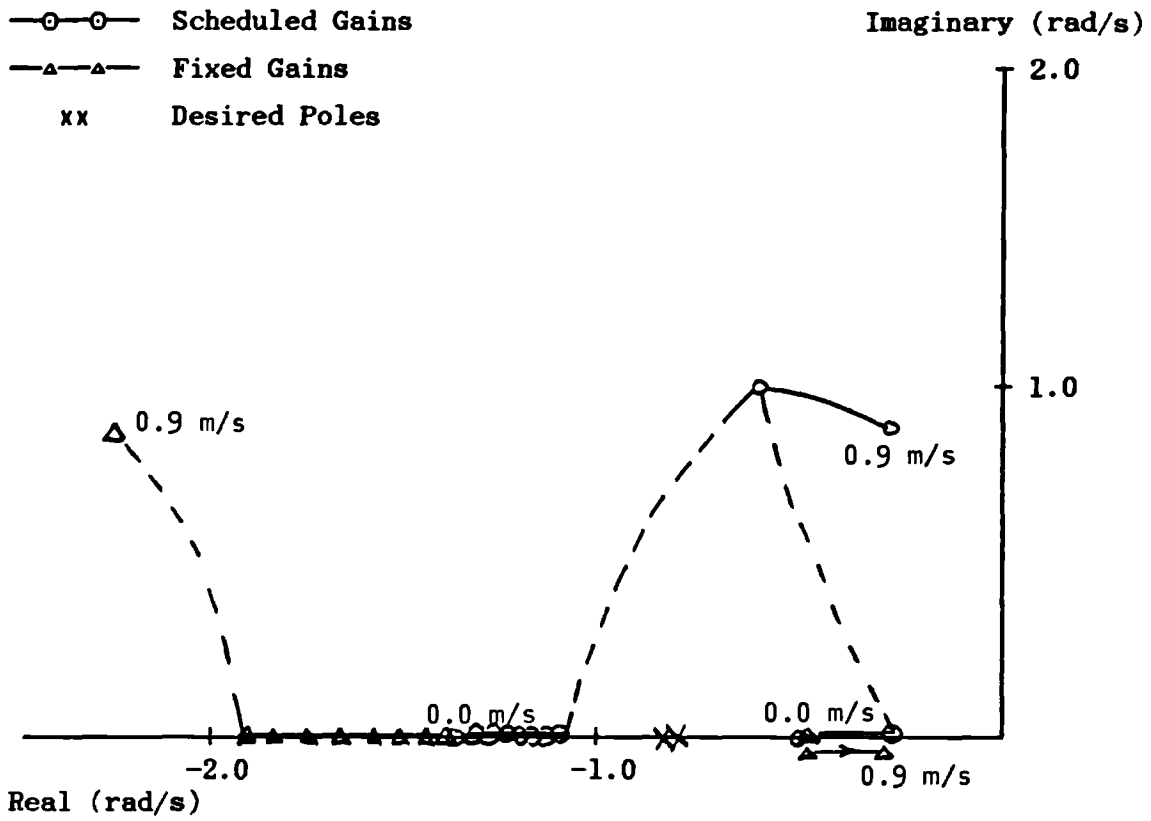

a) Sampling Frequency = 5 Hz

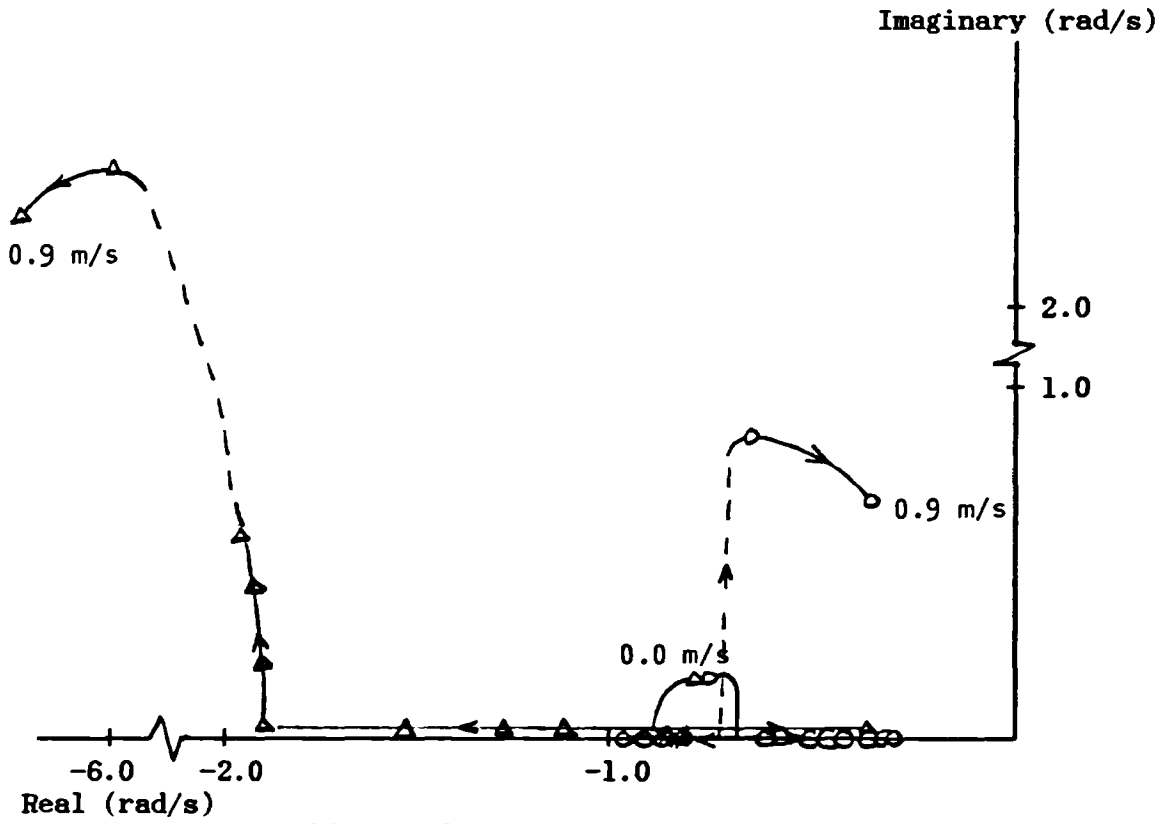

b) Sampling Frequency = 20 Hz

Figure 5.5 : Locus of Sway Mode Eigenvalues

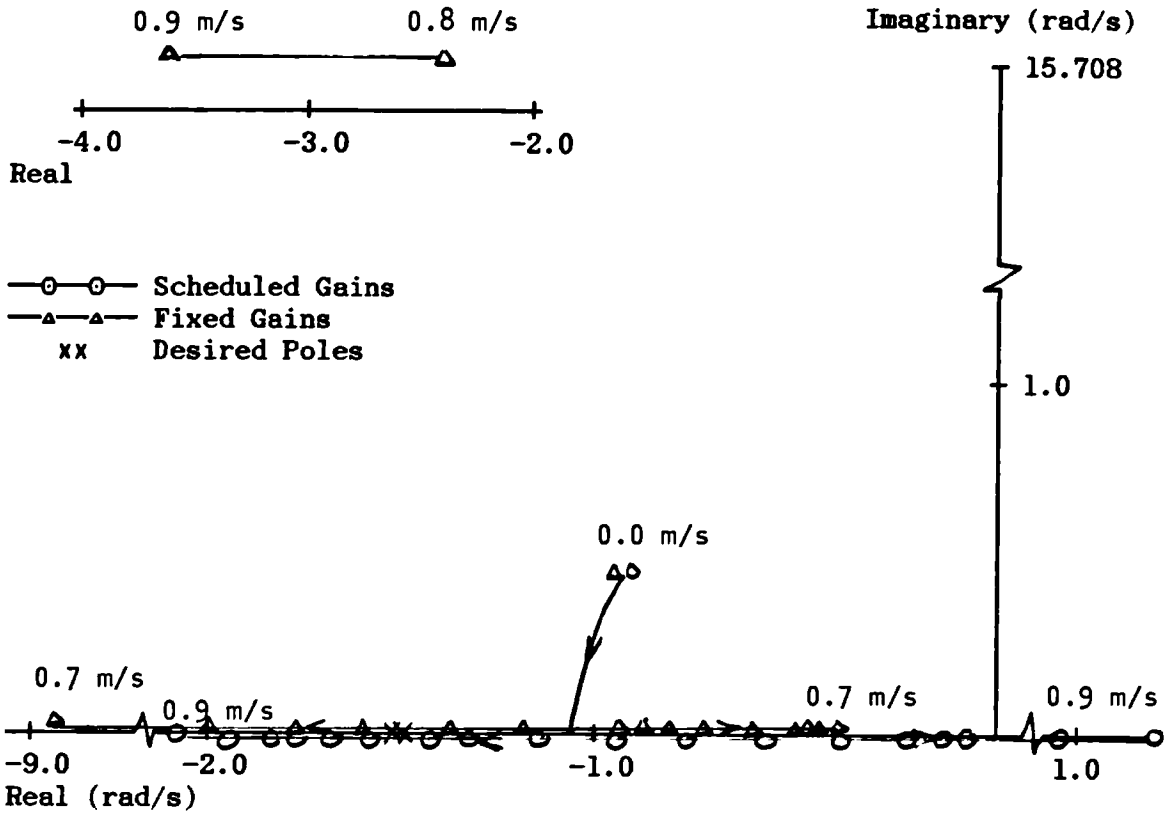

a) Sampling Frequency = 5 Hz

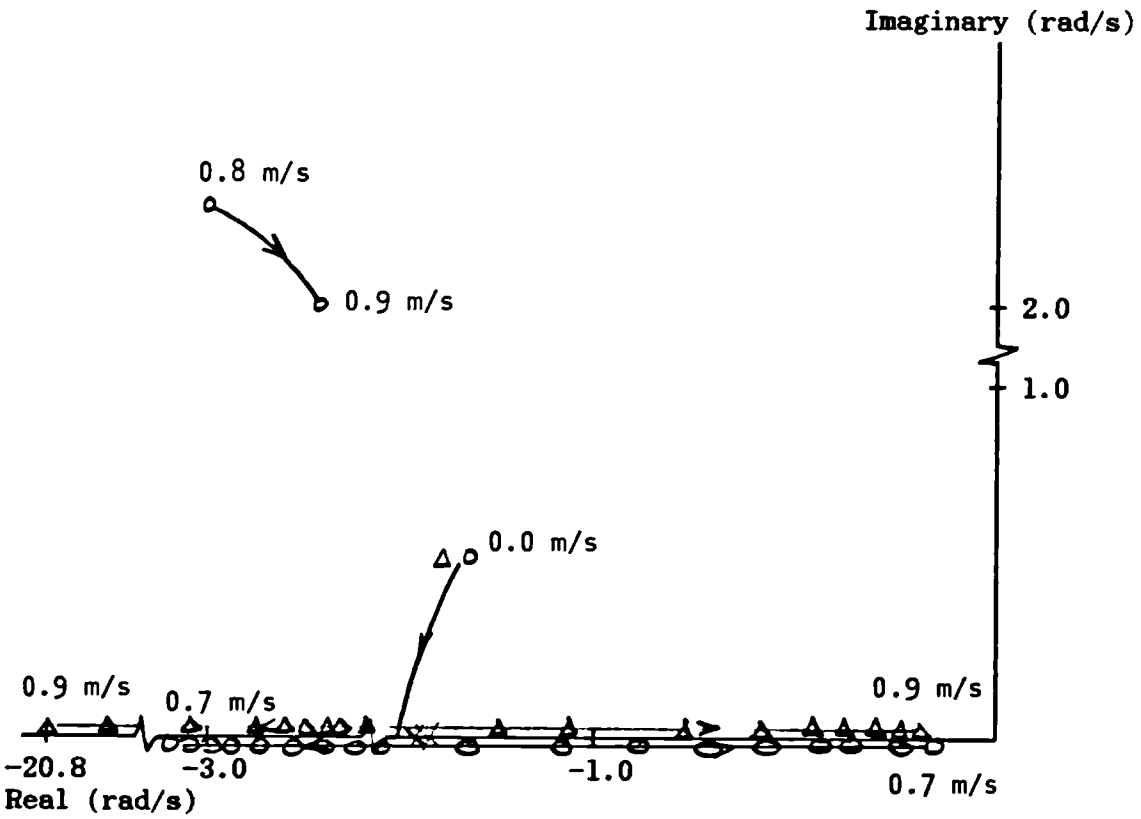

b) Sampling Frequency = 20 Hz

Figure 5.6 : Locus of Heave Mode Eigenvalues

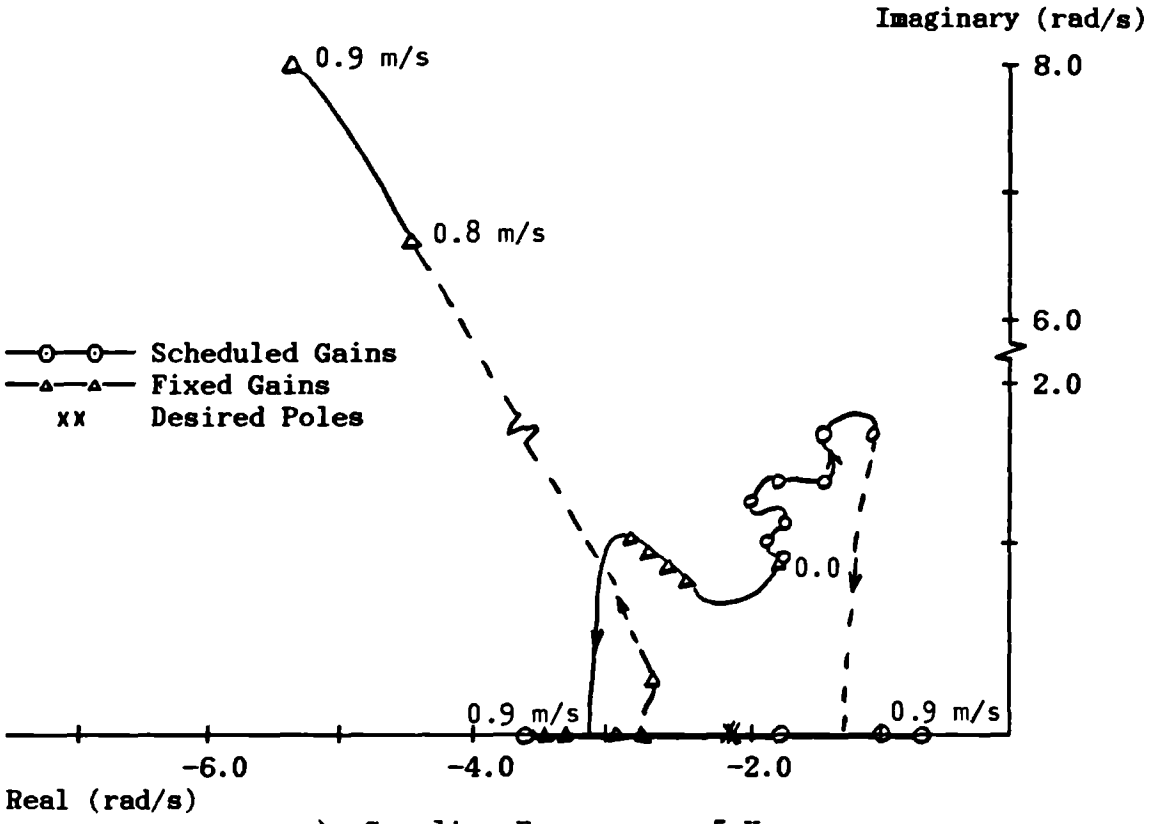

a) Sampling Frequency = 5 Hz

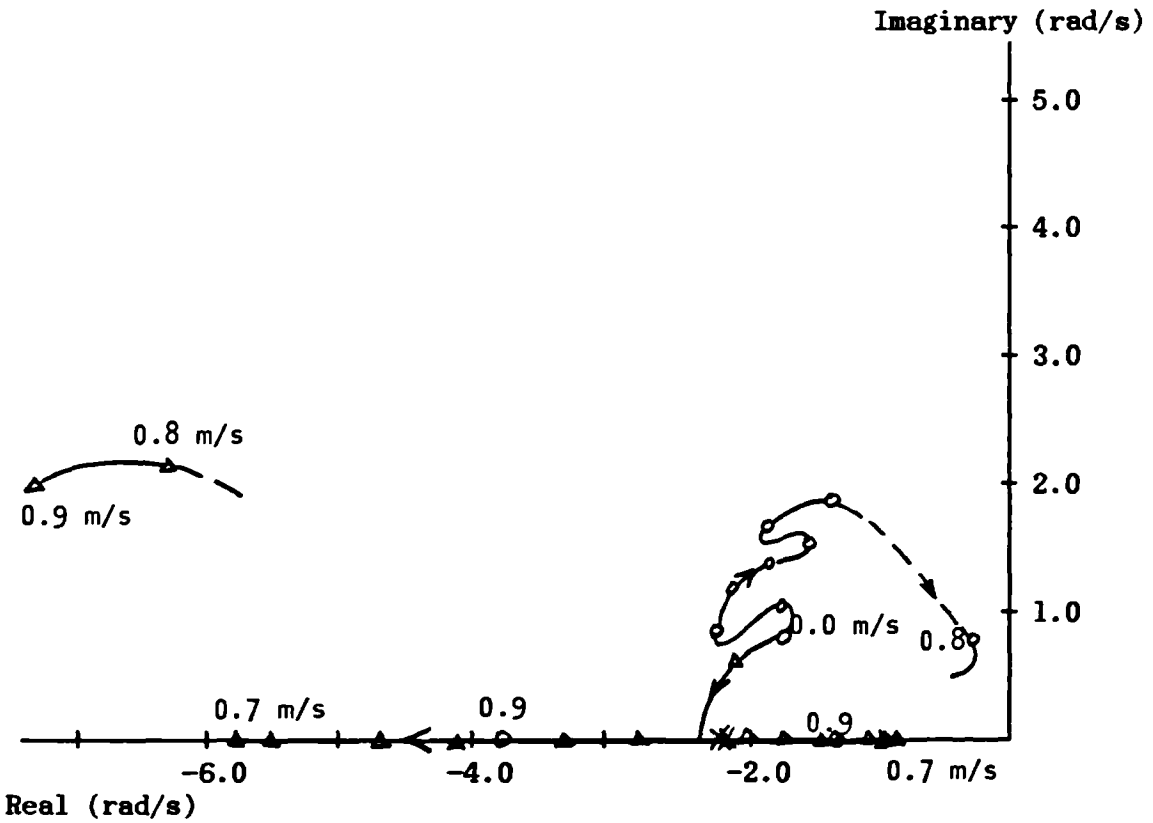

b) Sampling Frequency = 20 Hz

Figure 5.7 : Locus of Yaw Mode Eigenvalues

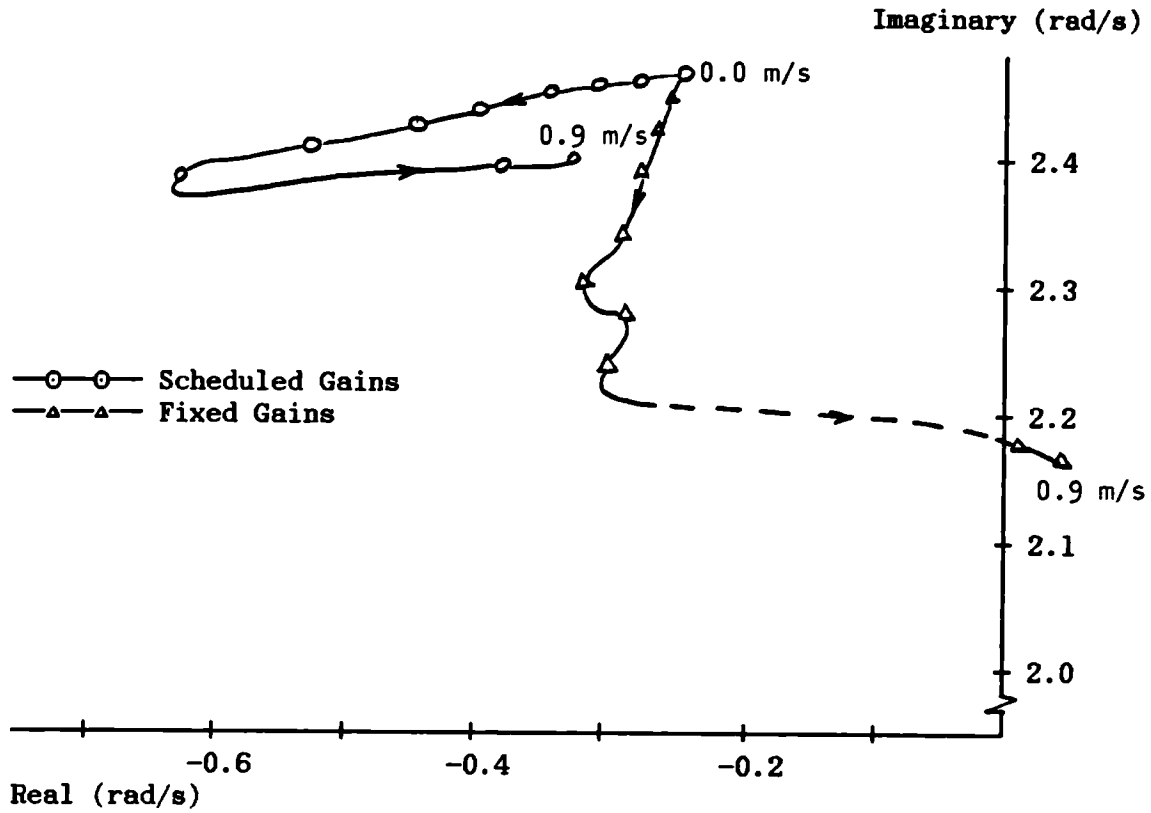

a) Sampling Frequency = 5 Hz

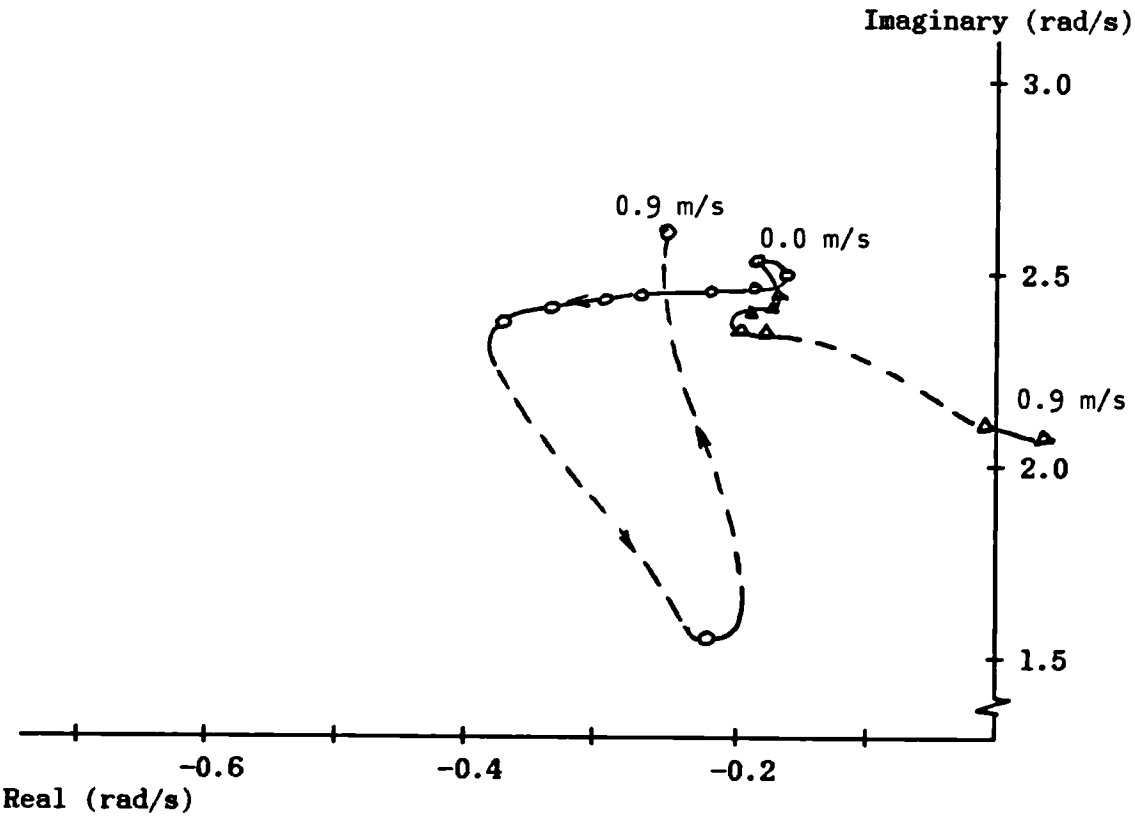

b) Sampling Frequency = 20 Hz

Figure 5.8 : Locus of Roll Mode Eigenvalues

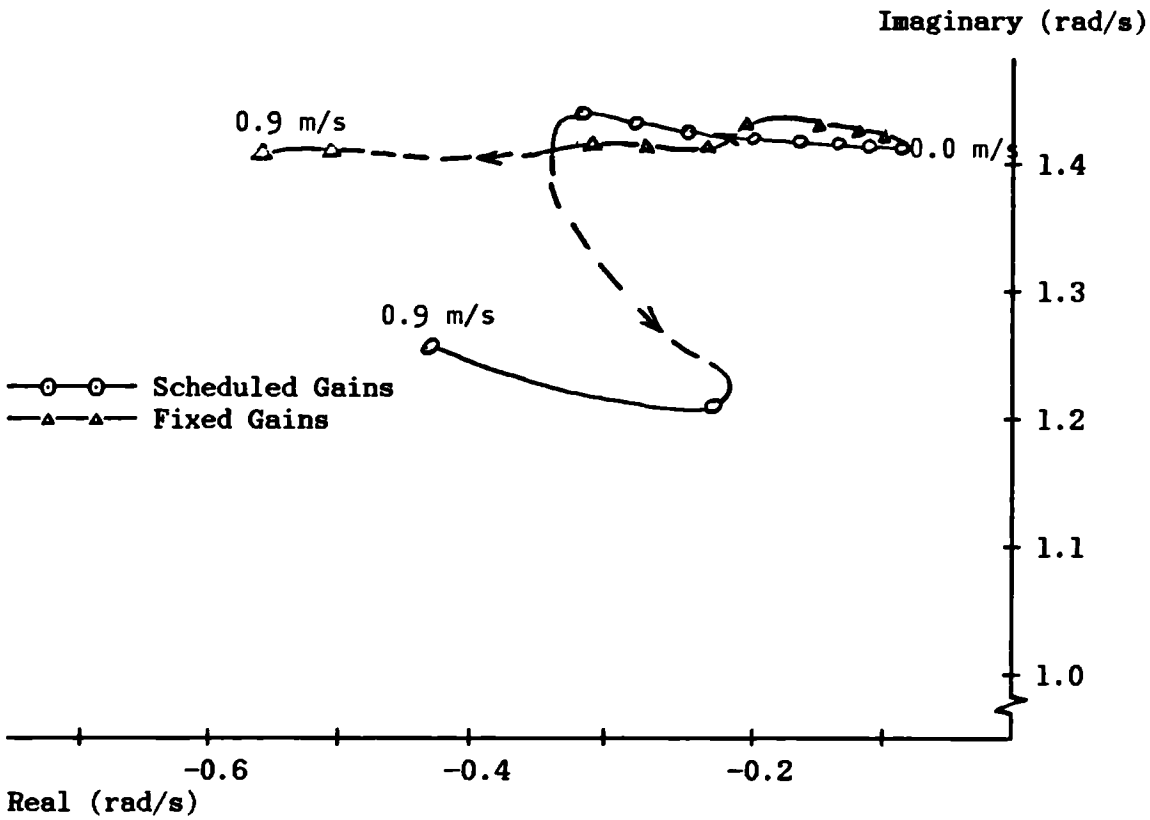

a) Sampling Frequency = 5 Hz

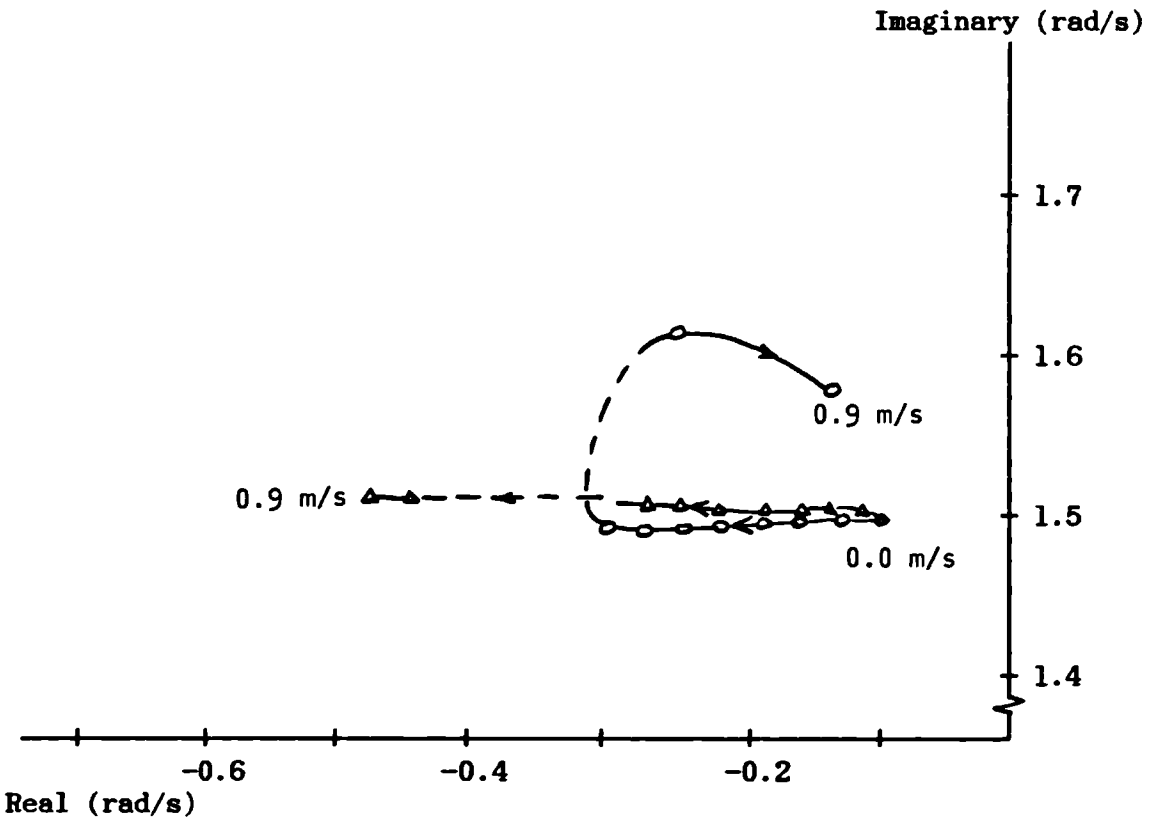

b) Sampling Frequency = 20 Hz

Figure 5.9 : Locus of Pitch Mode Eigenvalues

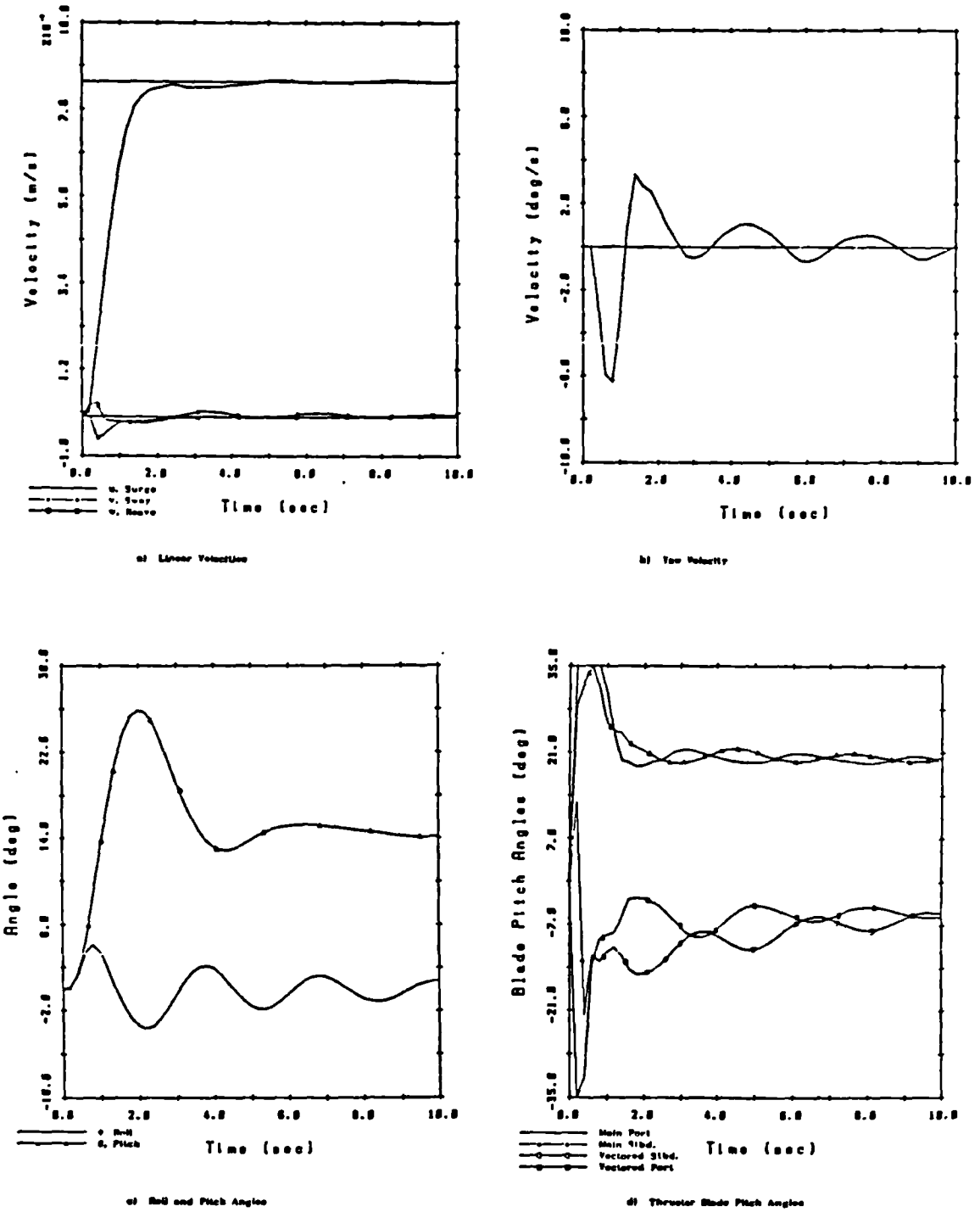

Figure 5.10 .: Closed-Loop Response to Step Change in Surge Velocity

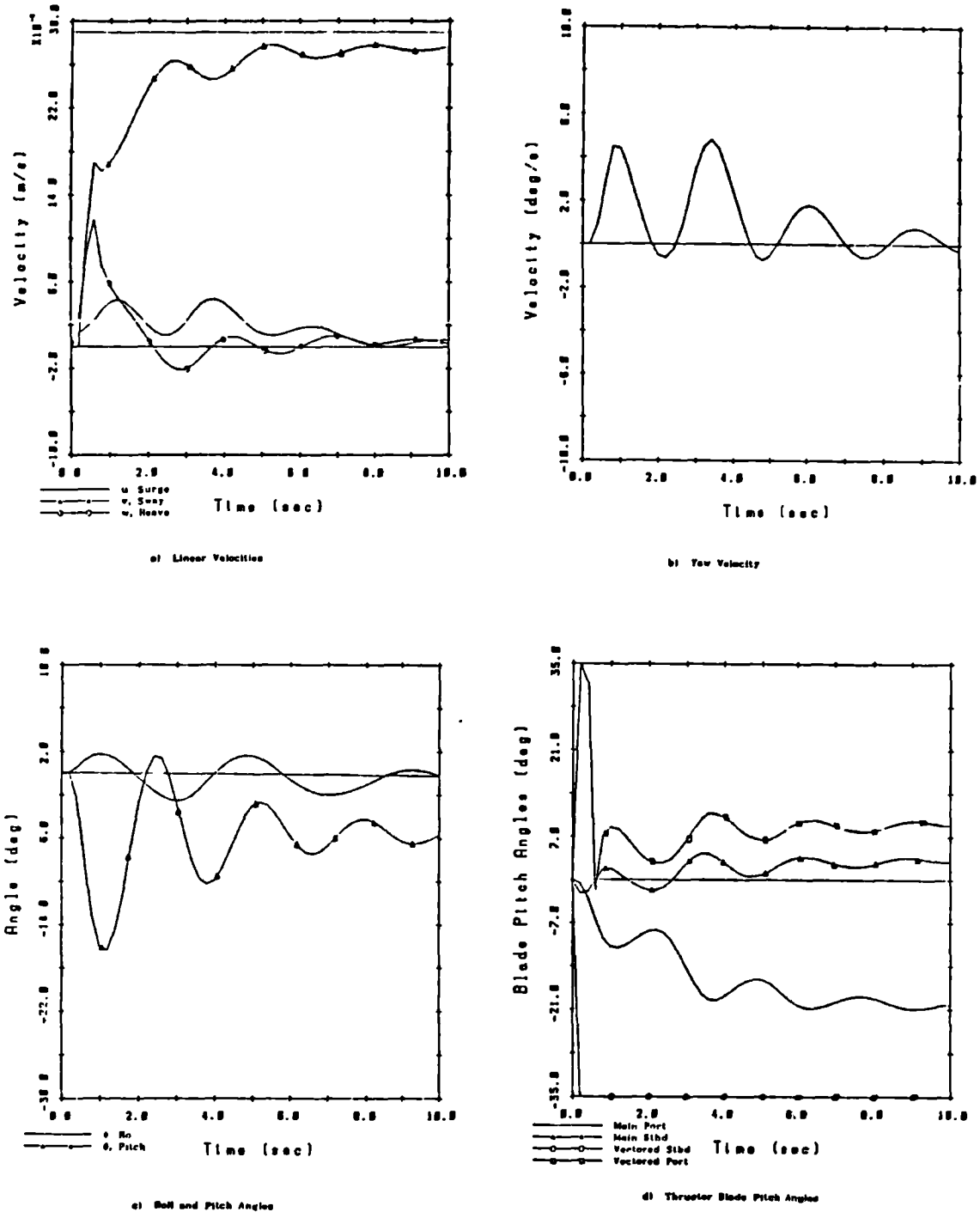

Figure 5.11 : Closed-Loop Response to Step Change in Sway Velocity

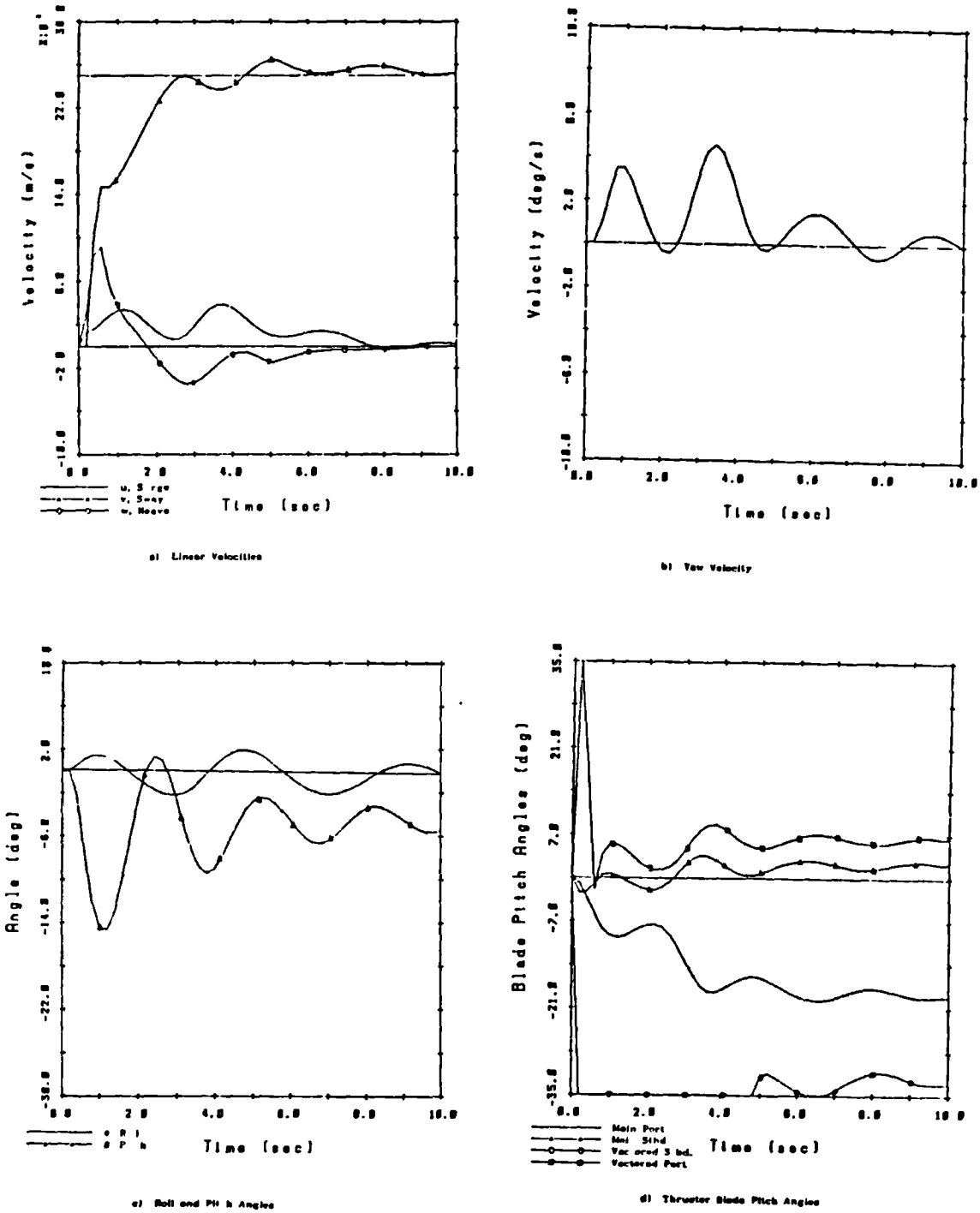

Figure 5.12 : Closed-Loop Response to Step Change
in Sway Velocity
Decreased Reference Velocity, v = 0.25 m/s

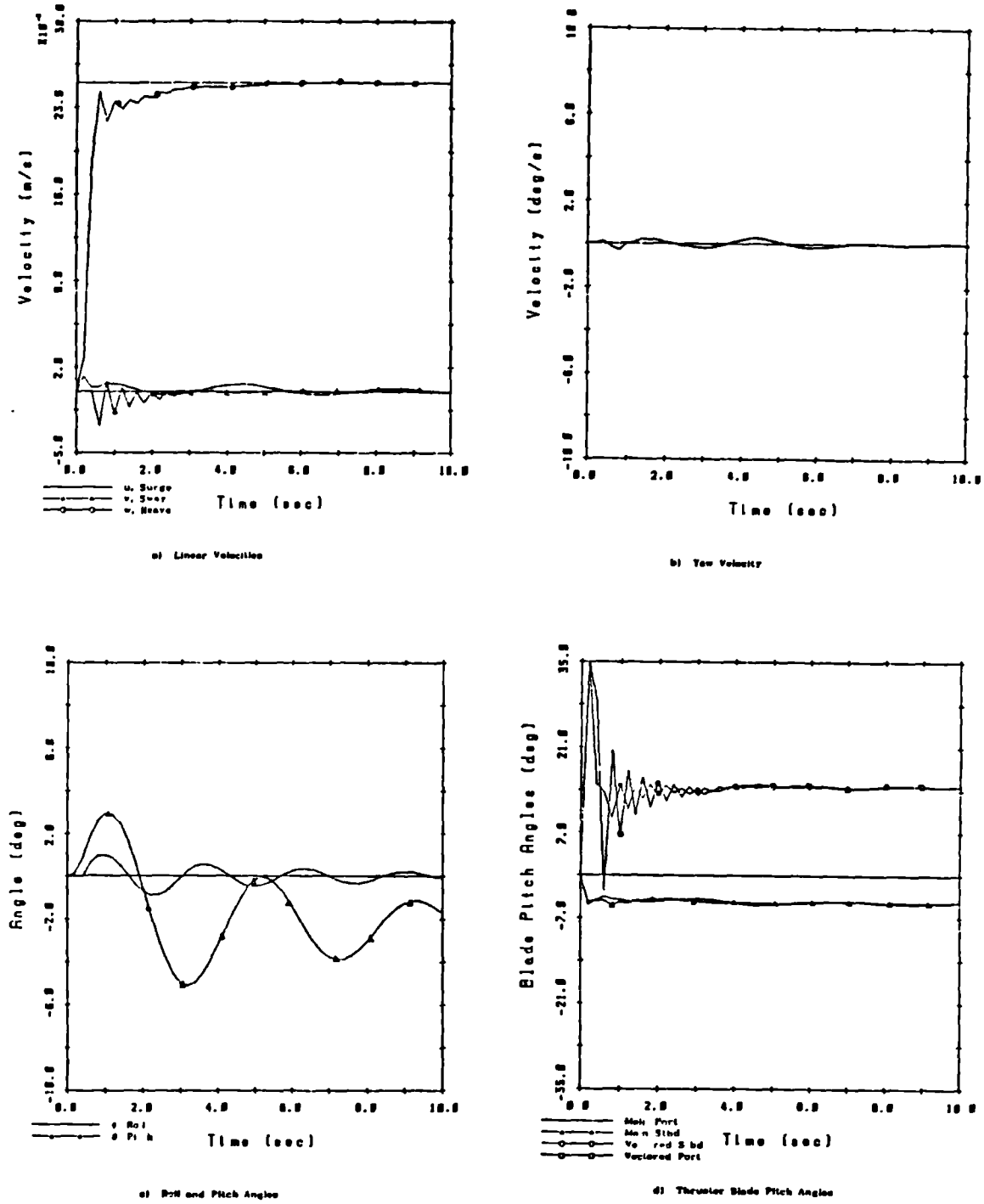

Figure 5.13 : Closed-Loop Response to Step Change in Heave Velocity

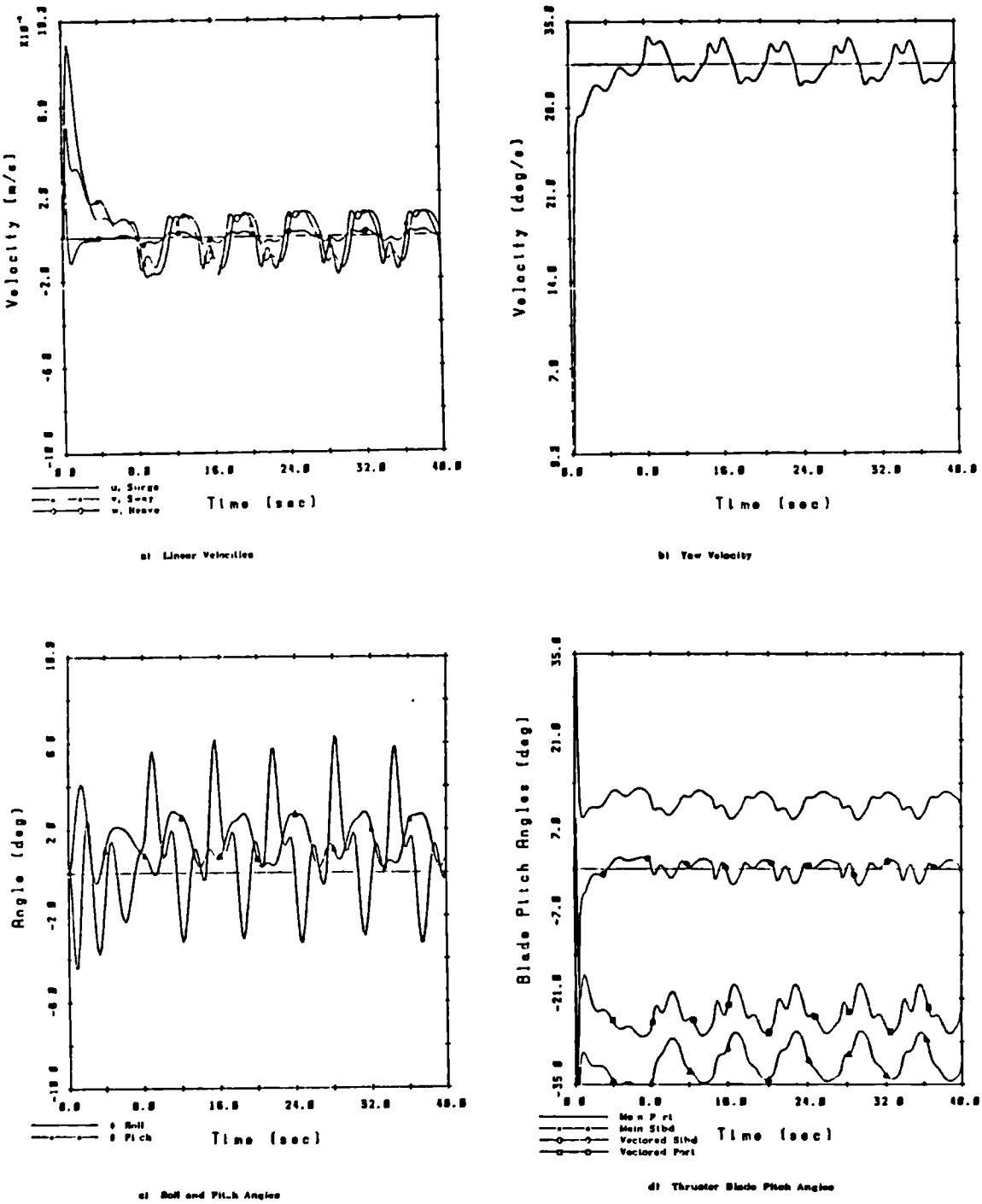

Figure 5.14 : Closed-Loop Response to Step Change in Yaw Rate

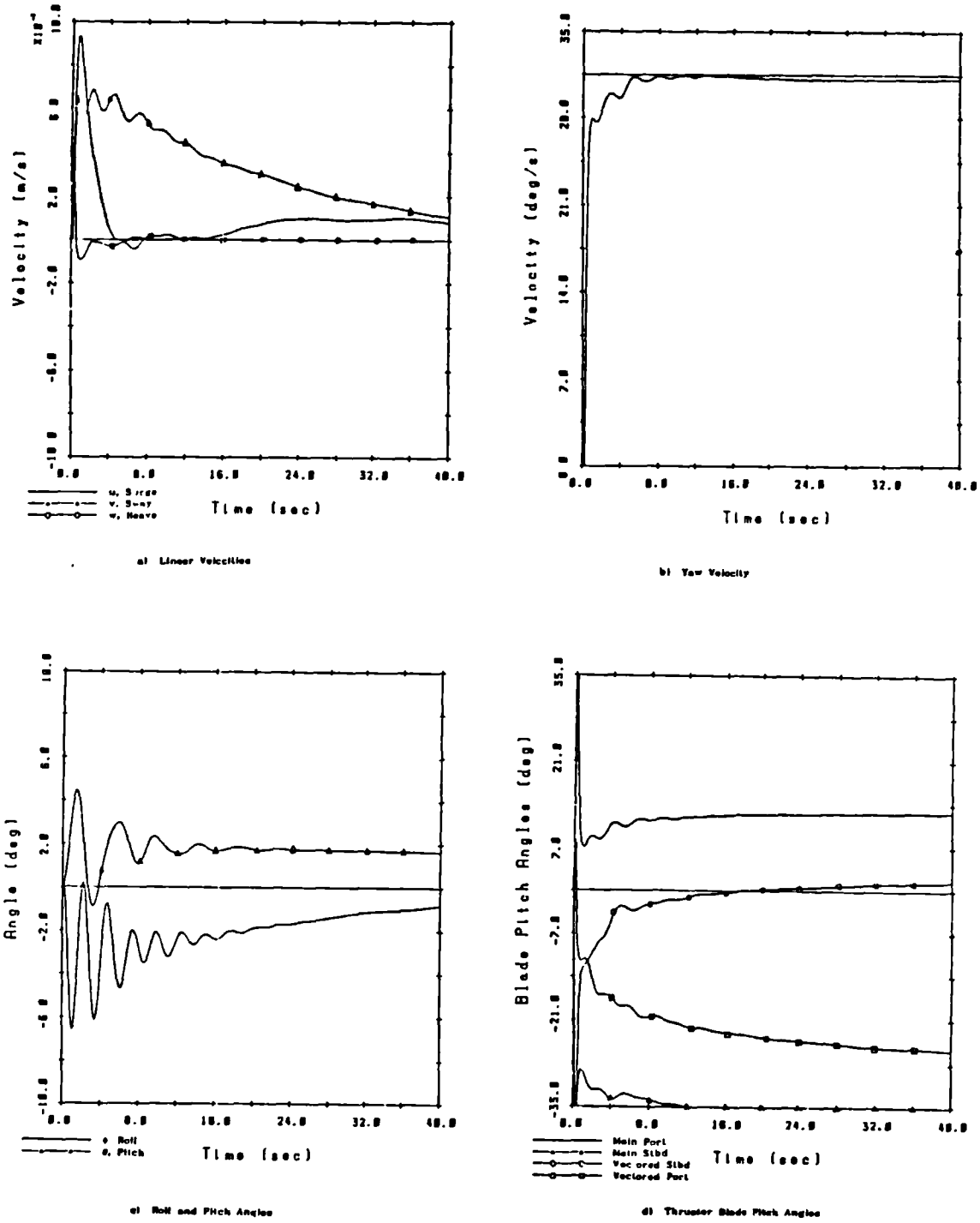

Figure 5.15 : Closed-Loop Response to Step Change in Yaw Rate; Slower Sway Poles, $k_2 = c_2 = 0.95$

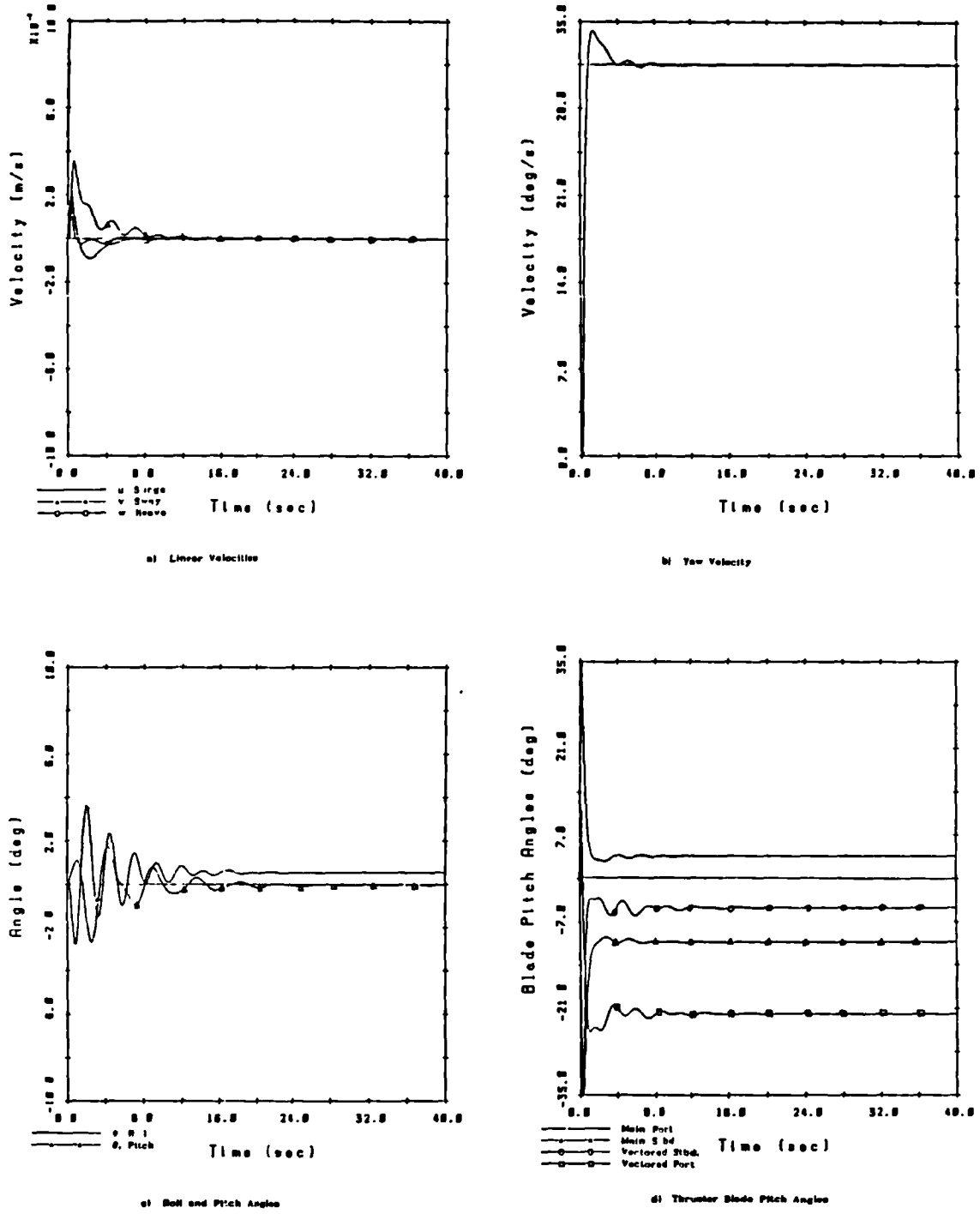

Figure 5.16 : Closed-Loop Response to Step Change in Yaw Rate; Linearised ROV Model

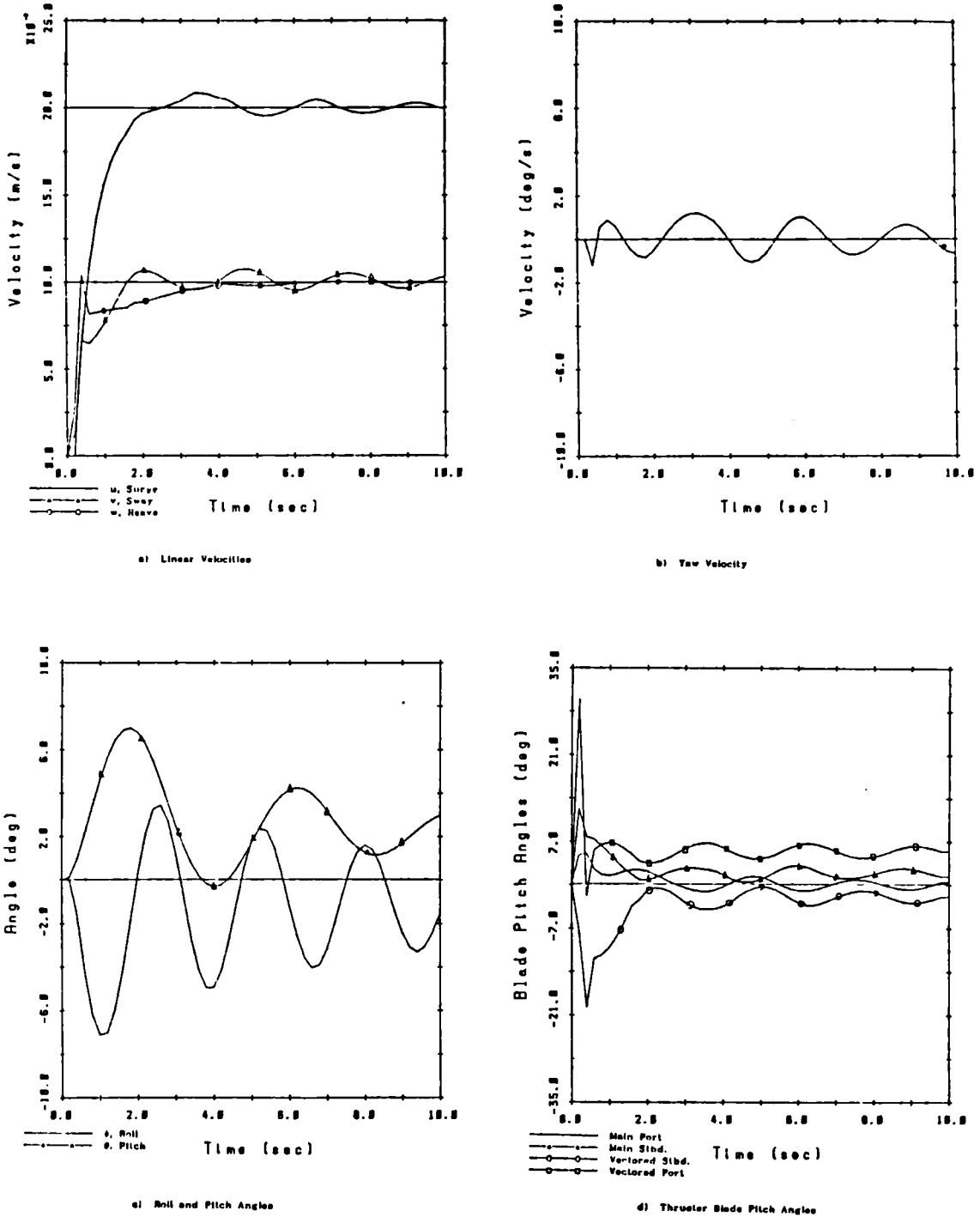

Figure 5.17 : Closed-Loop Response to Inspection Manoeuver Command

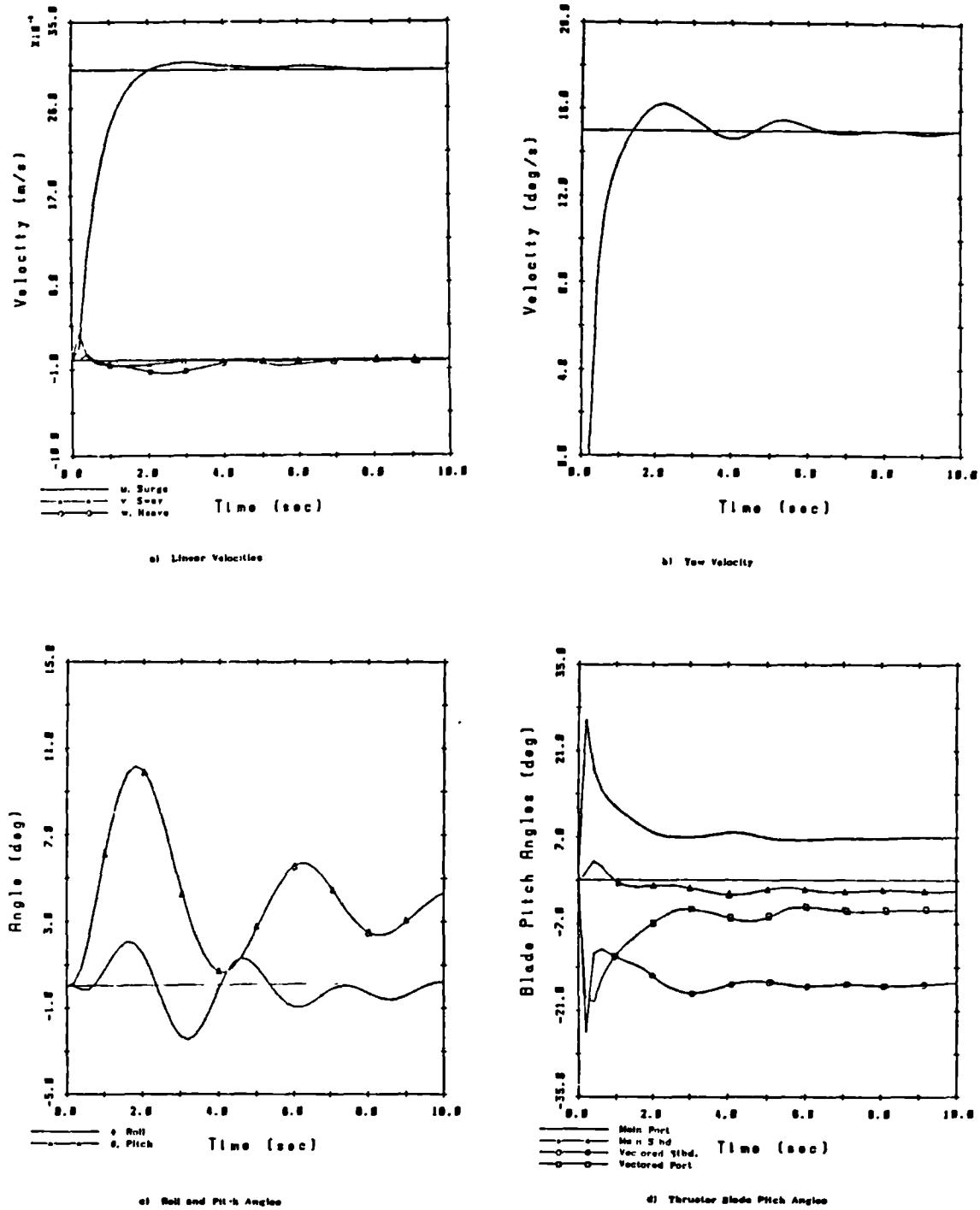

Figure 5.18 : Closed-Loop Response to Medium Speed Turn Command

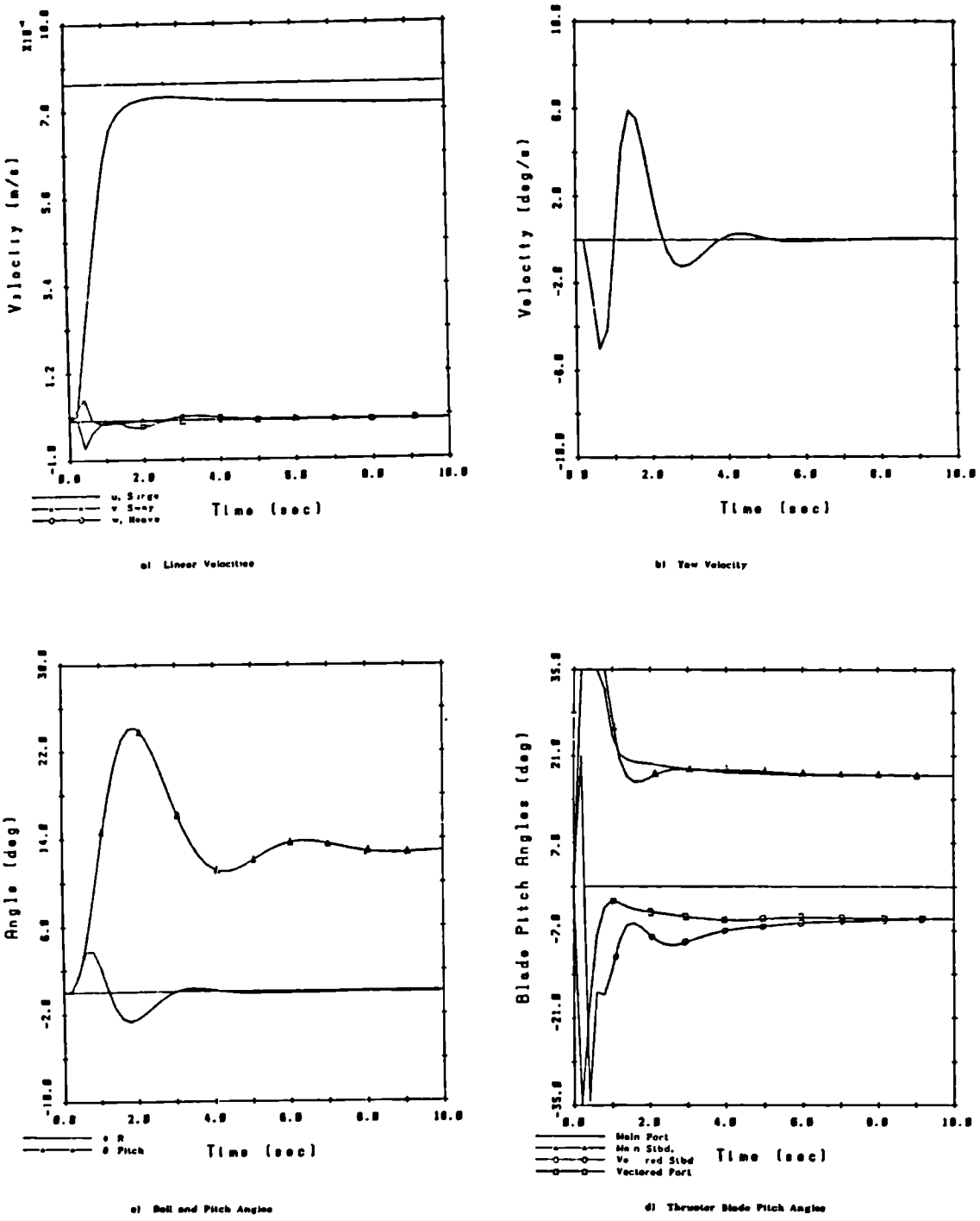

Figure 5.19 : Closed-Loop Response to Step Change in Surge Velocity; Linear Gain Scheduling

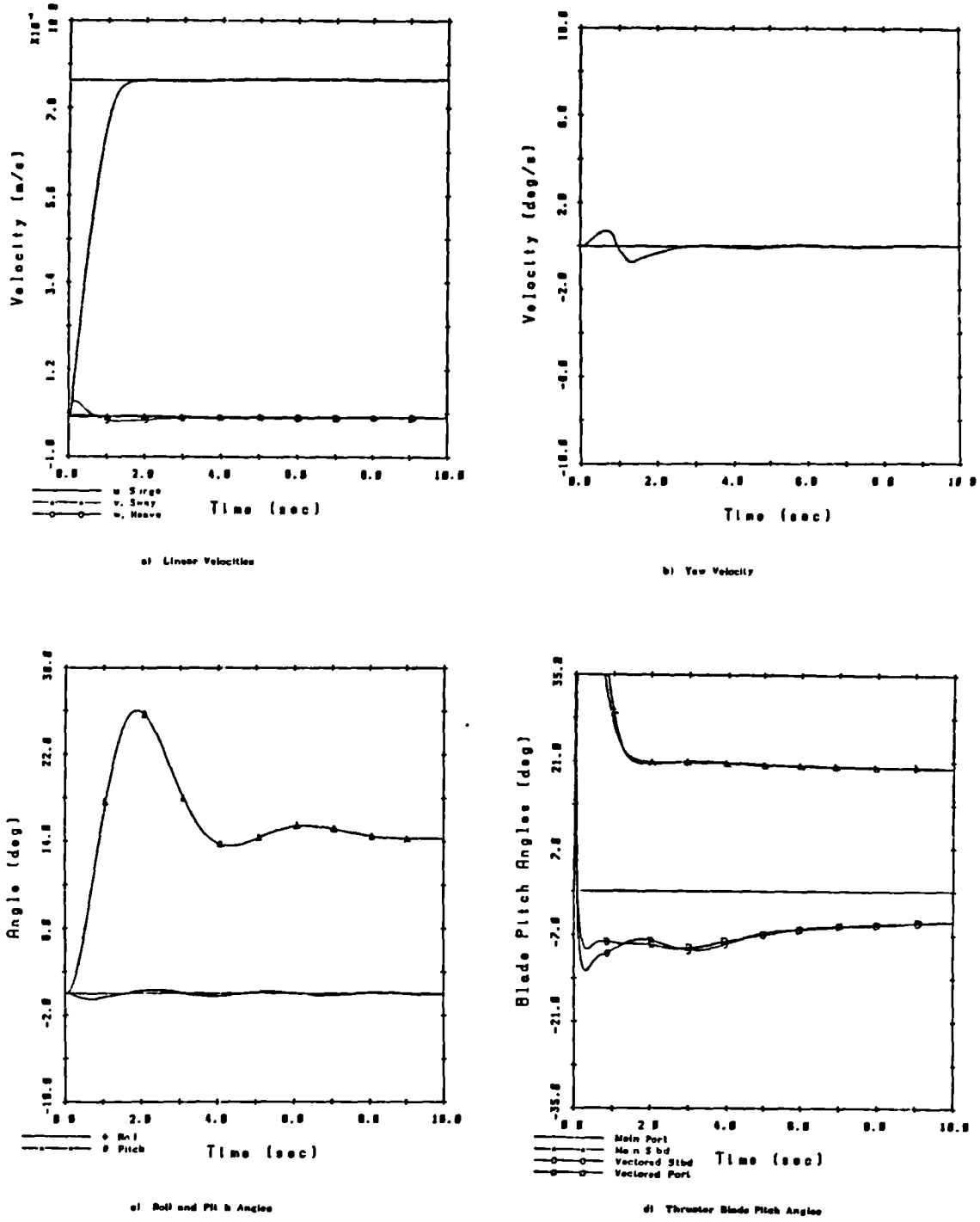

Figure 5.20 : Closed-Loop to Step Change in Surge Velocity; Faster Sampling Rate, 20 Hz

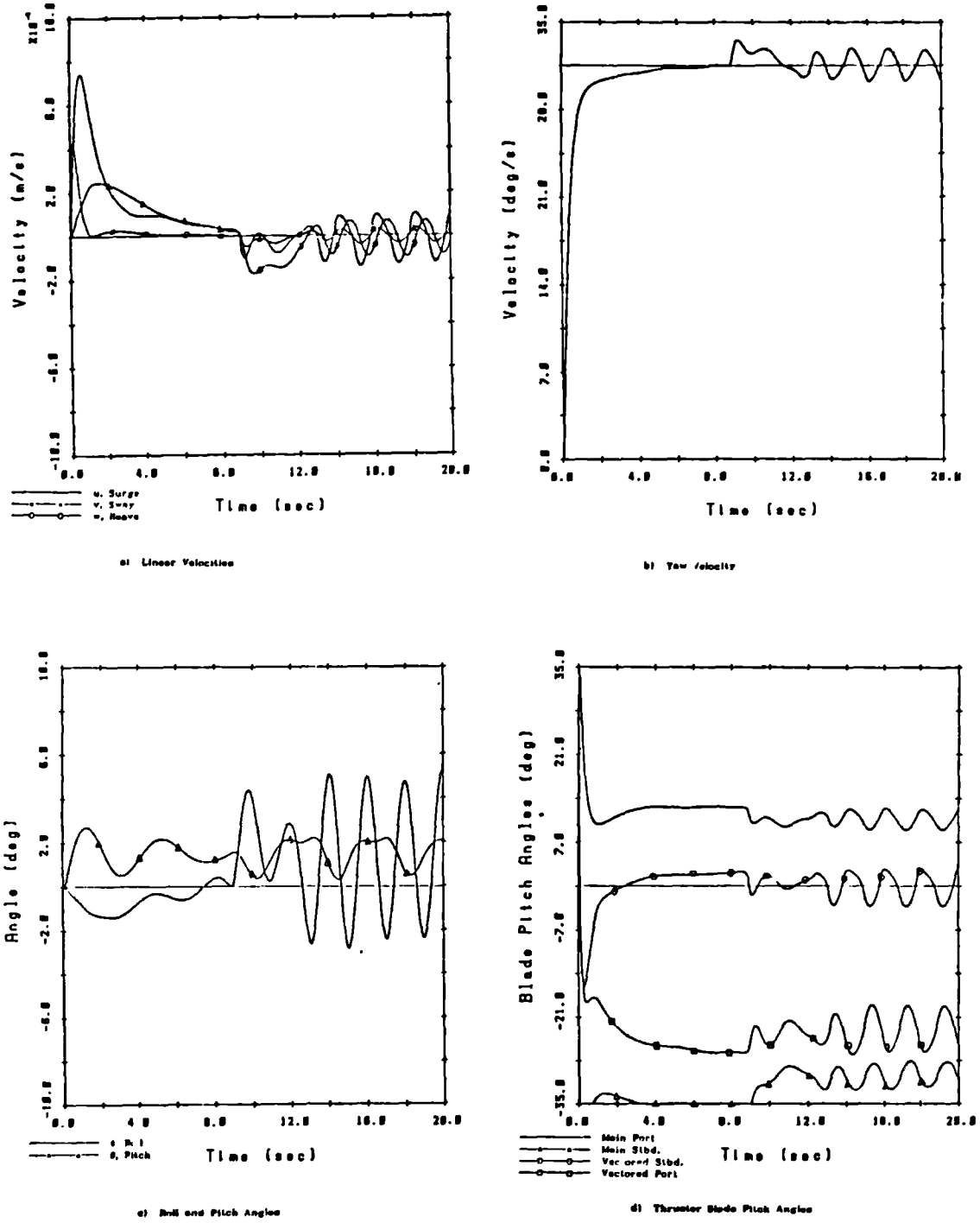

Figure 5.21 : Closed-Loop Response to Step Change in Yaw Rate; Faster Sampling Rate, 20 Hz

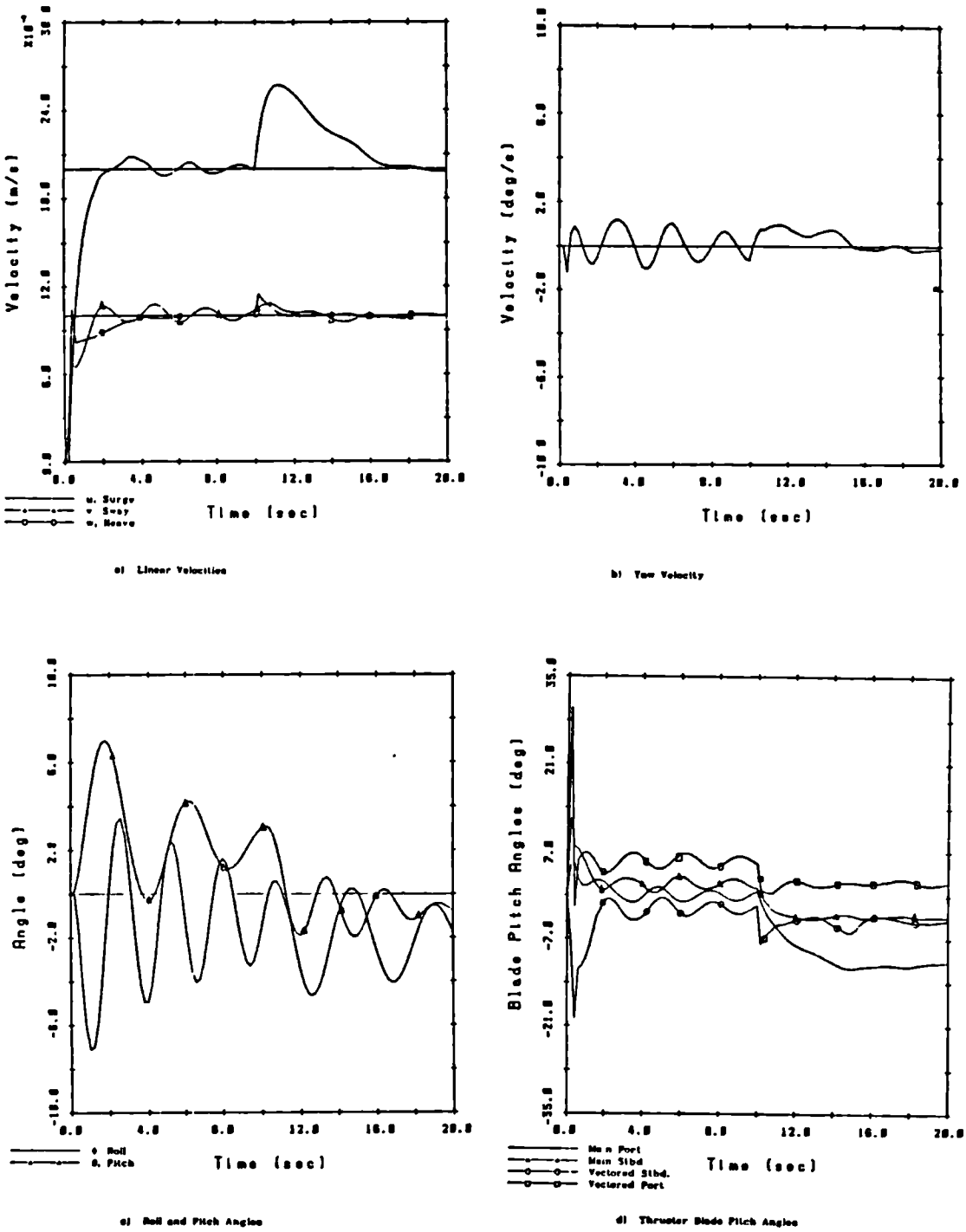

Figure 5.22 : Closed-Loop Response to Inspection Manoeuver Command; Step Change in Disturbance Current at 10s

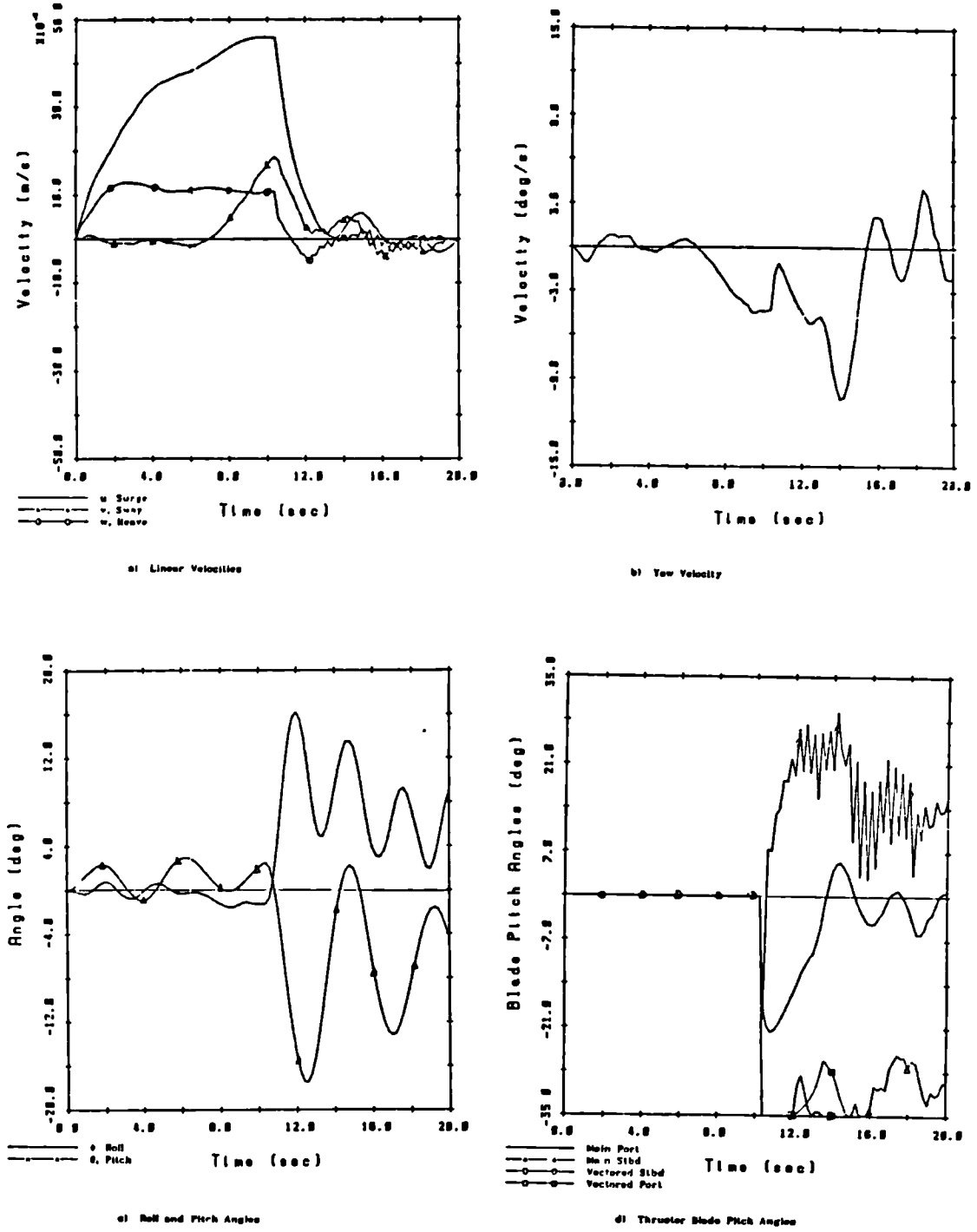

Figure 5.23 : Closed-Loop Response to Station Holding in a Stochastic Current

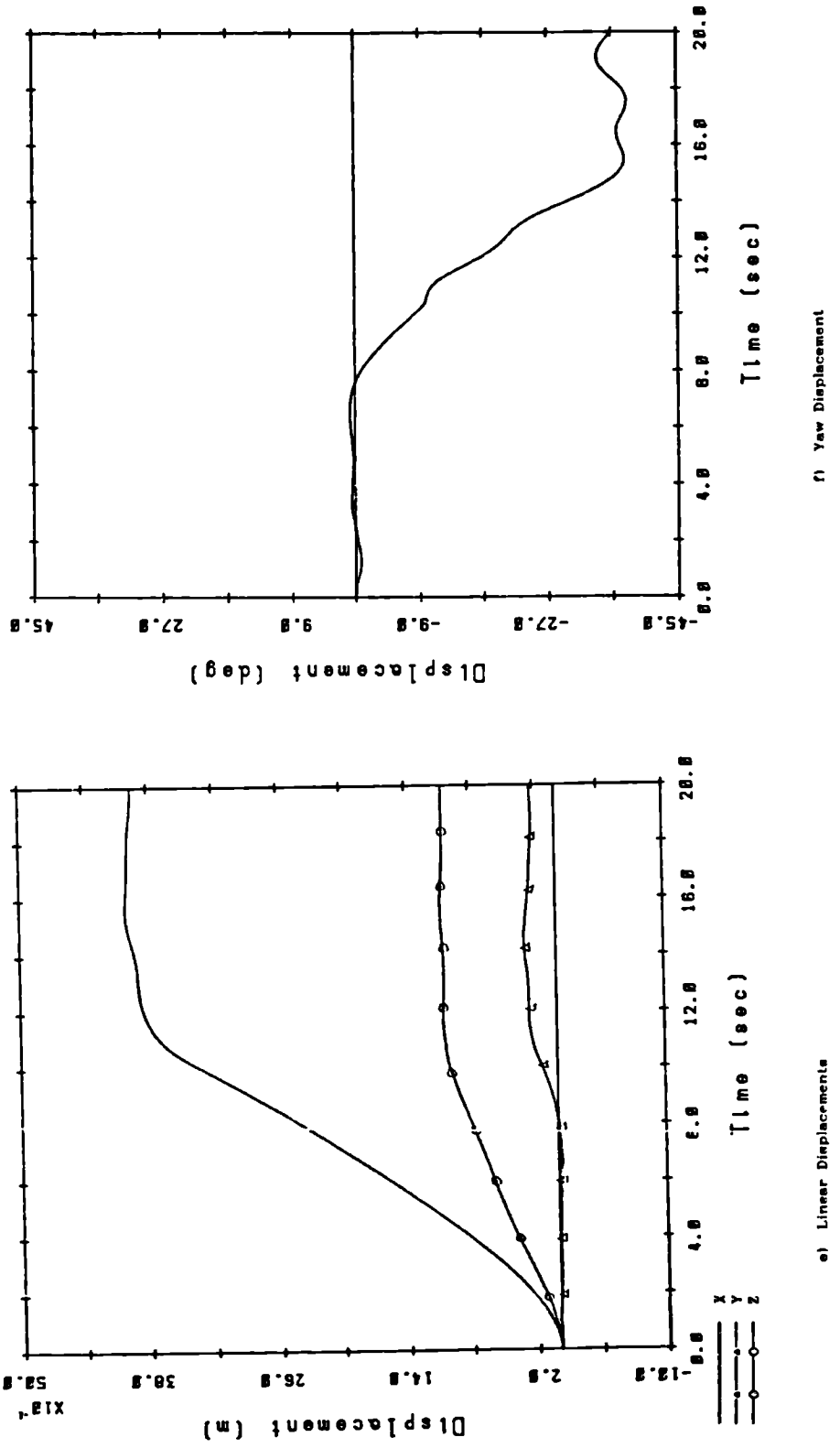

Figure 5.23 : Continued

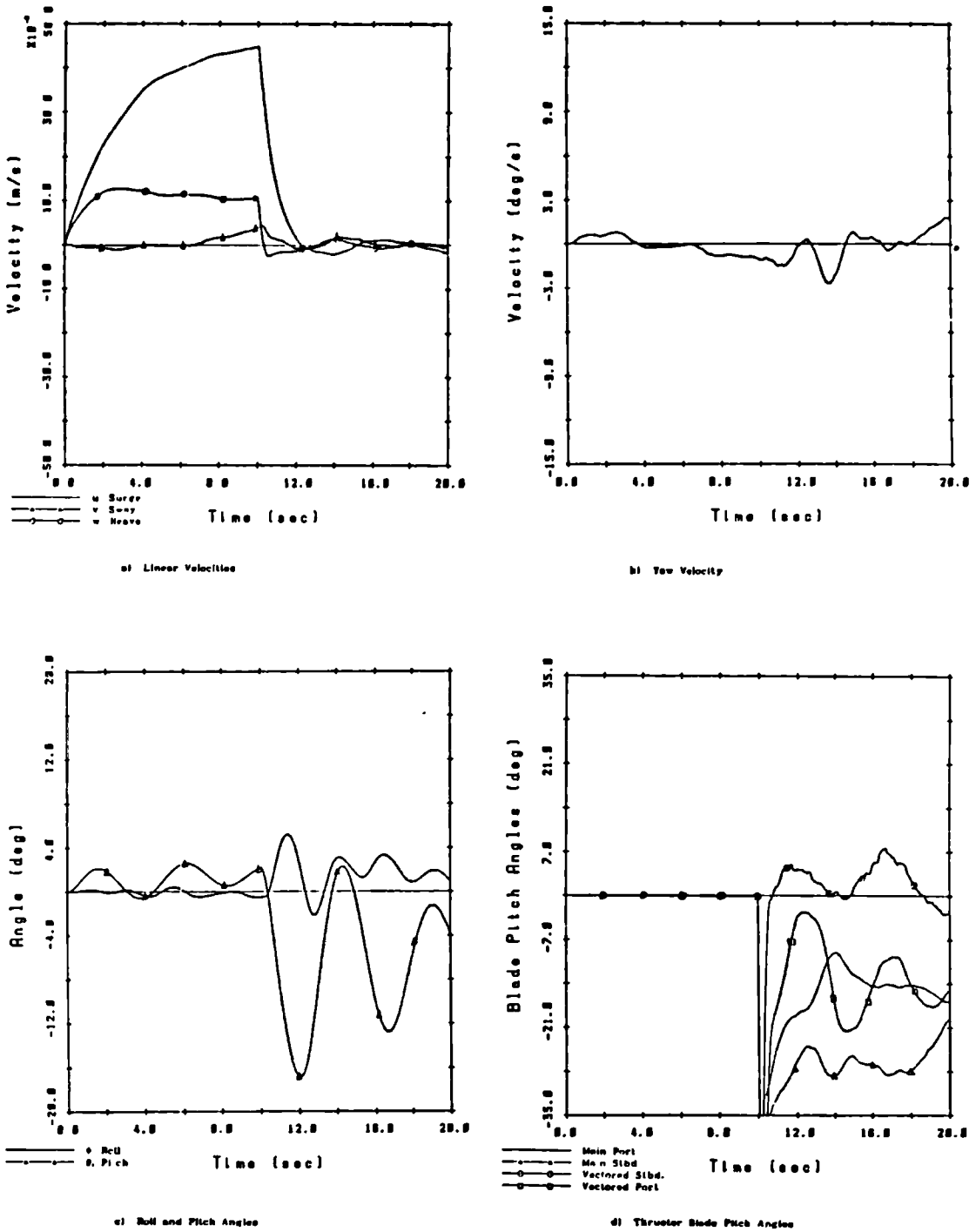

Figure 5.24 : Closed-Loop Response to Station Holding in a Stochastic Current; Faster Sampling Rate, 20 Hz

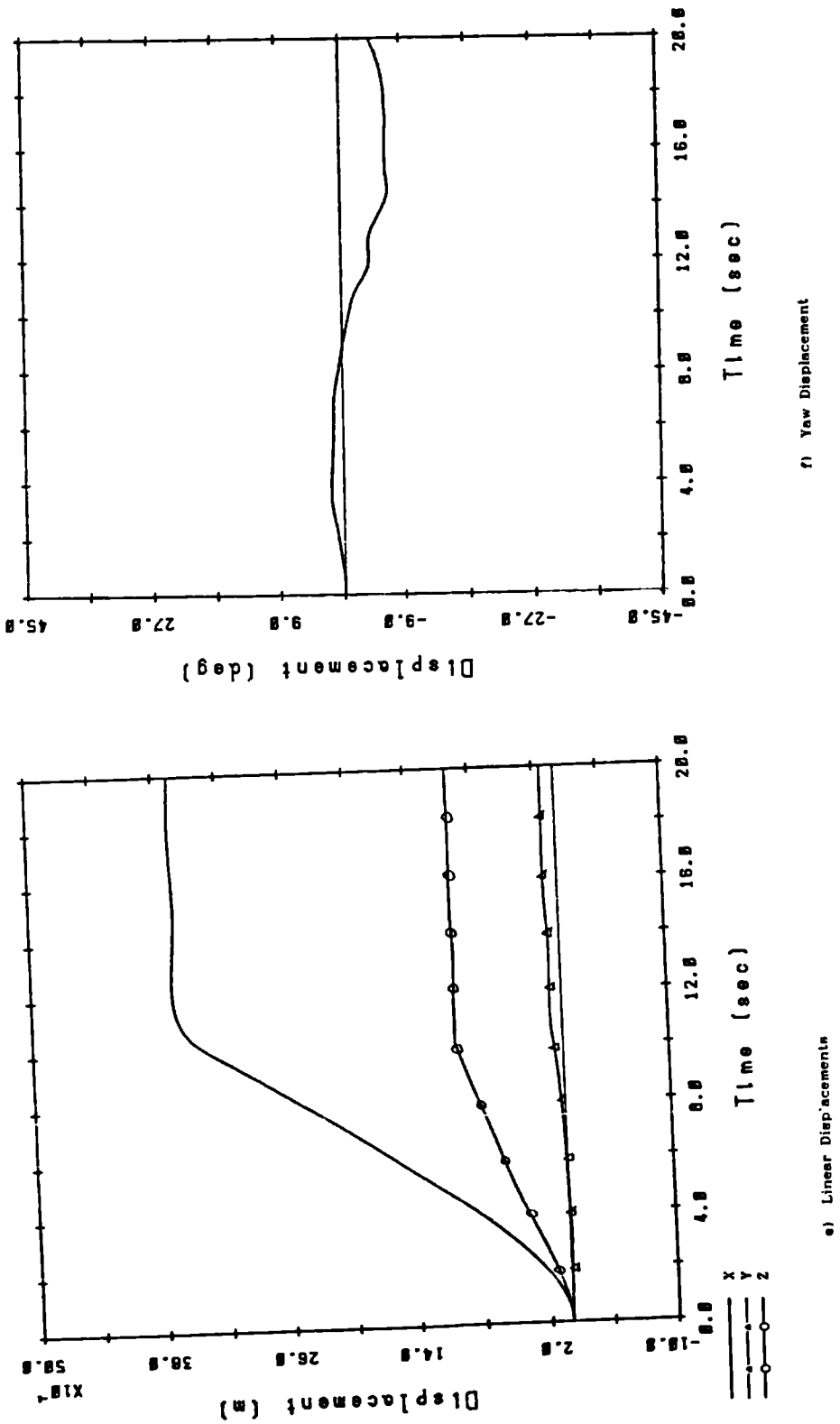

Figure 5.24 : Continued

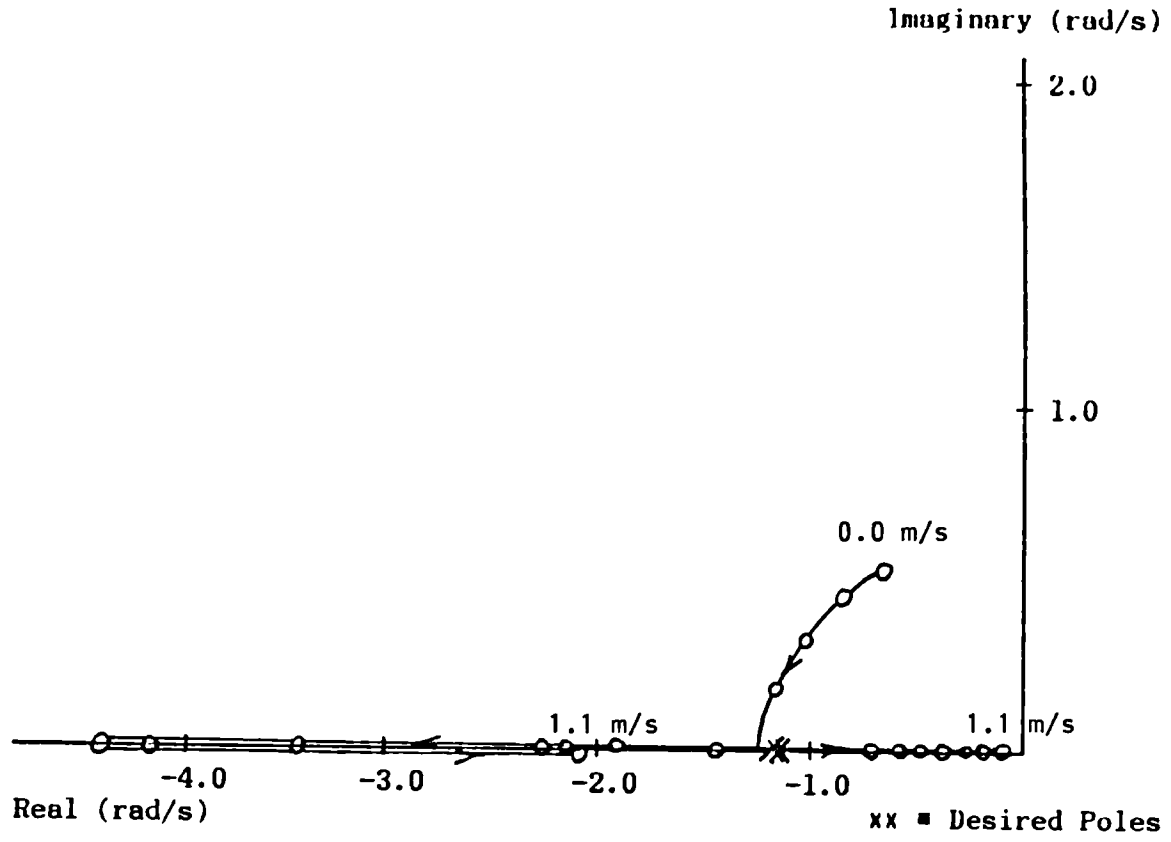

Figure 5.25 : Modified ROV Closed-Loop Poles; Surge Mode

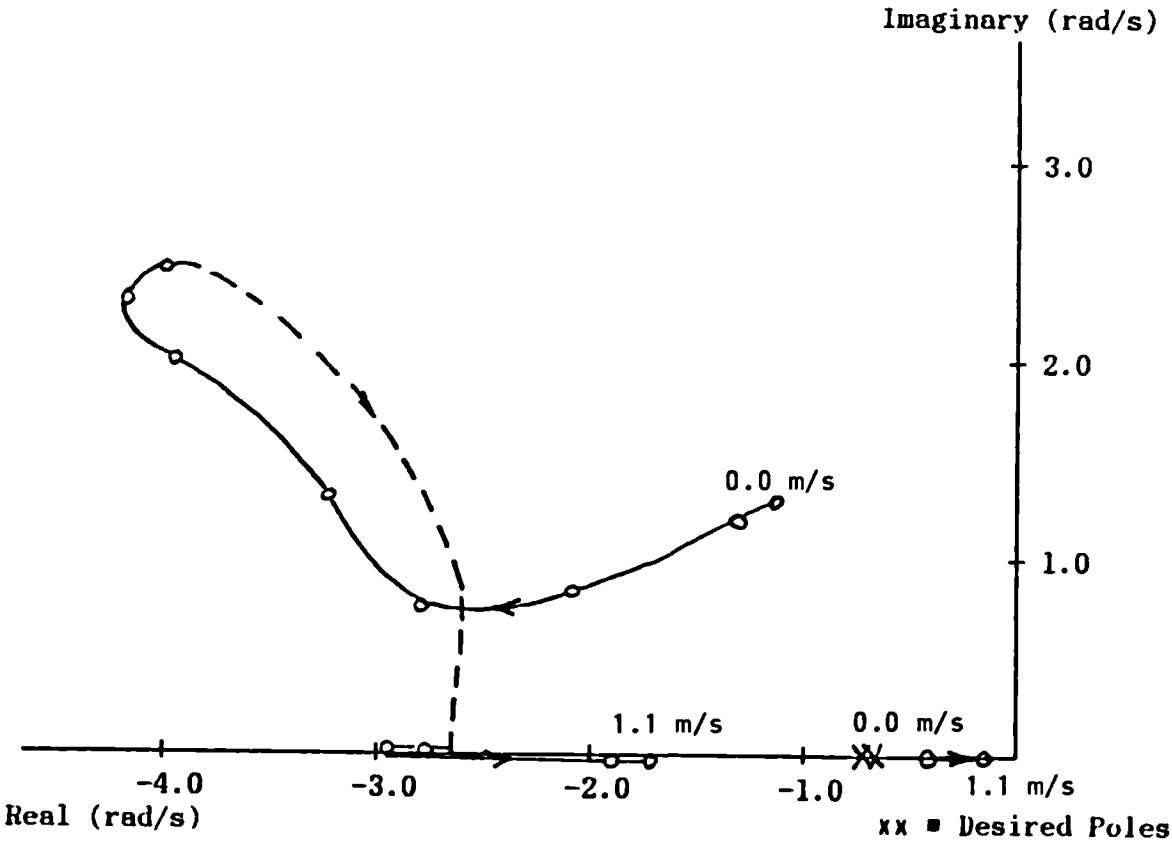

Figure 5.26 : Modified ROV Closed-Loop Poles; Sway Mode

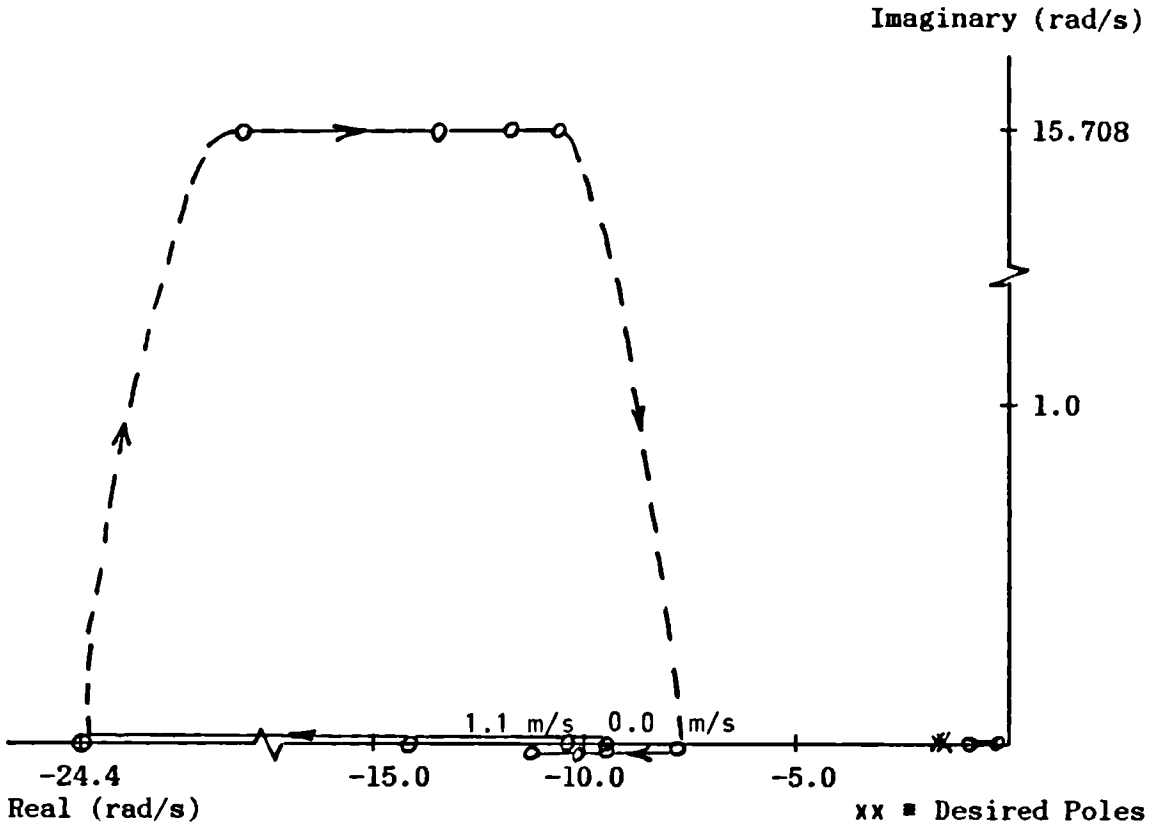

Figure 5.27 : Modified ROV Closed-Loop Poles; Heave Mode

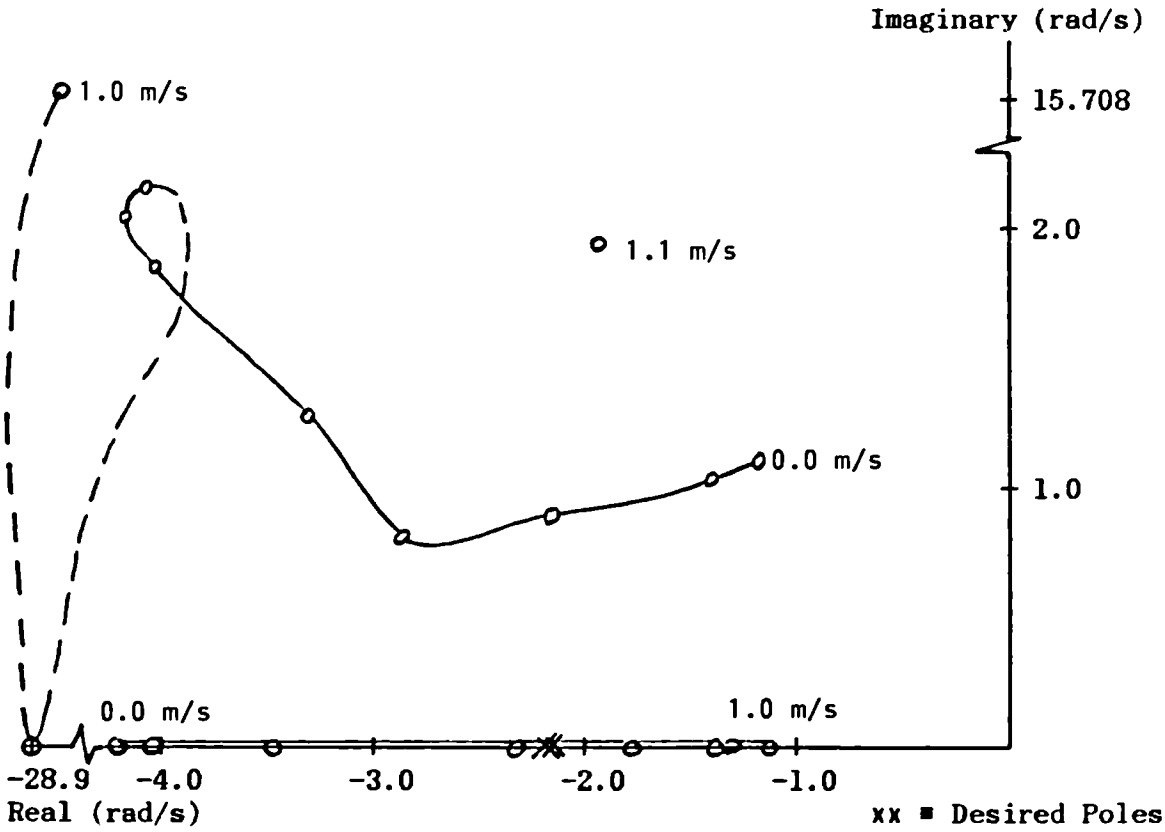

Figure 5.28 : Modified ROV Closed-Loop Poles; Yaw Mode

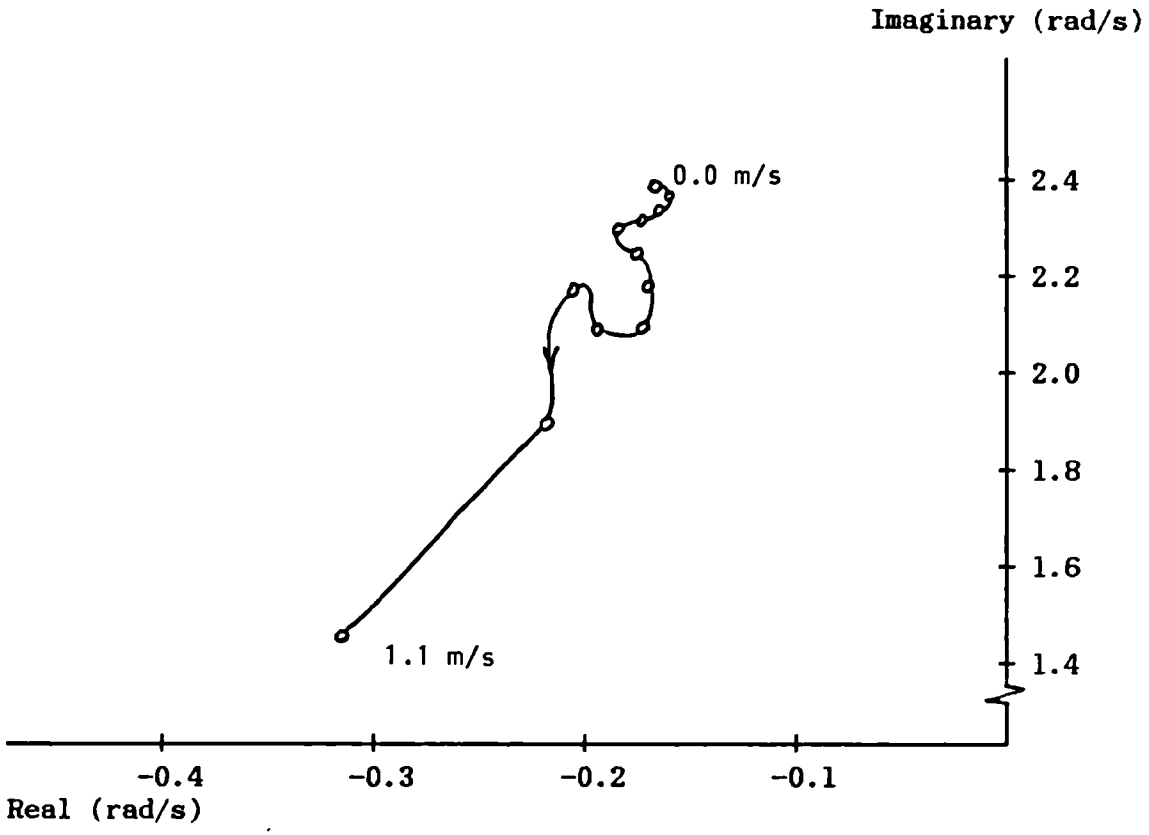

Figure 5.29 : Modified ROV Closed-Loop Poles; Roll Mode

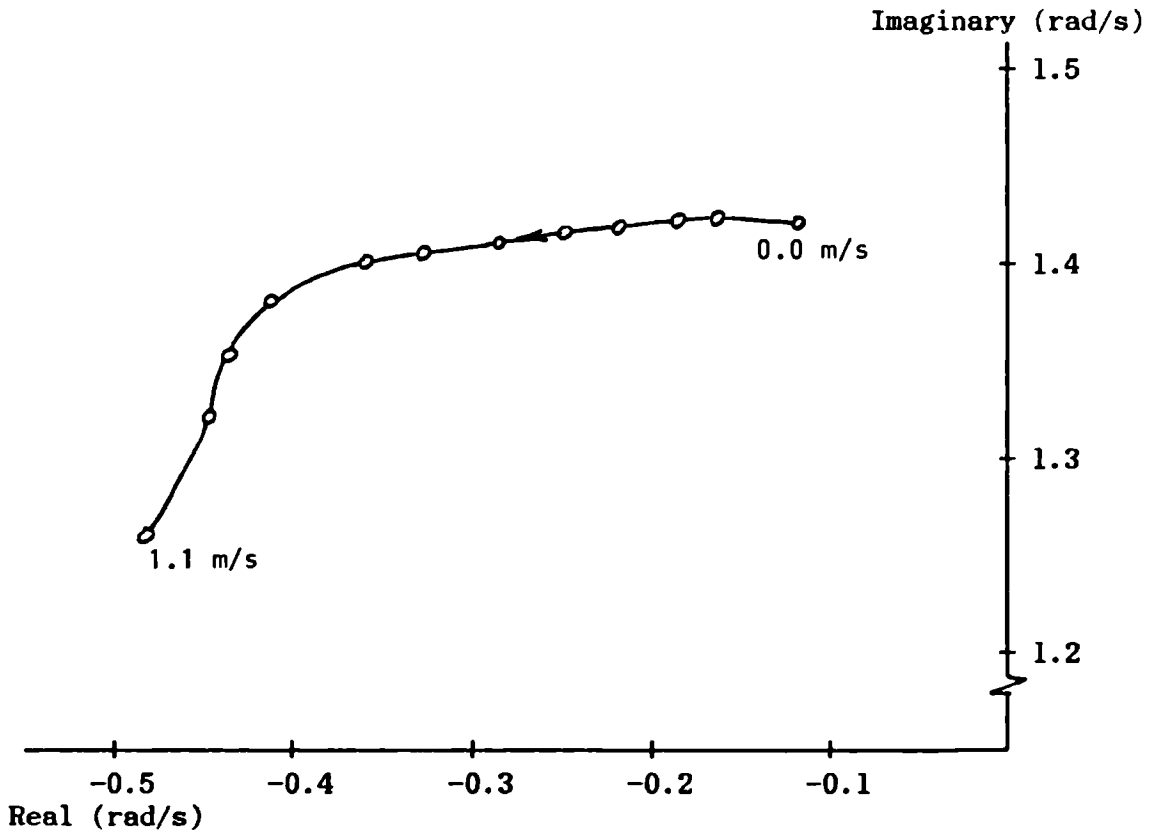

Figure 5.30 : Modified ROV Closed-Loop Poles; Pitch Mode

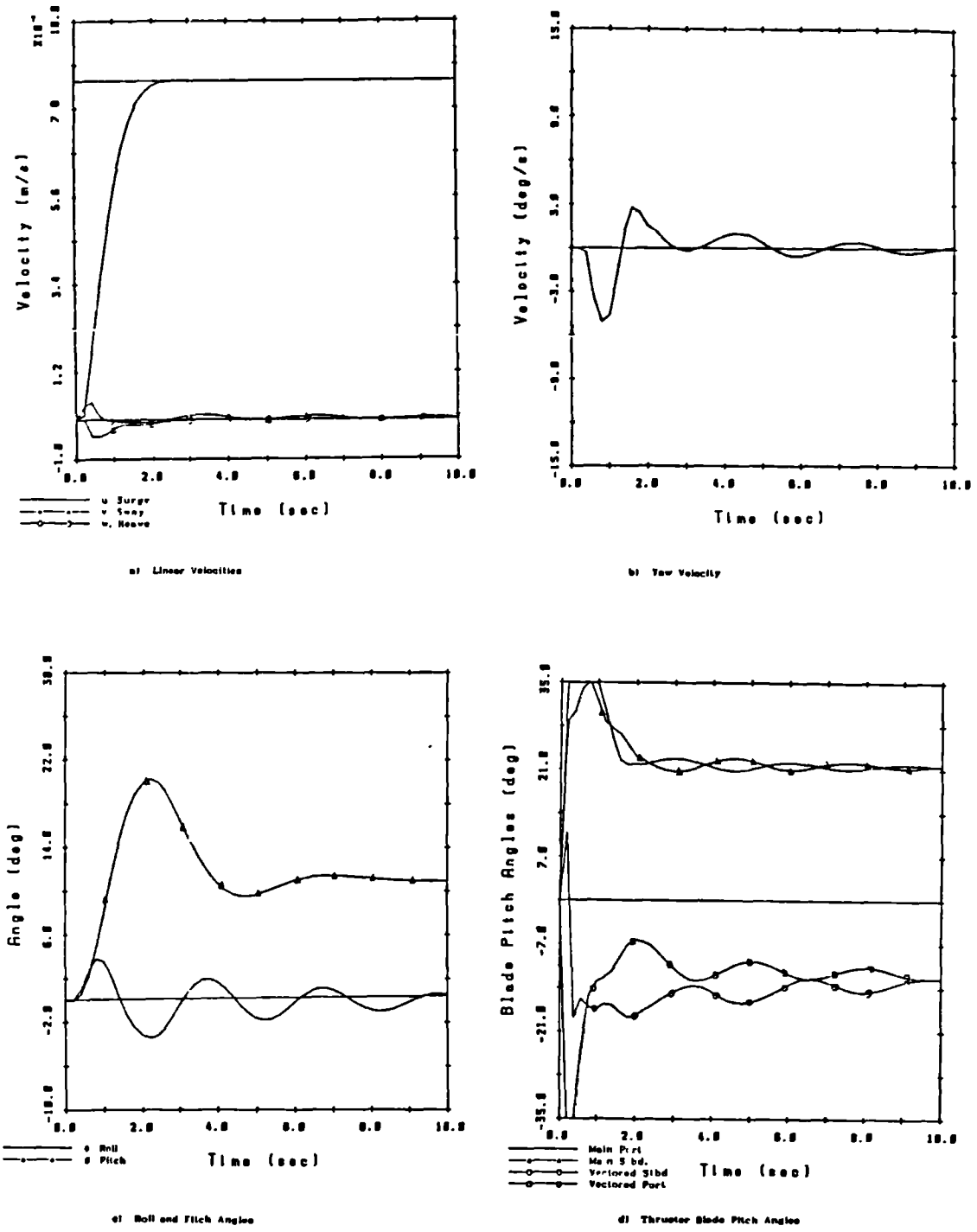

Figure 5.31 : Modified ROV Closed-Loop Response to Step Change in Surge Velocity

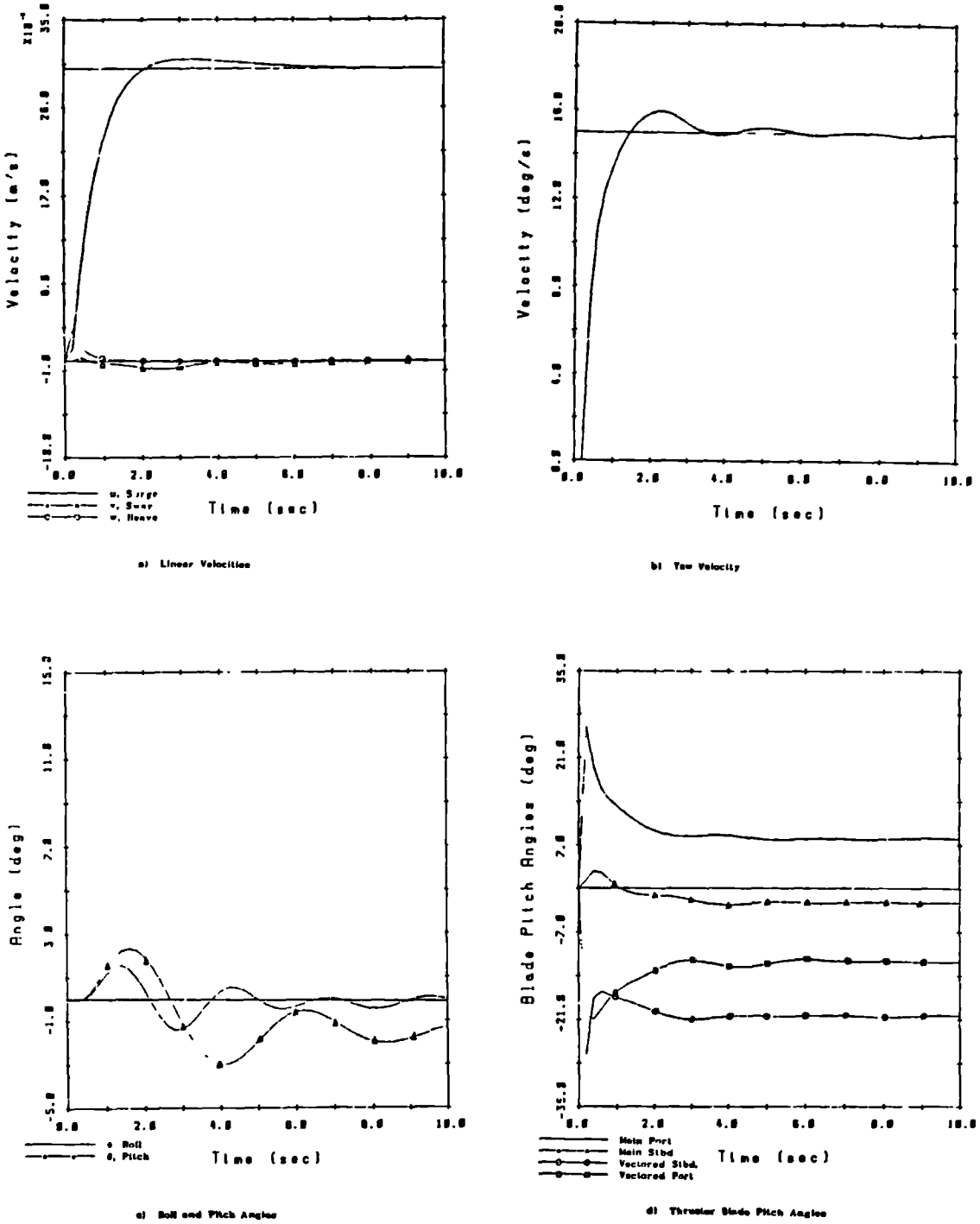

Figure 5.32 : Modified ROV Closed-Loop Response to Medium Speed Turn Command

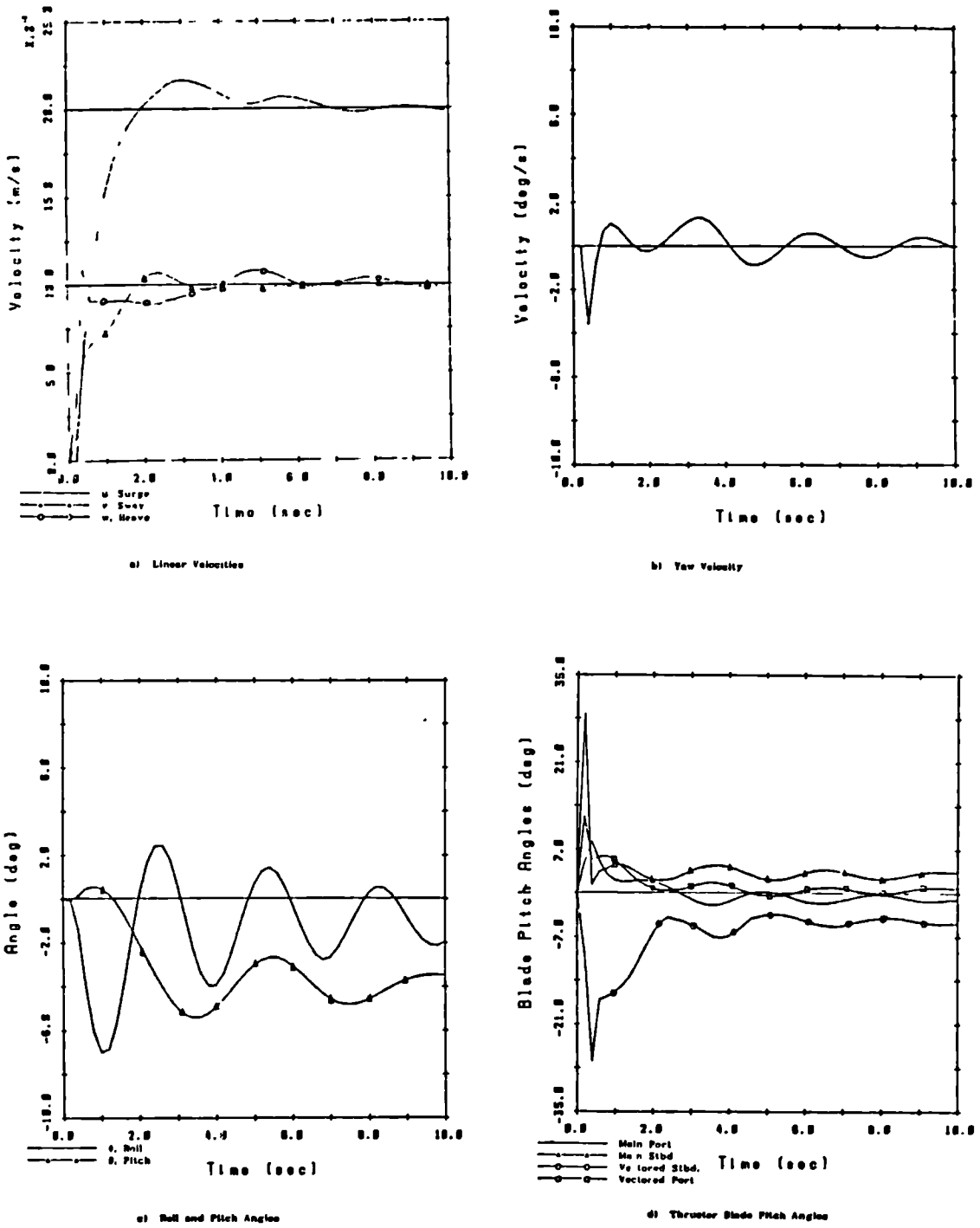

Figure 5.33 : Modified ROV Closed-Loop Response to Inspection Manoeuver Command

Chapter 6

Modelling ROV Dynamics by System Identification

6.1 Introduction

The topic of this chapter, Recursive System Identification (SI) and its application to modelling ROV dynamics, and that of the next, Adaptive Control, are very closely related. Authors of papers and books on recursive SI invariably include a section on how the mathematics they are discussing may be useful in real problems. A major application they note is adaptive or self-learning controllers. Chapter 4 described a few of the vast number of design techniques for generating control laws when the system model is known. Adaptive control considers the case when the open-loop dynamics are not known; instead they are estimated on-line by a recursive SI method and the controller is updated continuously.

The previous two chapters discussed a fixed-gain controller for the ROV which had some shortcomings; adaptive control appeared to be the most promising way of extending the autopilot's capabilities to cope with these problems, despite the reservations about this technique that were noted in section 4.3. Two adaptive controllers were implemented and their performance, documented in chapter 7, proved to be very satisfactory. However, since recursive SI forms the core of adaptive control, it is more appropriate to present this work on identification of open-loop dynamics first.

During the course of the adaptive autopilot study, it became apparent that the SI model description of the ROV was such that the closed-loop system had performance exceeding that achieved with the self-testing fixed-gain controller. It is known that feedback reduces the effects of modelling errors so the question remained whether SI techniques could produce an adequate open-loop model. If they could, the advantages over conventional modelling techniques would be substantial. Chapter 2 described the components which make up a ROV model while chapter 3 documented the validation exercise that was required to make the original Seapup model match its observed

performance. The effort, in terms of money and time, was considerable when the tank trials, the analysis of the experimental results and the model validation were taken into account and still doubts remain about the model's adequacy.

It is important to define what a SI modelling exercise will produce. Conventional tank trials and analysis yield hydrodynamic derivative based equations in the form of (2.3). During digital simulation, sums of large numbers of terms are made and divided by other long sums to yield output values. SI techniques would directly identify the quotient of the two sums i.e. state-space models such as (3.2); this possibly will be more accurate and definitely will require less effort at the experimental stage. Chapters 2 and 3 described conventional hydrodynamic modelling; a scale model of the marine vehicle or in the case of the ROV, the vehicle itself, is mounted in a Planar Motion Mechanism (PMM). This device oscillates the model in a prescribed manner, usually so that it moves purely in one degree of freedom only. The PMM itself is attached to the towing tank's carriage. A series of tests with each oscillatory mode and varying PMM oscillatory frequency and carriage speed yields a pair of hydrodynamic coefficients related to the in-phase and in-quadrature forces and their speed and frequency dependence.

Clearly, such a method is very time consuming and hence, expensive. The work in chapter 3 indicated that it is also of limited worth. A SI modelling trial would dispense with the need for a towing tank and PMM. Instead, the vehicle is run in a protected body of water, ideally a manoeuvering tank. The ROV is equipped with a navigation system for measuring positions and velocities and its control console is modified to accept thruster commands from a computer. This computer also logs the navigational data. Appendix A describes the experimental apparatus for a series of ROV trials which were held at Admiralty Research Establishment (Haslar) between 12 and 23 May, 1986. The tests were run jointly by personnel from ARE (Portland) and the Automatic Control Group, University College London. The appendix also contains details of the tests and a few preliminary results. Time constraints prevented most of the analysis of the trials data from being included in this thesis.

Multivariable SI methods operate on a series of data points and simultaneously estimate the ARMAX (autoregressive, moving-average with exogenous inputs) models which the data best fits. Hence, one experiment which excites all thrusters and degrees of freedom and is of sufficient duration to yield a few hundred input and output data samples could determine the entire model.

If only the relationships between inputs and outputs are required, then SI methods have clear advantages over hydrodynamic testing. This information would be sufficient for control system design or if the model was to be used in a simulator for pilot training. However, in some cases, specific hydrodynamic properties are required and conventional constrained tests are more appropriate. SI can be useful here to process the PMM data and make more accurate estimates of the slow motion derivatives than simpler analysis would allow.

After this brief introduction, system identification and its various divisions will be defined. The uses of the models are presented. Adaptive control requires the internal model to be continuously updated on-line which requires that the identification be recursive, as opposed to a batch method. A number of recursive SI algorithms are discussed and it is shown that they all fit a general framework with different choices to be made by the user. These techniques are presented, as is the organisation of suitable experiments and effective analysis of resultant data. Most SI references discuss the techniques in terms of single-input/ single-output (SISO) systems only. A simple extension to a MIMO model appropriate for the ROV is given. It is also possible to modify SI methods to cope with nonlinear systems; this is discussed briefly.

Applications of SI have been discussed extensively in the literature and a few are mentioned. Of particular interest are the marine oriented problems.

Because of the lack of real data, the appropriateness of SI is tested by using the existing Seapup model to produce time series data which is then analysed. This is done for different experimental

conditions and identification techniques and all results compared to the original simulated responses. Conclusions are drawn about the use of SI for modelling ROV dynamics.

6.2 System Identification

Models of systems are required for such tasks as control, signal processing and prediction. Ljung and Soderstrom [55] distinguish between 'mental' or 'intuitive' models, 'graphic' models and 'mathematical' models. A person summarises knowledge of a system's behaviour in a nonanalytic form in models of the first category. Graphic models have information in the form of tables or graphs eg. frequency domain methods of controller design which requires the system's response to be represented in Bode or Nyquist diagrams. Mathematical models have relations cast in the form of a functional relationship. Another important category often overlooked are physical models such as ship or submarine models for towing tests or plastic models of structures which aid visualisation of stress concentrations.

Reference [55] shows that models can be derived by two methods. The first, called appropriately 'modelling', determines the parameter values of the physical mechanisms which all together make up the system. Examples would be finding the values of mass, damping and stiffness in a second order system or conventional hydrodynamic modelling of a marine vehicle. It has been shown here that modelling of the latter can be time-consuming and inaccurate. An alternative is 'identification' where measured signals produced by the system are used to construct the model. If a mass/spring/dashpot system is set oscillating and the frequency and log decrement of the vibrations noted from the output, then the model has been derived by identification.

It is usually appropriate to begin a discussion of a topic by defining it. Zadeh [56] stated the following about the identification problem:

"Identification is the determination, on the basis of input and output, of a system within a specified class of systems, to which the system under test is equivalent."

This definition was also chosen by Astrom and Eykhoff in their survey of SI [57], a very complete review which is frequently drawn upon here.

Zadeh's definition requires that the user specify the class of systems, the type of input signal and the meaning of 'equivalent'. The latter is often cast in the form of a 'loss function', usually a measure of the difference between real and modelled output. When a loss function is used, the problem becomes that of optimising over the set of allowable models to minimise the loss.

Identification methods can be classified according to the type of model which results and whether the algorithm operates on- or off-line. Isermann, et al. [58] define models as either parametric or nonparametric. The former category produces models which are defined by a finite number of parameters eg. a state-space representation. All of the methods used in this chapter are of this type. Nonparametric models cannot be characterised by a finite number of values. An example is the impulse response of a system given by Fourier analysis.

Off-line methods are also referred to as 'batch' because they operate on a batch of data that has been gathered previously. Batch methods are no use in applications where the system is either constantly or intermittently changing, such as adaptive control or adaptive prediction. In such cases, on-line or 'recursive' SI is required; this will be treated separately in the next section.

SI and more generally, modelling, is useful in a number of different applications. It was mentioned briefly at the beginning of this section that models of systems are usually required for the purpose of either control, filtering or prediction. Chemical and production engineers need to model and control processes; the same applies to mechanical engineers designing controllers for vehicles ranging from aerospace to marine. Other examples of control

applications are modelling human actions in accomplishing tasks and biological functions such as arm or leg motion or the mechanism of pain [59]. Filtering involves, for example, determining models of various aspects of telecommunications channels which are then used for equalisation or noise cancellation. Another example is spectral estimation, which is utilised in the enhancement of visual and audio data. The third major use of models is prediction; future values of data, such as economic indicators or ship motion, are predicted from past and present data.

6.3 Recursive System Identification

Whether the purpose of a model is for control, prediction or filtering, if the underlying system changes over time, then the identification must take place continuously. Batch algorithms, i.e. those which operate on the entire data set, would be inappropriate for this purpose. Suppose that z(t) is a vector of measurements taken at time 't' (the notation of [55] is used here). Sampling takes place in discrete time, though this is not always the case, and at even time intervals, again not a necessary condition. Let:

$$z_t = \{ z(t), z(t-1), \ldots z(1) \} \qquad \ldots.(6.1)$$

be the entire data record up to time t. The 'identification problem' is to map z_t to an estimate of the model parameters θ:

$$z_t \rightarrow \hat{\theta}(t; z_t) \qquad \ldots.(6.2)$$

where ' denotes an estimate of the true values.

The model of the system is of the form:

$$y(t+1) = M(\theta(t), z_t) \qquad \ldots.(6.3)$$

In batch processing, data is first collected to time N and then a 'single-shot' estimate is made. It would be possible to use this scheme for the on-line case. At the next sampling instant, another

set of measurements are taken and a batch process of N+1 points is executed, i.e. the entire data set is operated on again. However, for on-line processing, computer memory and time should not increase with the length of the data set, which means z_t must be condensed into an "auxiliary memory quantity S(t) of fixed dimensions." Recursive SI algorithms are of the form:

$$\begin{aligned} \hat{\theta}(t) &= F(\hat{\theta}(t-1), S(t), z(t)) \\ S(t) &= H(S(t-1), \hat{\theta}(t-1), z(t)) \end{aligned} \qquad \ldots.(6.4)$$

Since the current parameter estimate $\hat{\theta}(t)$ is formed from the previous estimates, the current auxiliary variable and current measurement, there is only the need to store $\hat{\theta}(t)$ and S(t), arrays that do not increase in size with time.

There are other advantages in using recursive algorithms. Simple modifications allow different weightings to be given to data eg. higher to more recent readings or lower to those which are plainly wrong because of measurement errors. They can be used for off-line applications, dispensing with the need for two different algorithms. The data record is rewound and processed a number of times to improve the accuracy of estimates. The disadvantages are that model order must be decided upon 'a priori' and that results are usually not as accurate as achieved with batch methods, though it can be shown that for long data records, the differences are insignificant. Recursive methods also have a larger 'overhead' associated with them which makes batch algorithms attractive for short data series, but this disadvantage quickly disappears as the amount of data increases.

The recursive SI problem is simply to choose i) the model M (6.3), ii) the experimental conditions, including the input signal and iii) the functions F and H (6.4). However, the general opinion in the engineering and scientific community is that recursive SI is "a bag of tricks" [55] or "a fiddler's paradise" [57]. There are good reasons for these feelings. Depending on the chosen model, different approaches to the derivation of the algorithm and the use of various approximations and numerical tricks to aid performance, the resulting

methods all have different names, despite their underlying similarity. Reference [55] takes another attitude. "...There is only one recursive identification algorithm. It contains some design variables to be chosen by the user".

The first choice that has to be made is the model set which will represent the true system. If the data is sampled in discrete time, a natural selection would be a linear difference equation or ARMAX model:

$$A(z^{-1})\, y(t) = B(z^{-1})\, u(t) + C(z^{-1})\, e(t) \qquad ....(6.5)$$

Here, y is the value of the output variable (or vector of variables, if a MIMO system), u, the control variable and e, uncorrelated or 'white' noise. Here, z is the backward shift operator such that:

$$z^{-1}y(t) = y(t-1) \qquad ....(6.6)$$

The z polynomials in (6.5) are:

$$\begin{aligned} A(z^{-1}) &= 1 + a_1 z^{-1} + \ldots + a_n z^{-n} \\ B(z^{-1}) &= b_1 z^{-1} + \ldots + b_m z^{-m} \\ C(z^{-1}) &= 1 + c_1 z^{-1} + \ldots + c_r z^{-r} \end{aligned} \qquad ....(6.7)$$

Another possible model is a state-space form, such as (3.2). Here, the past values of y, u and e take the values of the extra states, x.

Equation (6.5) can also be written as:

$$y(t) = \theta^T \phi(t) + e(t) \qquad ....(6.8)$$

where $\theta^T = (a_1, \ldots a_n, b_1, \ldots b_m, c_1, \ldots c_r)$,

is the parameter vector and

$$\phi(t) = \{ -y(t-1),\ldots -y(t-n),\ u(t-1),\ldots u(t-m), e(t-1),\ldots e(t-r)\}^T$$

is the vector of regression variables.

With the chosen model set, there are different ways of calculating the 'best' estimate of θ. Least Squares (LS) strives to minimise the equation error:

$$V(\theta) = \frac{1}{N}\sum^{N} \alpha_t [\ y(t) - \theta^T\phi(t)\ ]^2 \qquad \ldots.(6.9)$$

Here, $C(z^{-1})$ is chosen to be unity and α_t is a factor which changes the weights given to different measurements. If the actual noise model $C(z^{-1})$ is not unity, then LS can give biased estimates of the parameters; this is because some of the regression variables become correlated with the equation error. The method of Instrumental Variables (IV) is designed to cope with biased estimates of this sort. The vector of regression variables $\phi(t)$ is replaced by $\psi(t)$, the 'instrumental variables' such that $\psi(t)$ and the equation error are uncorrelated. A common choice for these variables is:

$$\psi(t) = \{ -y_M(t-1),\ldots -y_M(t-n),\ u(t-1),\ldots u(t-m)\} \qquad \ldots.(6.10)$$

where y_M is the output of the estimated model driven by the input u.

These two methods have criterion functions which are quadratic in θ and so, can be minimised analytically. In general, this is not the case with other Recursive Prediction Error Methods (RPEM) and so approximations must be made in minimising the prediction error:

$$V(\theta) = \frac{1}{N}\sum^{N} [\ y(t) - \hat{y}(t/\theta)\ ]^2 \qquad \ldots.(6.11)$$

The approximations are dependent on the choice of model. An example is Extended Least Squares (ELS), another approach to eliminating bias due to correlated noise. Here, the noise model is estimated as well as the polynomials $A(z^{-1})$ and $B(z^{-1})$. LS and IV algorithms are linear

regressions, whereas ELS is a Pseudolinear Regression because the past values of the white noise, e, are not measured, but instead approximated by the equation error.

Yet another approach to parameter estimation considers the members of θ as random variables with an unknown probability distribution. This Bayesian approach uses the fact that observations are correlated with the parameters and so information can be inferred from them. The Recursive Maximum Likelihood (RML) method finds these distributions and then chooses the most likely value of θ. RML is another specific form of a RPEM. The Kalman Filter is another example of Bayesian estimation; here, the most likely values of the unobserved state are calculated from observations of input and output data.

Based of this array of parameter estimation methods, it is easy to sympathise with those who hold the "fiddler's paradise" opinion. However, all of these algorithms can be presented in the form:

$$\hat{\theta}(t) = \hat{\theta}(t-1) + \gamma(t)\, P(t)\, \eta(t)\, [\, y(t) - \hat{y}(t)\,] \qquad ....(6.12)$$

where

$\theta(t)$ is the current parameter estimate
$\gamma(t)$ is a scalar gain sequence, tending to zero
$P(t)$ is a matrix based on observations up to time t
$\eta(t)$ is the 'gradient' vector, related to $d\theta/dy$

and

$[\, y(t) - \hat{y}(t)\,]$ is the prediction error

The gain sequence is chosen such that time-varying systems may be tracked. There is a trade-off between tracking ability and noise rejection. A common choice is to introduce a 'forgetting factor', $\lambda(t)$, such that:

$$\gamma(t) = \frac{1 - \lambda}{1 - \lambda^t} \qquad , \lambda < 1,\ \lambda \cong 1 \qquad ....(6.13)$$

For λ close to unity, data is forgotten at a rate:

$$T_o = \frac{1}{1 - \lambda} \qquad ....(6.14)$$

This means prediction errors older than T_o units have weights less than 36 percent of the most recent. A refinement is to let:

$$\lambda(t) = \alpha\lambda(t-1) + (1-\alpha) \quad ,\alpha < 1, \alpha \simeq 1 \qquad ....(6.15)$$
$$\lambda(0) = 0.6 - 0.7$$

This gain sequence allows initial estimates, usually bad, to be forgotten quickly.

Special allowances can be made for nonlinear systems. When the reference output undergoes a large change, $\lambda(t)$ can be made small to cause the estimator to track rapidly. A similar scheme is to decrease the forgetting factor when the prediction error increases.

The search direction, $\eta(t)$, is normally chosen as either the Stochastic Gauss-Newton or the Stochastic Gradient direction. The choice will influence the asymptotic accuracy, convergence rate and algorithm complexity, the former direction involving more calculations.

For SISO systems, the matrix P(t) is the covariance of the parameter estimation $\theta(t)$. Hence, a good choice for the initial conditions of the estimated algorithm is:

$$P(0) = p\ I \qquad ....(6.16)$$

where p is a large number. One suggestion is to let p equal $100/E(y^2)$ in the scalar case. The large value of the diagonal elements of P(0) reflects the large uncertainty in the original guess of $\theta(0)$ and will cause the algorithm to move rapidly from these values.

In this study of modelling ROV dynamics, the methods of least squares, extended least squares and recursive predictive error will be compared. LS is simpler, always an advantage, because the observations do not have to be prefiltered as in RPEM or the noise model estimated as in RPEM and ELS. Another complication is that this filter, the estimated $C(z^{-1})$, must be monitored to ensure its stability. However, RPEM converges under more general conditions than

LS or ELS and is asymptotically more accurate. The RPEM algorithm used is that presented in [55] which has been modified to model MIMO systems. It uses a stability test presented by Kucera [60] for monitoring $C(z^{-1})$ as part of its so-called 'Projection Algorithm'. These are used when some parts of θ are known to lie in certain domains, eg. the noise model $C(z^{-1})$ or the autonomous system $A(z^{-1})$, is stable or the system is minimum-phase ($B(z^{-1})$). The new proposed $\theta(t)$ is tested; if it is not in the desired area, the correction factor, $\theta(t) - \theta(t-1)$, is made smaller and added to $\theta(t-1)$ again. This continues until the updated parameter vector obeys the constraints.

Other numerical 'tricks' both the LS and RPEM algorithms implement are methods of keeping P(t) positive definite and nonsingular. Each updates the matrix in the UD form such that:

$$P(t) = U\ D\ U^T \qquad \ldots.(6.17)$$

where U is an upper triangular matrix and D is a diagonal matrix. The LS method employs Peterka's 'Square Root' algorithm [61] for this purpose whereas the RPEM uses Levenberg-Marquardt regularisation [62, 63]; a small number is added to each diagonal element.

The type of identification algorithm is only one decision the user would have to make. Two other choices of particular interest here are the experimental conditions and the model order.

Experimental conditions to be designed include the sampling rate, what exactly to measure, how to prefilter the raw data and the choice of the input signals. Appendix A has a discussion of all of these issues for a set of ROV trials; here only the latter will be addressed.

A poor choice of input signal can lead to numerical difficulties, i.e. P(t) becoming singular, or, even more dangerous, poor estimates without any indication of numerical difficulties. The input must be 'persistently exciting', a term which can be defined mathematically; suffice it to say that over the course of the experiment, u must excite all modes of the system and all combinations of parameters.

Open-loop experiments are the most straightforward. Since the tests are often driven by computer, a good choice for the input signal is a Pseudo Random Binary Sequence (PRBS). In a PRBS, the signal randomly switches between two levels at a given clock period; this period can be varied to excite different spectral properties of the system. It is important to note that the predictor $\hat{y}(t/\theta)$ which is minimised by the estimation algorithm is the best "for the experimental condition used under the identification experiment" [55]. Therefore, it is best to choose u close to the set of signals to be input to the model in the application.

Closed-loop estimation can be difficult. This is most likely to occur when the system is operating under low-order feedback which allows the input to become perfectly correlated with the additive output noise. Instead of the open-loop system, the feedback model is identified. This can be solved by using a higher order control law, such as PI, or varying the setpoint rather than using the closed-loop system as a regulator. Though more difficult, closed-loop estimation is often necessary. Adaptive control is the obvious example. It is also needed when separate experiments would be prohibitively expensive, for example, with full scale ships or processes, or when feedback is needed to keep the system within safe operating limits [64].

The choice of model order is interesting in this study. Chapters 4 and 5 demonstrated that a portion of the system, surge, sway, heave and yaw, are explained sufficiently well by a first-order model while under feedback. The question remains whether this extends to open-loop applications of the model and whether it applies to pitch and roll as well. Model order is a compromise between a good description of the data and complexity. Most methods developed are for off-line analysis. Freeman [65] considers a number of tests of the variance of the parameters. Soderstrom [66] reviews many techniques, three which will be used here.

A model is correct if the residuals i.e. the 'a posteriori' output errors, are uncorrelated. This can be tested by calculating the correlation function for a series of residuals. Ninety-five

percent of the values of this function, $R_{xx}(t)$, for $t > 0$, should fall within 2σ limits if the residuals are white noise.

The loss function, $V_n(\theta)$ (6.11), decreases as the model order increases. Statistical tests can be used to determine whether this loss is significant. If $V_n(\theta)$ is achieved for a model with n parameters and $V_m(\theta)$ by a model whose number of parameters has been increased to m, then the statistic:

$$F_{n->m} = \frac{V_n - V_m}{V_m} \quad \frac{N - m}{m - n} \qquad ....(6.18)$$

is $F(m-n, N-m:\alpha)$ distributed, where N is the number of sampling points. If $F_{n->m}$ is less than $F(m-n,N-m:\alpha)$, then the model of order n is suitable; the risk of an error is only α. Typically, this risk is chosen to be between 0.005 and 0.1.

Various figures of merit or 'criterion functions' have been proposed for choosing model order, the most widely used being Akaike's Information Criteria (AIC) [67], given by:

$$AIC = -2 \log L + 2 v \qquad ....(6.19)$$

This represents a compromise between the maximum of the likelihood function, L, and the number of model parameters, v, and should be minimum for the correct model. The likelihood function is given by:

$$L = -\exp \left(\frac{N}{2} \log 2\pi + \frac{N}{2} \log R_v + \frac{1}{2 R_v} \sum^{N} e^2(k) \right) \qquad ....(6.20)$$

where $R_v = \frac{1}{N} \sum^{N} e^2(k)$ is the variance of the equation error.

By substituting (6.20) into (6.19), the expression for the information criterion becomes:

$$AIC = N(\log 2\pi + 1 + \log R_v) + 2 v \qquad ....(6.21)$$

6.3.1 A Note on Extensions to Nonlinear and Multivariable Systems

All of the SI methods discussed here have been, implicitly, applicable only to linear single input/single output models. The extension to certain nonlinear and multivariable forms is simple, however.

A typical example of a system which is nonlinear is the force acting on an object moving in a fluid with velocity u. The force is usually approximated by Morrison's Equation:

$$F = a_0\dot{u} + a_1 u|u| \qquad ....(6.22)$$

The square-law damping term is clearly nonlinear, but it is desired to estimate the discrete-time counterparts of the parameters in (6.22) by SI techniques. The solution is to cast the model in the form of (6.8), so that it is linear in the regression variables. This leaves the model of (6.22) as:

$$\dot{F}(t) = \{ A_0 \quad A_1 \} \{ u_0(t-1) \quad u_1(t-1)^T \} + e(t) \qquad ....(6.23)$$

where $\{ u_0(t-1) \quad u_1(t-1) \} = \{ \dot{u}(t-1) \quad u(t-1)|u(t-1)| \}$

SI would then take place as described previously.

The modification for multivariable systems is equally straightforward and is described by Goodwin and Sin [68] and Deng and Guo [69]. If the appropriate representation has been chosen, a MIMO system can be viewed simply as a collection of SISO models. Here, a multivariable ARMAX model is used; in linear regression form, it becomes:

$$y(t) = [A_1,\ldots A_n, B_1,\ldots B_m, C_1,\ldots C_r] x$$
$$\{ -\underline{y}(t-1)^T,\ldots -\underline{y}(t-n)^T, \underline{u}(t-1)^T,\ldots \underline{u}(t-m)^T, \underline{e}(t-1)^T,\ldots \underline{e}(t-r)^T]^T + \underline{e}(t) \qquad ....(6.24)$$

The array of parameters θ is now a two dimensional matrix, but this

and a few other trivial modifications are all that are necessary to adapt the standard LS, ELS and RPEM algorithms to this purpose. One limitation of (6.24) is that each output must have the same order of each component, i.e. $A(z^{-1})$, $B(z^{-1})$ and $C(z^{-1})$. The model order tests, described in the previous section, can be applied to each output's prediction error separately; the overall system order is chosen to be the largest indicated.

6.3.2 Estimating DC Values

All SI methods require that the input and output data have zero average values since the standard ARMAX model (6.5) does not allow for them to be estimated. If the actual measurements do not fit these conditions, the effects of d.c. levels may be removed in three ways [70]. The first method is to use differences between consecutive values rather than the measurements themselves, i.e.:

$$\begin{aligned} \underline{y}(k) &= \underline{y}(k) - \underline{y}(k-1) \\ \underline{u}(k) &= \underline{u}(k) - \underline{u}(k-1) \end{aligned} \qquad \ldots.(6.25)$$

The next solution is to estimate the average values, $\bar{\underline{y}}$, $\bar{\underline{u}}$ on-line. The recursive form of an estimate of these values is:

$$\bar{\underline{y}}'(k) = \bar{\underline{y}}'(k-1) + \frac{1}{k}\left(\bar{\underline{y}}(k) - \bar{\underline{y}}(k-1)\right) \qquad \ldots.(6.26)$$

The values $\underline{y}(k) - \bar{\underline{y}}(k)$ and $\underline{u}(k) - \bar{\underline{u}}(k)$ are then used in the data vector ϕ .

It is also possible to put the raw measurements in the data vector and estimate the offsets recursively. This is done by making an extension to the ARMAX model (6.5):

$$A(z^{-1})\, y = B(z^{-1})\, u + C(z^{-1})\, e + d \qquad \ldots.(6.27)$$

The value of the offset d is estimated simply by extending the

dimensions of ϕ and θ by one to become:

$$\theta = \{ a_1 \ldots a_n, b_1 \ldots b_m, c_1 \ldots c_r, d \}$$

$$\phi = \{ -y(t-1) \ldots -y(t-n), u(t-1) \ldots u(t-m), \dot{e}(t-1) \ldots \dot{e}(t-r), 1 \}$$

This latter method is employed in this study.

6.4 Previous Marine Application Studies

System Identification has, in recent years, become simultaneously a subject of serious academic research and a tool for scientists, engineers and economists working in more practical fields. Entire international conferences are now devoted to papers on the subject. A glance at the proceedings of such a conference [71] will give an indication to the myriad of applications of SI, too numerous to even begin to list here.

Of particular interest, though, are studies of marine-oriented applications. This field is very appropriate for adaptive SI especially, because of the uncertain, time-varying nature of the dynamics. Kallstrom [72] applied RML and output error methods to simulated and real data from three oil tankers and a cargo ship. This reference also lists many other previous studies of ship dynamics identification. Pioneering work was done by Nomoto [73] who suggested using least squares to estimate a ship's steering indices from zig-zag tests.

Jefferys and co-workers have considered a number of marine applications. Samra and Jefferys have developed an adaptive predictor with near-optimal performance for ship roll and pitch motion [74]; this could be of great use during aircraft and helicopter landings on ships and for oil-rig supply ships which must transfer cargo by crane in heavy seas. A method of using Inverse Fourier Transforms coupled with SI for deriving transfer functions of systems characterised by frequency response data has been considered by Goheen and Jefferys [75]. This study, still in progress, was motivated by the need for

simple models of wave-power devices. Robbins also used a wave power device, the Salter 'Duck', as one of his examples in his thesis on SI [76].

An application closely related to the present study is that of identifying submarine models. Tinker, Bowman and Booth [64] have used SI methods to analyse scale model data from harmonic response, pulse response and PRBS tests. It was this reference that was mentioned in the discussion of closed-loop identification in section 6.3. They found the model submarine would either hit the tank bottom or break the surface without the depth autopilot in the loop. However, with closed-loop control, there were difficulties in exciting the submarine's dynamics sufficiently.

6.5 Identification of Seapup

This section will examine the suitability of recursive system identification for modelling the dynamics of a ROV. Because experimental facilities were not available, the testing method was to use the linear and nonlinear Seapup simulations to generate the raw data series. Sensor and disturbance noise was added to see what detrimental effect they have on the estimation. Three SI algorithms, Least Squares, Extended Least Squares and Recursive Prediction Error was used and their performances compared. Optimal model order was determined using the three statistical tests described in section 6.3.

Though no general conclusions about the ability of SI methods can be made with only simulated data from one vehicle to work with, the results of this exercise indicate whether further study is worthwhile.

6.5.1 Linearised Simulation Model

In section 3.2, a linear approximation of the full Seapup model was derived for eigenvalue analysis. This model is only valid in operating regions close to the point of linearisation, but it is still useful for the first stage of this study. If SI fails on data

generated by this simulation, then there will be no point in proceeding with data from the nonlinear simulation or experiments.

Here, a model linearised about the quiescent state will be used. Measurement noise will be added corresponding to the accuracy reported by Kallstrom in his study of ship dynamics identification [72]. Amongst the ships used were the "Sea Scout" and "Sea Swift", both oil tankers. They were equipped with Atlas doppler logs with a stated accuracy of 0.02 knots and yaw rate gyros with 0.005 degrees/second accuracy. It will be assumed here that these figures represent the 3σ limits of Gaussian white noise. Pitch and roll gyros with an accuracy of 0.25 degrees will also be assumed to be available.

This assumed sensor model will not represent the fit used in the trials described in appendix A nor its associated problems. Again, this is because of lack of time to incorporate the trials into the main body of this thesis. Readers will wish to look at this appendix for a description of the inertial navigation system and analogue filters. Of particular interest are the problems of separating thruster induced vibration from the rigid-body motion that is to be modelled.

For this preliminary attempt at identification, disturbances caused by current and turbulence are not included. Later, in section 6.5.4, these will be added to the nonlinear simulation.

The input series considered is a PRBS of 10 sample clock cycles and magnitude $\pm$ 10 degrees. The standard sampling rate of 5 Hz, used for the numerical simulations and controller algorithms, is chosen here as well. Three hundred data points are generated for use in the LS algorithm. The covariance matrix, P(t), has an initial value of 100 I and θ is set to zero. The forgetting factor, $\lambda(t)$, is determined by (6.15) with $\lambda(0) = 0.6$ and $\alpha = 0.9$. Figure 6.1 shows the transient behaviour of the estimated model over this sixty seconds of real time. The model has matrix polynomials $A(z^{-1})$ and $B(z^{-1})$ of order 2.

While the performance during this run is obviously good, it is desirable to determine the most suitable model order in a systematic fashion. Clearly, with this simulated data, the correct model orders are known but this will not be the case with realistic data. The orders of $A(z^{-1})$ and $B(z^{-1})$ will be increased together starting from 1 until the optimal order is determined. Table 6.1 lists the values of the loss function $V_n(\theta)$ (6.11) and AIC_n (6.19) and the statistic F for n = 1,2,3. The LS algorithm as described above was used for all of these cases.

The values of AIC indicate that the output r is adequately modelled by a first order system while u, v, w, roll and pitch require second order representations. The F tests point to the same conclusions; the risk of error is zero here because the equation error variance actually increases for models larger than the optimal. Figure 6.2 shows the six correlation functions of the residuals for the model, order(A,B) = 2,2; the residuals of this model are close to white noise, as required.

The performance of the final model is compared with the real data in figure 6.3. In order to ensure that the parameters have converged, the 300 sample data series is rewound and passed through repeatedly until the algorithm has examined 2000 points. The models of surge, sway, heave and yaw match especially well; the output error is not visible. Roll and pitch errors are larger in proportion to the values of these two outputs.

6.5.2 Nonlinear Simulation Model

An attempt to identify the nonlinear simulation may now be made with increased confidence since the analysis of the linear simulation data was so successful. The procedure is exactly the same as with the linear simulation. PRBS input series are used to excite the thrusters and the input and output are logged for 60 seconds at a sampling rate of 5 Hz. Measurement noise is added to the output values.

This data is analysed with LS methods of increasing order; the

results are summarised in table 6.2. The minimum value of the criterion function shows that while a first order model is adequate to represent surge, second order descriptions are required for the other five degrees of freedom. Therefore, second order polynomials must be used throughout. The F statistics also indicate these model orders are best; again, this test is trivial because the variance is minimal for the optimal model order.

The correlation functions of the six residuals for the model, order (A,B) = 2,2, are shown in figure 6.4. These indicate that the residuals are probably not white noise as required, but instead weakly correlated. Identification has not been as successful as in the case of data generated by the linear model, not too surprising a result since in this case there is a mismatch between system and model structure. The comparison between the transient performance of the estimated model and the original nonlinear measurements is given in figure 6.5. Here, the rapid elimination of the output error is apparent.

In order to ensure that the parameters have converged, the LS algorithm is used to analyse 2000 data points. The performance of the resulting model is shown in figure 6.6. It is interesting to see how well the nonlinear simulation can be characterised by a low order linear model, even in open-loop operation. The weakly correlated residuals do not seem to be of much consequence. It is also possible that when the SI technique is used in an adaptive control scheme, feedback will reduce the effects of modelling errors even further.

6.5.3 Least Squares, Extended Least Squares and Recursive Prediction Error Methods

The simple LS identification method has been shown to produce models which characterise both the linear and nonlinear simulations very well. In some conditions however, other algorithms might prove to be more suitable. Reference [70] suggests circumstances when ELS and RPEM might be better. ELS estimates the noise model as well as $A(z^{-1})$ and $B(z^{-1})$; this is important in situations when the noise

affecting the system is not white since it prevents biased parameter estimates. The RPEM algorithm uses a more complex gradient approximation than the other two methods. However, this allows the RPEM to converge in more general circumstances than LS or ELS, leading to better accuracy for very long data series from linear systems. For short data series and systems with unmodelled dynamics, the accuracy of RPEM may not be as good as LS or ELS. The use of a factor for 'weakening' the filtering process of the RPEM during the initial phase allows its transient accuracy to be improved.

These three algorithms will be compared by considering their performance with the data generated by the nonlinear simulation driven by the same PRBS. Values of AIC will be used to judge which is best, remembering that models produced by ELS and RPEM will have more parameters than LS because of the noise model estimation. Table 6.3 lists the values of the information criterion for the first 300 points of the operation and for runs operating on 2000 data points.

LS and ELS produce models with nearly identical AIC values. This indicates that modelling $C(z^{-1})$ is really not essential for this data, but it is of some slight value.

It is interesting to note how much worse the RPEM method performed relative to the more simple algorithms, especially for the shorter data series. Quite possibly the RPEM could be 'tuned' by modifying its filtering factors to improve its performance, an exercise which will not be attempted here. The RPEM estimations in this form are adequate however and this method is definitely worth further study. In an effort to determine the cause of this poor behaviour, the tests of table 6.3 were repeated with data from the linear Seapup simulation. It was thought the combination of the unmodelled nonlinearities and the strong convergence properties of the RPEM might have led to this problem, since a nonlinear system will be modelled better by an estimator which adapts more quickly. The results of this exercise seem to support this theory.

The models produced from the nonlinear simulation data are compared in figures 6.7 (LS), 6.8 (ELS) and 6.9 (RPEM). Each shows

the error of the final model produced after a 2000 point run relative to the original measurements. These final modelling errors are nearly identical for all three SI methods, showing that the models have converged to nearly the same values, independent of the technique used. This is also an indication that estimating $C(z^{-1})$ is really of no use here.

6.5.4 Effects of Environmental Disturbances

Though it is assumed that experiments to gather data for SI analysis of ROVs would always be carried out in still bodies of water, most likely manoeuvering tanks, effects of current and turbulence will be considered here briefly.

The nonlinear simulation driven by the same PRBS is used again. A current with a mean speed of 0.26 m/s and standard deviation 0.086 m/s is added. The average current direction is zero degrees with a standard deviation of 20 degrees. Of particular interest during identification is the effect of estimating the noise model; here LS of order (2,2) will be compared with ELS of order (2,2,2). The results of SI runs of 300 and 2000 data points are listed in table 6.5.

As in the undisturbed case summarised in table 6.3, ELS performs better than LS, both for short and long data series. Here, the advantage of ELS over LS is more apparent in the transient case. Plots of the measurements compared to the adapting model output are given in figures 6.10 (LS) and 6.11 (ELS). ELS is especially impressive during the initial 60 samples; its model output does not 'burst' as did the estimated LS output.

6.5.5 Closed-Loop Estimation

It was noted in section 6.3 that closed-loop identification has unique difficulties, but is essential in certain circumstances, e.g. when the plant must be maintained within safe operating limits or when adaptive control is to be implemented. The case considered here will

be the nonlinear simulation driven by the fixed-gain 'self-testing' controller. Measurement noise is included in the feedback loop. The reference velocity vector is a square wave of half-period 10 seconds. During the first half period, this reference is:

$$r^T = (\ 0.2\ m/s,\ 0.0\ m/s,\ 0.0\ m/s,\ 15.0\ deg/s\ )$$

For the second half:

$$r^T = (\ 0.0\ m/s,\ 0.1\ m/s,\ -0.1\ m/s,\ 0.0\ deg/s\ )$$

The response of the simulated ROV to this reference input is shown in figure 6.12.

It can be seen from the data in table 6.6 that different optimal model orders compared to those determined during the open-loop tests apply here. First order models can be used for sway and heave for certain and for surge with the risk of error being less than 0.5 percent. Yaw velocity, roll and pitch require second order models; therefore, the entire system will be represented by second order polynomials. The performance of second-order LS, ELS and RPEM algorithms are compared in table 6.7. Their relative abilities are very close to the open-loop case, as presented in table 6.3. As before, ELS is marginally better than LS, but here RPEM is closer in performance to the other two than previously. This is perhaps because the simulation is operating in a smaller state-space region than in the open-loop case, making the measurements 'less nonlinear'.

The transient performance of the ELS estimation is shown in figure 6.13; again, rapid reduction of the equation error can be seen. This is compared with the final model, achieved after 2000 data points, in figure 6.14. It is obvious that none of the difficulties associated with closed-loop identification have occurred in this one example. This is very encouraging because the subject of the next chapter, the performance of adaptive controllers for ROVs, is very dependent on closed-loop SI working well.

6.6 Summary

It has been shown that multivariable recursive SI methods can be applied to the problem of modelling ROV dynamics. Since experimental data was not available, the information for the tests was generated by the nonlinear Seapup simulation, described in chapters 2 and 3. Unfortunately, this limitation weakens any general conclusions that can be made about the suitability of this technique.

Least Squares, Extended Least Squares and Recursive Prediction Error Algorithms were all used successfully. ELS produced slightly lower values of Akaike's Information Criterion than did LS, indicating that the estimation of the noise model $C(z^{-1})$ is worthwhile. RPEM had relatively poor performance compared to LS and ELS; it was thought that the nonlinearities in the simulation combined with the slow, yet strong convergence properties of the algorithm might have caused this. LS and ELS converge more rapidly, but with less strong asymptotic behaviour.

The results of statistical tests indicate that all of the nonlinear dynamics which are thought to be essential in modelling a ROV are conveniently lumped into first and second order linear models. The improvement in the speed of a simulation using a linear model can be important, especially in cases where it must run in real time, such as for pilot training. As an example of this improvement, the computer programme used for this study was linked with the nonlinear and second-order linear models and their speeds compared for a simulation of 60 seconds real time:

Nonlinear	:	207 seconds
Linear	:	77 seconds

If only an ARMAX model is required, modelling ROVs by SI methods compared with the conventional hydrodynamics approach can result in great savings, both in time and cost. These savings occur because specialised testing equipment such as planar motion mechanisms are no longer required while the velocity and position measuring equipment that is needed for SI is more commonly available. The work presented

here also suggests that the analysis of the data is simpler and more easily checked for errors. Either the model matches the original measurements or it does not; it is not necessary to go through a lengthy validation exercise of the type described in chapter 3.

Table 6.1

Determination of Optimal Model Order; Linear System

Data: Linear Seapup model with measurement noise
PRBS input, clock cycle 10 samples, ± 10 degrees
Sampling rate: 5 Hz

S.I.: Least Squares , $\underline{P}(0) = 100\ \underline{I}$, $\underline{\theta}(0) = \underline{0}$
$\lambda(0) = 0.6$, $\alpha = 0.9$
$N_{data} = 300$

Output	Model Order, N	V_N	AIC_N	$F_{N \to N+1}$
u	1	0.1552×10^{-4}	-2449.	13.15
	2	0.1056×10^{-4}	-2527.	-4.190
	3	0.1250×10^{-4}	-2512.	
v	1	0.1612×10^{-4}	-2437.	15.61
	2	0.1035×10^{-4}	-2533.	-0.05207
	3	0.1037×10^{-4}	-2527.	
w	1	0.1561×10^{-4}	-2447.	17.66
	2	0.9591×10^{-5}	-2556.	-0.2372
	3	0.9676×10^{-5}	-2533.	
r	1	0.2579×10^{-5}	-2989.	-23.51
	2	0.1609×10^{-4}	-2401.	-21.21
	3	0.7503×10^{-4}	-1923.	
ϕ	1	0.1165×10^{-3}	-1844.	388.4
	2	0.7833×10^{-5}	-2616.	-0.06533
	3	0.7852×10^{-5}	-2595.	
θ	1	0.2969×10^{-3}	-1563.	900.7
	2	0.8951×10^{-5}	-2576.	-0.1976
	3	0.9017×10^{-5}	-2554.	

Table 6.2

Determination of Optimal Model Order; Nonlinear System

Data: Nonlinear Seapup model with measurement noise
PRBS input, clock cycle 10 samples, ± 10 degrees
Sampling rate: 5 Hz

S.I.: Least Squares , $\underline{P}(0) = 100\ \underline{I}$, $\underline{\theta}(0) = \underline{0}$
$\lambda(0) = 0.6$, $\alpha = 0.9$
$N_{data} = 300$

Output	Model Order, N	V_N	AIC_N	$F_{N \to N+1}$
u	1	0.1984×10^{-4}	-2375.	-0.2933
	2	0.2005×10^{-4}	-2344.	-0.3038
	3	0.2880×10^{-4}	-2208.	
v	1	0.2945×10^{-4}	-2256.	2.769
	2	0.1922×10^{-4}	-2357.	-0.1119
	3	0.1930×10^{-4}	-2327.	
w	1	0.1837×10^{-4}	-2398.	4.909
	2	0.1563×10^{-4}	-2418.	-0.3411
	3	0.1583×10^{-4}	-2386.	
r	1	0.8184×10^{-4}	-1950.	52.26
	2	0.2855×10^{-4}	-2238.	-18.81
	3	0.9411×10^{-4}	-1855.	
ϕ	1	0.2888×10^{-3}	-1572.	818.5
	2	0.9553×10^{-5}	-2565.	-0.1350
	3	0.9601×10^{-5}	-2535.	
θ	1	0.1845×10^{-3}	-1706.	549.1
	2	0.8951×10^{-5}	-2585.	-1.111
	3	0.9335×10^{-5}	-2547.	

Table 6.3

Comparison of LS, ELS and RPEM Algorithms

Data: Nonlinear Seapup model with measurement noise
PRBS input, clock cycle 10 samples, ± 10 degrees
Sampling rate: 5 Hz

S.I.: $\underline{P}(0) = 100\ \underline{I}$, $\underline{\theta}(0) = \underline{0}$
$\lambda(0) = 0.6$, $\alpha = 0.9$
For RPEM: $K(0) = 0.1$, $\gamma = 0.98$
Model Order: LS: (A,B) = (2,2)
ELS and RPEM: (A,B,C) = (2,2,2)

N_{data}	Output	Values of AIC		
		LS	ELS	RPEM
300	u	-2344	-2357	-1713
	v	-2357	-2343	-2072
	w	-2418	-2473	-787.5
	r	-2238	-2476	-1485
	ϕ	-2565	-3066	-2305
	θ	-2585	-3228	-1478
2000	u	-15,620	-15,840	-13,590
	v	-15,480	-15,820	-15,270
	w	-15,990	-16,360	-11,150
	r	-16,100	-16,970	-14,200
	ϕ	-19,730	-22,140	-17,060
	θ	-22,410	-23,550	-12,920

Table 6.4

Comparison of LS, ELS and RPEM Algorithms; Linear System

Data: Linear Seapup model with measurement noise
PRBS input, clock cycle 10 samples, ± 10 degrees
Sampling rate: 5 Hz

S.I.: $\underline{P}(0) = 100\ \underline{I}$, $\underline{\theta}(0) = \underline{0}$
$\lambda(0) = 0.6$, $\alpha = 0.9$
For RPEM: $K(0) = 0.1$, $\gamma = 0.98$
Model Order: LS: (A,B) = (2,2)
ELS and RPEM: (A,B,C) = (2,2,2)

N_{data}	Output	Values of AIC		
		LS	ELS	RPEM
300	u	-2527	-2565	-1856
	v	-2533	-2572	-2120
	w	-2556	-2594	-2307
	r	-2401	-3293	-2089
	ϕ	-2616	-3177	-2716
	θ	-2576	-3326	-2555
2000	u	-16,680	-17,310	-18,260
	v	-16,690	-17,210	-18,310
	w	-16,840	-17,430	-18,620
	r	-20,140	-25,330	-27,440
	ϕ	-21,170	-23,100	-24,100
	θ	-23,980	-24,700	-26,090

Table 6.5

Comparison of LS and ELS Algorithms;
Nonlinear Simulation with Turbulence

Data: Nonlinear Seapup model with measurement noise
Current/Turbulence model added
PRBS input, clock cycle 10 samples, ± 10 degrees
Sampling rate: 5 Hz

S.I.: $\underline{P}(0) = 100\ \underline{I}$, $\underline{\theta}(0) = \underline{0}$
$\lambda(0) = 0.6$, $\alpha = 0.9$
Model Order: LS: (A,B) = (2,2)
ELS: (A,B,C) = (2,2,2)

N_{data}	Output	Values of AIC	
		LS	ELS
300	u	-2106	-2202
	v	-2112	-2144
	w	-2273	-2331
	r	-2179	-2470
	ϕ	-2514	-2539
	θ	-2581	-2657
2000	u	-14,050	-14,630
	v	-13,840	-14,160
	w	-14,850	-15,350
	r	-15,480	-16,160
	ϕ	-16,470	-16,960
	θ	-16,950	-17,810

Table 6.6

Determination of Optimal Model Order;
Nonlinear Closed-Loop System

Data: Nonlinear Seapup model with measurement noise
Fixed-gain closed-loop velocity controller input
Reference: Square wave of half-period 10 seconds

$\underline{r}^T_0$= { 0.2 m/s, 0.0 m/s, 0.0 m/s, 15.0 deg/s }
$\underline{r}^T_1$= { 0.0 m/s, 0.1 m/s, -.1 m/s, 0.0 deg/s }

Sampling rate: 5 Hz

S.I.: Least Squares , $\underline{P}(0) = 100\ \underline{I}$, $\underline{\theta}(0) = \underline{0}$
$\lambda(0) = 0.6$, $\alpha = 0.9$
$N_{data} = 300$

Output	Model Order, N	V_N	AIC_N	$F_{N \to N+1}$
u	1	0.2010×10^{-4}	-2371.	0.9357
	2	0.1945×10^{-4}	-2353.	-19.88
	3	0.7374×10^{-4}	-1928.	
v	1	0.1092×10^{-4}	-2554.	-9.480
	2	0.1651×10^{-4}	-2402.	-1.278
	3	0.1733×10^{-4}	-2359.	
w	1	0.1061×10^{-4}	-2563.	-19.67
	2	0.3568×10^{-4}	-2171.	-0.7647
	3	0.3672×10^{-4}	-2136.	
r	1	0.1418×10^{-4}	-2476.	73.41
	2	0.3092×10^{-5}	-2903.	-26.57
	3	0.1930×10^{-3}	-1641.	
ϕ	1	0.7070×10^{-4}	-1994.	1230.
	2	0.1574×10^{-5}	-3105.	-0.3220
	3	0.1593×10^{-5}	-3071.	
θ	1	0.6242×10^{-4}	-2031.	5154.
	2	0.3373×10^{-6}	-3565.	-21.08
	3	0.1539×10^{-5}	-3081.	

Table 6.7

Comparison of LS, ELS and RPEM Algorithms;
Nonlinear Closed-Loop System

Data: Nonlinear Seapup model with measurement noise
Fixed-gain closed-loop velocity controller input
Reference: Square wave of half period 10 seconds

$\underline{r}^T_0$= { 0.2 m/s, 0.0 m/s, 0.0 m/s, 15.0 deg/s }
$\underline{r}^T_1$= { 0.0 m/s, 0.1 m/s, -.1 m/s, 0.0 deg/s }

Sampling rate: 5 Hz

S.I.: $\underline{P}(0) = 100\ \underline{I}$, $\underline{\theta}(0) = \underline{0}$

$\lambda(0) = 0.6$, $\alpha = 0.9$

For RPEM: $K(0) = 0.1$, $\gamma = 0.98$

Model Order: LS: (A,B) = (2,2)
ELS and RPEM: (A,B,C) = (2,2,2)

N_{data}	Output	Values of AIC		
		LS	ELS	RPEM
300	u	-2353	-2485	-1756
	v	-2402	-2580	-2101
	w	-2171	-2562	-1830
	r	-2903	-2990	-2123
	ϕ	-3105	-3327	-2914
	θ	-3565	-3315	-2568
2000	u	-15,720	-16,690	-15,900
	v	-16,030	17,160	-15,180
	w	-14,890	-17,050	-13,270
	r	-19,040	20,110	-17,550
	ϕ	-21,010	-24,200	-19,970
	θ	-24,110	-25,300	-18,140

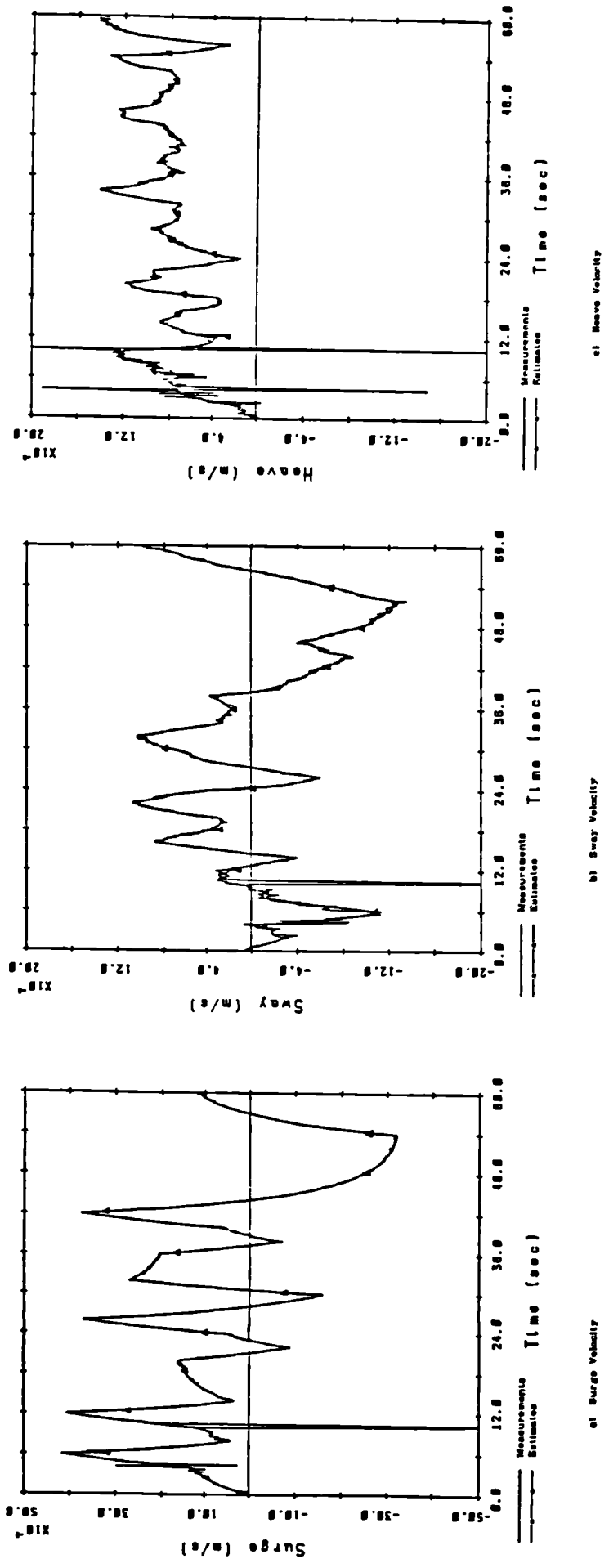

Figure 6.1 : Transient Performance of LS Method; Linear PRBS Data

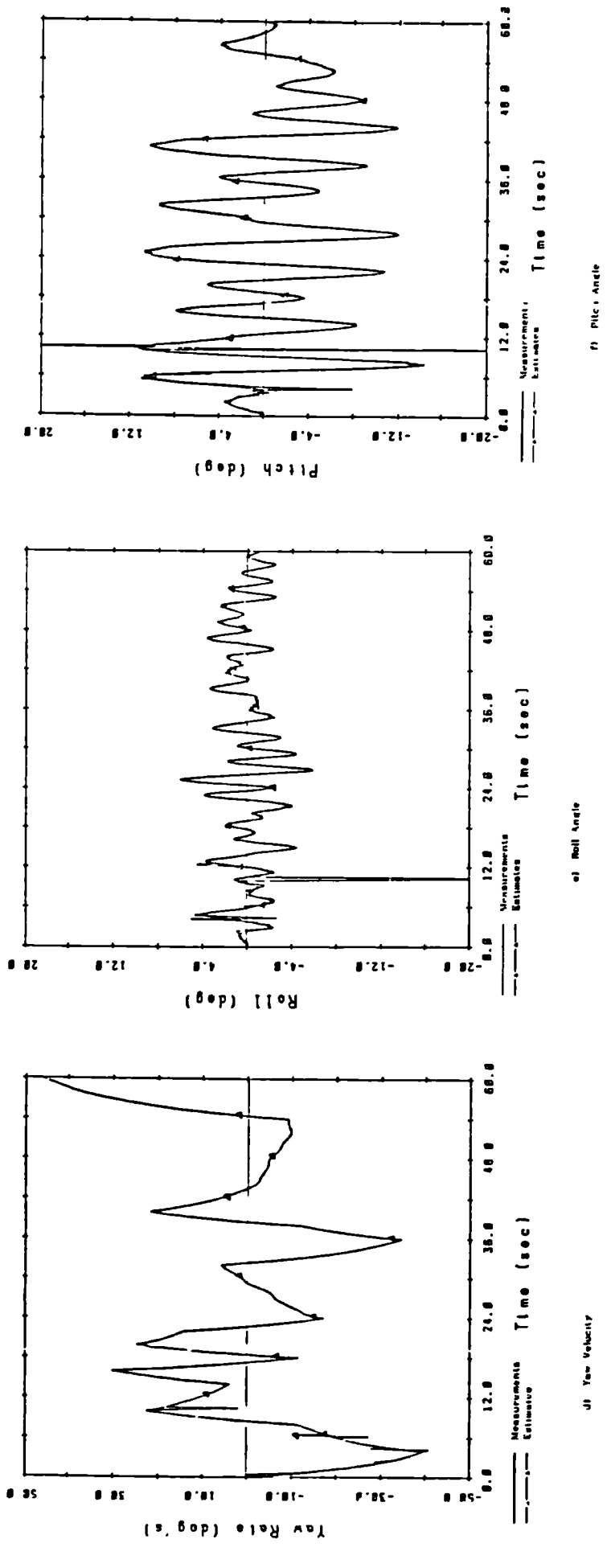

Figure 6.1 : Continued

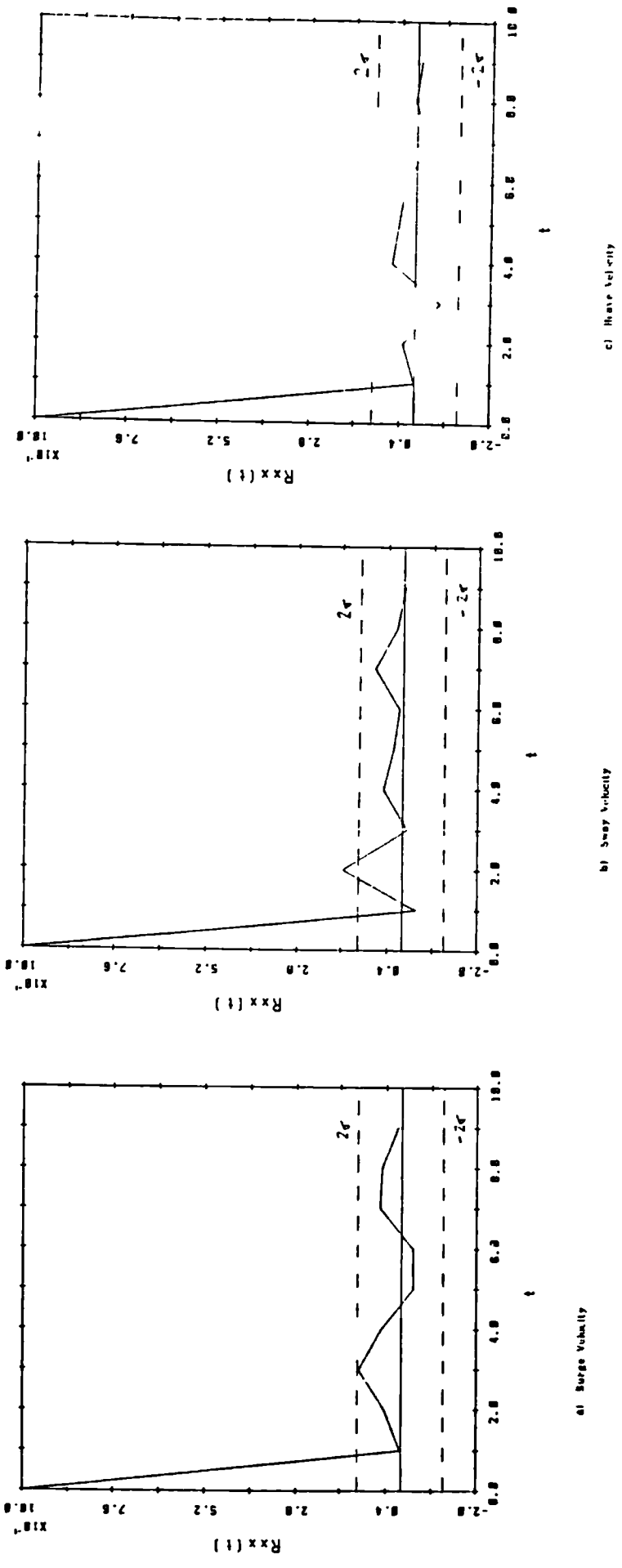

Figure 6.2 : Correlation Functions of LS Residuals; Linear PRBS Data

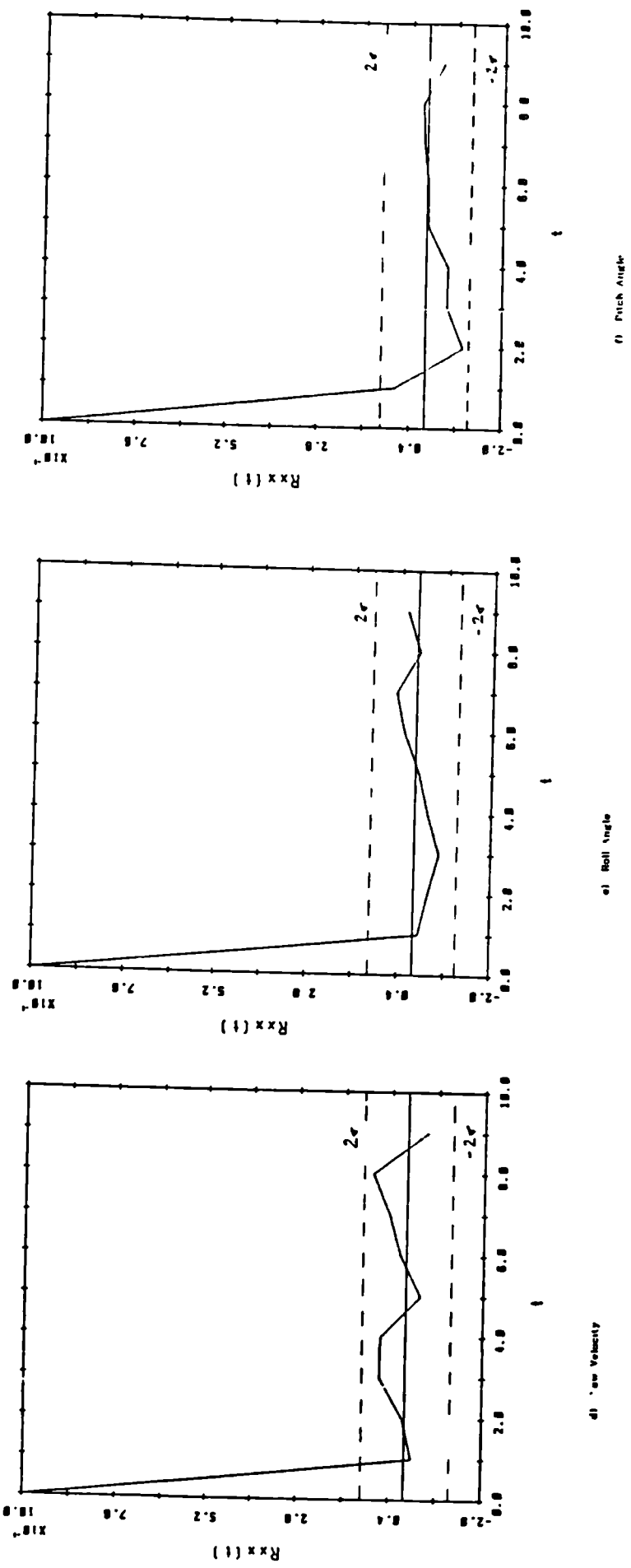

Figure 6.2 : Continued

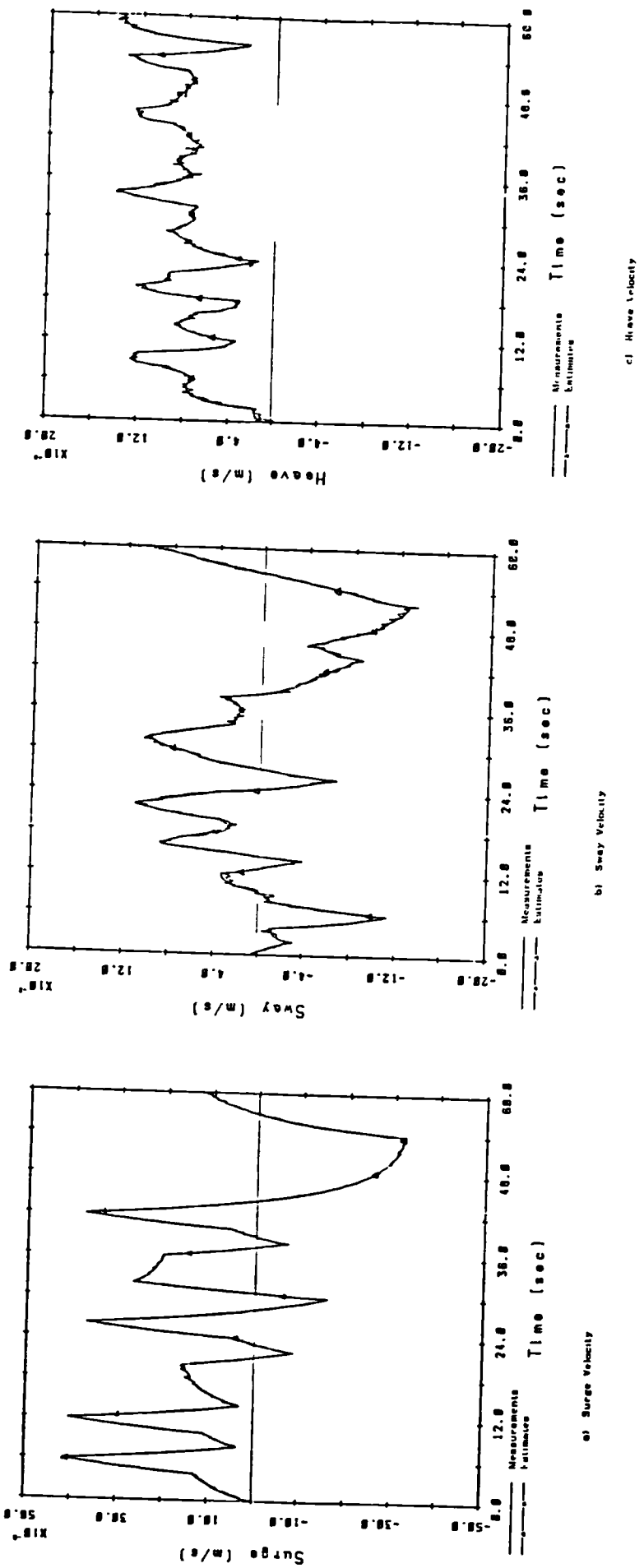

Figure 6.3 : Performance of Final LS Model; Linear PRBS Data

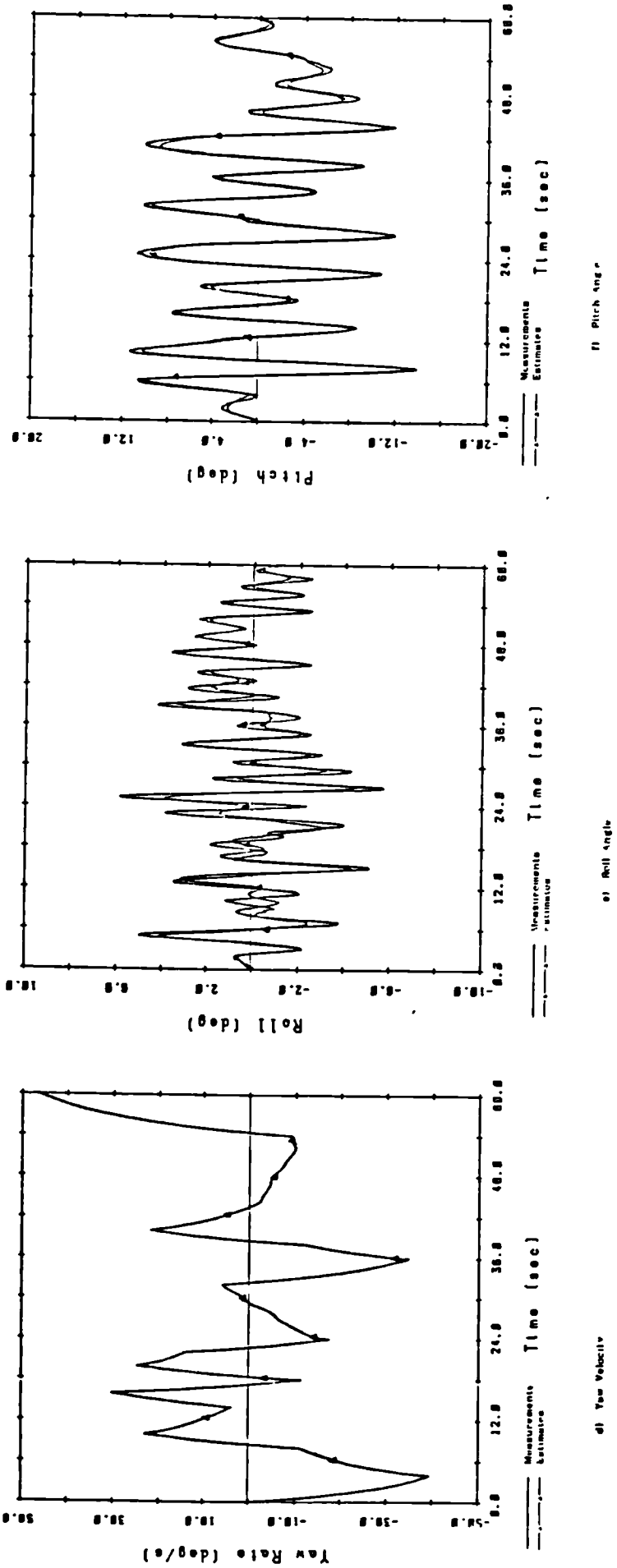

Figure 6.3 : Continued

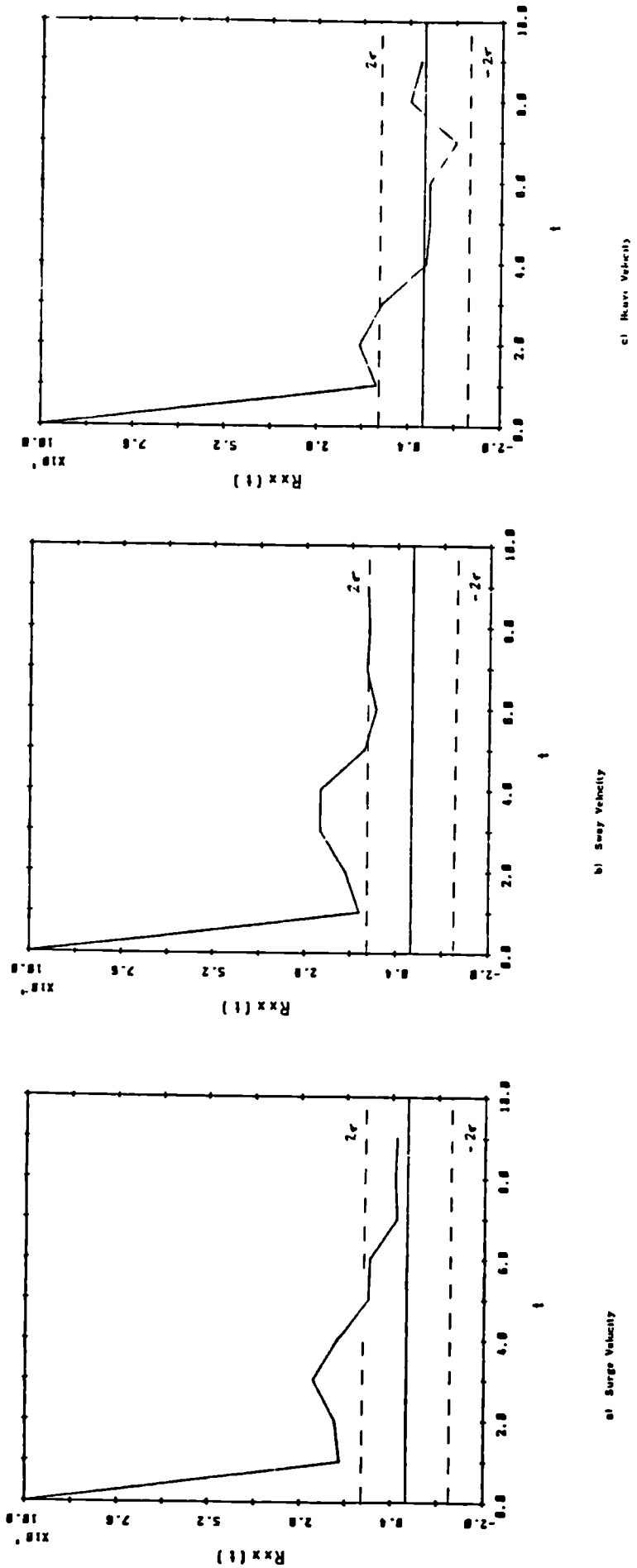

Figure 6.4 : Correlation Functions of LS Residuals; Nonlinear PRBS Data

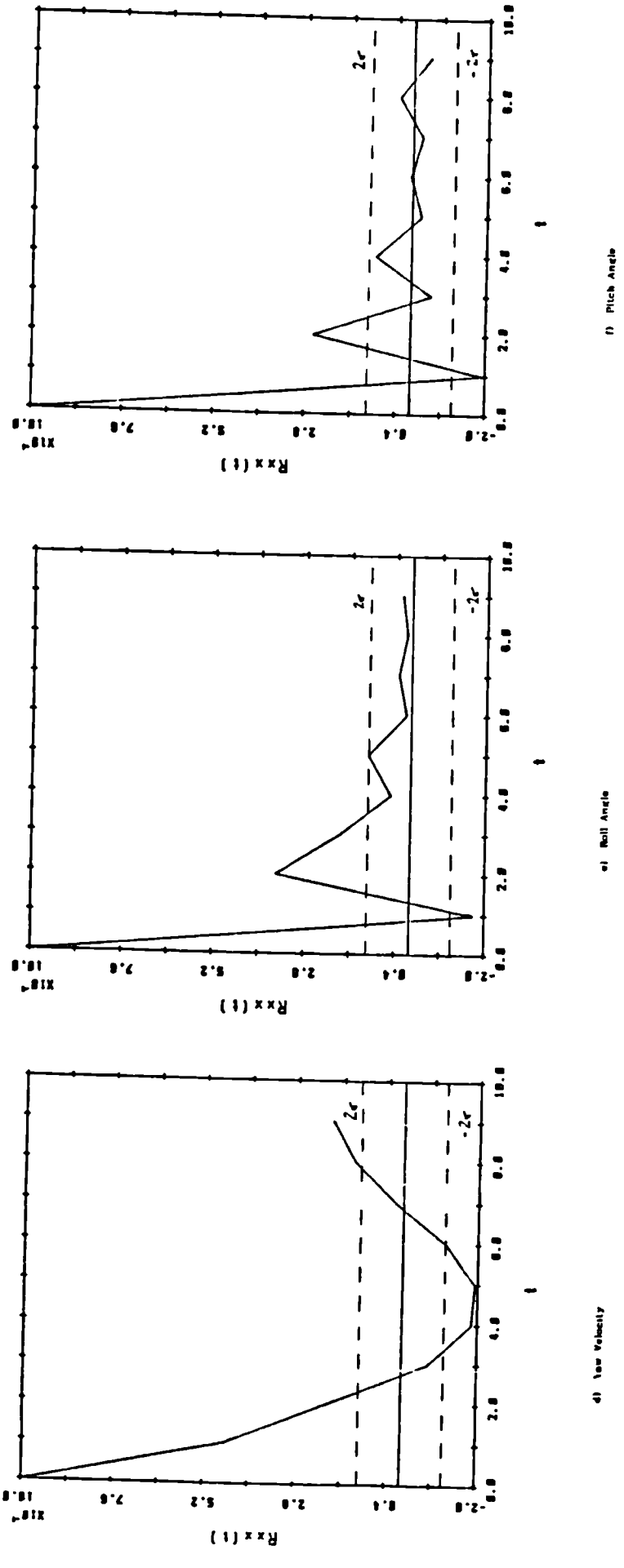

Figure 6.4 : Continued

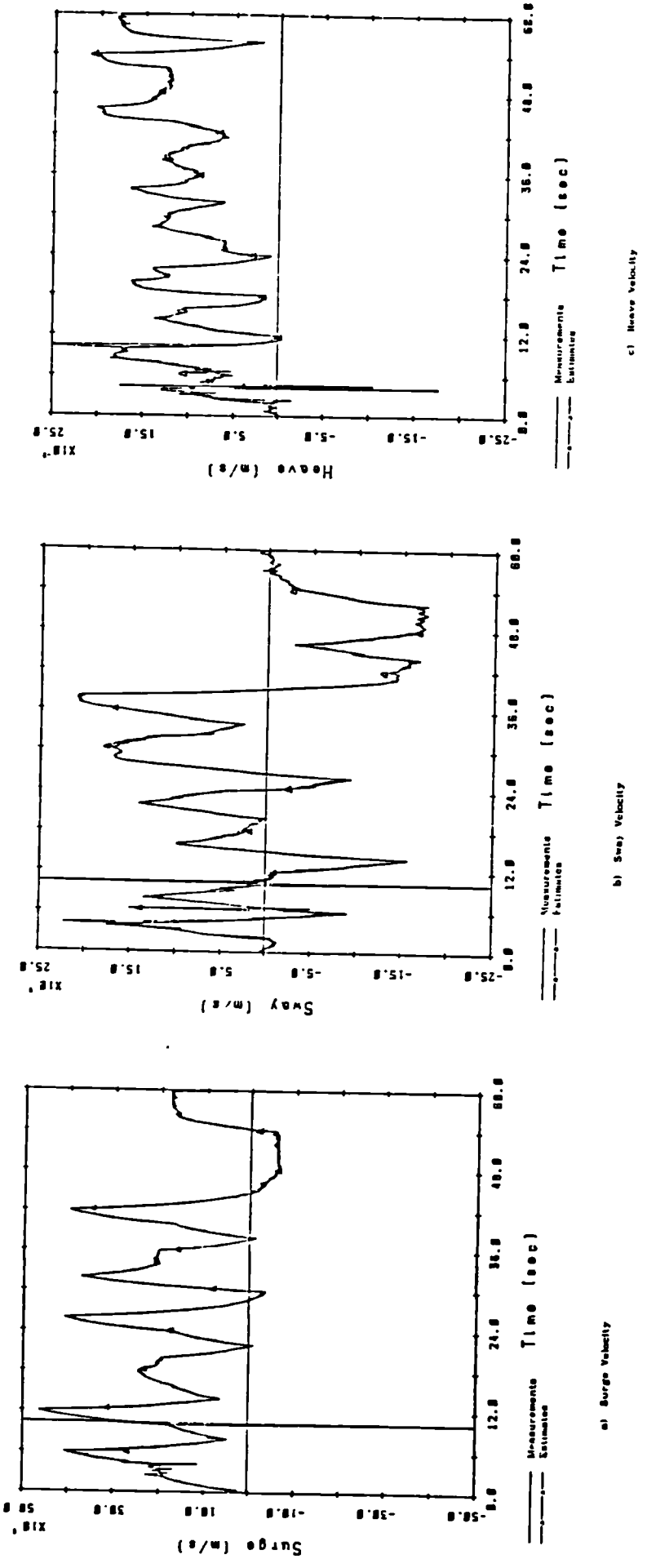

Figure 6.5 : Transient Performance of LS Method; Nonlinear PRBS Data

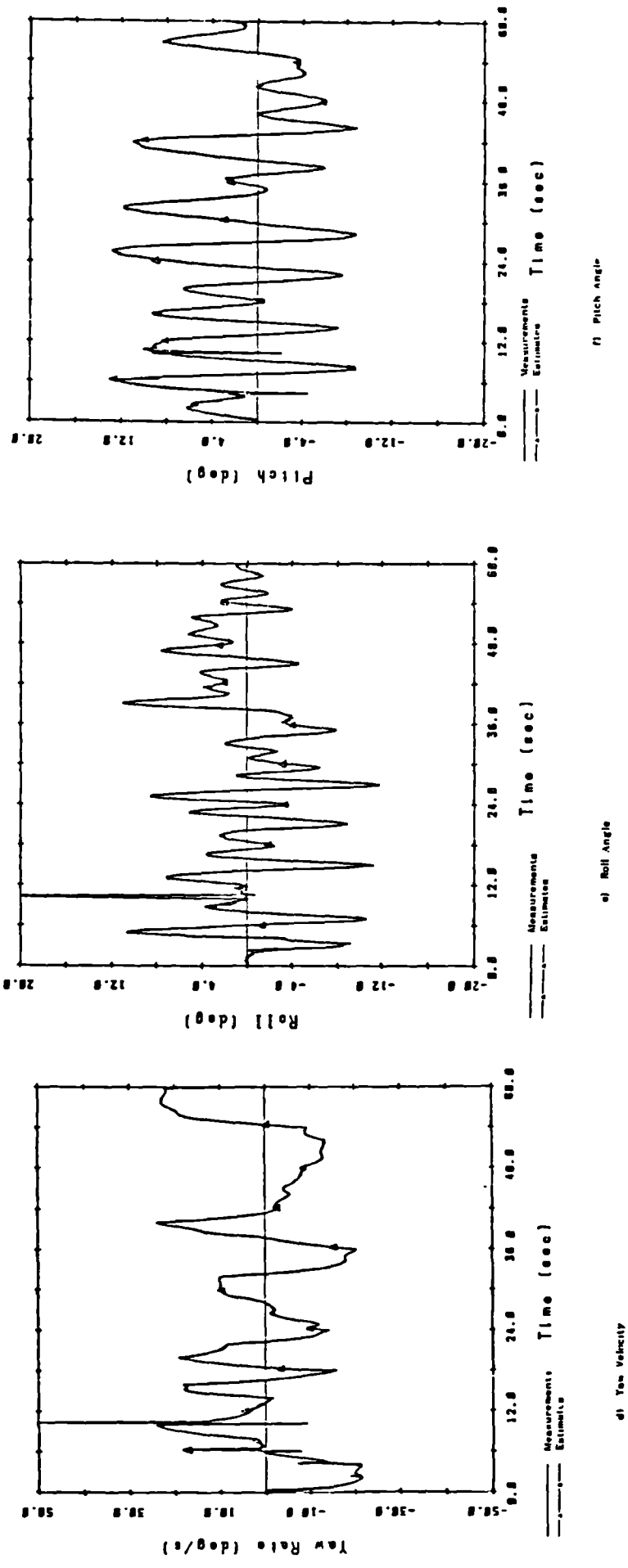

Figure 6.5 : Continued

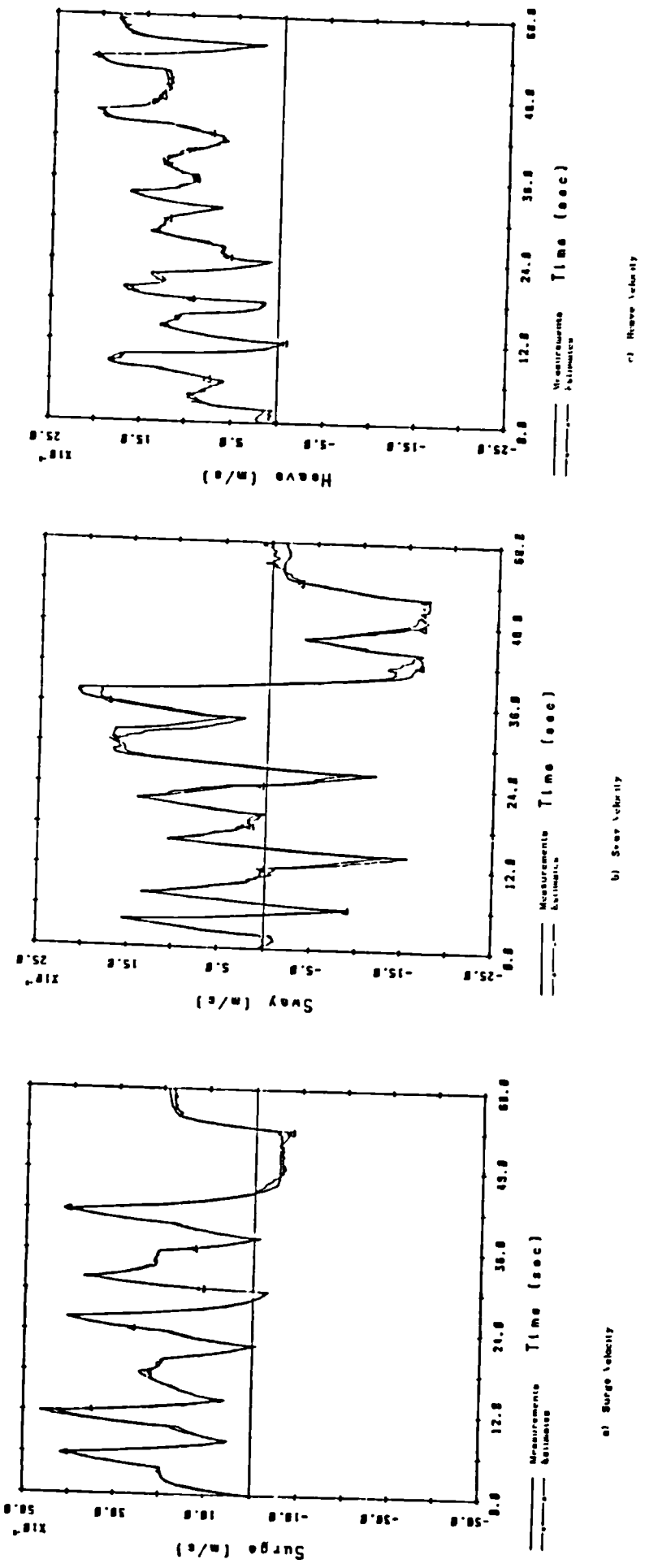

Figure 6.6 : Performance of Final LS Model; Nonlinear PRBS Data

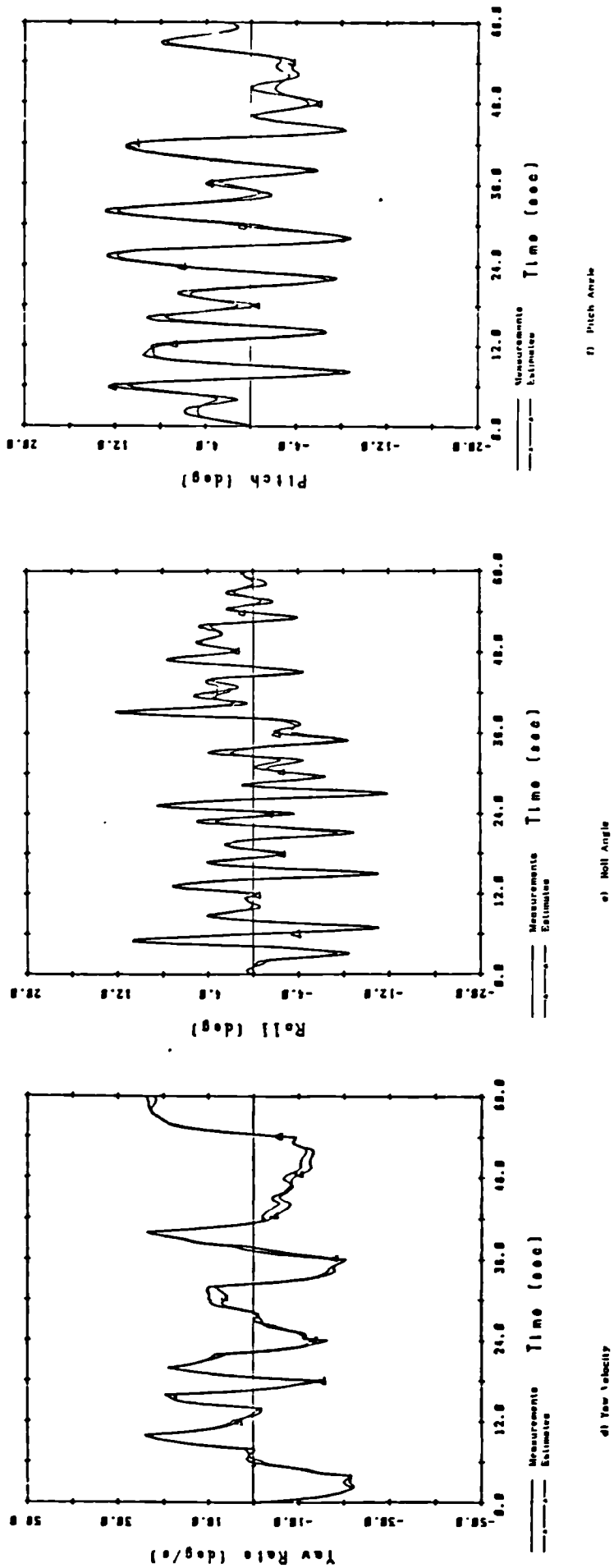

Figure 6.6 : Continued

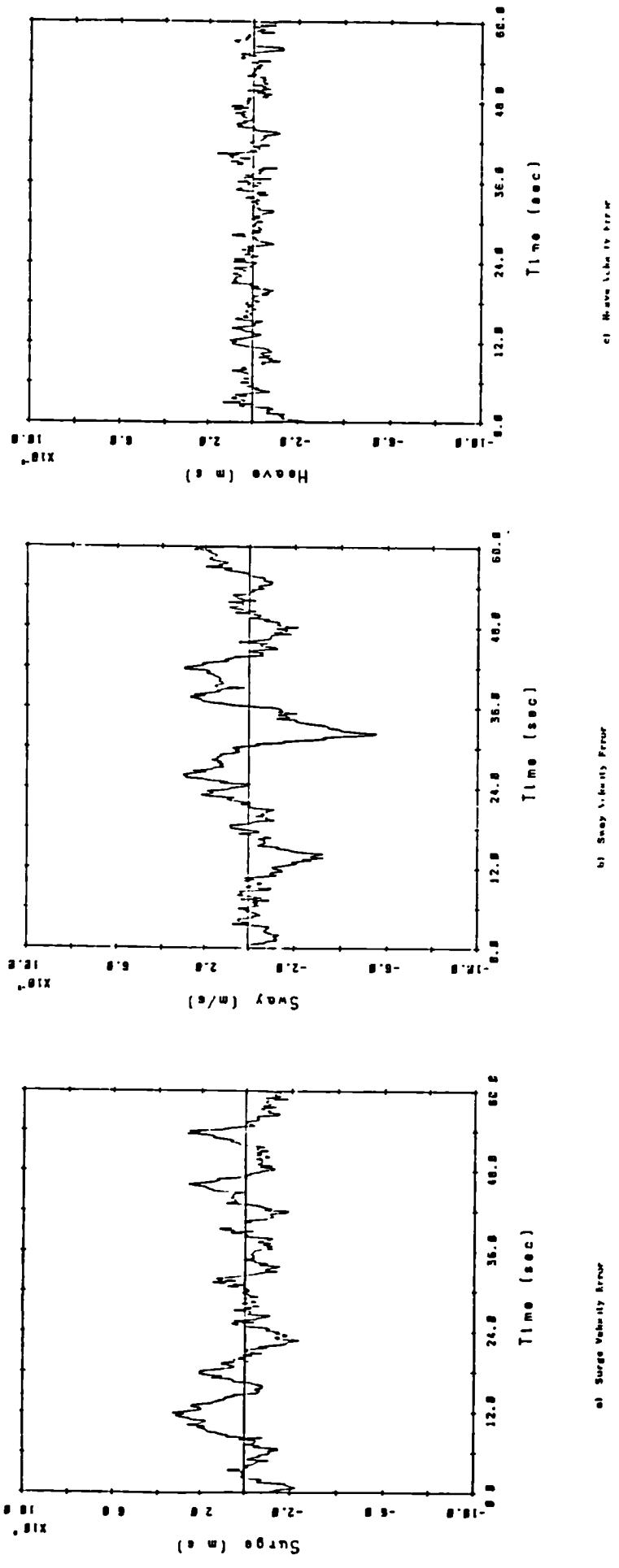

Figure 6.7 : Errors of Final LS Model; Nonlinear PRBS Data

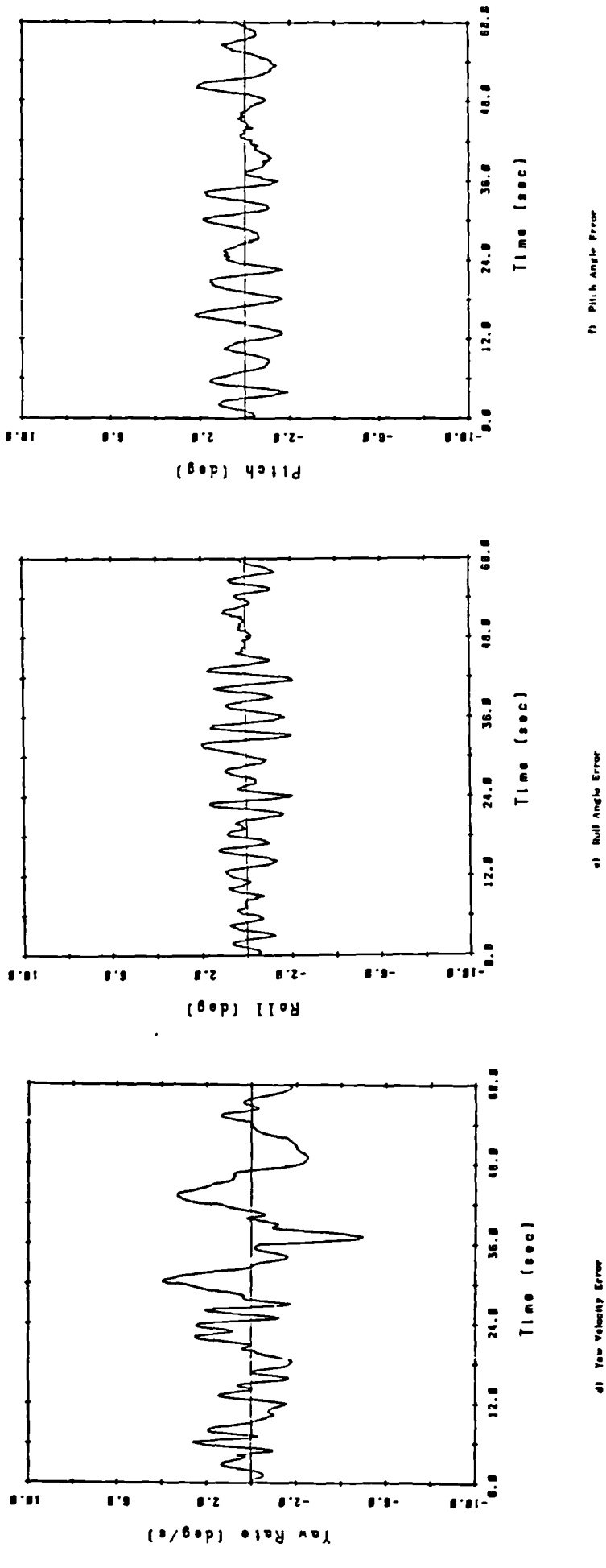

Figure 6.7 : Continued

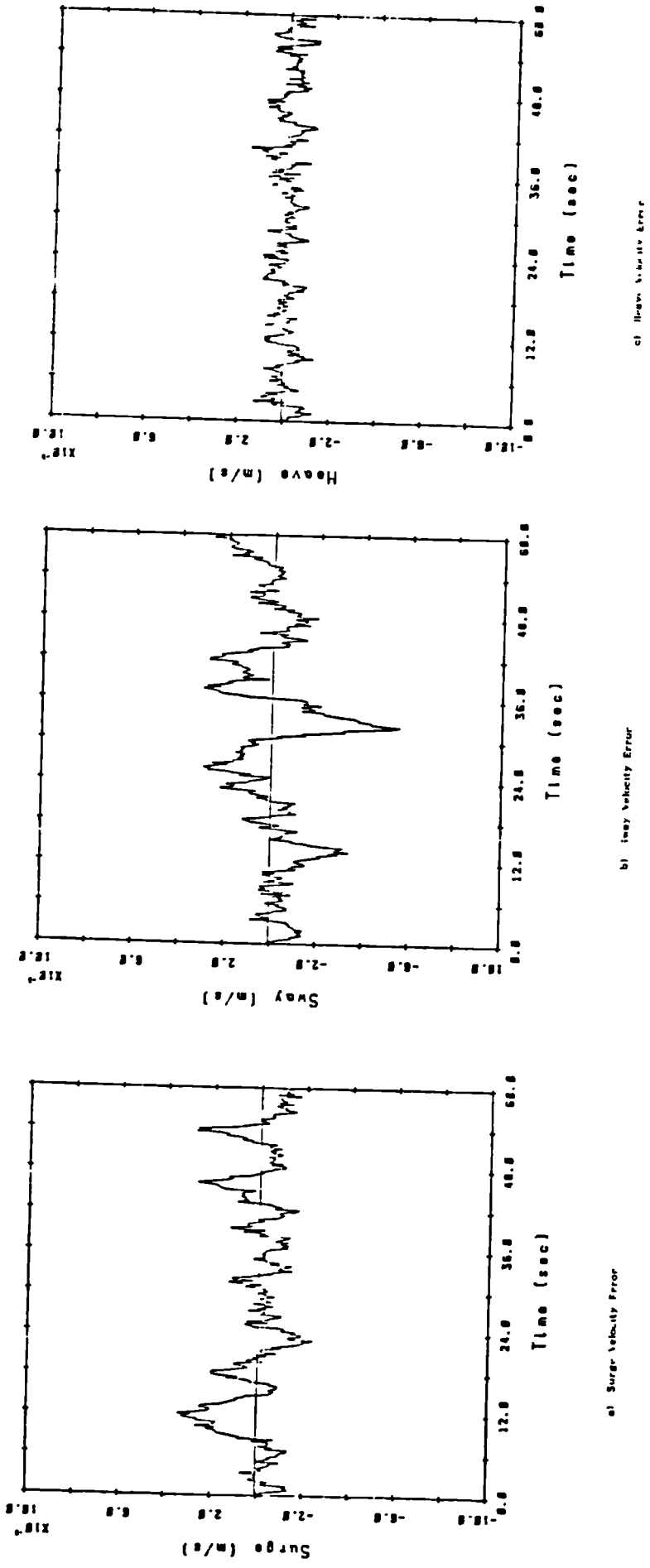

Figure 6.8 : Errors of Final ELS Model; Nonlinear PRBS Data

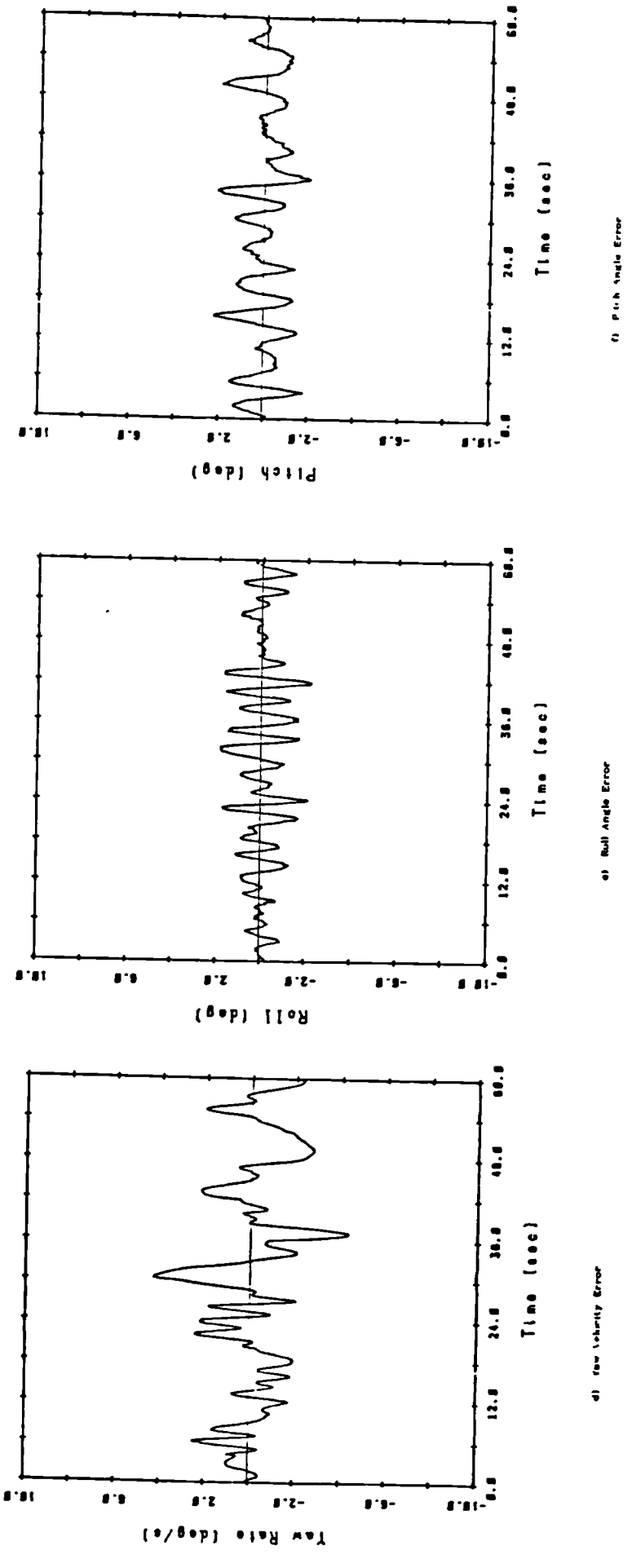

Figure 6.8 : Continued

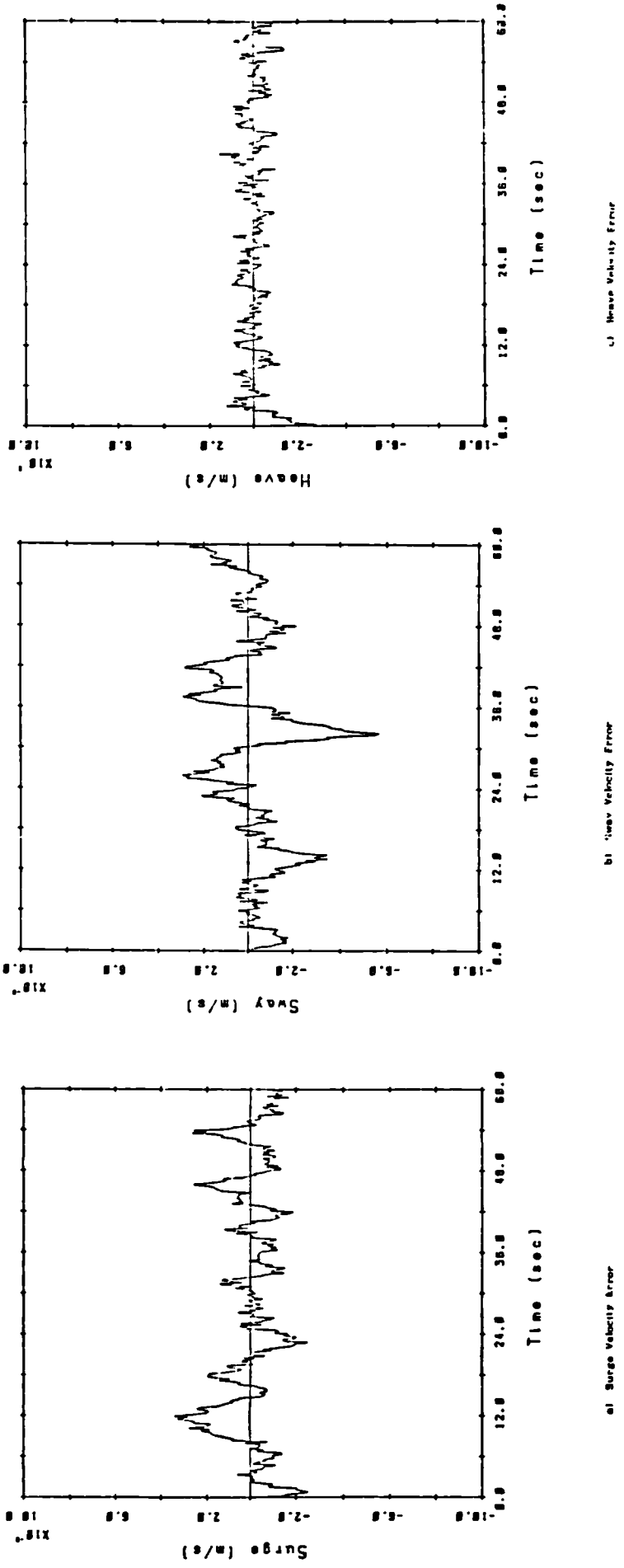

Figure 6.9 : Errors of Final RPEM Model; Nonlinear PRBS Data

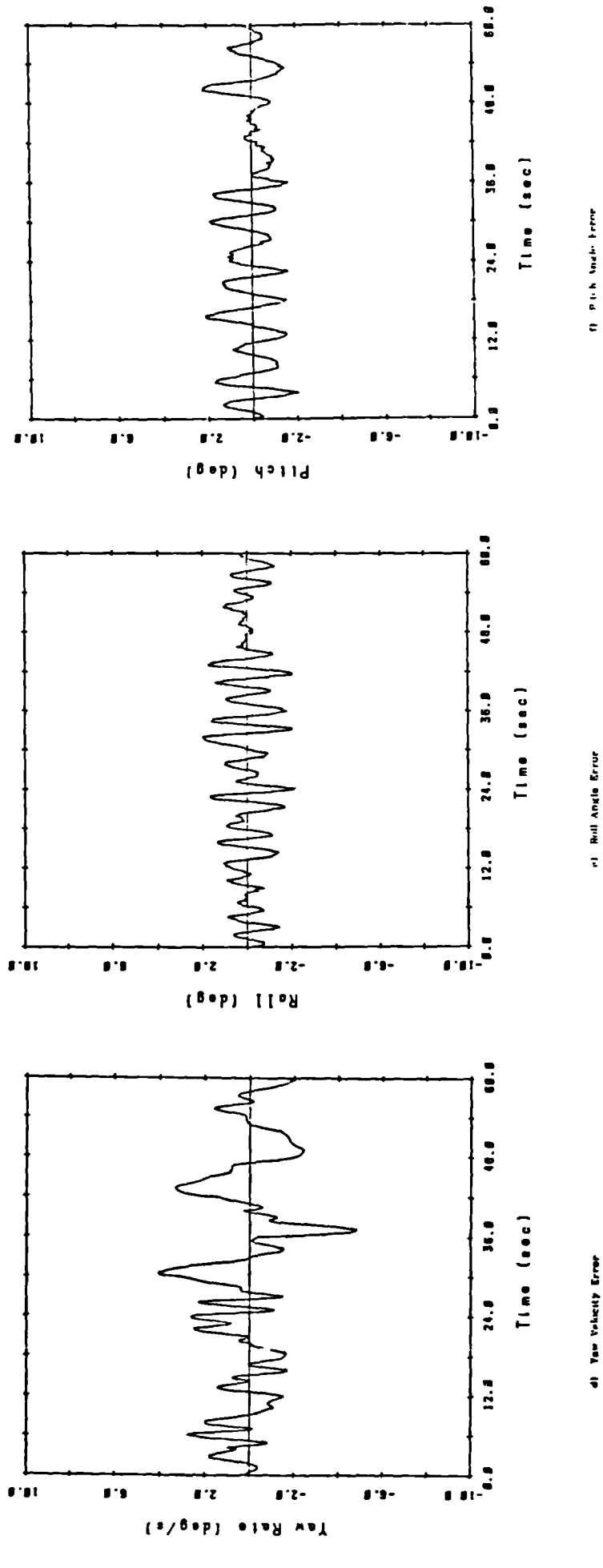

Figure 6.9 : Continued

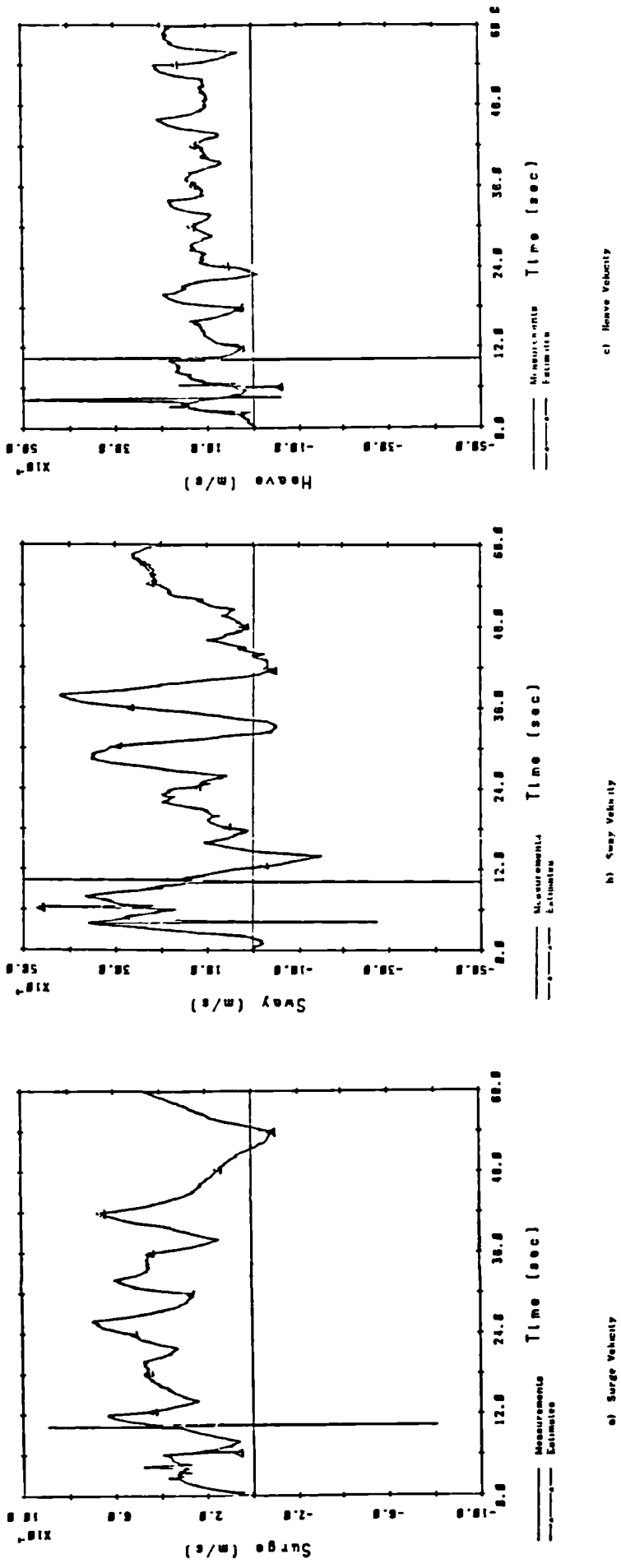

Figure 6.10 : Transient Performance of LS Method; Nonlinear PRBS Data with Turbulence

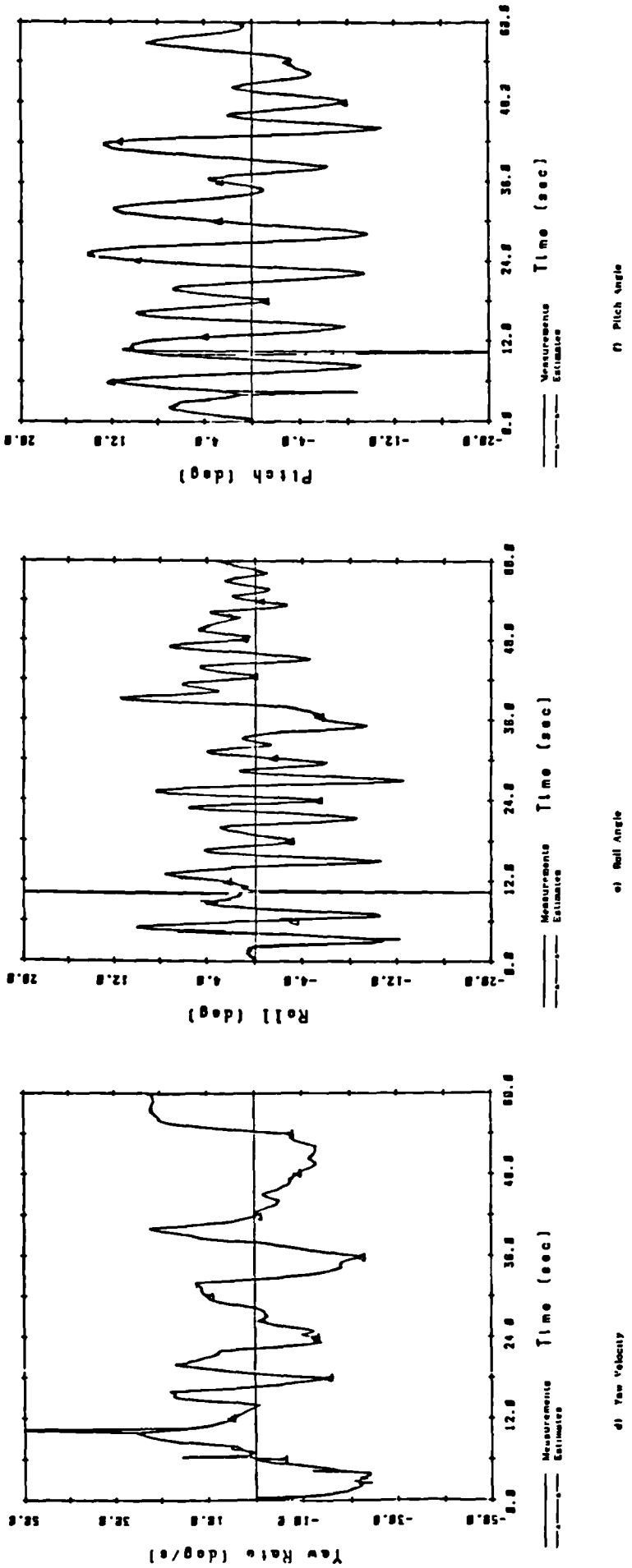

Figure 6.10 : Continued

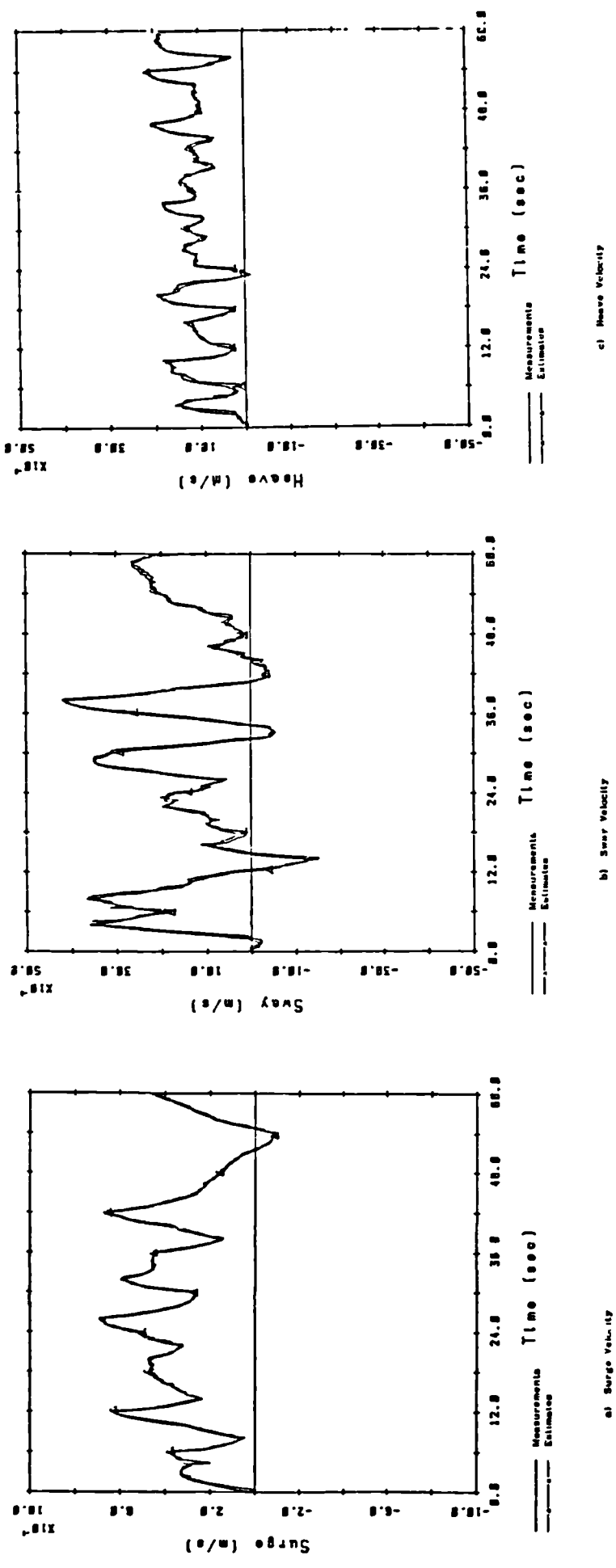

Figure 6.11 : Transient Performance of ELS Method; Nonlinear PRBS Data with Turbulence

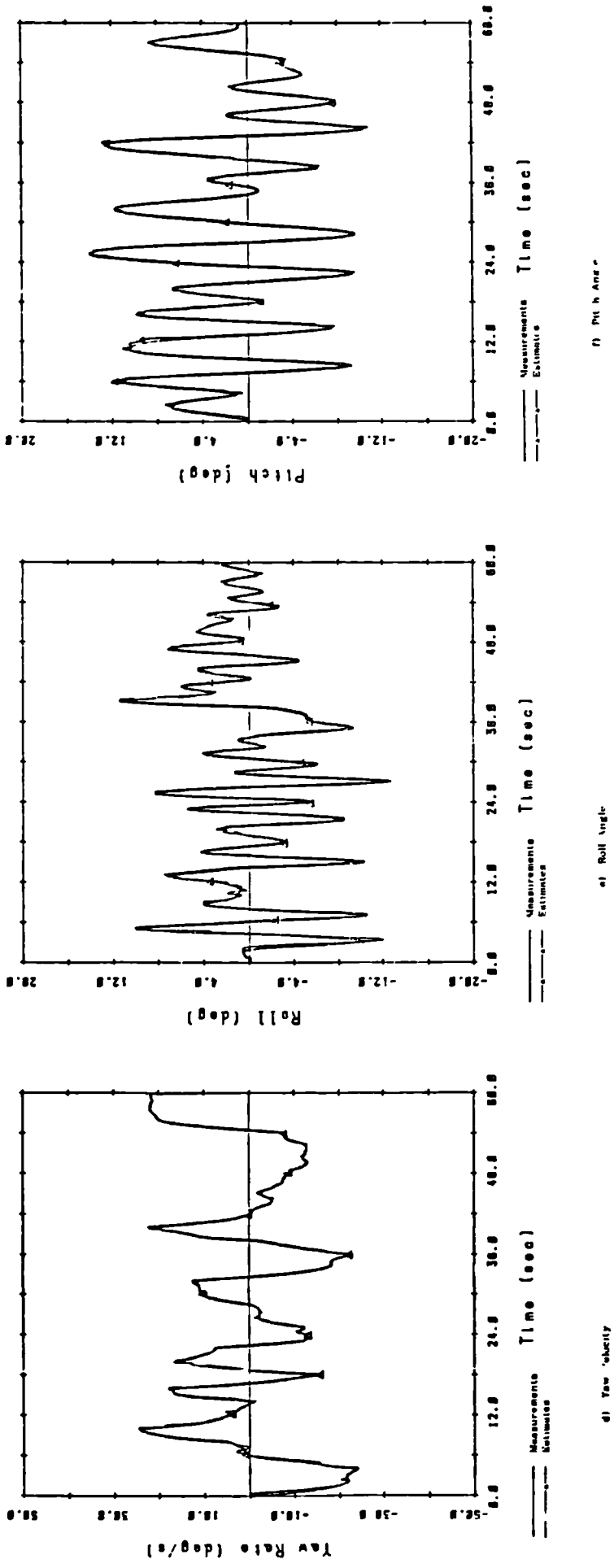

Figure 6.11 : Continued

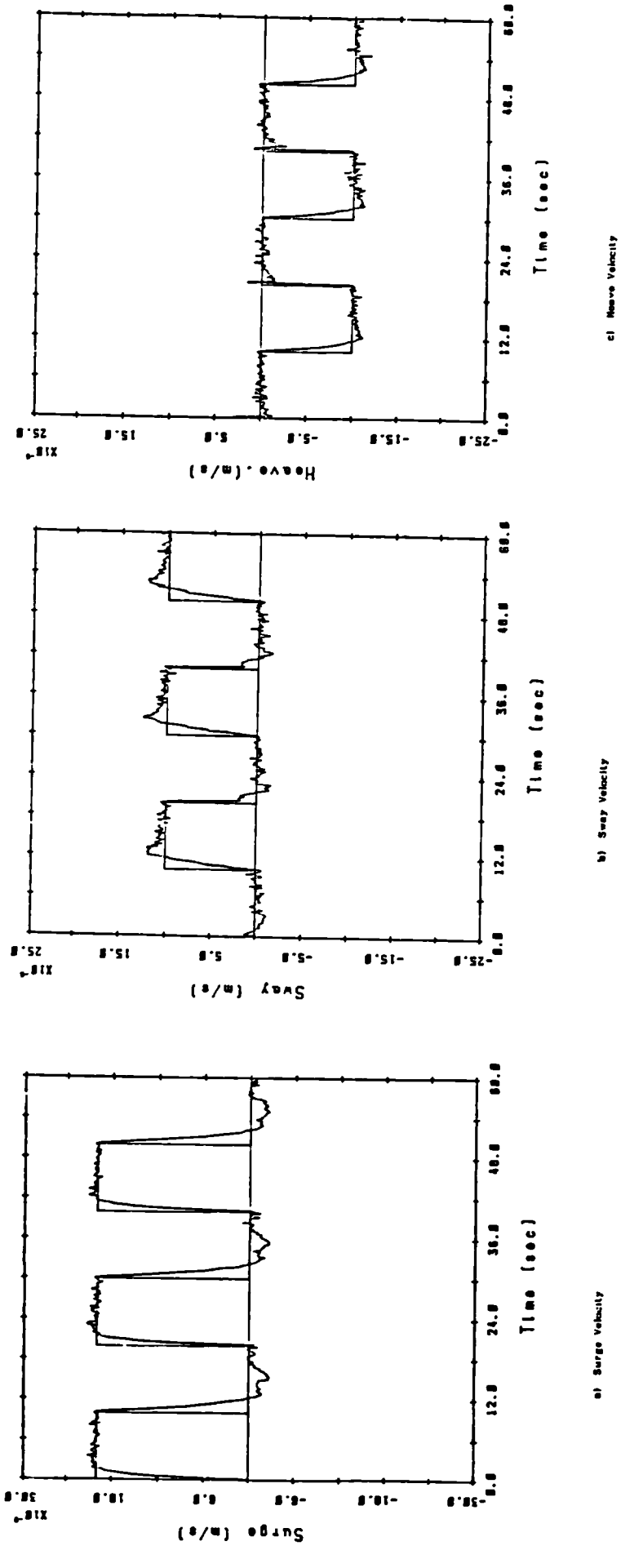

Figure 6.12 : Response of Nonlinear Simulation to Fixed-Gain Velocity Controller

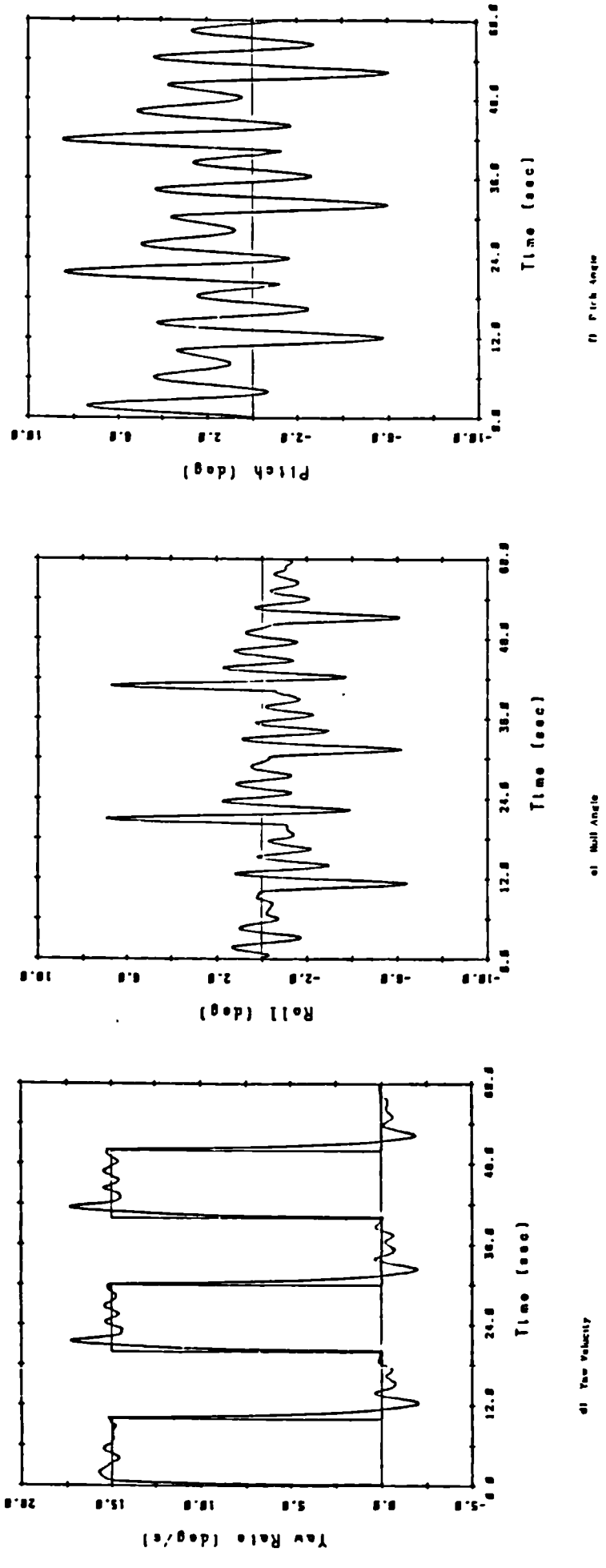

Figure 6.12 : Continued

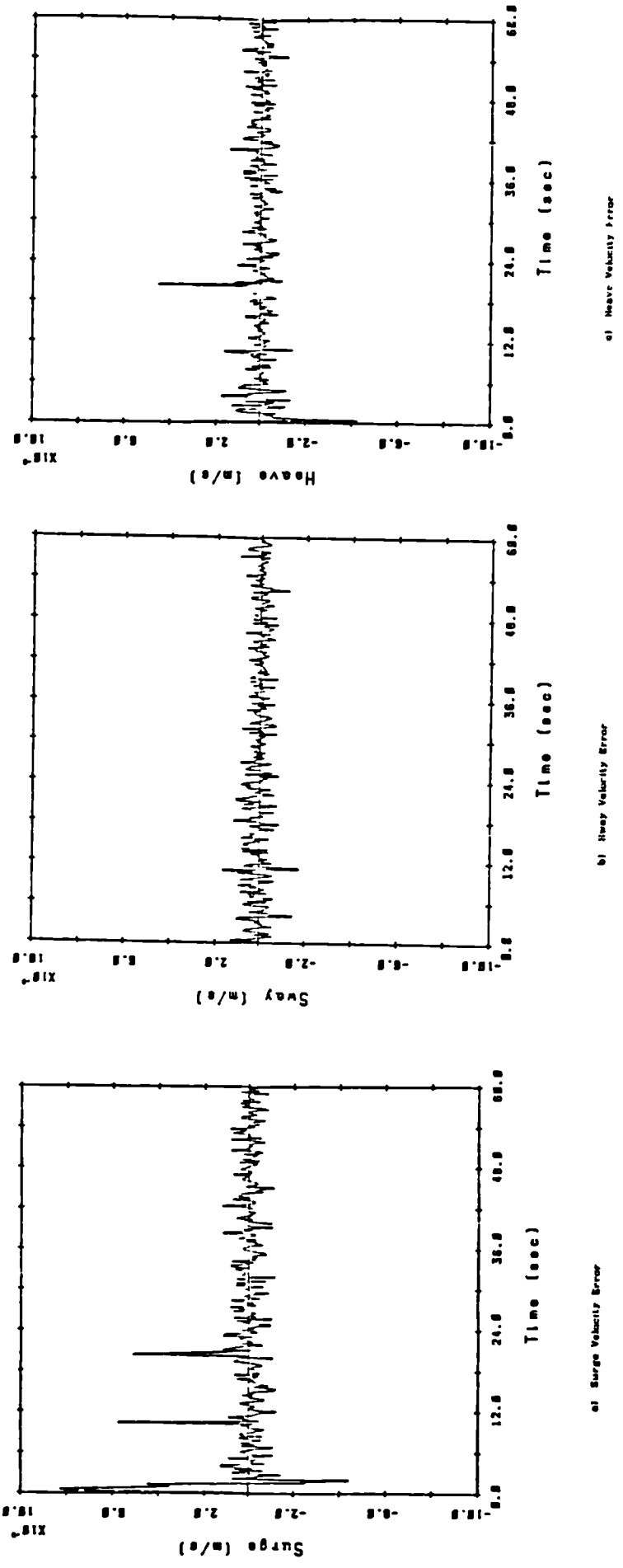

Figure 6.13 : Transient Errors of ELS Model; Nonlinear Closed-Loop Data

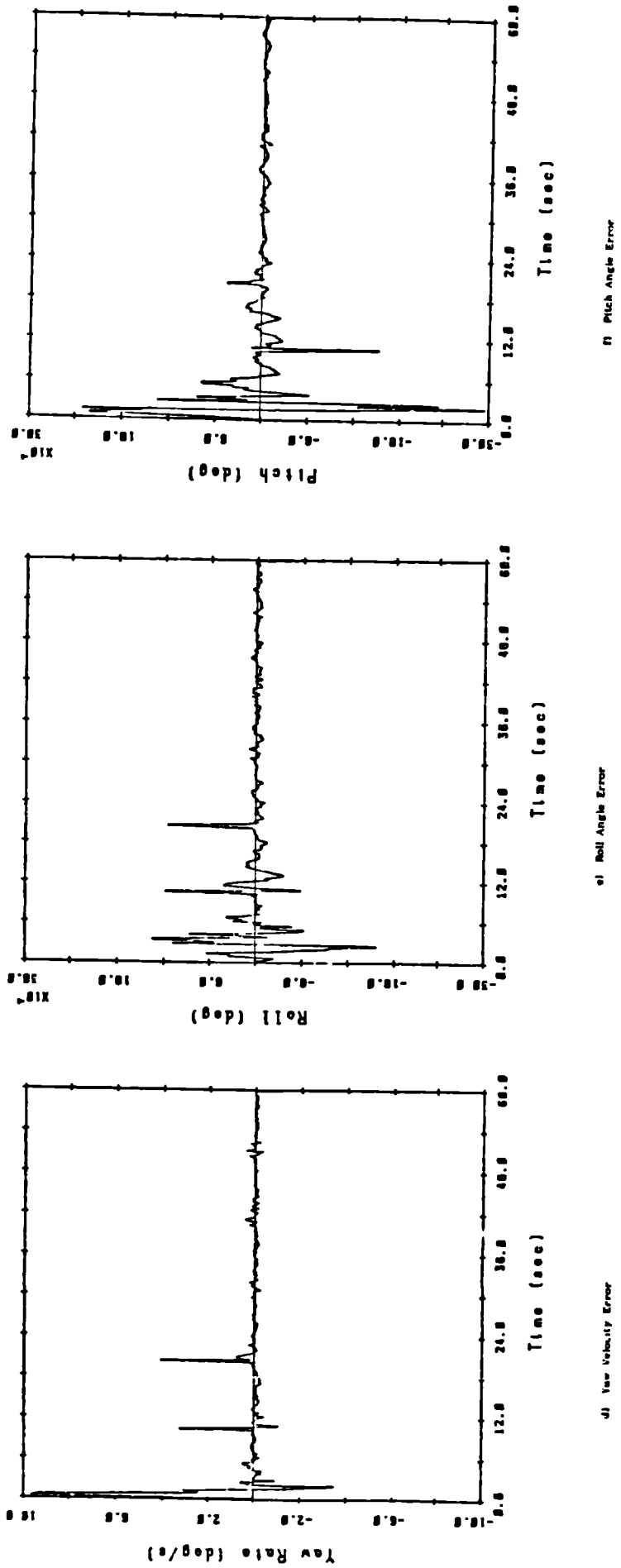

Figure 6.13 : Continued

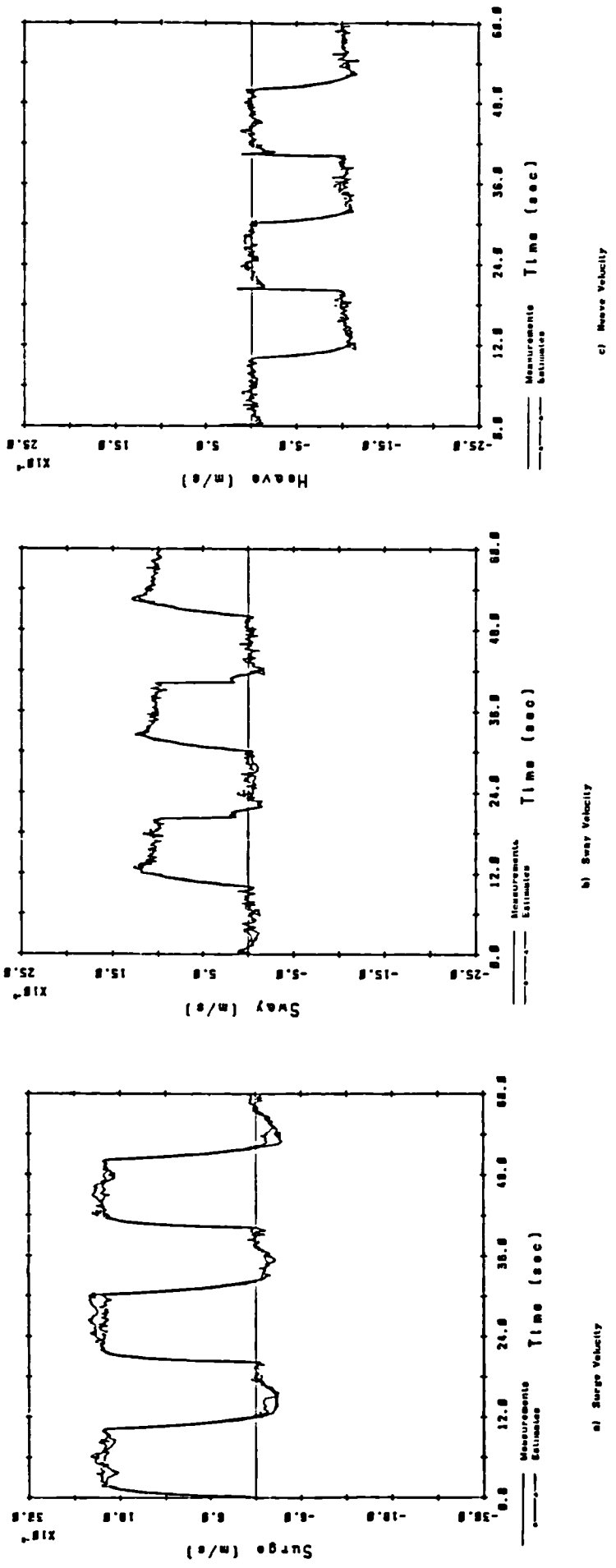

Figure 6.14 : Performance of Final ELS Model; Nonlinear Closed-Loop Data

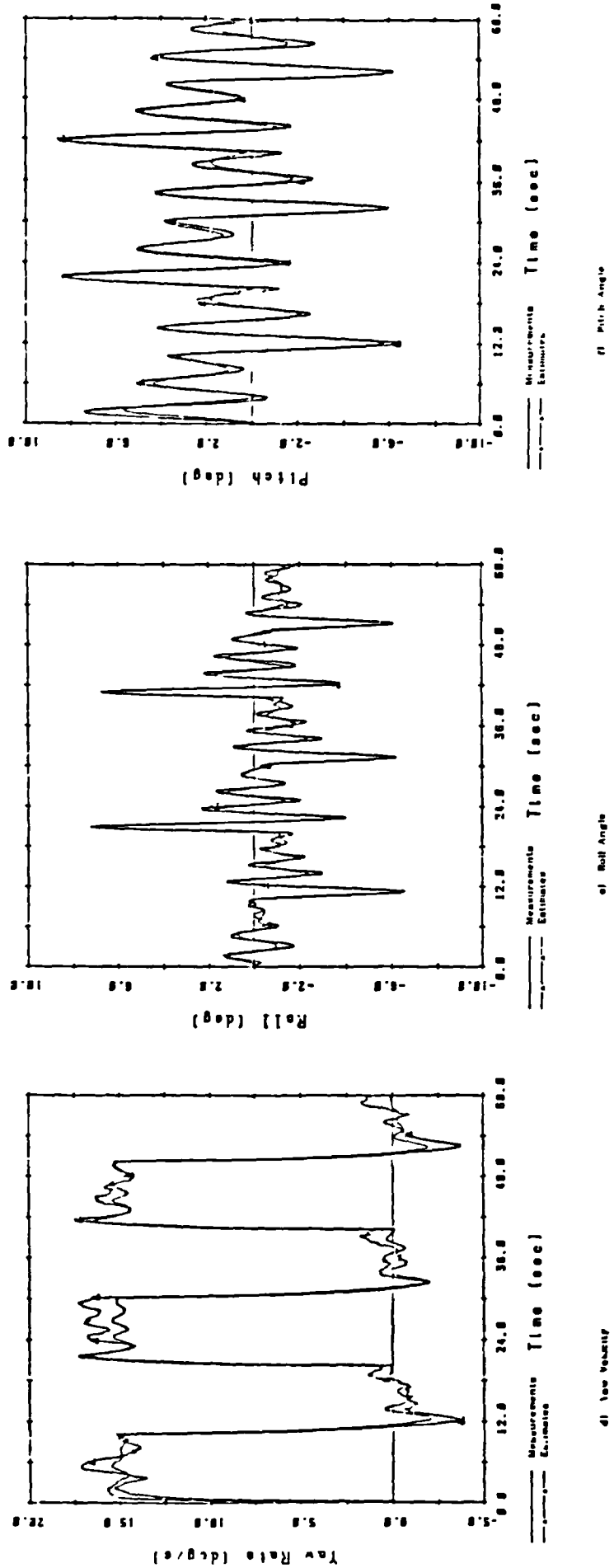

Figure 6.14 : Continued

Chapter 7

Adaptive Control of ROVs

7.1 Introduction

The fixed-gain 'self-testing' autopilot described in chapters 4 and 5 was shown to be very effective in controlling the ROV's velocity. The method combined a robust multivariable control law with a self-tuning period prior to operations during which the parameters of the controller were determined. These two features, robustness and adaptiveness, were necessary in a controller for a system characterised by a large degree of uncertainty in its modelling and major nonlinear and time varying features in its dynamics.

The self-testing controller provided good performance in step tests of individual output references and combinations of references as well as effective rejection of deterministic and stochastic disturbances. However, the closed-loop system did exhibit some shortcomings. During the test of the yaw rate step response, a limit cycle involving yaw, sway and roll occurred. An effort to introduce surge velocity scheduling of the controller gains failed because the self-test produced an incorrect model about one of the points in the scheduling range. The original aim of this study was to produce a controller design method which could be applied to any ROV with minimal modifications by operators who did not necessarily have extensive knowledge of control theory. The self-test only partially fulfils this goal. The operator must still choose quiescence speed limits for the self-testing procedure as well as the desired closed-loop poles. Another failing of this autopilot is that it cannot adapt to changes that occur during a mission, such as a manipulator arm reaching out and grasping a load, without breaking off from the task and repeating the self-test. Fortunately this is not always necessary since the fixed-gain controller was shown to be robust with respect to changes such as this. Still, this method of adaptation is not at all suitable for continuous changes in dynamics, but only those which occur intermittently.

Section 4.3 discussed a few of the potential difficulties of using fully adaptive control in this application. It is known that the gains, poles and zeros of the ROV are strong functions of its operating point and that an adaptive controller might not be able to track the vehicle's dynamics quickly enough. The computational burden and complexity of these control schemes could make them less attractive to offshore operators than a simpler fixed gain autopilot.

Despite these possible problems, the advantages of a fully adaptive autopilot make a study of its feasibility worthwhile. This chapter will describe the simulated implementation of two adaptive control schemes.

Following this introduction, adaptive control will be defined and a representative list of previous theoretical and practical studies cited. Of particular interest are those references which considered marine applications. Two main divisions of adaptive control, explicit and implicit schemes, are defined and compared. One of the controllers implemented with the Seapup simulation is an explicit law based on the same robust controller used with the self-testing method. The other is an implicit scheme which minimises a generalised output variance. The theory of each of these is presented along with its performance in a selection of situations. A comparison is made of the three autopilots, fixed-gain, explicit adaptive and implicit adaptive, in terms of performance and computational burden.

7.2 History, Theory and Past Applications

Such are the number of books and papers on adaptive control produced in recent years that here only a brief introduction to the subject is possible. Each of the many survey papers and texts invariably begins with a definition. In [77], Jacobs states that when the term 'adaptive' is used to describe a controller, it implies that while the process is being controlled, the algorithm should simultaneously be learning about the process and the environment and adjusting itself to produce better control. This is more restrictive than a very early definition which said that adaptive control allows

for "self-adjustment in accordance with changing conditions" [78]; this does not exclude conventional feedback which also decreases the effects of unmodelled dynamics and disturbances.

Reference [77] defines the three classes of adaptive control as 'self-tuning', 'model reference' and 'suboptimal'. The first two categories are similar in that the control signal they produce is 'certainty-equivalent', i.e. stochastic effects are ignored and the control generated is the same to that which would be produced if there was no uncertainty about the parameters or the state of the process.

The structure of self-tuning control systems is shown in figure 7.1. The scheme assumes the process satisfies the ARMAX model (6.5), with $C(z^{-1})$ set to unity. This allows the simplest parameter estimation algorithm, Recursive Least Squares, to be used, along with an equally simple deterministic control law.

Clarke [79] mentions three key papers in the development of self-tuning control. Kalman's 'self-optimising' control system [80] in 1958 was the first attempt at adaptive control; he implemented the algorithm using a special hybrid computer, not well suited for general usage. The emergence of relatively inexpensive mini and micro computers in the 1960's revived interest in the subject. Stochastic aspects were covered by Peterka [81] in 1970. However, in 1973, Astrom and Wittenmark [82] introduced the now standard stochastic self-tuning regulator which minimised the output's variance. This development sparked the current widespread interest in the subject.

Figure 7.2 depicts a model reference adaptive control system. The error between the actual closed-loop system and a reference closed-loop model is driven to zero by the adaptation mechanism which adjusts a classical feedback controller. The input signal produced by this controller is certainty equivalent. Model reference methods were originally devised for aerospace applications, where the controllers were to be implemented using analogue hardware [83].

The third class of adaptive controllers, suboptimal methods, allows for some or all of the nonlinearities ignored by self-tuning

and model reference controllers. An example of this is the use of an Extended Kalman Filter, a nonlinear estimator, to approximate simultaneously the unknown parameters and states of equation (6.5). Another feature of suboptimal controllers is that they augment certainty-equivalent control with two components, caution and probing. The cautious control component accounts for the uncertainty in state estimates and generally results in less strong action than certainty-equivalent control. Probing is introduced to the control signal to reduce future uncertainty, e.g. in the form of a test signal.

Both of the adaptive controllers considered in this chapter are self-tuners. This class is divided further into explicit and implicit methods; one of each is used in this study. In explicit adaptive self-tuners, the model of the open-loop process is estimated recursively from input/output data. This model is then used by a conventional design algorithm which updates the parameters of the control law. Implicit adaptive controllers are formulated such that the parameters of the feedback law are estimated directly, eliminating the design stage.

A very complete survey of adaptive control has been compiled by Wittenmark [84] while Astrom, et al. have reviewed self-tuning control in particular [85]; these references should be consulted for further information.

Despite the proliferation of theoretical studies, the number of successful implementations of adaptive controllers remains comparatively small. A possible reason is that conventional two or three term regulators are entirely adequate for most applications. There is no need to sacrifice the robustness and simplicity of classical feedback loops for only the potential of enhanced performance adaptive controllers might deliver. Another drawback of self-tuning is the extra computing power that is required; however with the recent increased availability of inexpensive microprocessors, this limitation is no longer as restrictive.

A small sample of applications shows the variety of problems to

which adaptive control is applicable. Reference [85] discusses implementations of self-tuning regulators on such industrial processes as paper machines, pulp digesters, ore crushers and enthalpy exchangers. A recent conference on control theory and applications [86] included papers on adaptive regulation of pH levels in a waste brine treatment plant, muscle relaxation during surgery and the heating system of a 3000 m^2 building.

Of particular interest are the marine systems which have been studied. Kallstrom [72] simulated the performance of two adaptive autopilots guiding tankers of 255,000 and 356,000 tdw and reported speed increases of 0.1 to 0.4 percent over those achieved by a well-tuned PID regulator. The autopilots employed Kalman filters for state estimation and a linear quadratic control law. The autopilots were tested in sea trials with three tankers and drag reductions of 0.5 to 2.0 percent were observed, a significant improvement given the price of fuel at that time. Adaptive control was of most benefit in rough weather. This reference also contains a review of other adaptive ship steering studies.

Most of the other applications of adaptive techniques to marine problems used conventional controllers with self-tuning only employed for the state estimators. Much work has been done by Reid and co-workers from the University of Illinois. A recent paper [87] described an autopilot which employed adaptive Kalman filtering. A maximum likelihood technique selects the best 'a priori' Kalman filter for the current sea state. A LQG control law is used; this is very appropriate for ship steering because the quadratic cost function actually represents ship drag whereas in other applications the cost function is not so naturally applicable.

A mention was made in chapter 1 of the work of Fung and Grimble on adaptive control applied to ship dynamic positioning [14]. A self-tuning filter was used to remove the high frequency motion from the measurements; this is necessary since the ship's thrusters can only counteract low frequency disturbances. An attempt to use the unfiltered measurements directly would cause the thrust devices to wear excessively and waste energy.

7.3 Explicit Adaptive Control

The first adaptive autopilot considered will be an explicit scheme using the control law discussed in section 4.4. In summary, this design technique models all of the unknown or complex open-loop dynamics by a multivariable first order lag. With two pieces of information about each input/output path, typically the initial and steady-state response, and the desired closed-loop poles for each loop, a PI digital control law is calculated readily, as described by equations (4.9) to (4.11).

In the fixed-gain case, the simplified model is estimated during a 'self-test', where the thrusters are perturbed in turn and the output velocities recorded for a short period. Fifty samples at 5 Hz was used here successfully. The data is then analysed by the Batch Least Squares method to yield the best discrete-time first-order model of the ROV. This control method is transformed into a continuously adaptive scheme by introducing recursive parameter estimation into the algorithm.

Multivariable recursive least squares (LS) was discussed in section 6.3 and will be used here for the closed-loop identification. It was shown in the last chapter to model the ROV's dynamics very well, with rapid elimination of the output error. LS is simpler than Extended Least Squares and Recursive Prediction Error Method, the other two algorithms that were used previously. Here, the algorithm has to operate in real time, and the method requiring fewest calculations has a distinct advantage. It was also shown in the section 7.2 that self-tuning adaptive controllers do not require the noise model to be estimated; this is another reason to employ LS.

The algorithm used for open-loop identification needs to be modified slightly for this application. In the open-loop case, it was desired to model all of the output degrees of freedom, namely surge, sway and heave velocities, yaw rate and roll and pitch angles. Here, the simplified ROV model only contains those outputs that are to be controlled: surge, sway and heave velocities and yaw rate. The inputs in both cases are the four thruster blade pitch angle commands. The

other change is to the order of model that will be used. Tests presented in the previous chapter showed that during closed-loop estimation, first-order models were sufficient for surge, sway and heave, while a second-order description was required for yaw rate; hence the latter was employed for all outputs. Because of the nature of the control law, only first-order versions of $A(z^{-1})$ and $B(z^{-1})$ are modelled here.

Only three functional blocks, namely the parameter estimator, the control law design and the control law itself, are necessary for an explicit adaptive controller; however a number of additional features are desirable to safeguard the closed-loop system's integrity during a simulated or real implementation. Reference [79] discusses the causes of adaptive control failure and suggests a number of solutions.

One common cause of failure often occurs when the plant is operating in steady-state with no load disturbances; for these conditions the input and output signals will no longer 'persistently excite' the estimator. If this happens, the elements in the covariance matrix, P, become larger, reflecting increasing uncertainty in parameter values. This is not a problem when the modelling errors are small but if the plant should happen to move rapidly away from its set point, then the estimator can 'burst' (see equation (6.12)). A solution to this phenomena of the estimator 'going to sleep' is to skip the estimation stage of the control algorithm and either use the existing control law or revert to the default fixed-gain law that was controlling the process during the commissioning stage of the self-tuner. For the ROV autopilot, the controller derived during the self-test could be used as the back-up. It is recommended that estimation be stopped when the output is 'close' to its set point or when the change in the input signal is 'small'. For strongly nonlinear systems, estimation errors can become very large when the output is changed rapidly. In this case, estimation is stopped when the output is 'far away' from its set-point. Yet another solution is to monitor some measure of the estimation error, such as the trace of P, and change to the default controller when it exceeds some limit. However, in this case, the parameter estimates are still updated.

Note that no jacketing software was used in any of the simulations presented in this chapter, simply because none of the difficulties just described ever occurred.

Clarke [79] goes on to suggest further modifications for adaptive control of nonlinear systems, a topic of particular interest here. One possibility is to place a fixed-gain control loop about the plant, with the adaptive controller monitoring the reference and output signals and modifying a precompensator; the first level of feedback partially linearises the open-loop process. Since in this case a conventional controller needs to be designed, some model of the process will be required. This requirement partially negates the prime advantage of adaptive control. A more extreme example of this type of modification is to use parameter scheduling along with estimation to track rapidly time-varying systems such as found in aerospace applications. This would only be appropriate when it is obvious which state variables should characterise the scheduling. Another option is to use a conventional adaptive controller whose parameter estimator is adjusted to track rapidly, i.e. $\lambda = 0.95$, say (6.13). This latter method will be employed in this study because of its simplicity, though it requires that the level of measurement noise is relatively small. This is to ensure that the estimator can differentiate between signal and noise. Recall that an estimator with a forgetting factor closer to unity would reject noise better.

Numerical behaviour of the LS estimator is further improved by Peterka's Square Root algorithm which was discussed in section 6.3. This ensures the covariance matrix remains positive definite, as required.

7.4 Explicit Adaptive Autopilot Simulation Results

The feasibility of an explicit adaptive ROV autopilot will be tested by examining its performance in guiding the simulation of 'Seapup'. Situations considered will be identical to those used in the study in chapter 5 of the fixed-gain autopilot. The first cases will be step changes in individual outputs; complications are then added in the form of more realistic commands.

Effects of different levels of measurement noise are examined. The instrument fit described by Kallstrom [72] and simulated in chapter 6 is used as the 'base-line' case here.

The ability of the autopilot to reject stochastic disturbances is tested by adding the effects of turbulence while the vehicle is attempting to manoeuver.

The chief advantage of fully adaptive control is that it should be able to improve the ROV's performance despite sudden or continuous changes in vehicle behaviour. The robustness studies in section 5.5 considered the baseline Seapup modified by the addition of a bow-mounted camera; this vehicle will be tested here as well. Another typical change that is introduced is the sudden loss of efficiency in a thruster due to foulling.

All of the simulations in this chapter will use a 5 Hz sampling rate. Results obtained with a 20 Hz fixed-gain controller did not indicate a vast improvement in performance. Preliminary results of tank trials showed that a typical computer that could be used for a commercial autopilot is hard-pressed to operate at 5 Hz (see appendix A). However, it should be noted that the IBM AT employed during these trials was not as powerful as other computers available for the same or less cost.

7.4.1 Step Changes in Reference Velocities

For simplicity these tests will, at first, only consider the case of measurement noise from the 'base-line' instrument fit. The reference signals will request 85 percent of the maximum levels available in that output while running in open-loop conditions. The exception is sway velocity. Recall that in chapter 5, this level, 0.29 m/s, was not obtainable because of thruster saturation and so it was reduced to 0.25 m/s. All of the references are square waves with half-period 10 seconds. The second half of this cycle is set to quiescence. Note that these rapid and extreme changes in reference velocities are a severe test of the tracking ability of the adaptive algorithm.

Parameter estimation is, as previously mentioned, by recursive least squares. The forgetting factor is set to 0.999 for this first attempt and the parameter matrix, Θ, is initialised to zero. The first five samples of each test are considered to be the 'commissioning' stage. During this time, the fixed-gain controller derived form the 'self-test' is used for generating the thruster commands. Meanwhile, the input and output signals are monitored by the estimator. Though at first the model derived with so few samples is not very good, at least the control law design stage does not fail because of singularities. This would have happened if $\Theta = 0$ had been used for the controller calculations.

a: Surge Velocity (figure 7.3)

It is apparent from the figure when the adaptive controller is used first. Up to one second, the response is very smooth, but just after this, the velocities jump. Obviously the estimated model at this early stage is a great deal poorer than that derived during the self-test. However, the second step in reference signals at $t = 10s$ is handled much better. The same can be said at $t = 20s$ when $u = 0.85$ m/s is demanded again. The performance at the succeeding reference changes is roughly similar, indicating that the internal model may have converged within 200 samples. The next section will examine this convergence.

The surge response shows a ninety-five percent rise time of approximately 1.0 second. Integral action in the control law eliminates steady-state errors. There is little interaction between surge demand and sway and yaw velocities but there is a noticeable change in heave velocity whenever the demand in surge changes from 0.0 to 0.85 m/s. This pulse is of very short duration.

The control effort, characterised by the thruster blade pitch angles, shows that, as expected, the levels reached are roughly the same as demanded by the fixed-gain controller (figure 5.10). The effect of measurement noise is apparent here; the duration of the commissioning stage, during which the thrusters have thrashed about for approximately 1.6 seconds, is also obvious. Note that for the

other step responses simulated in this section (figures 7.4 to 7.8), the thruster inputs are not shown in the interest of brevity. All are similar to their counterparts in chapter 5 except for the effects of measurement noise and the preliminary action of the adaptive controller, as was the case with this example.

b: Sway Velocity (figure 7.4)

The addition of adaptive control has had a number of benefits here. Comparing figure 5.12 with the results here shows that the level of interaction with surge, heave and yaw is very much less than in the fixed gain situation. The response in the sway velocity has a similar rise time of approximately 2.0 seconds. Again, the estimator and control law have coped well with the levels of measurement noise added.

c: Heave Velocity (figure 7.5)

After the 'tuning-in' period, the controller brings the vehicle to ninety-five percent levels within 2.6 seconds. The performance over the second and third cycle are very similar, indicating internal model convergence. The interaction with sway and yaw is very low but the surge level is greater than with the fixed-gain controller. However, the surge velocity is eliminated quickly.

d: Yaw Velocity (figure 7.6)

The difficulties with limit cycle behaviour observed during the yaw rate simulation in chapter 5 unfortunately occur here as well. The range of motion during the cycle is less than that caused by the fixed-gain controller. The limit cycle is not obvious from figure 7.6, so another simulation, not shown here, was run. The reference signal for the yaw rate was left at 31.5 degrees/second throughout the 60 seconds and measurement noise was eliminated. The period of the limit cycle was very long at approximately 20 seconds and not as obvious as in the fixed-gain case. The variations in the outputs from their references were less than half those noted in chapter 5.

Thus, it may be said that this controller produces less than ideal performance in this example but that an improvement has been made by the addition of adaptive estimation.

The two 'combination' demands that were introduced in chapter 5 are used here. The first, shown in figure 7.7, is the 'inspection manoeuver'. The reference signal for the first half of the cycle is:

$$r^T = \{\ 0.2\ \text{m/s},\ 0.1\ \text{m/s},\ 0.1\ \text{m/s},\ 0.0\ \text{deg/s}\ \}$$

As a reminder to the reader, this was designed to simulate a diagonal creeping motion that an ROV operator may adopt when inspecting the sloping section of an oil rig. The response is very good, with fast rise times and zero steady-state errors. The interaction with yaw rate demand is low after the tuning-in period.

The 'medium speed turn' is defined as:

$$r^T = \{\ 0.3\ \text{m/s},\ 0.0\ \text{m/s},\ 0.0\ \text{m/s},\ 15.0\ \text{deg/s}\ \}$$

It can be seen in figure 7.8 that the response is adequate though with larger overshoots of surge and yaw velocities than were seen with the self-test controller in figure 5.18. The interaction between surge demand and heave velocity which was not evident during the surge step test is noticeable here also.

7.4.2 Estimator Convergence and the Effect of Measurement Noise

Preliminary results of the ARE Haslar trials indicate that the instrument fit that was used has a higher level of noise than the measurements described by Kallstrom in his study [72]. A simulation of the latter set of instruments, comprising linear velocity logs and a yaw rate gyro, was used here as the 'baseline' case. Appendix A describes completely the measurement equipment used in the Haslar trials and the procedure that was used to integrate them with the data acquisition software. In summary, the instrument fit consisted of

three strapdown accelerometers which would provide velocity values in the surge, sway and heave direction when integrated and three gyros for measuring roll, pitch and yaw rates. Factors contributing to the inaccuracy of the measurements include line noise and the limited signal/noise ratio of the 12 bit A/D converters but the overwhelming problem was that gravity dominated the acceleration levels of the ROV. This effect, in theory, could be accounted for if the Euler angles of the vehicle were known, but this in turn was very dependent on knowing the initial orientation and integrating the angular rates accurately.

This section will examine the effects on performance and estimated parameter convergence by higher levels of measurement noise such as may be produced by this instrument fit. Difficulties with unknown initial conditions and gravitational effects are ignored here. The noise is assumed to be white and Gaussian distributed with standard deviations given by:

$$\sigma_u = 0.0172 \text{ m/s}$$
$$\sigma_v = 0.0172 \text{ m/s}$$
$$\sigma_w = 0.0172 \text{ m/s}$$
$$\sigma_r = 0.0083 \text{ degrees/s}$$

The inspection manoeuver described in the previous section will be used for comparisons. Figure 7.9 depicts the performance of the vehicle autopilot; here, the forgetting factor of the LS estimator has been set to 0.999 as in section 7.4.1. The estimated model has thirty-two parameters and the convergence of a selection of the most significant is shown in figure 7.10. Here, the diagonal elements of the [A] matrix are presented as a very approximate measure of the time constants for this multivariable system. A comparison is made between the modelling errors and measurement noise on all four output channels in figure 7.11. Ideally, if the modelling has been exact, the output error of the estimator will correspond to the measurement noise after the algorithm has converged. Of course, strong noise rejection and parameter convergence is a conflicting goal if it also is desired to track a nonlinear system. The effect of changing the forgetting factor to 0.950 so that the algorithm is more easily able to track is seen in figures 7.12 to 7.14.

It is apparent from these two cases that the 'slower' forgetting factor is much more appropriate with this high level of noise. When λ is set to 0.950, the estimator has great difficulty separating the signals from the noise; the values of the parameters do not converge and controller performance suffers. Figure 7.10 demonstrates the noise rejection properties of the algorithm when it is tuned to have a much longer 'memory'. The parameters have converged essentially within sixty samples and the set point velocities are held well. However in neither case do the modelling errors converge to the measurement noise. This implies that the chosen estimated model structure does not match the real system exactly; since the real system is nonlinear and the estimated system a first-order ARMAX, this result is not surprising.

7.4.3 Disturbance Rejection

The inspection manoeuver is used again to demonstrate the ability of the adaptive autopilot to reject a stochastic change in current. Measurement noise has been simulated from the baseline instrument fit. A stochastic current is simulated using the first-order Gauss-Markov model. Measurement noise has been simulated from the baseline instrument fit. The LS estimator is started at the beginning of the simulation; five samples later, the adaptive control law is substituted. Figure 7.15 shows that vehicle guidance is not as good as in the case of zero current, but still acceptable.

7.4.4 Sudden Configuration Changes

A major reason for adding the extra complication and cost of an adaptive controller is that the sudden and continuous changes that occur in a ROV's dynamics may be better compensated than by a fixed-gain controller. This section will consider two such possible variations.

The first change will be the addition of a bow mounted camera which was originally described in section 3.6. The robustness of the

'self-test' controller allows the vehicle to perform adequately despite none of the controller's parameters changing from those derived from the baseline vehicle (see section 5.5). The adaptive control should produce better results.

Figure 7.16 presents this situation; the controller has been estimating the unmodified vehicle's dynamics since t = 0s and driving the ROV through the inspection manoeuver. Note that the set point has been left at a constant level and measurement noise set to zero in this example and the next; this was done in order to emphasise the parameter variations due to vehicle configuration changes. The performance has reached as steady level, as in figure 7.7. At t = 65s, the effects of the camera are added. Though it is impossible, of course, to add a camera in mid-flight, this change in dynamics would be similar to that which would occur if a manipulator arm was suddenly extended to grab a load. As can be seen, the controller quickly modifies its performance to compensate for the new configuration. The diagonal elements of the estimated [A] matrix, shown in figure 7.17, also demonstrate how the controller has changed. The values of the parameters and the velocities have reached steady-state values within 100 sampling times of the vehicle change.

Another situation which may occur is the sudden loss of efficiency in a thruster due to foulling. This simulation is depicted in figures 7.18 and 7.19. As in the previous example, the ROV has been executing the inspection manoeuver under adaptive control since t = 1s. The installation coefficients of the main port thruster (see section 2.3.3) are reduced by 50 percent at 65s. The performance is quickly returned to its original level. In figure 7.18(e), it can be seen that the setting for the main port thruster is at a higher level after the disturbance while the other three remain at their original values.

Figure 7.19 shows how the relevant elements in the estimated [B] matrix change i.e. those relating the main port thruster to the output velocities. These decrease from their initial values, though not as much as anticipated because some of the effect of the thruster change has been taken up by changes in other parameters.

7.5 Implicit Adaptive Control

An alternative to the explicit adaptive controller just considered is an implicit method presented by Koivo [88]. His multivariable self-tuning controller is an extension of the SISO controller of Clarke and Gawthrop [89] and is comparable also to a multivariable self-tuning regulator which was presented by Borrison [90]. However, unlike the latter method, the controller used here can handle nonmimimum-phase systems and track time-varying reference signals. All of these features indicate that this controller may be suitable for the ROV autopilot.

The controller derivation assumes that the process model is a multivariable ARMAX (6.24) with the number of inputs equal to the number of outputs. The two other restrictions are that the noise model $C(z^{-1})$ must be stable and that the matrix associated with the most recent input vector, B_0, must be nonsingular. A term corresponding to the zero-input level, d, is allowed. It is wished to minimise the cost function:

$$I = E \{ ||P(z^{-1})\, y(t+k) - R(z^{-1})\, r(t)||^2 + ||Q(z^{-1})\, u(t)||^2 \} \qquad ....(7.1)$$

where $|| x ||^2 = x^T x$ and r(t) is the output reference signal.

If $Q(z^{-1})$ is restricted to λI, then the algorithm consists of forming the alternative output:

$$\phi(t) = y(t) - R\, r(t-k) + \lambda\, u(t-k) \qquad ....(7.2)$$

and choosing the control signal to set the k-step ahead predictor of $\phi(t)$ to zero:

$$\phi^*(t+k/t) = \tilde{F}(z^{-1})\, y(t) + \tilde{G}(z^{-1})\, u(t) + \tilde{H}(z^{-1})\, r(t) + \gamma = 0 \qquad ....(7.3)$$

This control signal is given by:

$$\tilde{G}_0\, u(t) = -\, [\, \Sigma\, \tilde{F}_i y(t-i) + \Sigma\, \tilde{G}_i u(t-i) + \Sigma\, \tilde{H}_i r(t-i) + \delta\,] \qquad ....(7.4)$$

The parameters of $\tilde{F}_i$, $\tilde{G}_i$, $\tilde{H}_i$ and δ are estimated directly from a recursive SI method; hence the implicit nature of the control law. The matrix $\tilde{G}_0$ is fixed in order to allow an unique solution.

Integrators can be introduced to eliminate steady-state errors by using an alternative generalised output given by:

$$\phi(t) = y(t) - R\, r(t-k) + \lambda\,(u(t-k) - u(t-k-1)) \quad ....(7.5)$$

In [88], Koivo suggests that identification should take place by an algorithm such as Peterka's square-root method in order to ensure that the covariance matrix remains positive definite. This reference demonstrates by simulation that the implicit adaptive controller can work with a variety of systems, including those that are nonmimimum-phase, have a time delay or are open-loop unstable.

7.6 Implicit Adaptive Autopilot Simulation Results

The multivariable generalised minimum-variance control law will be tested by considering the same situations that were used to examine the explicit adaptive controller. A selection of the results will be presented.

Throughout these simulations, the sampling rate will be set to 5 Hz and the baseline measurement system will be used. The effect of varying the control effort weighting will be examined as well as the controller's load disturbance rejection properties. ROV configuration changes will also be simulated. The square-root algorithm will be used for parameter estimation for all the simulations, with the forgetting factor set to 0.999.

7.6.1 Model Order Determination

Koivo's control law has an advantage over that used for the explicit adaptive scheme in that model orders higher than first are easily incorporated. However, it is left then to determine how complicated a model should be used.

Section 6.3 described three statistical tests which can determine optimal model order. These tests, the autocorrelation function of modelling errors, Akaike's Information Criterion and F-tests of modelling error variance, were used in chapter 6 to find the best model for system identification purposes. In closed-loop estimation (table 6.6), a second-order model was chosen for yaw rate, while first-order models were sufficient for the other output velocities. Therefore, second-order models were used throughout for identification purposes and will be used for the implicit adaptive controller.

7.6.2 Step Changes in Reference Velocities

The effect of varying the relative penalty given to thruster efforts will be examined by considering the vehicle response to the inspection manoeuver demand. In figure 7.20, the weighting factor has been set to zero. It has been changed to 0.1 in the simulation depicted in figure 7.21. The effects of this modification are obvious. Though the output response is very fast in the first example, it comes at the price of large and quickly varying thruster commands. The thruster commands are very much smoother and of lesser magnitude in figure 7.21(e). However, this is no great advantage since, as can be seen in figure 7.21, the velocity set points are not held at all well.

A compromise between these two fairly extreme examples is the choice of 0.001 for the weighting factor. This was chosen qualitatively after comparing a few responses and will be used for the rest of this section's simulations.

The vehicle's response to the other step tests presented in section 7.4.1 were simulated and because none of the results were remarkable, they are not shown here. All performance figures, such as rise times, settling times and steady-state errors, were very adequate.

However, the response to the step change in yaw demand is worthy of comment. It is apparent from figure 7.22 that the limit cycle

behaviour associated with this test observed previously does not occur. Instead, the yaw velocity rises very quickly to its set point and remains there. Surge, sway and heave velocities are kept near zero successfully.

In an effort to attribute this improvement to either the different control law goal, minimised variance of generalised output, or the inclusion of the second order model, the controller was modified so that the internal model was first order. Though not shown here, the performance was very similar to that depicted in figure 7.22, where the higher order model was used. However, rise times were approximately ten percent greater and the variations about the set points were larger.

7.6.3 Disturbance Rejection

The implicit adaptive autopilot is requested to manoeuver against a stochastic current in the situation shown in figure 7.23. Features of this simulation are similar to that described in section 7.4.3. Though sampling the performance of the vehicle since t = 0s, the adaptive controller does not guide the ROV until five samples later. Comparing figure 7.23 to 7.15, where the explicit adaptive controller was used, shows that guidance is substantially quicker. This is most apparent in the case of yaw velocity.

7.6.4 Sudden Configuration Changes

The ability of this controller in tracking the time-varying performance of the ROV is tested by simulating a loss of efficiency in a thruster. This situation was described fully in section 7.4.4. Figure 7.24 shows the outputs of the system and the thruster commands; at t = 65s, the installation coefficients of the main port thruster have been reduced by fifty percent and it is obvious that the controller has compensated for the change very quickly. The combination of feedback and adaptation has reduced the disturbance from the set points to virtually nil.

The changes in the most relevant elements of the two estimated [B] matrices are shown in figure 7.25. Their values are modified somewhat but not as much as originally anticipated; this is because other parameter values change as well to compensate.

7.7 Relative Computing Requirements

To be of practical use, the controllers described here and in chapter 5 would be required to operate in real time when installed on a commercially available microprocessor. Preliminary results of trials (appendix A) indicate that this computer must also be available for measurement processing during a large fraction of the sampling time.

Though no absolute measures of processing time can be given here, relative values are available. The simulation was run on a PDP 11/73 computer and though the TSX multi-user operating system was installed, care was made to ensure that only this simulation was running for these tests. All of the tests were simulations of 60 seconds of real time.

The difference between the times for a controlled simulation and the open-loop run are a guide to the time required by the control algorithm. A open-loop simulation of sixty seconds real time took 207 seconds. The extra time required by the controlled simulations were:

Fixed-Gain Control	:	35 seconds
Explicit Adaptive Control	:	88 seconds
Implicit Adaptive Control	:	133 seconds

7.8 Summary

Though requiring more computer resources to operate in real time, the two adaptive controllers described in this chapter demonstrated a number of advantages over the fixed-gain 'self-testing' autopilot. These may be sufficient to warrant the extra cost. However, with the increased availability of inexpensive and powerful microprocessors

such as the National Semiconductor 16032, this may no longer be a limitation.

The 'self-test' required that a number of parameters, such as zero-input speed, be known 'a priori'; additionally, the test was shown to fail occasionally. Simulations of the adaptive controllers has not shown a case of poor vehicle performance or numerical difficulties. The requirement for 'a priori' knowledge is reduced considerably, especially in the case of the implicit control law where the problem of tuning the closed-loop system is reduced to varying a single parameter. Since ROV operators would most likely lack a knowledge of control theory, this simplicity would be very advantageous. Of course, the disadvantage of this is that a degree of flexibility is lost over the control law used for the fixed-gain and explicit adaptive autopilots, where loops could be tuned individually.

Continuous adaptation would be advantageous when coping with sudden or continuous changes in vehicle performance since it would not be practical to repeat the 'self-test' whenever a change in the ROV was noted.

Implicit adaptive control was shown to eliminate limit cycle behaviour that occurred in certain circumstances with the other two autopilots. This was attributed to the different control law goal rather than the higher order model used during the design stage.

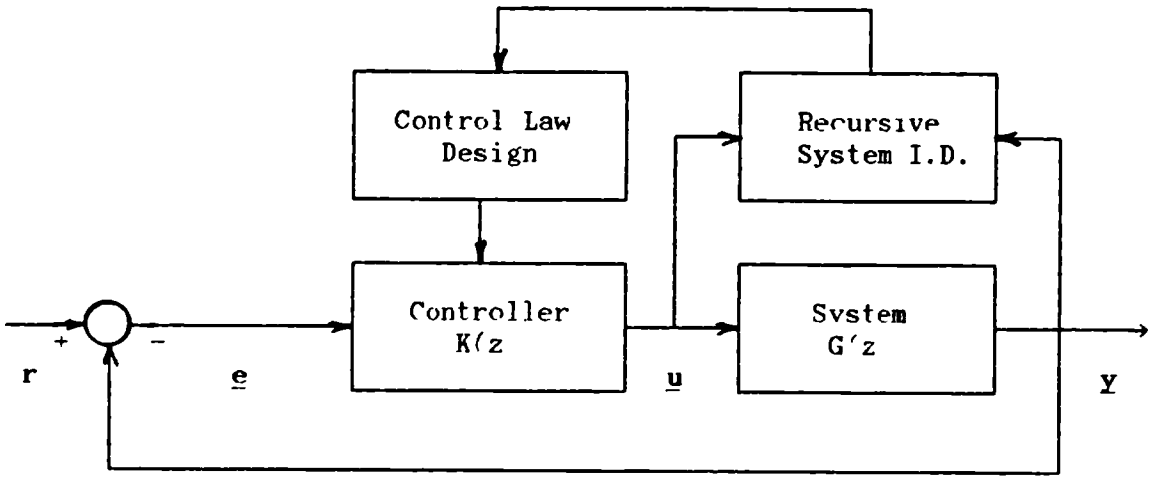

Figure 7.1 : A Self-Tuning Control System

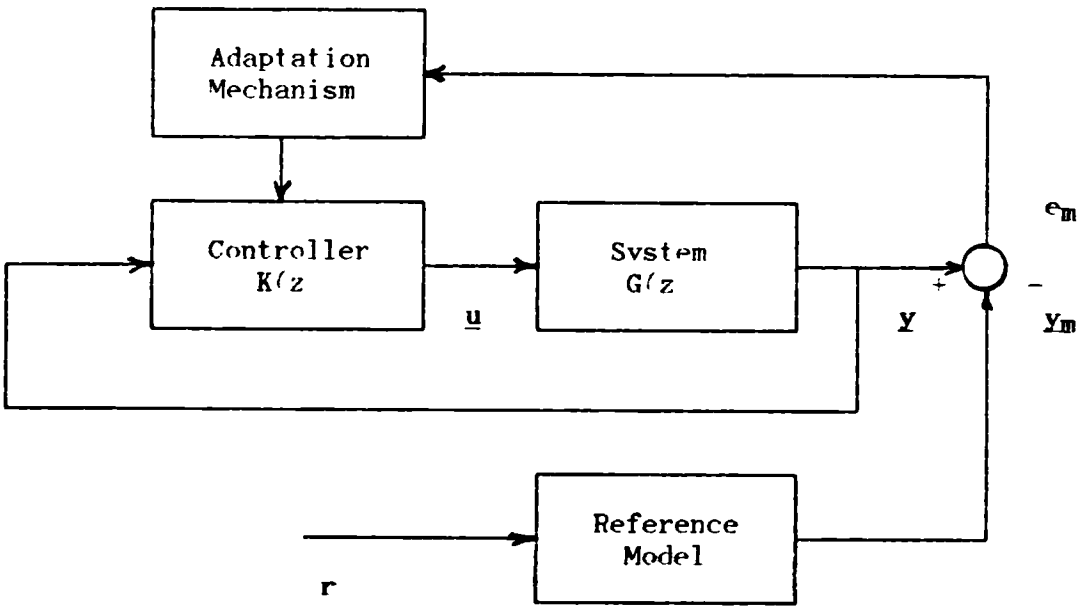

Figure 7.2 : A Model Reference Adaptive Control System

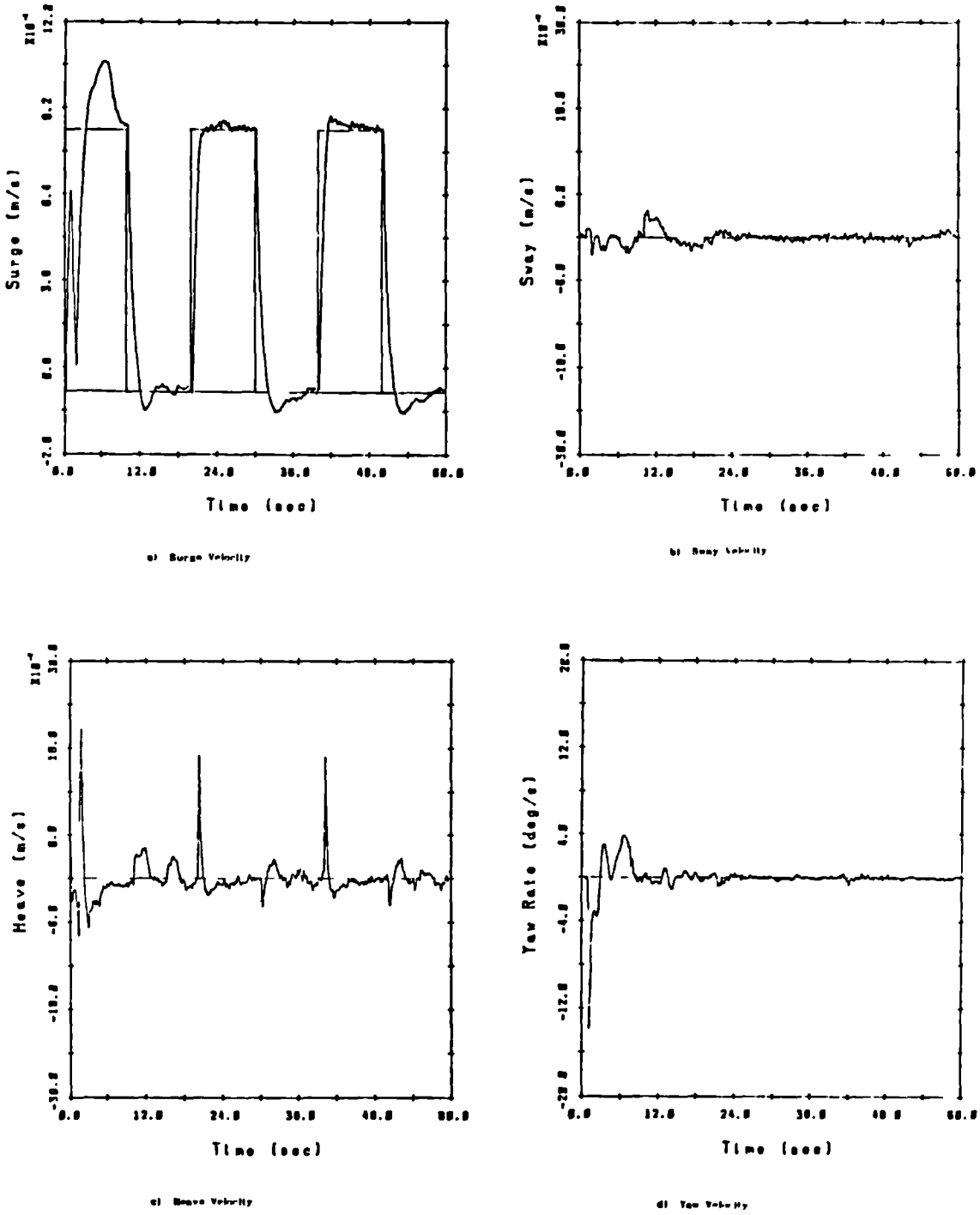

Figure 7.3 : Explicit Adaptive Control; Surge Test

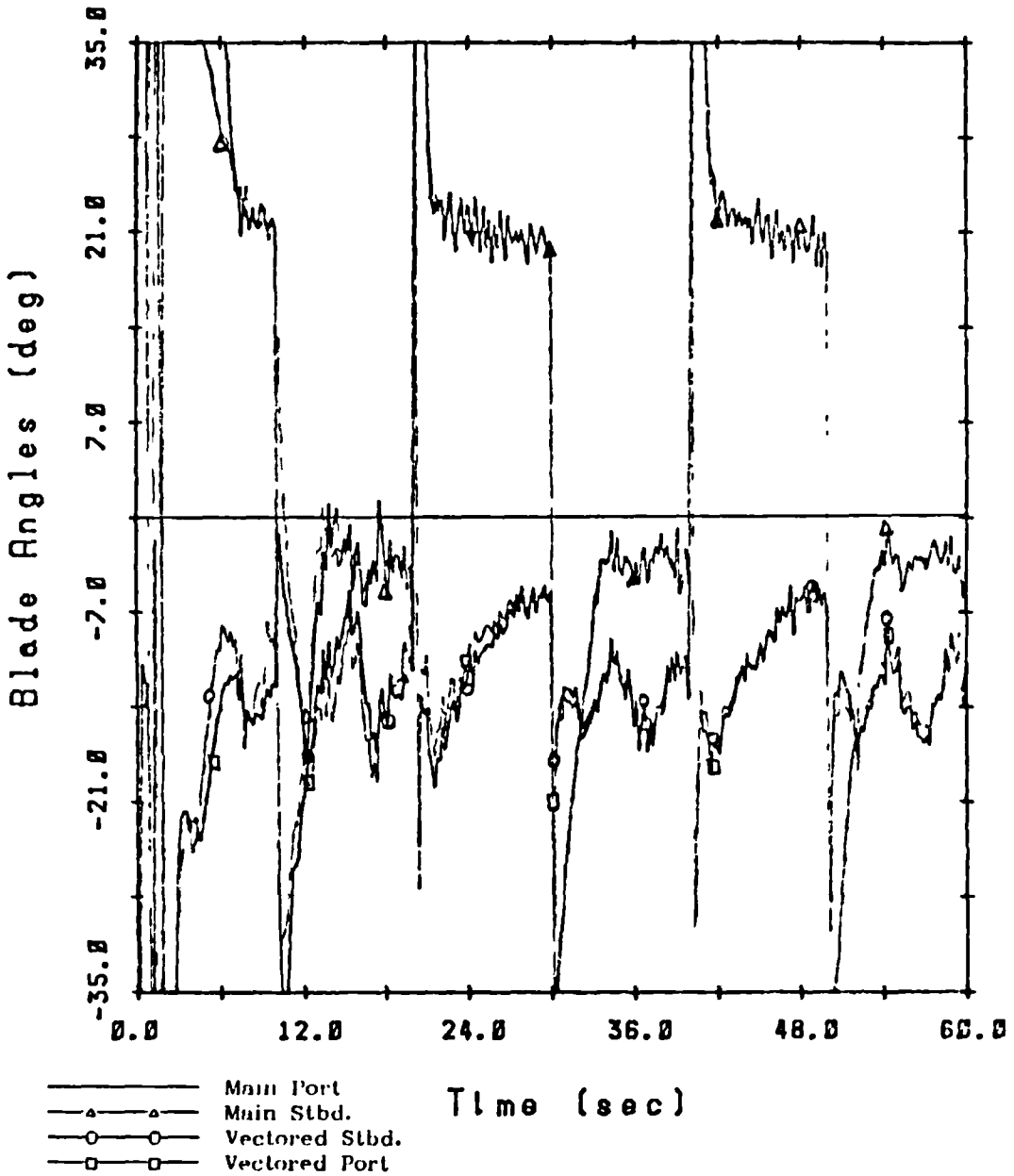

c) Thruster Blade Pitch Angles

Figure 7.3 : Continued

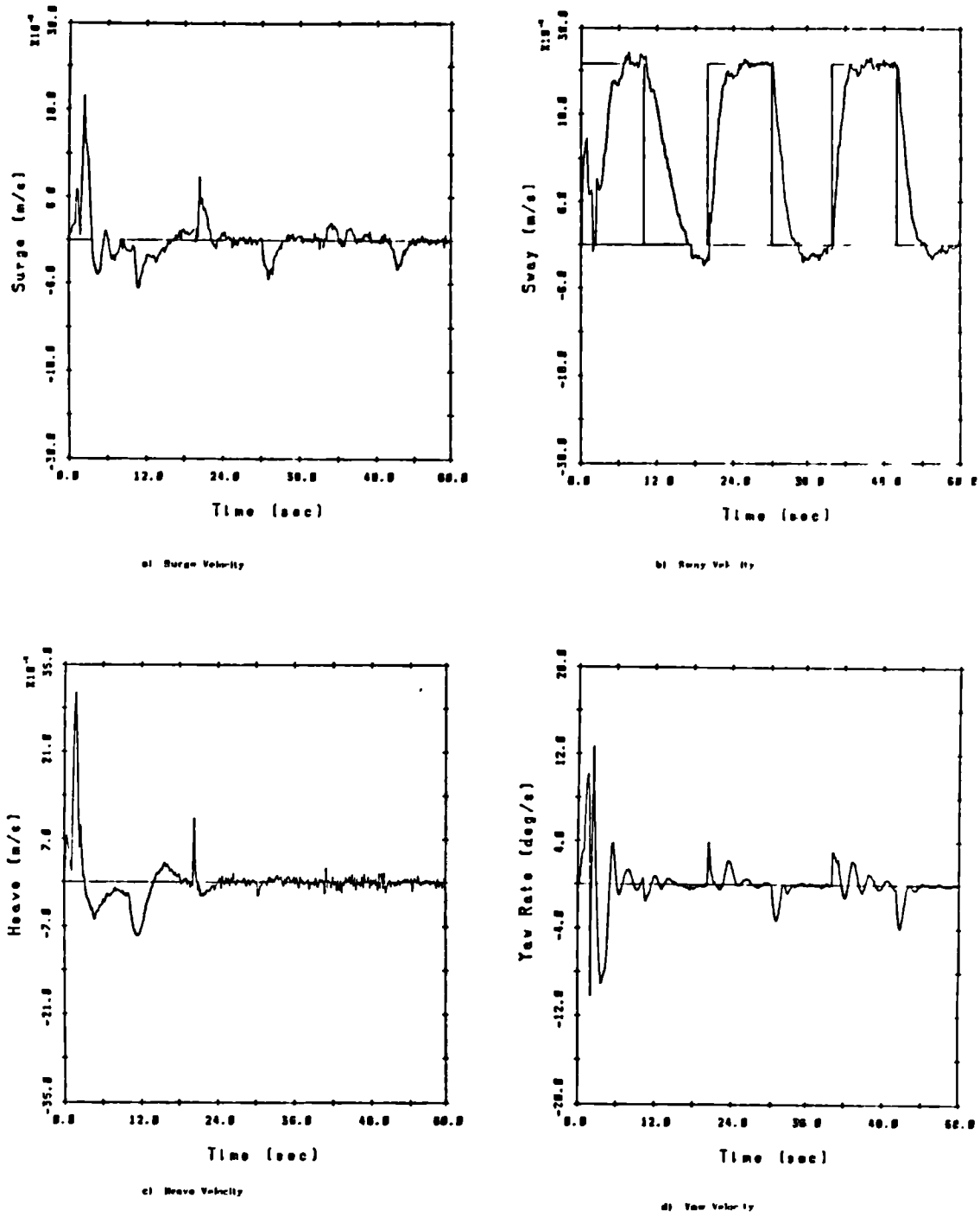

Figure 7.4 : Explicit Adaptive Control; Sway Test

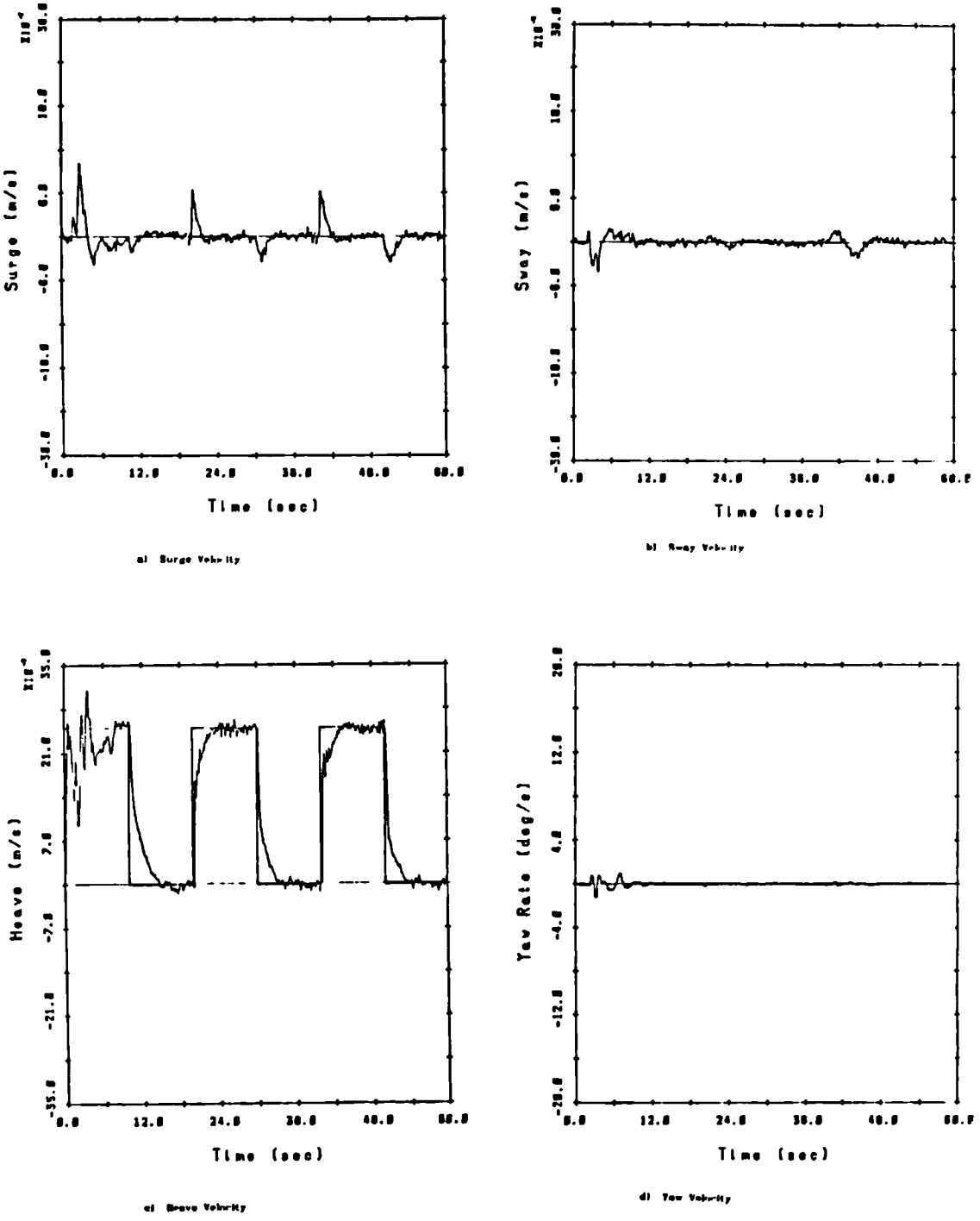

Figure 7.5 : Explicit Adaptive Control; Heave Test

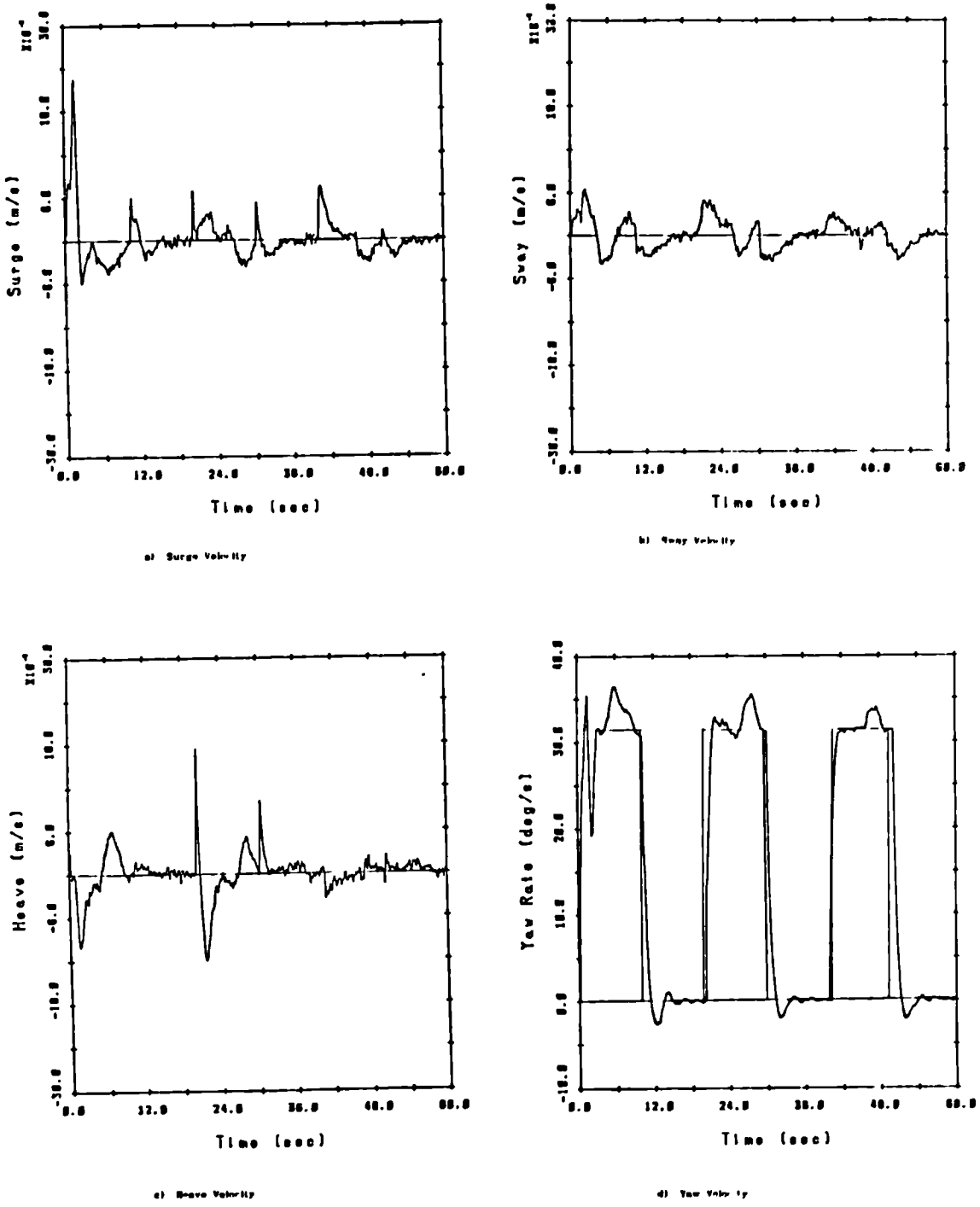

Figure 7.6 : Explicit Adaptive Control; Yaw Test

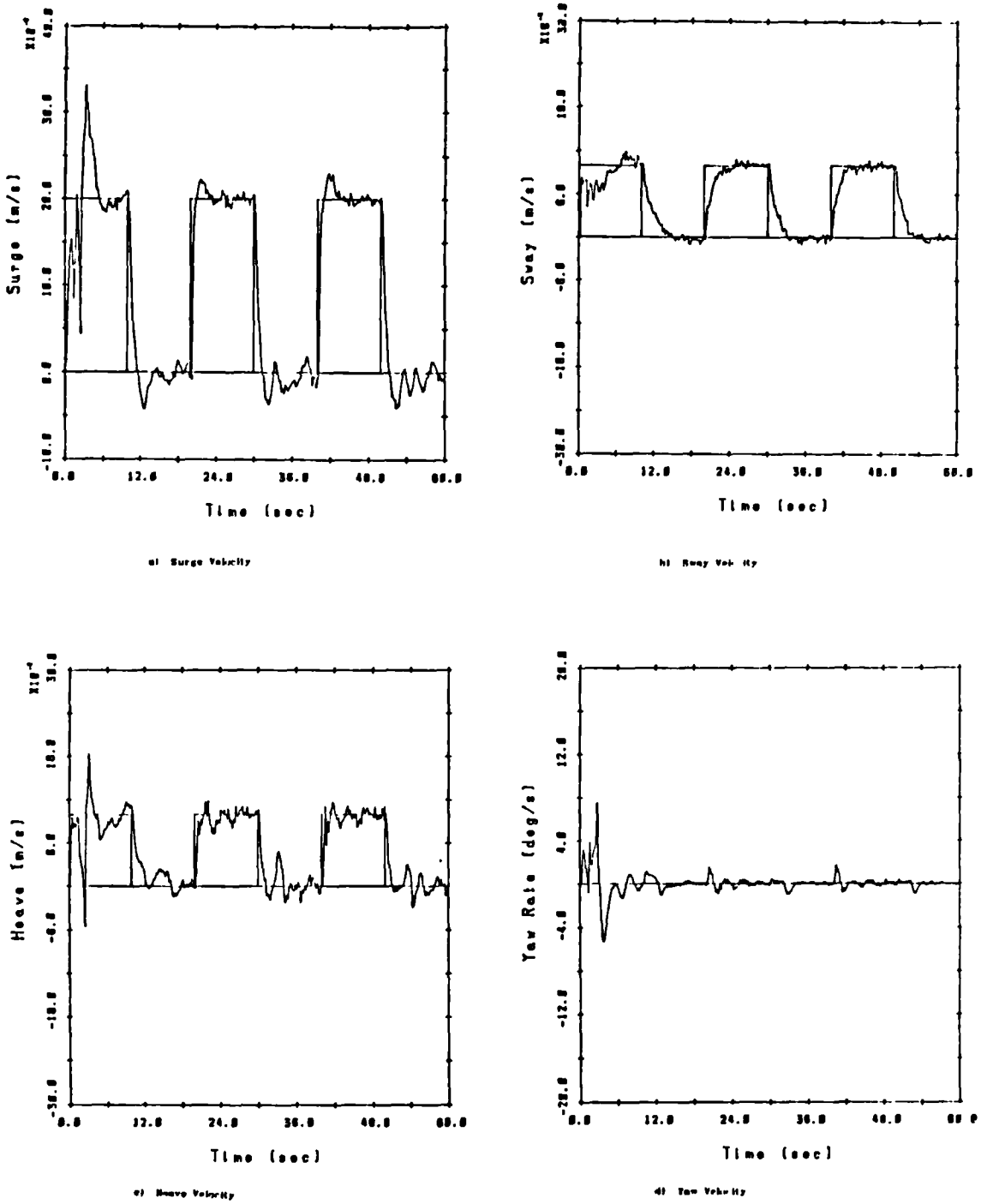

Figure 7.7 : Explicit Adaptive Control;
Inspection Manoeuver

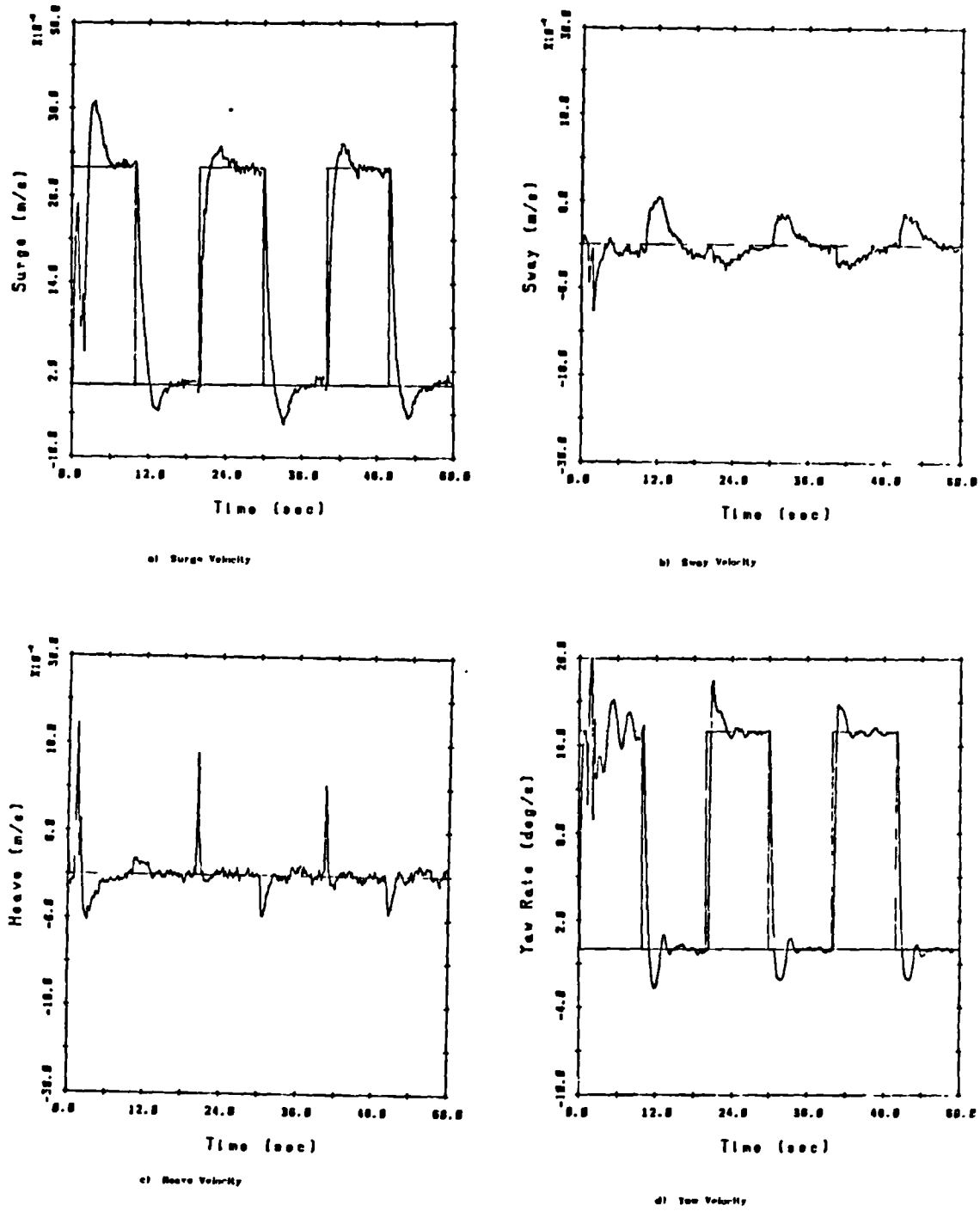

Figure 7.8 : Explicit Adaptive Control; Medium Speed Turn

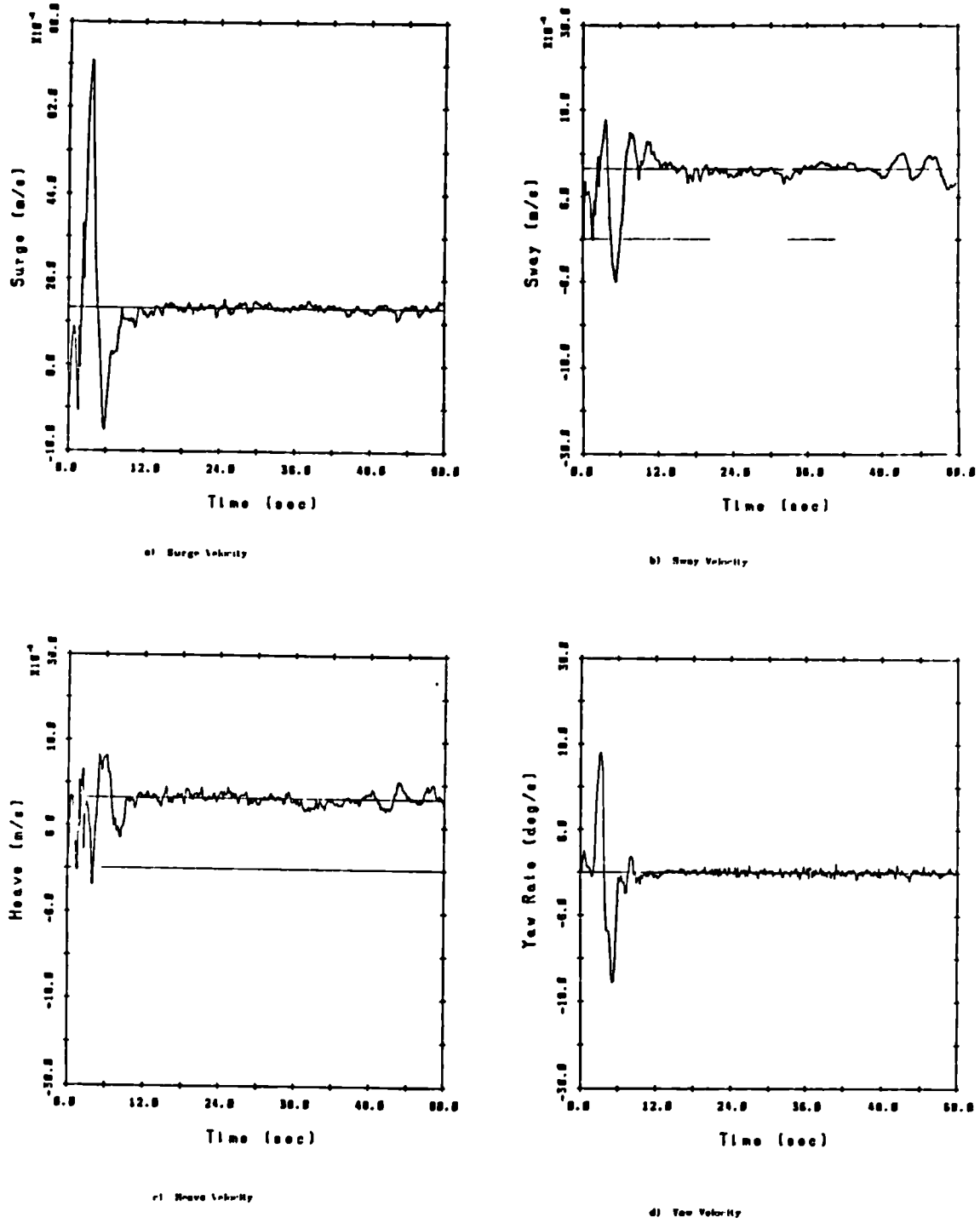

Figure 7.9 : Explicit Adaptive Control with High Measurement Noise

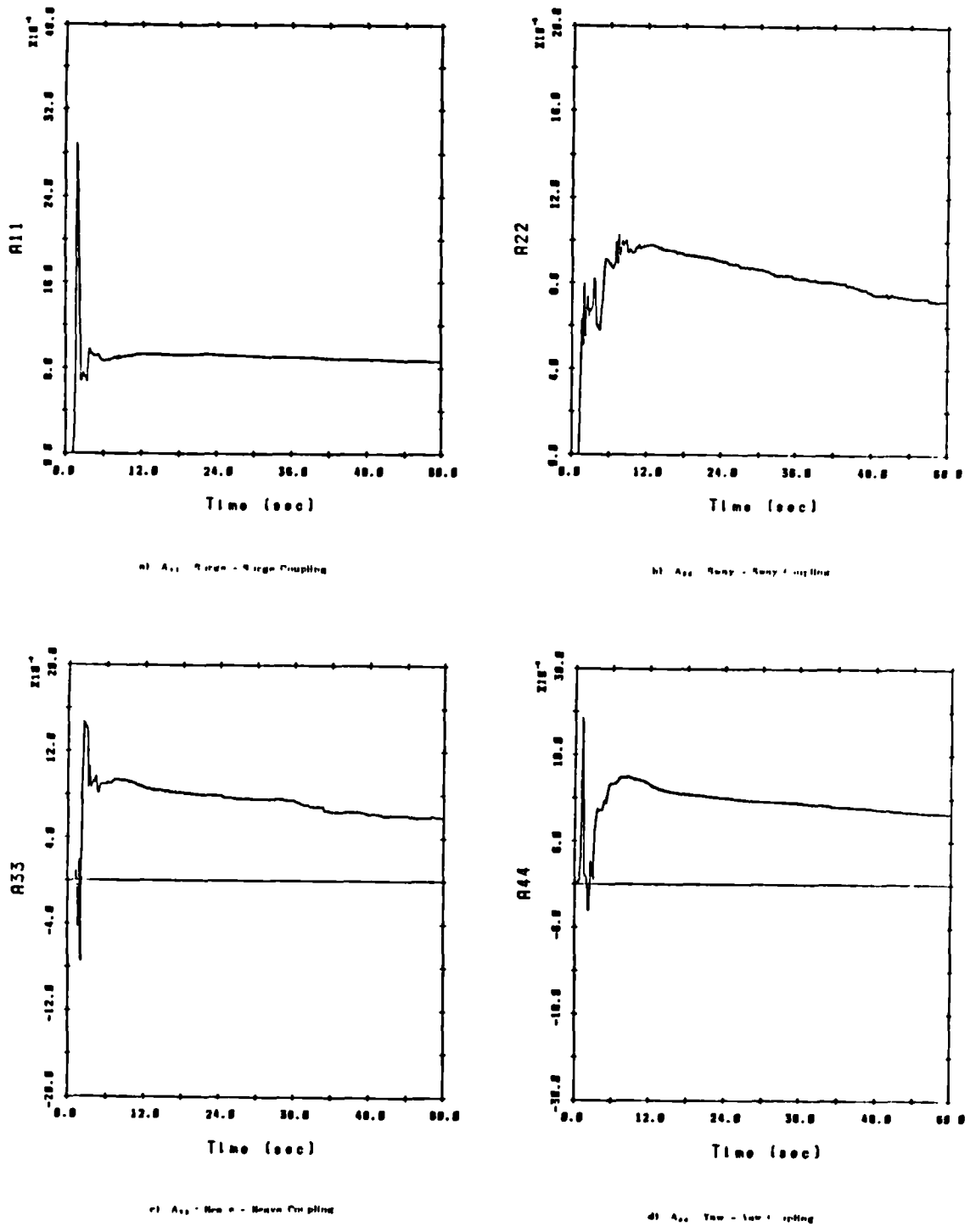

Figure 7.10 : Explicit Adaptive Control with High Measurement Noise; Parameter Convergence

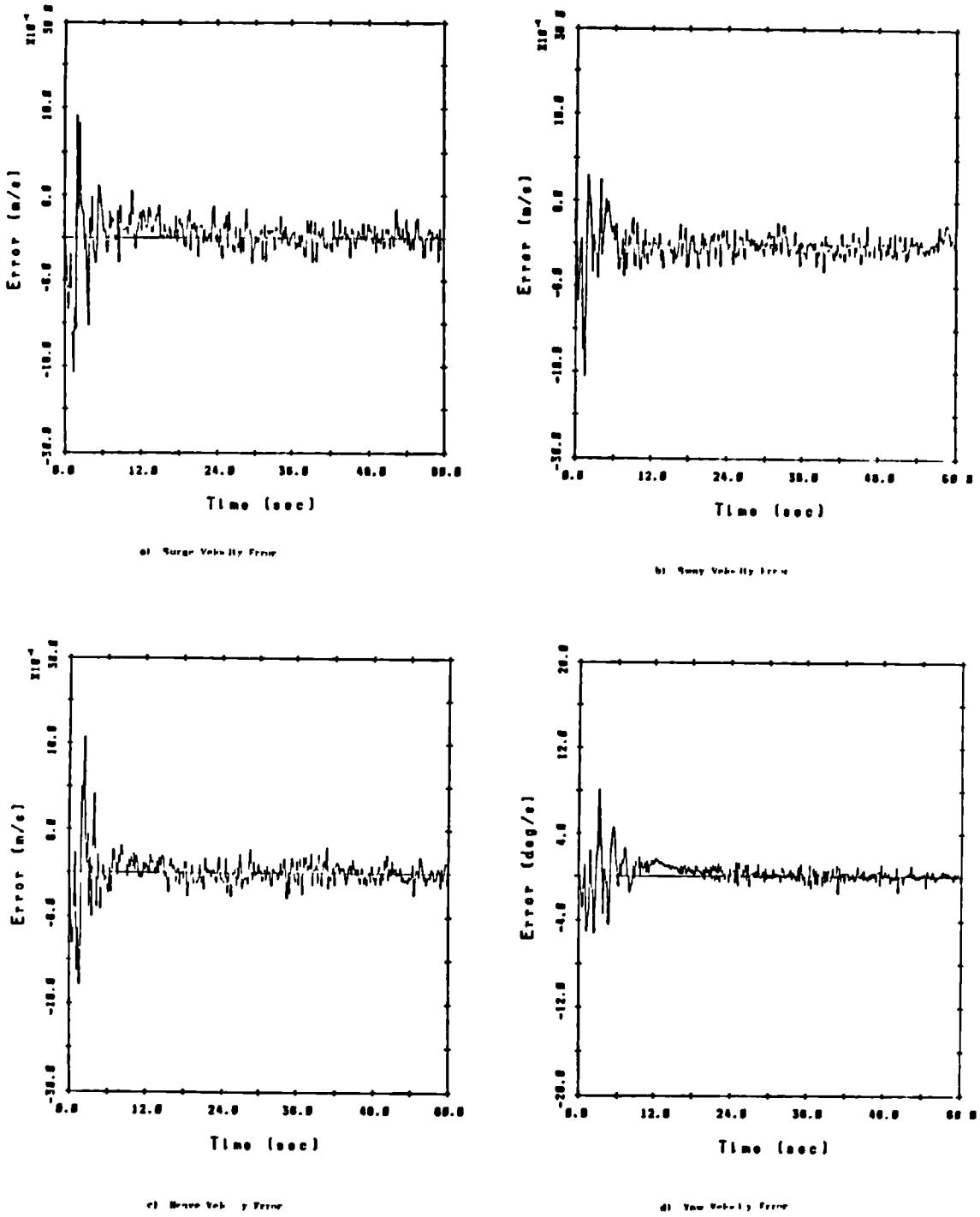

Figure 7.11 : Explicit Adaptive Control with High Measurement Noise; Differences between Measurement Noise and Modelling Errors

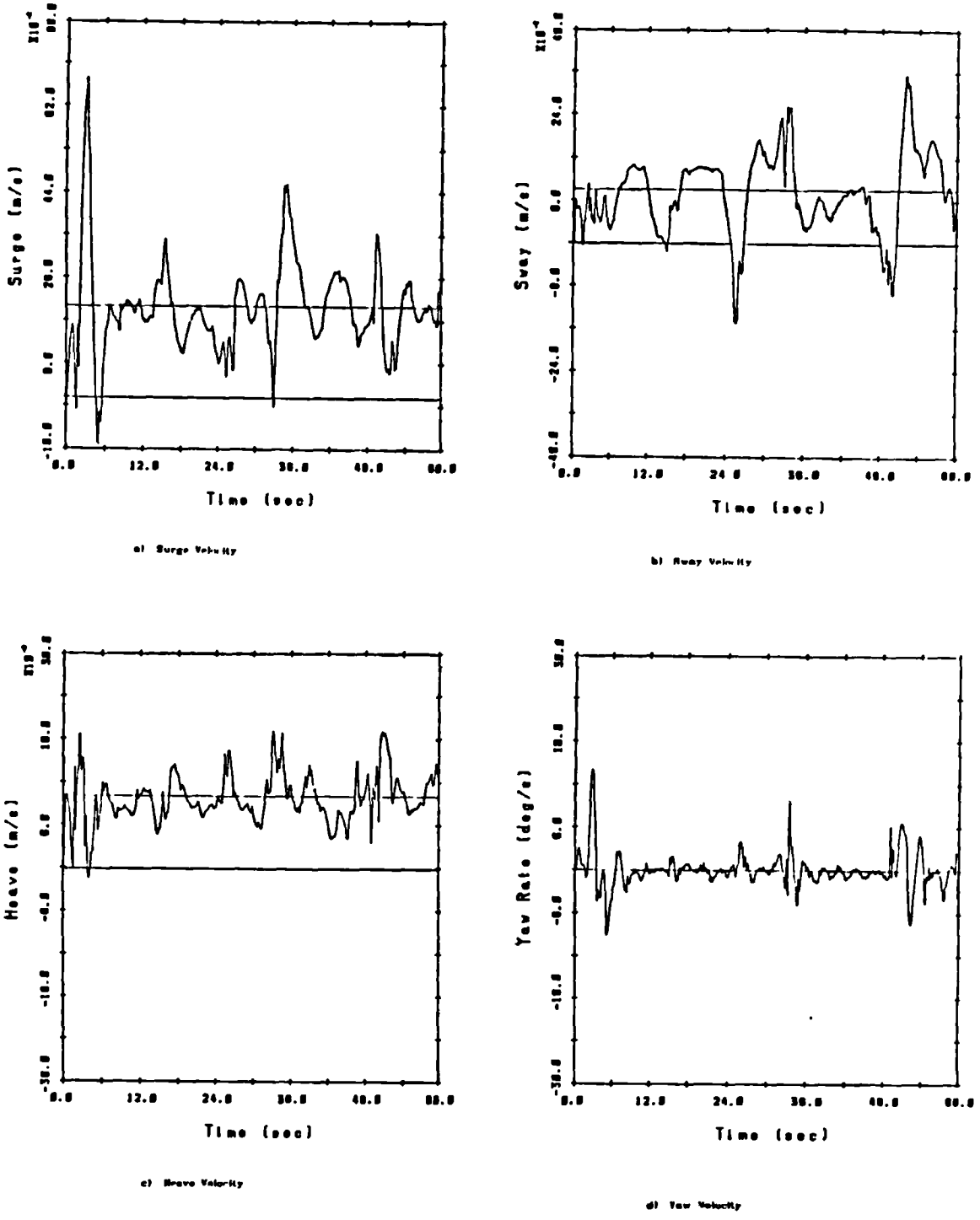

Figure 7.12 : Explicit Adaptive Control with High Measurement Noise; Forgetting Factor = 0.950

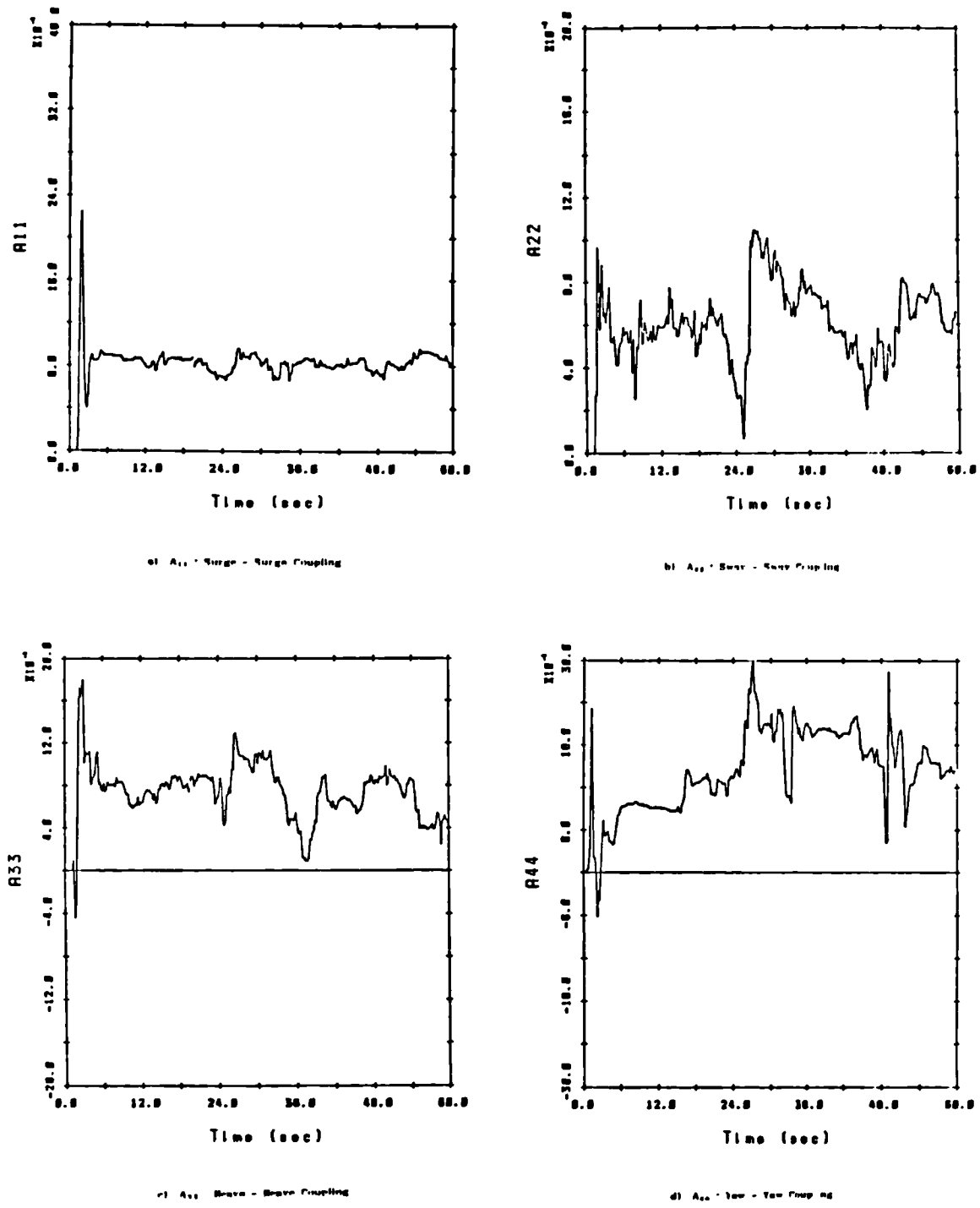

Figure 7.13 : Explicit Adaptive Control with High Measurement Noise; Parameter Convergence, Forgetting Factor = 0.950

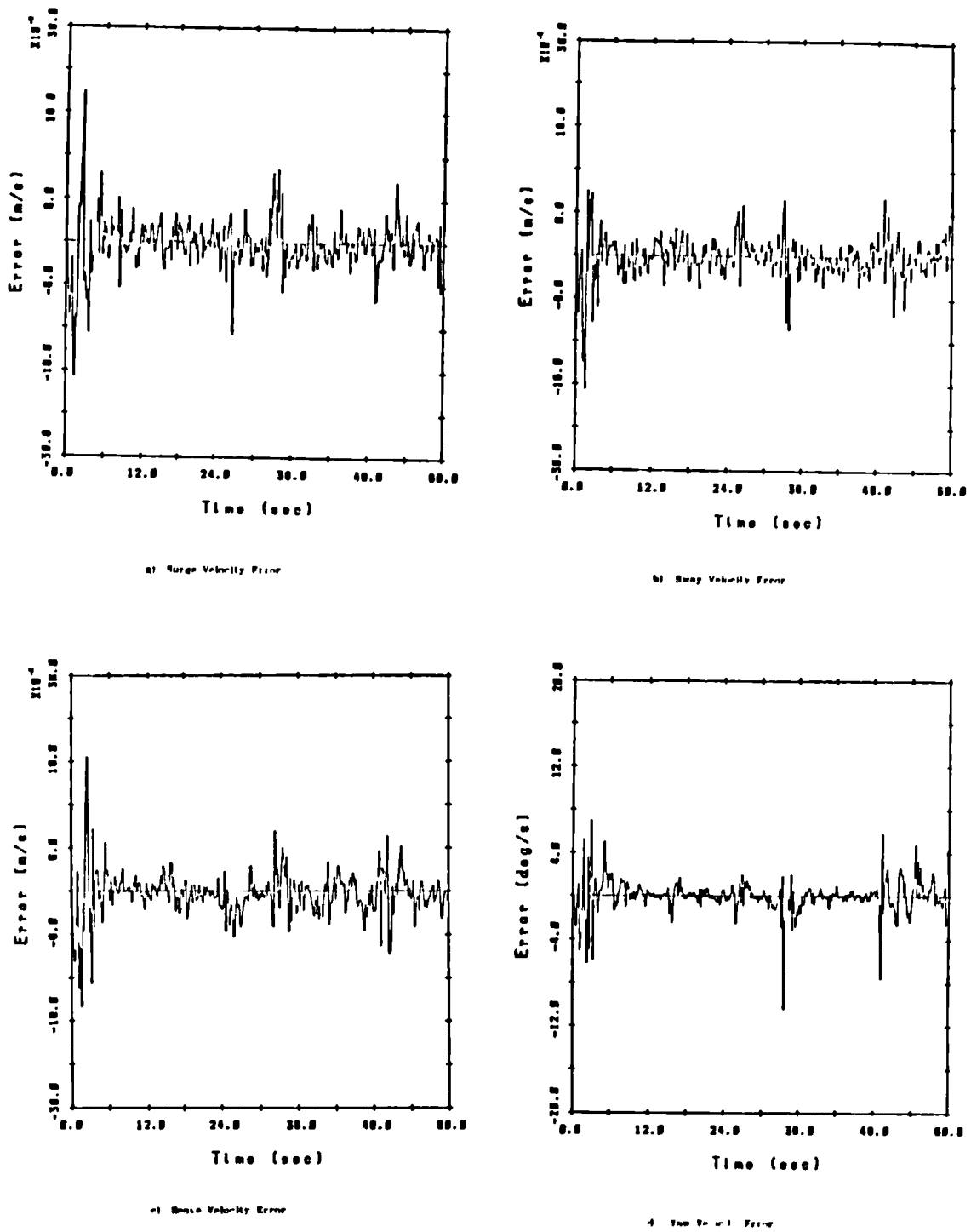

Figure 7.14 : Explicit Adaptive Control with High Measurement Noise; Differences between Measurement Noise and Modelling Errors, Forgetting Factor = 0.950

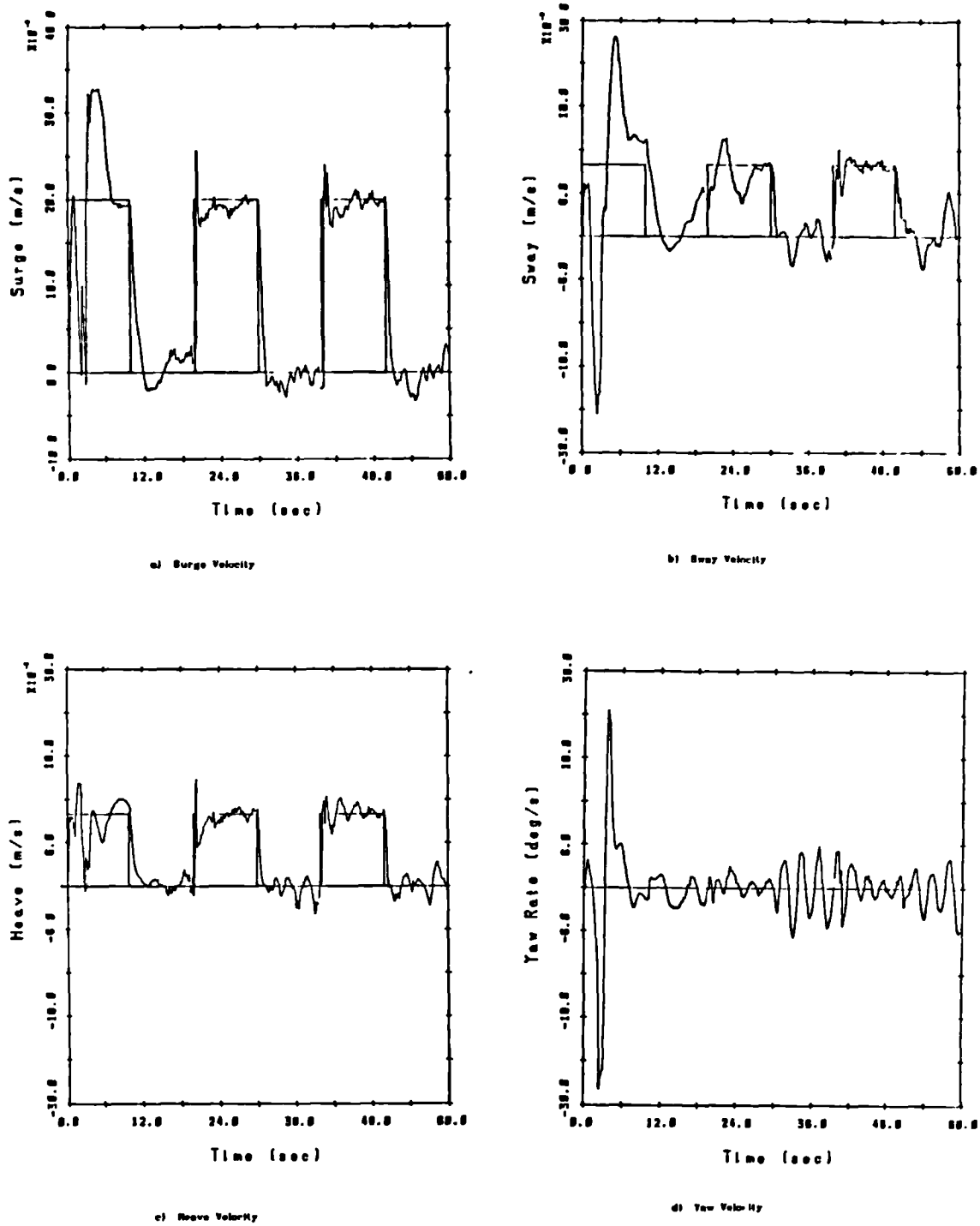

Figure 7.15 : Explicit Adaptive Control; Disturbance Rejection

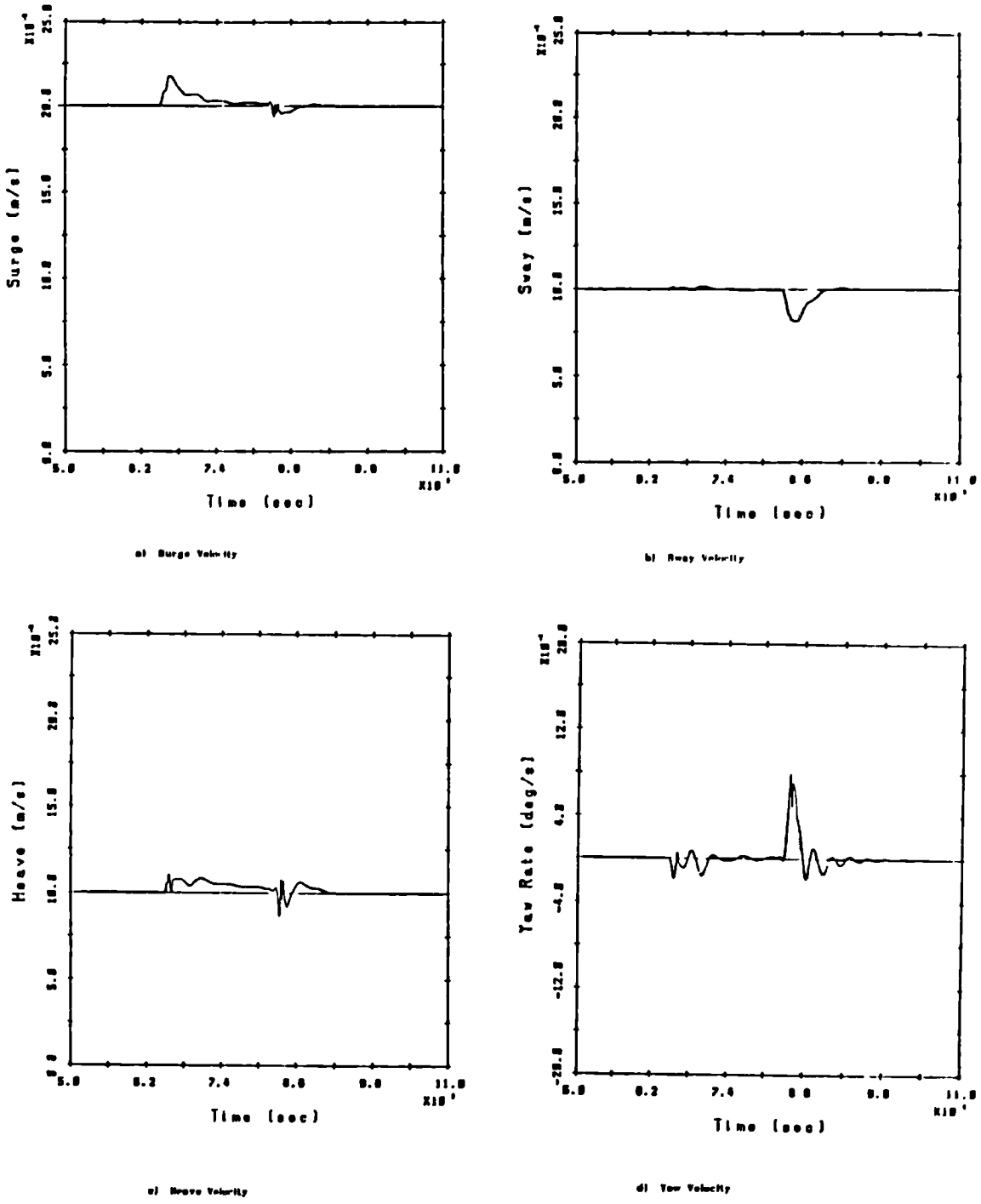

Figure 7.16 : Explicit Adaptive Control with the Modified ROV

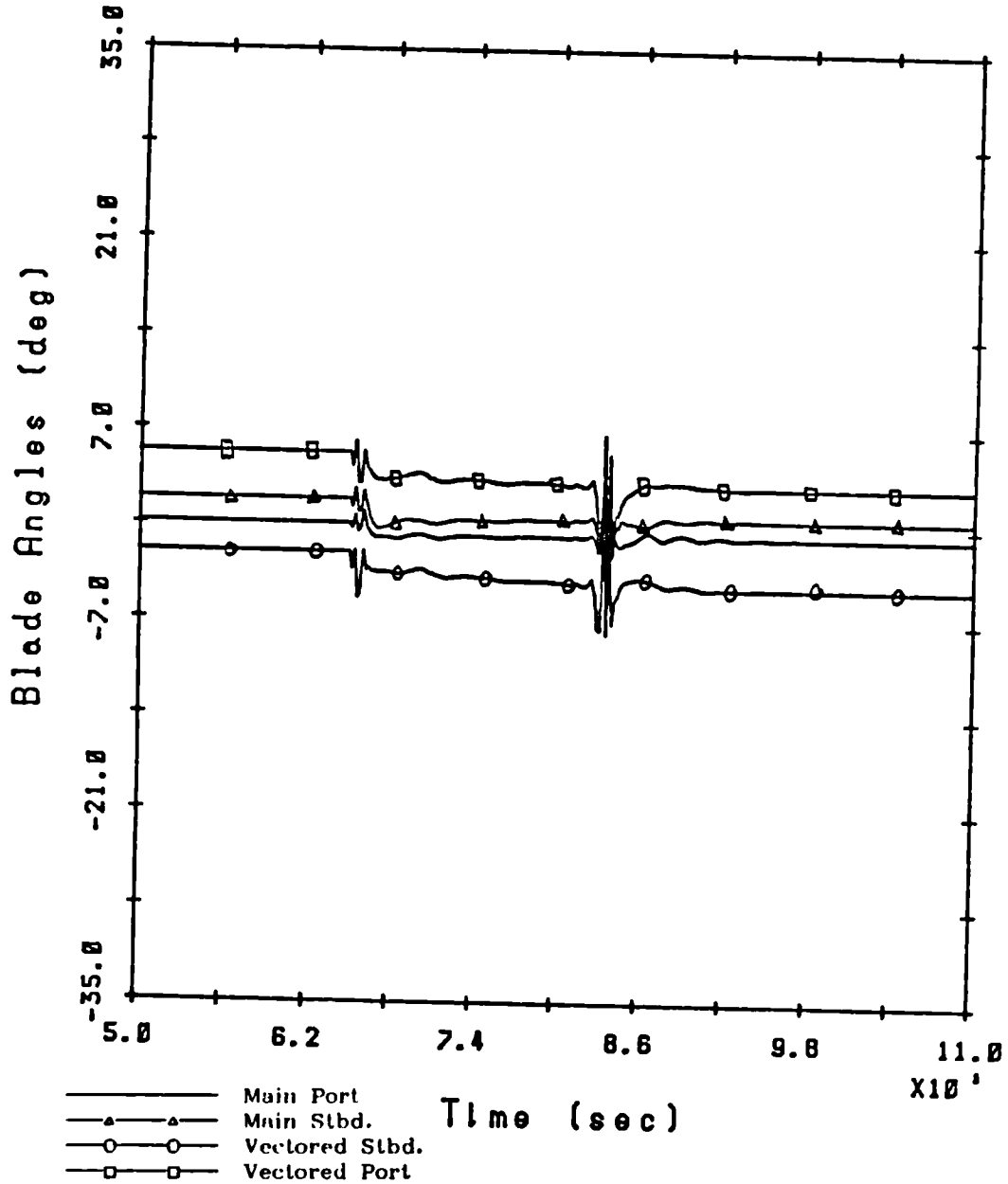

e) Thruster Blade Pitch Angles

Figure 7.16 : Continued

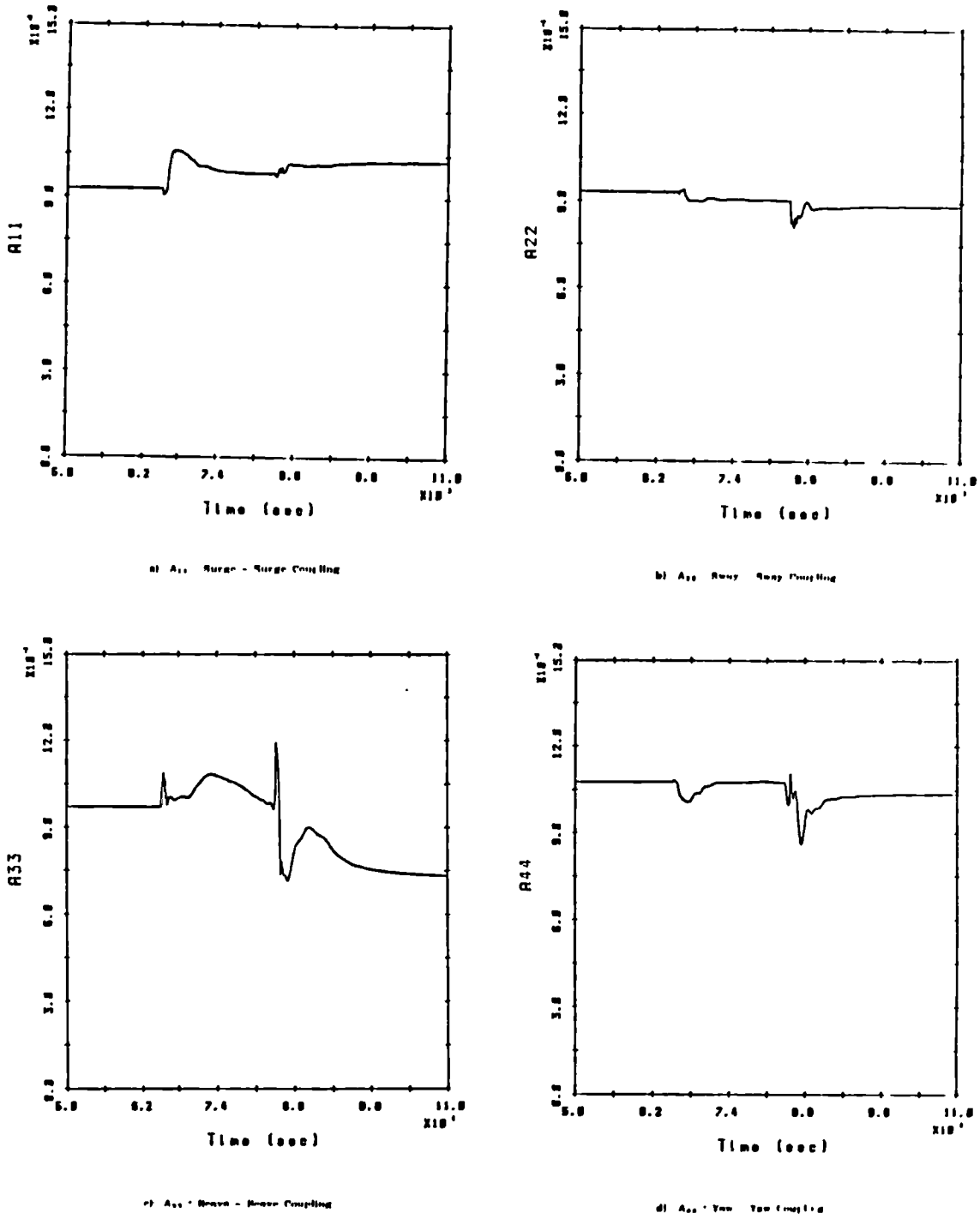

Figure 7.17 : Explicit Adaptive Control with the Modified ROV; Parameter Variations

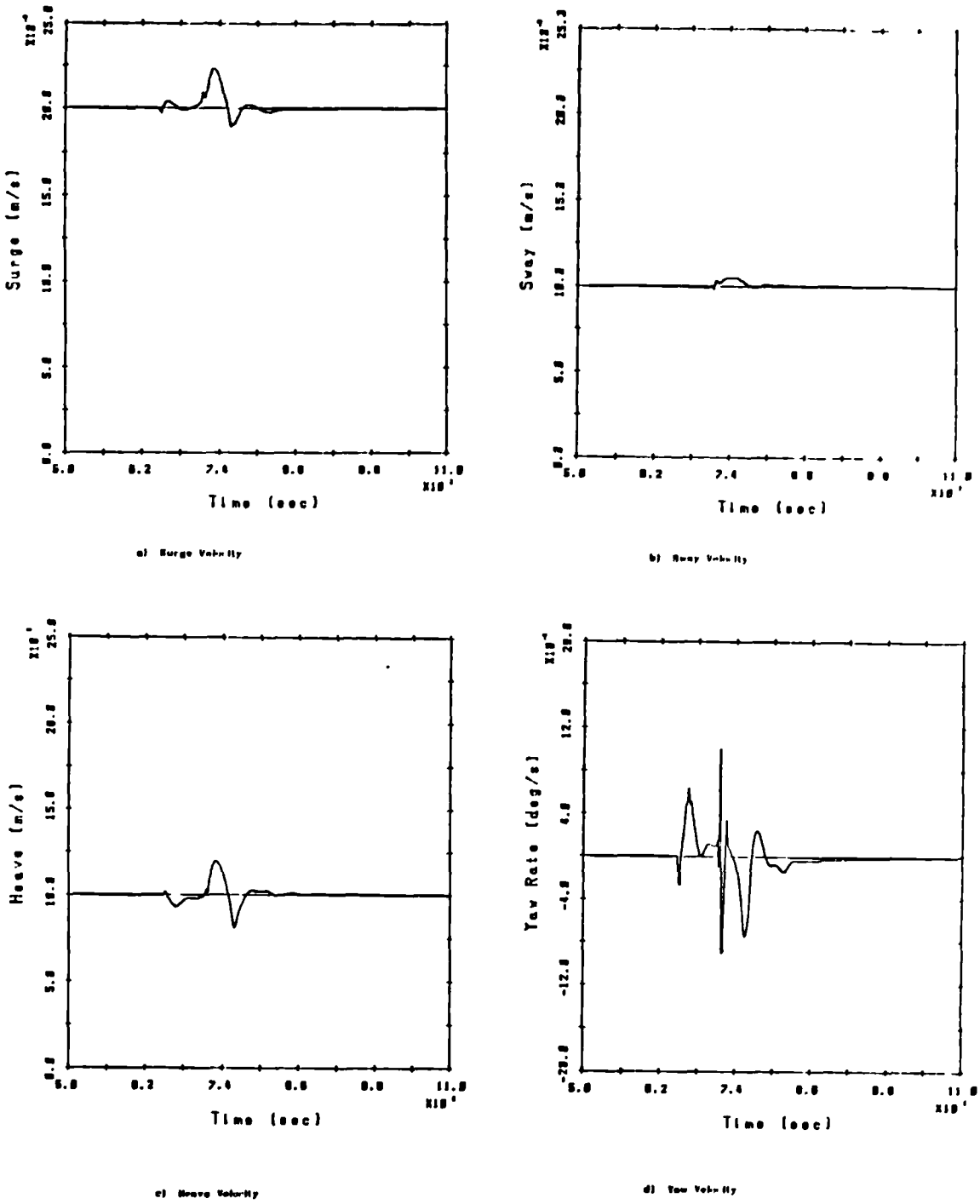

Figure 7.18 : Explicit Adaptive Control with Thruster Foulling

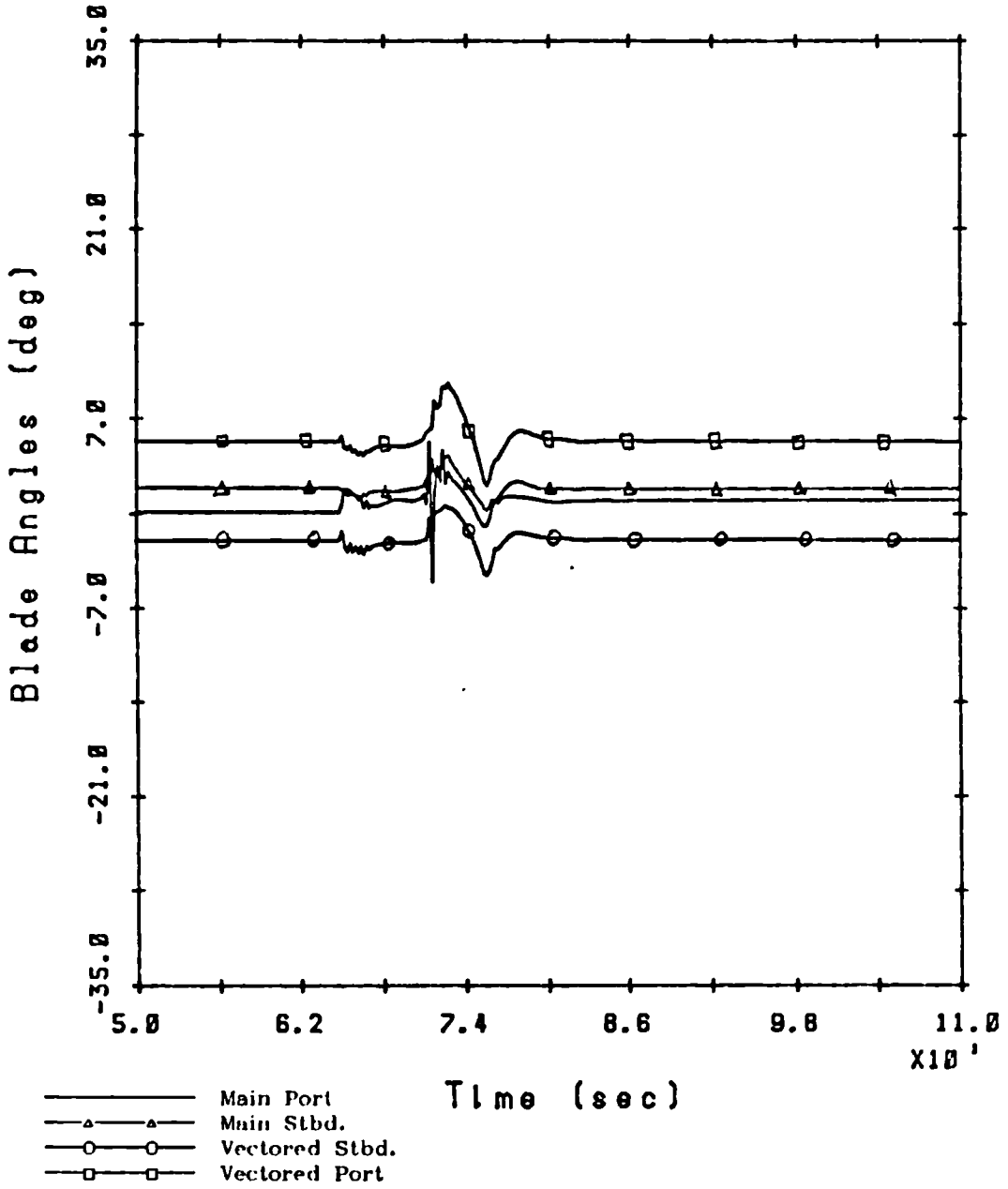

e) Thruster Blade Pitch Angles

Figure 7.18 : Continued

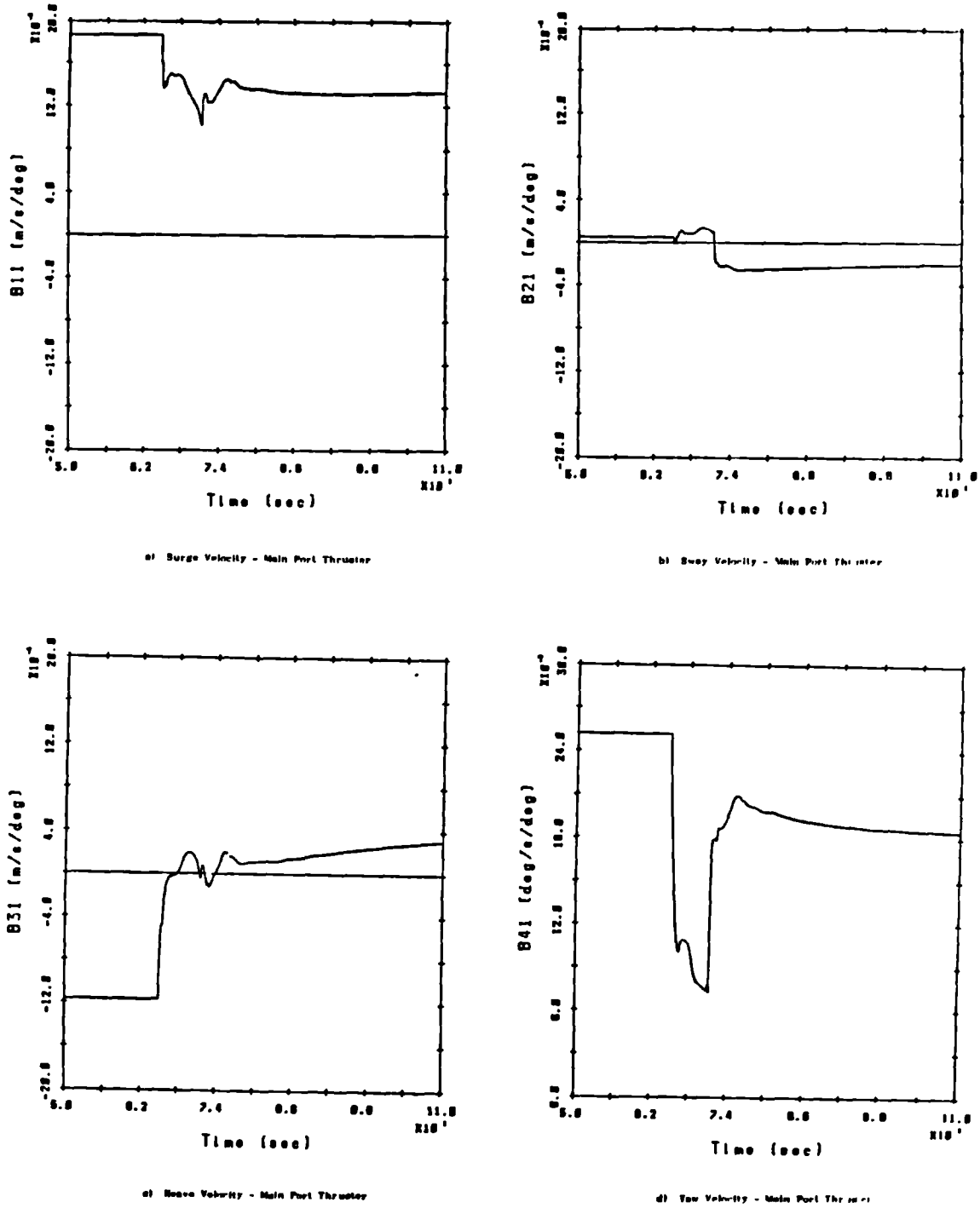

Figure 7.19 : Explicit Adaptive Control with Thruster Foulling; Parameter Variations

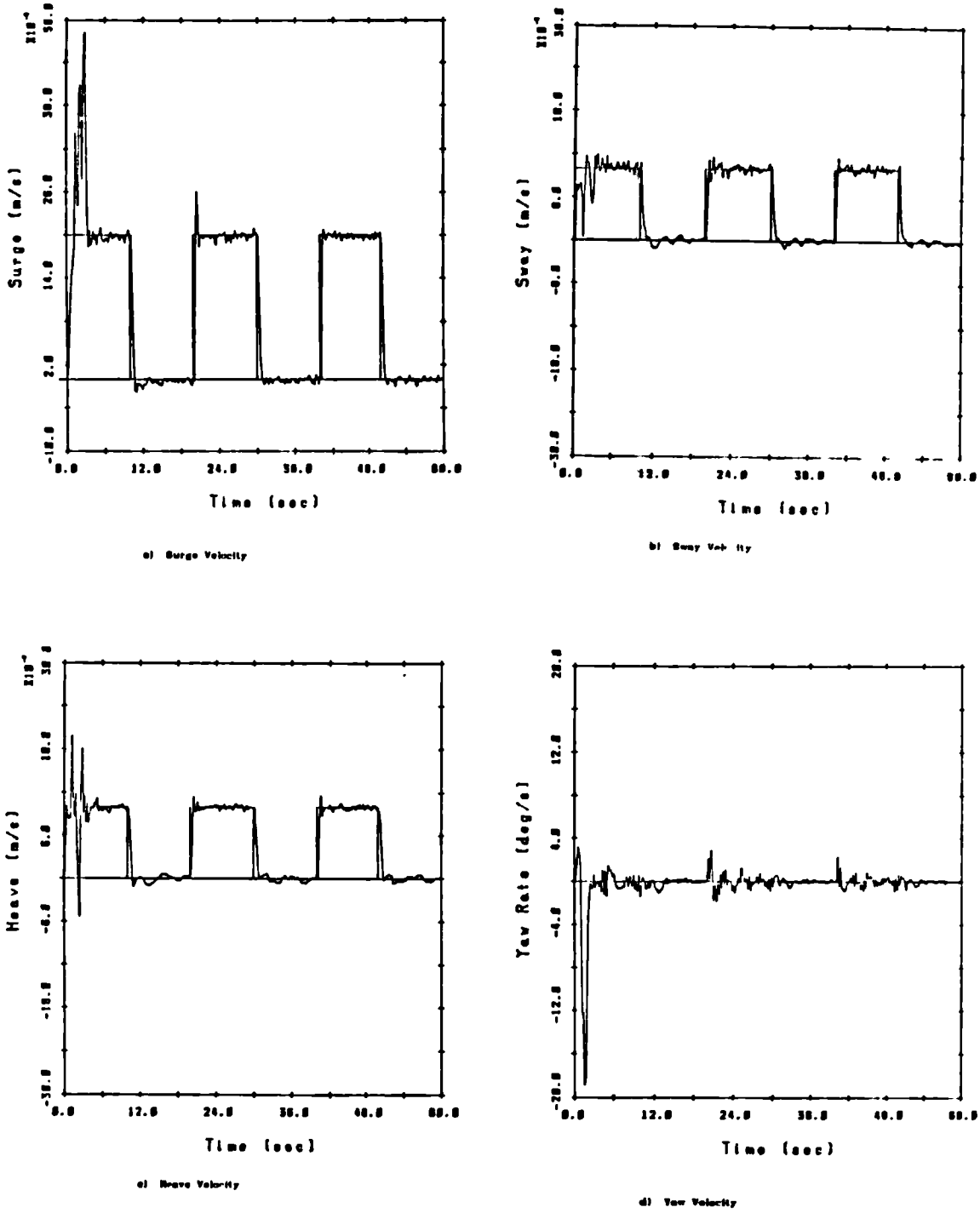

Figure 7.20 : Implicit Adaptive Control;
Inspection Manoeuver,
Thruster Penalty Factor = 0.0

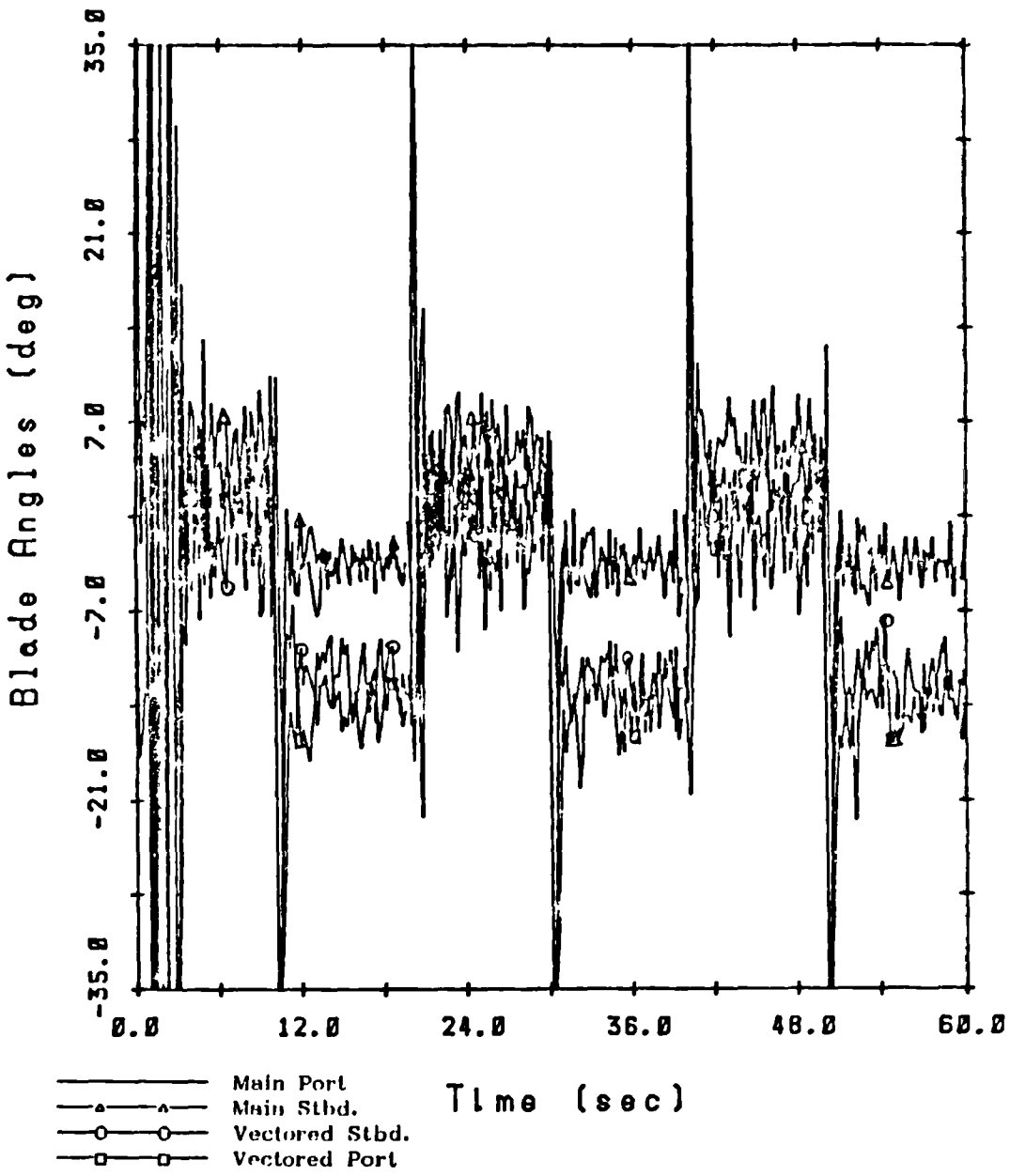

e) Thruster Blade Pitch Angles

Figure 7.20 : Continued

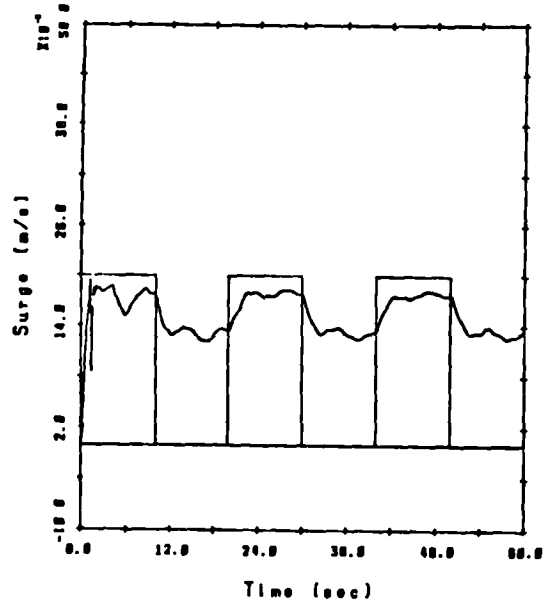

a) Surge Velocity

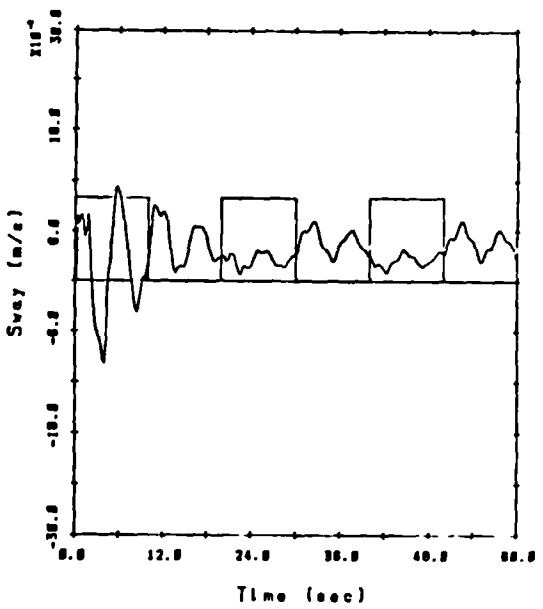

b) Sway Velocity

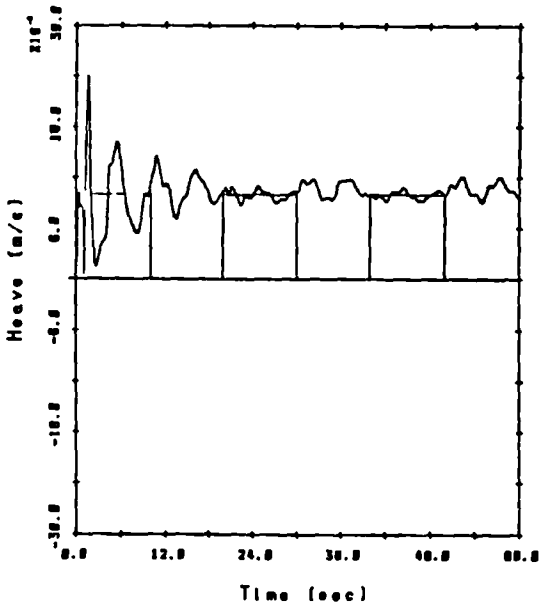

c) Heave Velocity

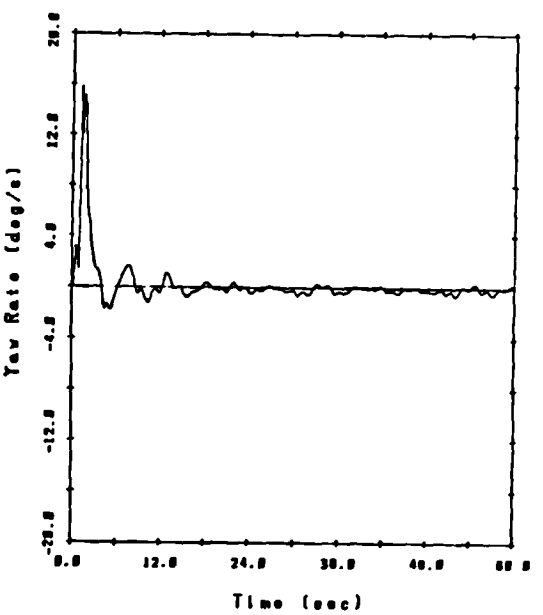

d) Yaw Velocity

Figure 7.21 : Implicit Adaptive Control;
Inspection Manoeuver,
Thruster Penalty Factor = 0.1

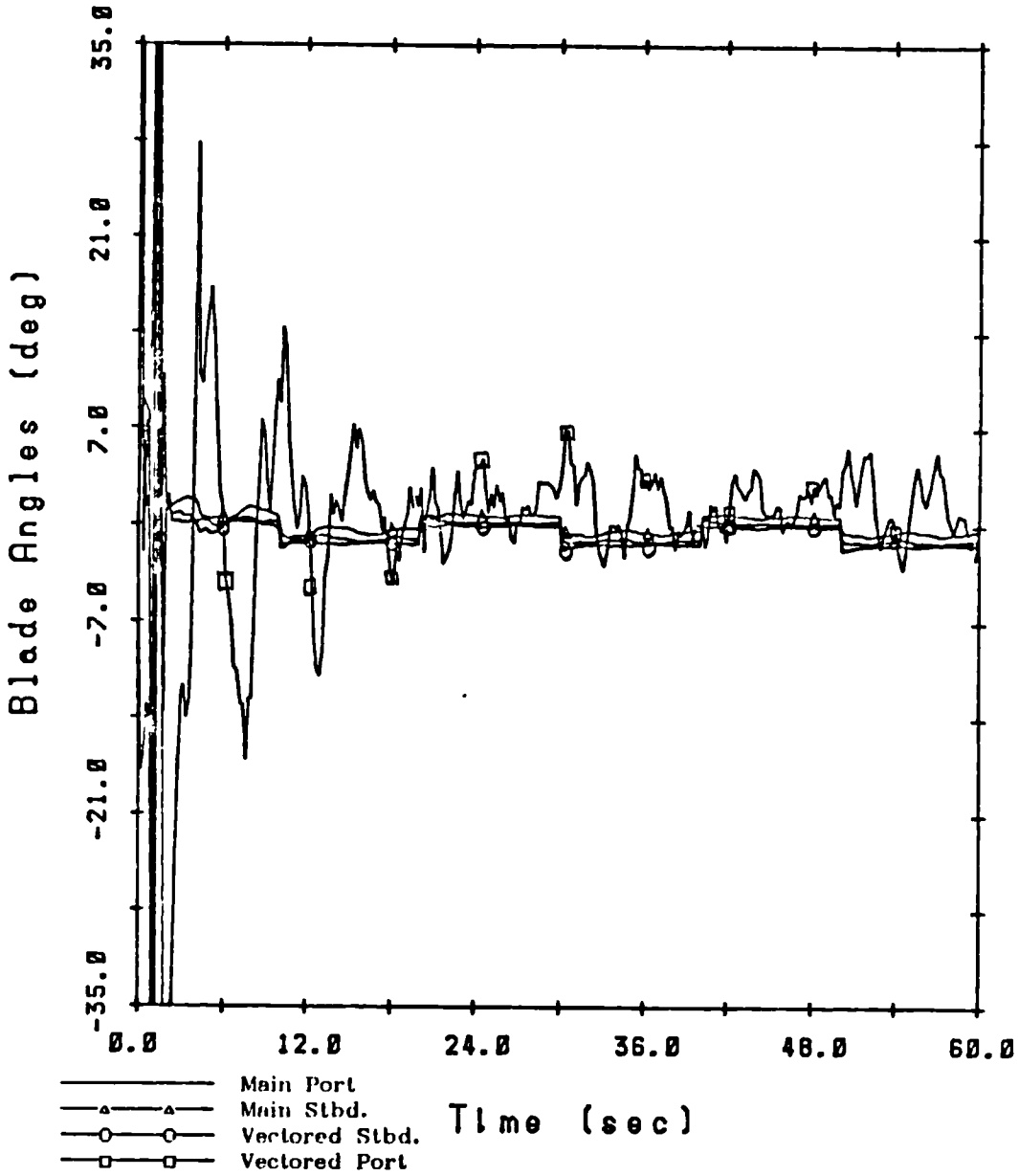

e) Thruster Blade Pitch Angles

Figure 7.21 : Continued

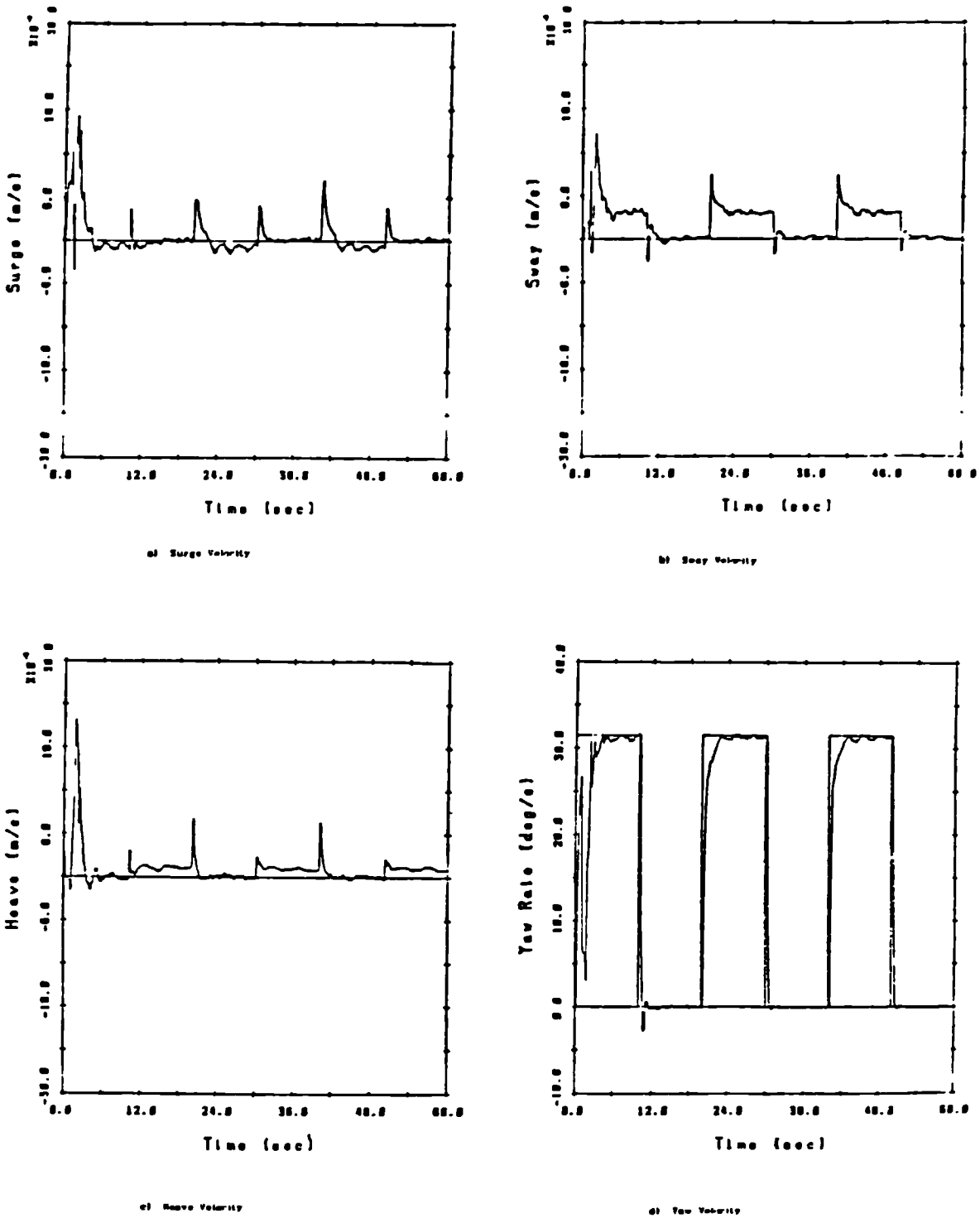

Figure 7.22 : Implicit Adaptive Control;
Yaw Test

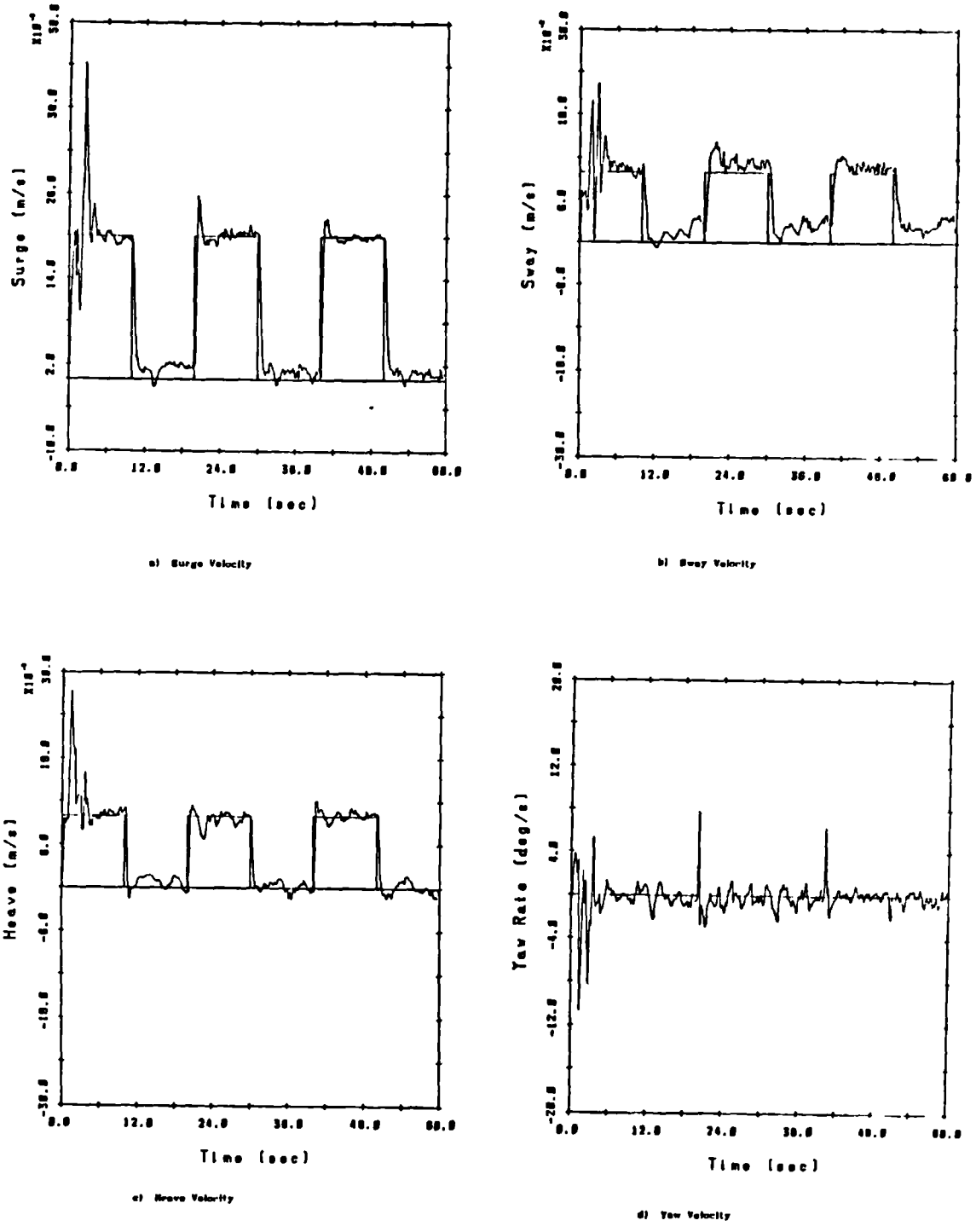

Figure 7.23 : Implicit Adaptive Control; Disturbance Rejection

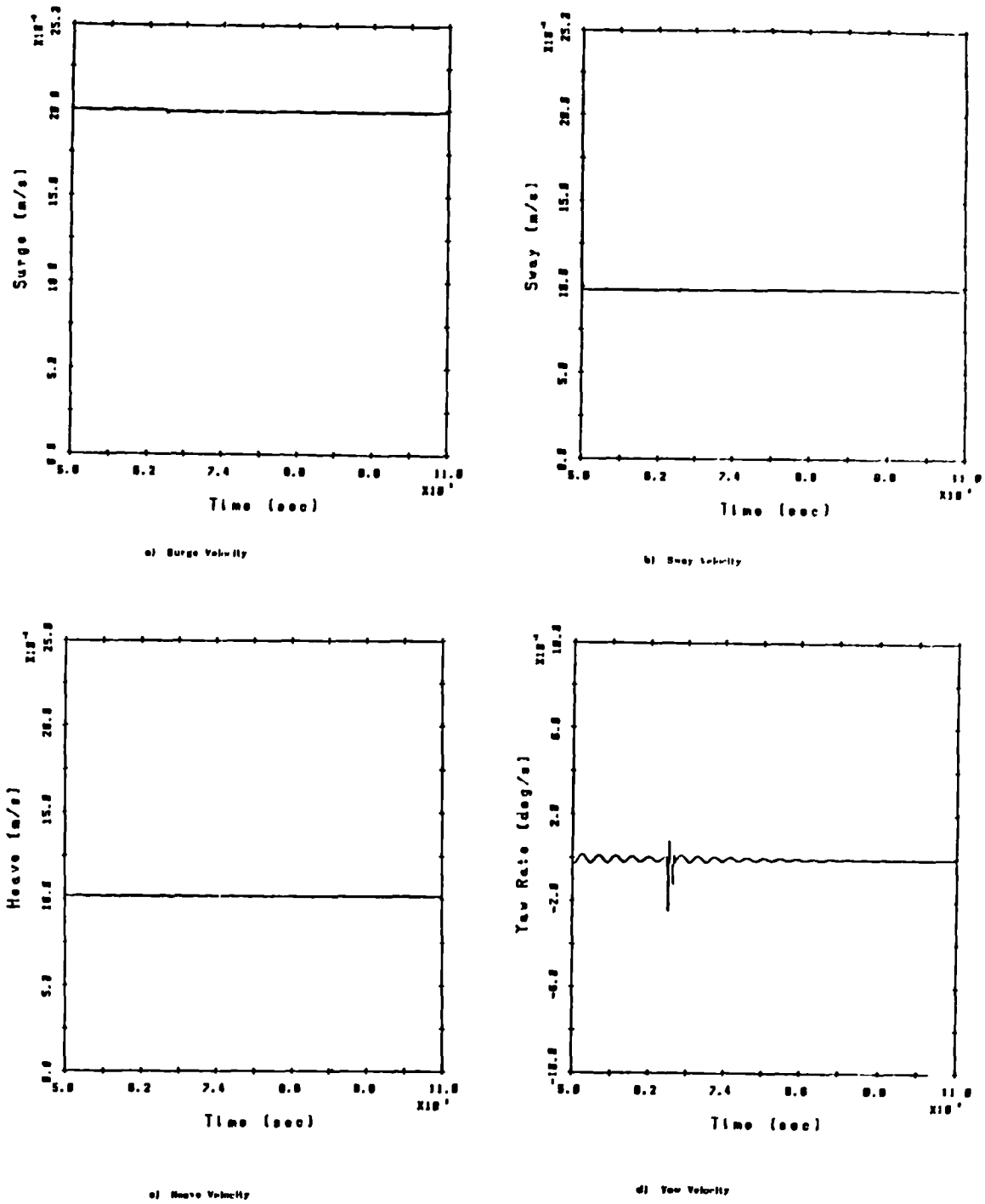

Figure 7.24 : Implicit Adaptive Control with Thruster Foulling

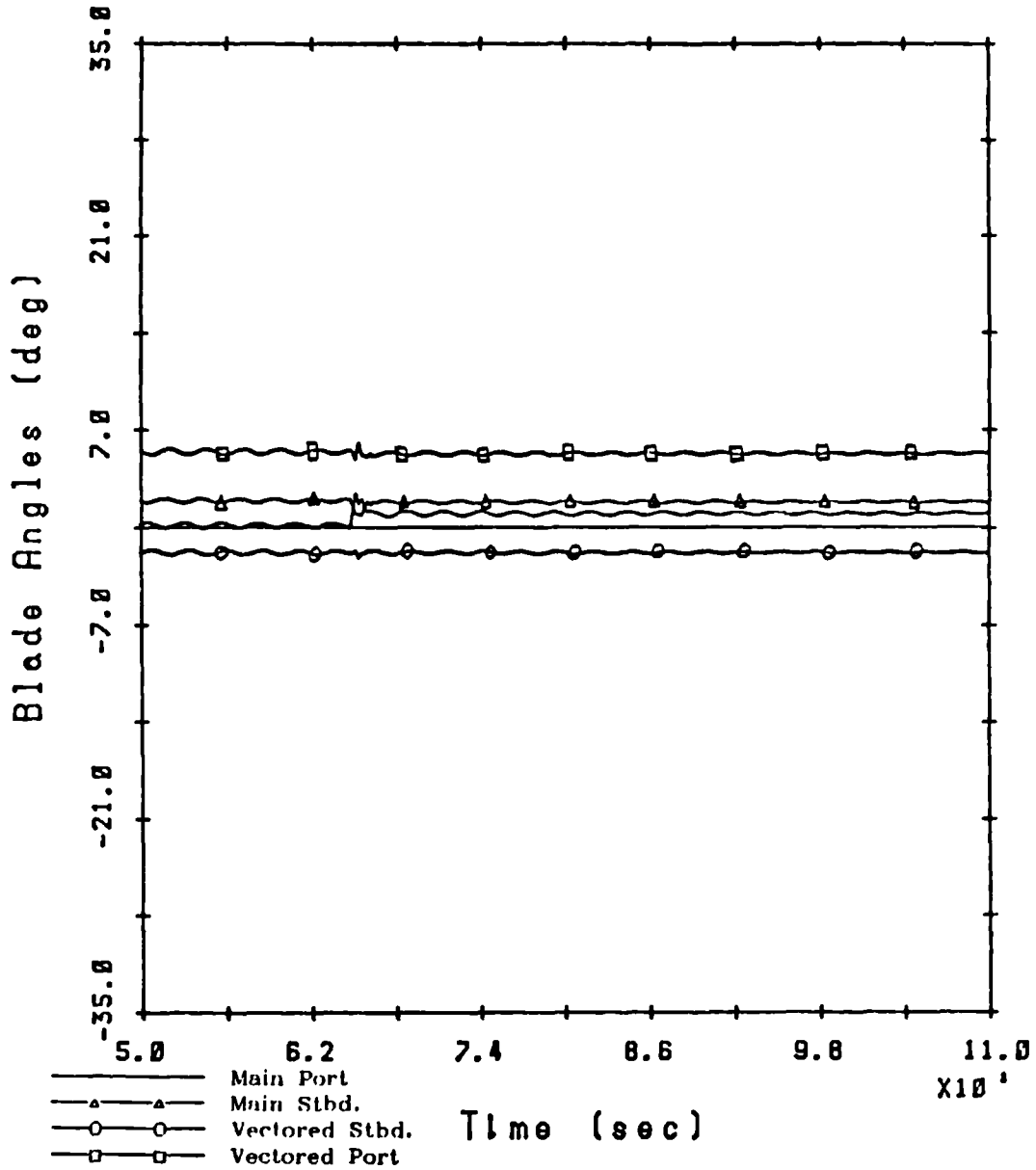

e) Thruster Blade Pitch Angles

Figure 7.24 : Continued

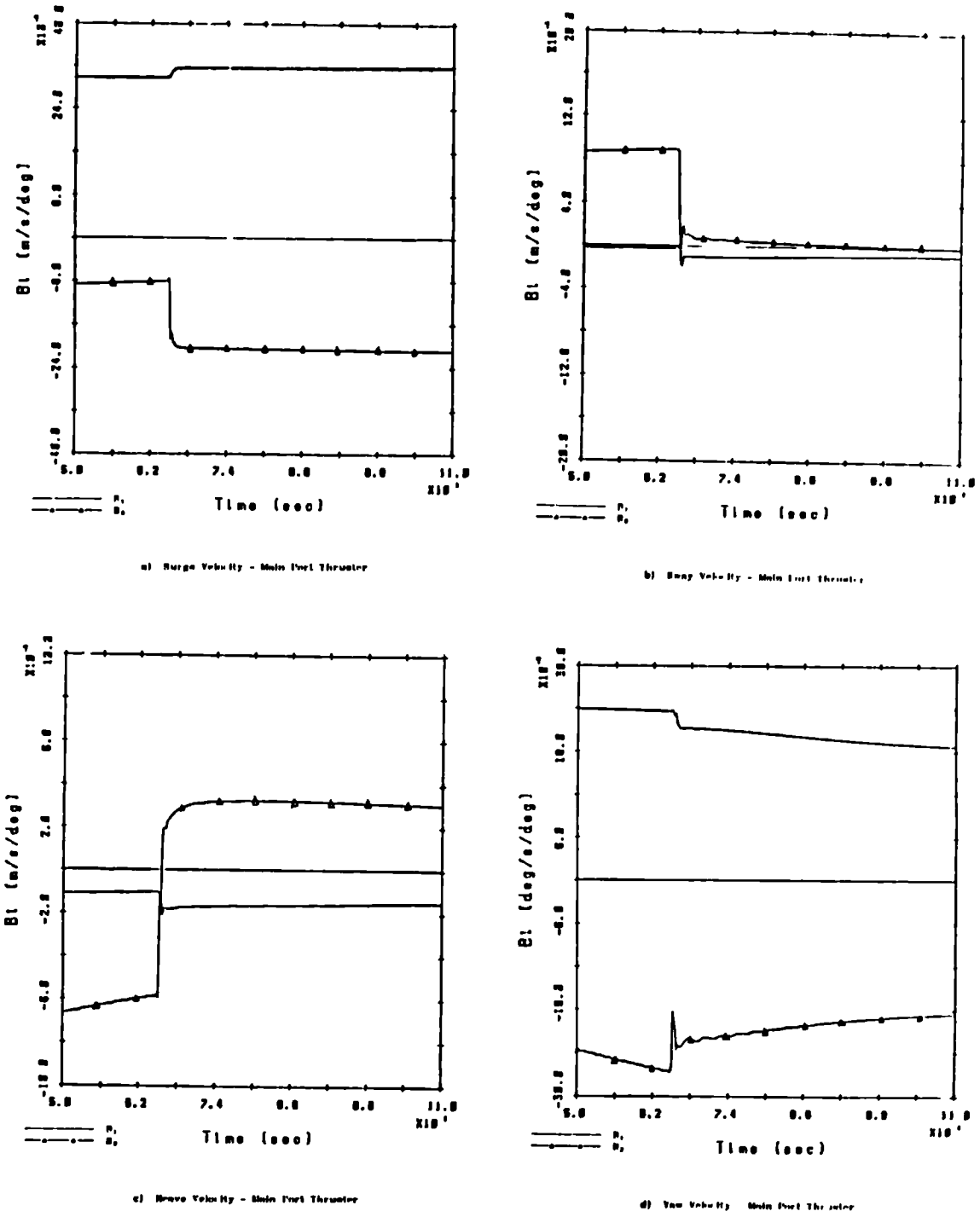

Figure 7.25 : Implicit Adaptive Control with Thruster Foulling; Parameter Variations

Chapter 8

Conclusions and Recommendations for Further Work

8.1 Introduction

The objective of this chapter is to give a summary of the work already presented, reach conclusions about its significance and suggest areas where additional study would be beneficial.

8.2 Summary and Conclusions

The original aim of this thesis was to investigate the modelling, simulation and control of Remotely Operated Underwater Vehicles (ROVs). An introduction to the history and capabilities of these vehicles illustrated the need for some form of automatic guidance system. Past and current research in this area was reviewed; this revealed many advances over manual guidance strategies but the studies all shared the weakness of requiring knowledge of the ROV's dynamics 'a priori'. The extent of this requirement varied from study to study.

A conventional hydrodynamic-based model of a ROV contains a number of components: vehicle hydrodynamics and hydrostatics, rigid-body kinematic forces, thruster forces and momentum drag effects and forces caused by the ROV's umbilical cable. Also required is an approximation for the current and turbulence in which these vehicles work. All of these elements were discussed with emphasis on the compromise between accuracy and complication which occurs when simplifications are made.

A comprehensive ROV model, derived experimentally by the National Maritime Institute, was made available for the present study by the model's sponsors, the UK Department of Energy Offshore Supplies Office. This model was validated and it was found that numerous changes were necessary in order to match the model's behaviour with the vessel's observed free-running performance. Furthermore, the time

and financial costs of the derivation were considerable and certainly more than a ROV manufacturer or operator would be willing to spend in order to have an autopilot.

The design of such an autopilot is best approached as a hierarchical scheme. A task controller next to the human operator will request a global position controller to move the ROV through a series of displacements and attitudes. The local velocity controller will receive references from the global position level and vary the thruster commands. These velocity references produced by the position controller should take the vehicle's capabilities into account. The advantage of a hierarchical system is that the design of the overall system is more manageable when broken into levels. Since each controller 'sees' a nice, decoupled system with constant dynamics below it, the overall design task is made less complex.

The remainder of the thesis concentrated on the requirements for the local velocity level. Conventional multivariable controller design methods require a reasonably reliable open-loop model and because of the experience with the ROV model verification exercise, these are rejected. Adaptive controllers do not require a model 'a priori' since they learn about the process on-line by examining the input and output data. However, they are set aside initially because ROV operators might be more prone to accept a simpler fixed-gain controller which is easier to understand and which would have a smaller computational requirement.

The scheme considered as an alternative uses a multivariable decoupling control law which only requires an approximate model of the ROV. This law is robust; that is, with fixed gains, it is able to maintain closed-loop performance for a range of open-loop systems. The parameters of this simplified model are identified by an off-line batch least squares technique during a 'self-test' executed autonomously by the ROV. This was found to provide very adequate closed-loop performance with the exception of some limit-cycle behaviour. Simulation also showed that the autopilot was able to hold a zero velocity in a stochastic current and, in this example, even displacement keeping was good. However, another loop with position

references would improve this property considerably. The robustness of the system was demonstrated by adding a camera to the bow of the vehicle. Despite the large change in open-loop dynamics caused by this extreme modification (the camera's mass was 13 percent that of the unmodified ROV's), there was little deterioration in performance.

A method for scheduling the controller gains with surge speed was devised, but it was found that starting the self-test at the correct nominal steady-state was difficult. An incorrect model was produced at the higher surge speed and this, of course, caused poorer performance.

Despite the reservations held about fully adaptive control, the potential of improved performance and the recent increased availability of inexpensive, powerful microprocessors encouraged studies of their suitability. Two adaptive controllers were considered. The first was an explicit method which combined the control law of the self-testing autopilot with recursive least squares system identification. An implicit generalised minimum variance adaptive controller was also simulated. These two methods have the distinct advantage of minimising the requirement for 'a priori' knowledge of the ROV's dynamics even more than did the self-test controller. Furthermore, the implicit adaptive controller has a simpler 'performance-oriented knob' than the law used for the other two systems. This consists of a single parameter which varies the relative penalty given to reference velocity errors and thruster effort; the other controller requires the designer to choose two poles for each loop. The first method would be more attractive to operators with little knowledge of control theory.

Thruster foulling and vehicle modifications were simulated in order to evaluate the ability of the adaptive controllers in coping with sudden configuration changes. It was shown that the controller parameters, after converging at the beginning of the simulation, quickly take up new values after the modification is introduced. This causes the SI algorithm's modelling errors to reduce and the closed-loop performance to return to its original level.

As an offshoot from the work on adaptive control, it was shown that multivariable recursive SI methods can be applied to modelling ROV dynamics. Input/output data sets were generated from the nonlinear vehicle simulation and then processed by three different SI algorithms: Least Squares, Recursive Least Squares and the Recursive Prediction Error Method. All produced ARMAX models which matched the original data very closely. Three statistical tests, namely the F-test for analysis of error variance, autocorrelation of the output modelling errors and Akaike's Information Criterion, a quantitative compromise between model complexity and accuracy, were used. These determined that the nonlinear models thought to be essential for a ROV simulation are conveniently characterised by first and second order linear equations.

If details of a ROV model, such as a particular hydrodynamic derivative, are not required, then SI can result in great savings of time and cost as compared with the conventional hydrodynamics approach. Additionally, it is easier to validate such a model by monitoring the modelling errors rather than having to perform a model validation exercise as was done in the present study. The ARMAX models produced would be especially useful for ROV pilot training simulators, which must run in real time.

All of the controllers and system identification methods studied require that the velocities and orientation of the ROV are measurable. Previous studies of marine systems have emphasised that this is difficult to achieve. Admiralty Research Establishment (Portland), JH Division, who are concerned with the mine countermeasures capabilities of ROVs, made available the manoeuvering tank at ARE (Haslar), support staff and an instrumented vehicle similar to that which was simulated in the rest of this thesis. Velocity measurements were to be achieved by integrating the signals from three mutually perpendicular strapdown accelerometers and three angular rate gyros. These proved to be unsuitable in this role for a number of reasons. However, some measurements were valid and closed-loop control of the yaw response was achieved. These measurements helped validate the simulated results presented here.

8.3 Recommendations for Further Work

Additional study into a number of practical and theoretical aspects of this project would be valuable. The most immediate need is for another attempt at instrumenting a ROV for SI and closed-loop control. It is hoped that ARE (Portland) will be supplying a gimballed accelerometer pack for the next test and this should largely eliminate the velocity measurement problems. However, further analysis of the last trial should determine exactly why these difficulties occurred and prevent a repetition. Another valuable project would be to develop an accurate sensor model. The inclusion of this model in the nonlinear simulation would predict problems before the expensive tank trials begin. Depending on the next instrumentation fit used, advanced filtering techniques may have to be employed for combining measurements from dissimilar sensors. Simulation could also be used to check their performance.

Section 7.3 discussed the jacketting software that is required to guarantee the integrity of an adaptively controlled system. None of these safeguards were implemented for the simulation studies of chapter 7, but they would be required for the manoeuvering tank trials.

There are a few aspects of the system identification research which require more work. Additional study is required to evaluate the effect of different excitation series on the models obtained during SI experiments. Changing the magnitude and cycle time of the PRBS signal could improve matters. Of particular interest are the effects of the thrusters' response time; if the PRBS cycle time is too fast, it is possible the thrusters will attenuate the signal excessively.

It would be interesting to determine if SI techniques could be used to derive simple models for umbilical disturbance forces. This would be very useful for real time applications, such as simulators, but the difficulty is discovering which state variables characterise the cable's dynamics.

Finally, there are some doubts about the results obtained in

chapter 6 with the Recursive Prediction Error SI method. Although the explanation for its barely adequate performance is plausible, it is unusual that it was so much worse than LS or ELS. It is possible that the modifications to the algorithm which allowed it to produce multivariable ARMAX models are incorrect. Ljung and Soderstrom [55] present a state-space form of the algorithm which might be more appropriate.

The theoretical work on ROV autopilots could benefit from studies of four different areas. The first idea is to take a step back from the multivariable fixed-gain that was described in chapters 4 and 5. It is known approximately how each thruster affects the vehicle's motions e.g. the two main thrusters acting differentially will cause the vehicle to yaw. There is potential for designing the closed-loop system as a series of single-input/single-output loops combined with a simple thruster allocation matrix. Output feedback would hopefully reduce errors introduced by ignoring any interaction.

Section 4.2 described the supervisory control system that would guide the ROV. Only the lowest level of this hierarchical scheme, the local velocity autopilot, was studied in depth in this thesis. The design of the global position controller would be reasonably straightforward but the task controller might possibly require artificial intelligence capabilities in order to cope with the uncertainties of the ocean environment. An example of this would be the inclusion of an oil rig geometry model in the autopilot. Another area which requires attention is dealing with ROVs which have more thrusters than controllable outputs. The difficulty then is allocating the demands to each thruster subject to the constraints that the power to each individual unit as well as the total power is limited. In the present study, thruster saturation was avoided by detuning the autopilots and limiting the reference velocities' magnitudes.

Support has been secured for a study of H_∞ controller design methods as applied to ROV autopilots. This seems an ideal application for these robust techniques which were derived specifically to cope with model uncertainties.

Appendix A

ARE Haslar Trials

[Note: This appendix is based extensively on a report that was written by M.S. Greenshields, D.R. Broome and K.R. Goheen which summarised tests carried out at ARE Haslar between 12 and 23 May, 1986.]

A.1) Introduction

These tests form part of a collaborative programme of work by the Automatic Control Group of the Department of Mechanical Engineering, UCL and JH Division of ARE Southwell to provide an overall system design capability for mine countermeasure ROVs. The tests were conducted using a UMEL Seapup ROV in the manoeuvring tank at ARE Haslar.

The objectives of the tests were:

i) To run the Seapup under full computer control.

ii) To validate K.R. Goheen's version of the NMI dynamic simulation of Seapup and NMI's published data on its performance with measurements from ARE Southwell's vehicle.

iii) To collect vehicle motion time history data for offline System Identification of the vehicle's dynamics.

iv) To operate the vehicle under Autopilot control using different closed-loop decoupling controllers.

This short report describes the tests and includes some preliminary analysis of the data.

A.2) Equipment

The Seapup ROV used for the tests was standard except for the mounting of an additional cylindrical instrumentation pack within the vehicle frame, below the drive motor. The instrumentation pack was supplied by AUWE and is normally used to measure the motions of a 1/5 scale torpedo model during its launching phase. The watertight pack contained three mutually perpendicular pairs of accelerometers and rate gyros and the small number of electronic components necessary to drive them.

Signals from the pack were sent to a distribution box at the surface via a thin cable fixed to the main vehicle umbilical, through which power and communications are carried. Conditioning of the signals was carried out by a 6 channel buffer amplifier/anti-aliasing filter unit and secondary four pole Butterworth adjustable turnover frequency anti-aliasing filter unit. A Data Translation 16 channel 12 bit A/D unit converted these signals, together with the four joystick output voltages, into digital form.

A modified joystick connection harness was used, which allowed switching between normal manual control and computer control. In the computer control mode the joystick position was read by the computer and a separate set of control voltages, produced by a DADIO D/A unit in the computer, was sent to the ROV control console, in place of that from the joystick. This arrangement and a thruster demand scrambling and unscrambling routine in the software allowed the inputs from the joystick to be added to individual thruster demands generated by the programme. Thus, in the event of the vehicle getting too close to fixed objects during the tests, the operator could override manually.

The computer used to process the acceleration data and run the controller algorithms was an IBM PC/AT. Acceleration, velocity and position data were logged to files on the 20 Mb internal hard disc as this minimised the time overhead. Subsequently, files were copied to floppy discs for transfer to a PDP 11 minicomputer for analysis and plotting.

A Hewlett Packard spectrum analyser was used to examine the frequency spectra of the instrumentation channels and identify noise or flexible body vibration components which were expected to affect the signals.

A.3) Measurements

Before any tests were performed with the vehicle, it was necessary to carry out an initial calibration of the instrumentation. This was done with the instrumentation pack free from the vehicle so that it could be put in various orientations to calibrate the accelerometers against gravity. The rate gyros were zeroed while held stationary. The figures obtained from these procedures gave the A/D levels for zero inputs and, in the case of the accelerometers, the readings for $\pm$ 1g. These figures were used in the data conversion routines in the programme.

The instrumentation channels were then tested with the spectrum analyser; the noise and flexible body vibration amplitudes with the thruster drive motor running were found to be acceptably low. The flexible body vibrations were mainly at the third harmonic of the thruster rotational frequency (28 Hz) and increased with blade pitch, showing them to be due to thruster blade interference.

The first run, a 6 D.O.F. closed-loop velocity controller test, caused unstable vehicle motions and gave very large recorded linear velocities and displacements, which were visibly not occurring. The recorded linear velocities increased in a monotonic fashion with time on each run, causing the controller outputs to saturate. The vehicle rotational motion records were plausible and matched visual observations.

Closed-loop control of yaw motion only was achieved by setting the surge, sway and heave errors to zero artificially. A square wave yaw velocity demand was used and good angular velocity data obtained from several runs. The results of one of these tests are shown in figure A.1.

The incorrect linear velocity logs could have been due to three factors, which were addressed separately:

i) The ranges of the accelerometers were not well matched to the range of actual vehicle accelerations. The sway and heave accelerometers had a range of $\pm$ 4g and the surge accelerometer a range of $\pm$ 40g. The estimated maximum accelerations occurring in these directions were a little over 1g in heave and about 0.75g in sway and surge. A method was found to alter selectively the A/D gains on different channels and was used to minimise this source of error.

ii) Drift of the instrumentation and/or data acquisition equipment zeros was found to be altering the accelerations read from one run to the next while the vehicle was stationary. To remedy this several iterative self-calibration procedures were devised and tried during the tests. One method successfully found the zero levels at the beginning of each run.

iii) The data logging programme assumed a completely level vehicle orientation at the start of the test run. This was not the case in practice, as the instrumentation pack was not guaranteed to be mounted exactly flat in the vehicle and the vehicle did not sit flat on the bottom of the tank before the test runs. Three wooden blocks were fixed to the skids under the vehicle to ensure a non-rocking stance on the bottom and the vehicle held there by a mild positive thruster heave input during calibration. The starting vehicle angular position was then evaluated before each run by reading the accelerometers and using the component of gravity present on each. However, there may have been difficulties in tracking the vehicle's orientation with sufficient accuracy during the test run. This was attempted by integrating angular rates and should have been held within 0.01 degrees of the true values if linear velocities were not to be too adversely affected. For example, a roll angle error of 0.1 degrees would cause a sway velocity error of 0.17 m/s after 10 seconds.

While these problems were being addressed, the ROV was put through simpler gross performance tests. The maximum heave and yaw velocities were measured by timing the appropriate manoeuvers. Signals from the

rate gyros were processed by the spectrum analyser to yield the roll and pitch natural frequencies.

The maximum velocity in heave was recorded as 0.233 m/s up. This was the mean value of six trials. The average of four yaw rate tests in each direction yielded a maximum value of 53.0 degrees/s to starboard and 51.7 degrees/s to port. This compares favourably with the yaw rates measured with the instrument package, 53.3 degrees/s to starboard and 50.0 degrees/s to port.

As derived by the spectrum analyser, the roll and pitch natural frequencies, 2.6892 rad/s and 1.5080 rad/s, agreed closely with the behaviour predicted by the simulation programme though damping values were substantially different. Simulation yielded a roll eigenvalue of $-0.18508 \pm 2.5638i$ rad/s. The time domain autonomous roll test, as shown in figure A.2, indicated that this eigenvalue should be $-0.38100 \pm 2.5130i$ rad/s. The simulation of pitch motion had a eigenvalue of $-0.16659 \pm 1.4632i$ rad/s, as compared with $-0.33010 \pm 1.3960i$ rad/s derived from the time domain data shown in figure A.3.

The linear velocity problem was not completely solved by any of the measures used and it was decided to concentrate further efforts on carrying out tests for which comparisons of angular data were available in NMI publications [20, 21]. These were:

1) Response to full surge input.
2) Response to full surge and full negative heave input ('climb').
3) Response to full yaw input ('Zero radius turn').
4) Response to full sway input.
5) Response to full surge and full yaw input ('High speed turn').

Comparisons between the performance figures measured here and those observed by NMI during their trials are given in table A.1; also shown are the values predicted by the UCL simulation. It is possible that some of the discrepancies between the two sets of measurements can be explained by the differences in trim condition of the two vehicles. Additionally, NMI did not give details of many of the tests they performed and hence there may have been differences in experimental conditions.

Six D.O.F. random excitation tests were also carried out, where uncorrelated PRBSs were sent to all thrusters simultaneously to excite all modes of vehicle motion. The linear data from these were no more reliable than from the other tests but it was felt that some system identification might later be possible.

A.4) Conclusions

The complete lack of mechanical or electrical problems during the tests, the consistent control of the vehicle, and the performance of the interfaces in acquiring good signals all demonstrate the suitability and reliability of the combination of equipment used, with the obvious exception of the sensors themselves. The accelerometers were particularly troublesome, though many of the difficulties which occurred when deriving linear velocities were caused by inaccurate angular measurements. The vehicle itself was completely reliable throughout, despite spending most of each day submerged.

Automatic control of the vehicle was thus demonstrated to be completely practicable if suitable sensors could be used to provide the velocity information required by the controller.

Good measurements of vehicle manoeuvring capabilities were obtained, which correlated well with NMI's results, as did the vehicle's natural frequencies in pitch and yaw. These results help to validate the dynamic simulation of the Seapup.

This test programme has demonstrated that a very good experimental system has been established; more detailed discussion between UCL and ARE will be necessary to define an adequate sensor fit. This will probably be base on a fully inertial gyro and accelerometer platform,as used in aerospace IN systems, rather than the 'strap down' system employed for these tests. Direct measurement of linear velocity and position should also be included eg. by doppler logs and USB acoustics.

Another test programme using upgraded sensors should be planned for late 1986, both to provide reliable data for complete multivariable SI, and to attempt full closed-loop control.

Table A.1: Seapup Performance Figures

a) National Maritime Institute Trials

b) ARE Haslar Trials

c) NMI/UCL Model Simulation

Test	a) NMI Trials	b) Haslar Trials	c) Simulation
1) Maximum pitch angle in a climb (degrees)	48	+ 32.9	35.4
2) Maximum rate of turn with zero ahead speed (degrees/sec)	57.2	+ 53.3 - 50.0	45.0
3) Maximum roll angle in zero radius turn (degrees)	14	- 6.2 + 3.6	4.2
4) Maximum pitch rate in zero radius turn (degrees/sec)	28	+ 9.8 + 9.4	9.4
5) Maximum rate of turn in full-speed, non-banked turn (degrees/sec)	27	- 31.0	25.9
6) Maximum pitch angle during impulsive start (degrees)	22	+ 22.7	32.5
7) Maximum pitch rate during impulsive start (degrees/sec)	18	+ 11.4	23.2
8) Maximum roll angle during pure lateral translation (degrees)	15	+ 11.0 - 11.2	24.8
9) Maximum roll rate during pure lateral translation (degrees/sec)	7.5	+ 8.5 - 11.6	32.7

Note: When two values have been reported, they correspond to a pair of trials which examined the asymmetric modes of the vehicle.

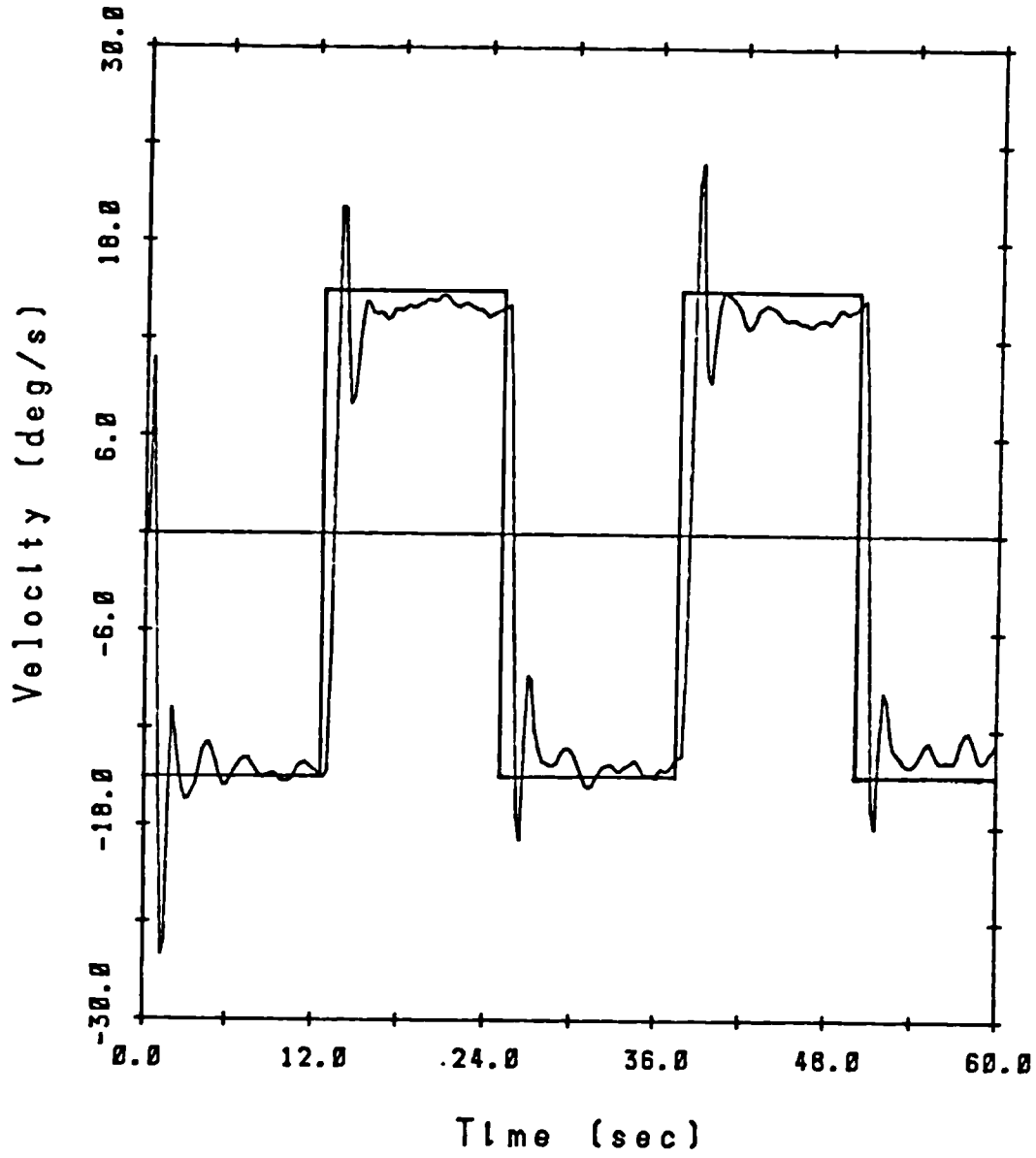

Figure A.1 : ARE Haslar Trials; Closed-Loop Yaw Response

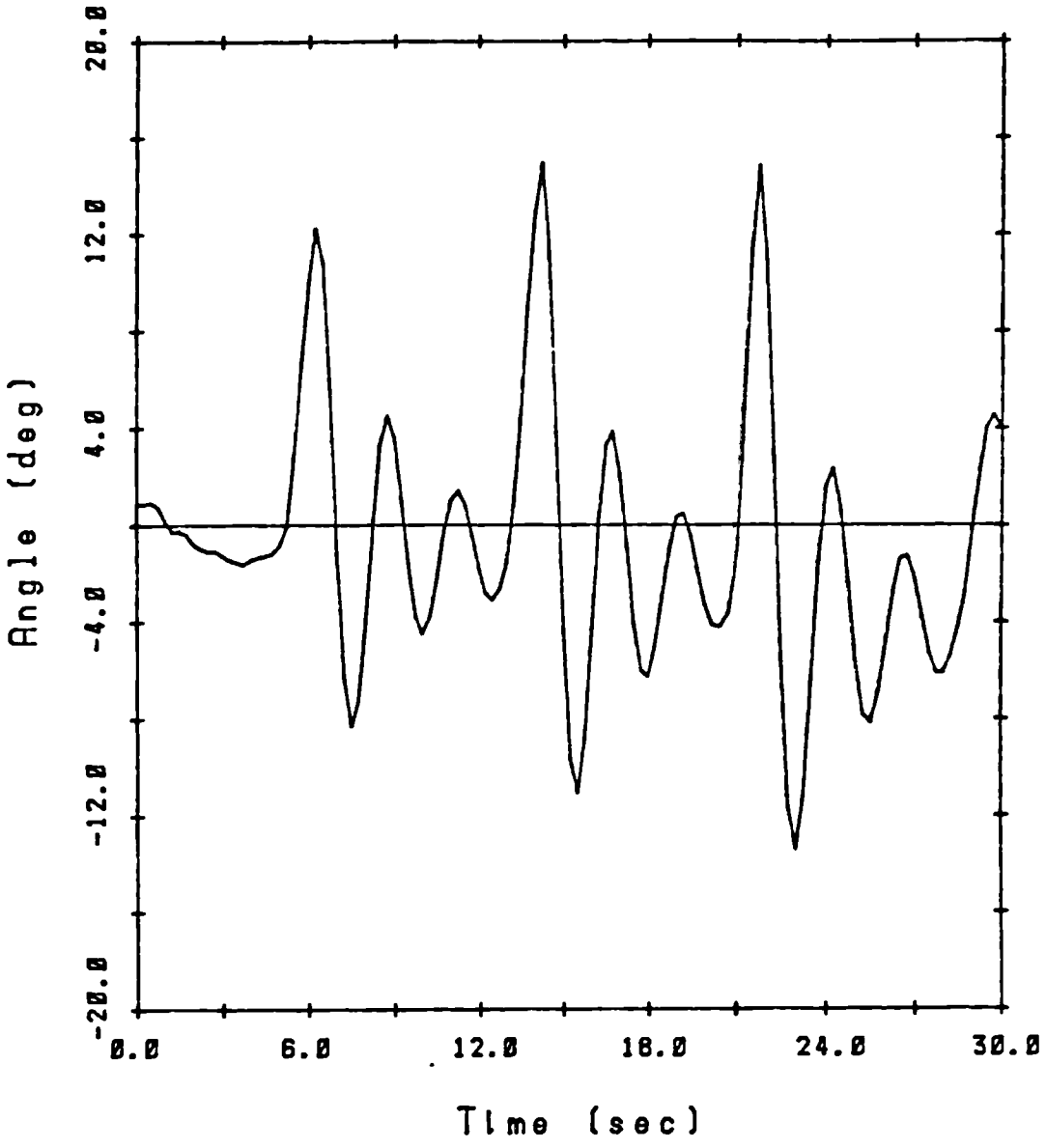

Figure A.2 : ARE Haslar Trials; Autonomous Roll Test

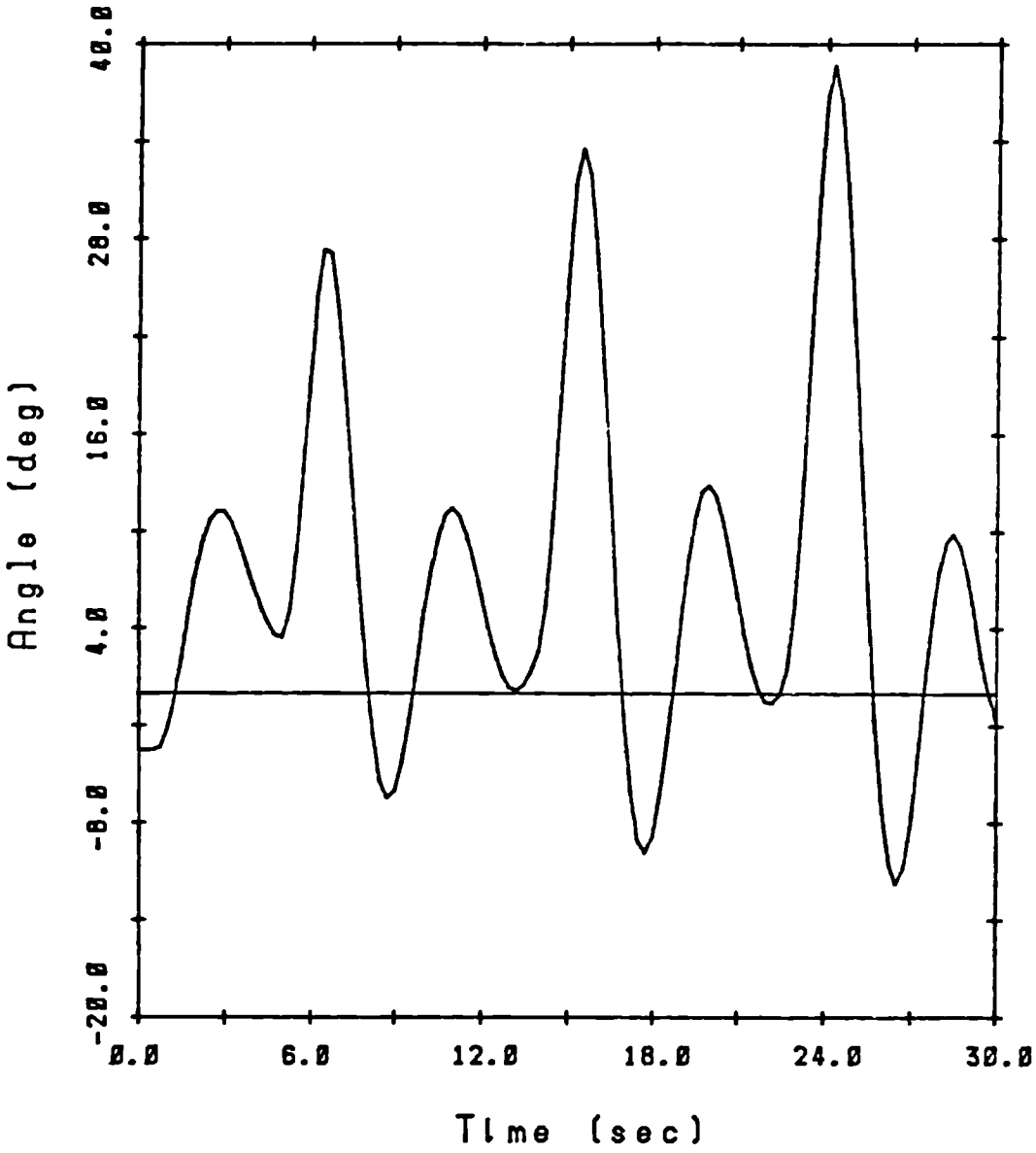

Figure A.3 : ARE Haslar Trials; Autonomous Pitch Test

Appendix B.1

Underwater Vehicle Controller Design by Self-Test Algorithm

Mr. K R Goheen
Research Student
Dept of Mechanical Engineering
University College London
Torrington Place
London, WC1 7JE

Dr E R Jefferys
Lecturer
Dept of Mechanical Engineering
University College London
Torrington Place
London WC1 7JE

Remotely operated vehicles (ROVs) are unmanned underwater craft in widespread use in the offshore oil industry. They can be used for observation only or they can be equipped with manipulator arms and a variety of tools to assist or replace a diver.

Thruster units, often manually controlled, manoeuvre the vehicle. In strong currents, taking up and holding station can be time consuming and exhausting as the operator must continuously adjust thruster levels. Underwater operations are expensive and there is a great incentive to reduce operation time. A recent study showed that during a trial series of typical tasks, taking up and holding station took up to 35% of the total time (1).

An automatic control system is not easy to design; ROVs are multivariable, interacting dynamic systems containing nonlinearities due to rigid-body coupling, hydrodynamic forces on the vehicle and its umbilical and advance coefficient and momentum drag effects in the thrusters. The dynamics can also be time-varying as manipulator position and load can radically change the kinematics and hydrodynamics of the vehicle.

A good model of the ROV and its thrusters, is needed for the design of a decoupling controller. However, expensive specialised laboratory facilities are needed to identify the vehicle and thruster characteristics. The model may be affected by experimental errors so the control engineer must verify that it is sufficiently accurate for design purposes.

Initially, an adaptive control system appeared ideal; it would be unaffected by inaccuracies in any model since it would identify the plant parameters on-line. Adaptive control works for nonlinear plants since they are represented by the "best" instantaneous linear model. The dynamics of the plant must not change too quickly if the controller is to adapt as fast as the plant is evolving. However, since the eigenvalues of a ROV are strong functions of its speed, adaptive control has been rejected in favour of an unique robust controller.

Owens and Chotai have developed a simple scheme for the design of robust controllers for unknown multivariable systems (2). The time constant and steady-state gain of each output in response to steps at each input is measured. A decoupling proportional plus integral control law is calculated after the designer has specified the desired closed-loop poles. There are minimal restrictions on the plant; it must be minimum-phase to guarantee stability for large controller gains.

This is the basis of the "self-test" ROV controller. Before operations begin, the ROV

PROCEEDINGS OF THE TENTH CANADIAN CONGRESS OF APPLIED MECHANICS • COMPTES RENDUS DU DIXIEME CONGRES CANADIEN DE MECHANIQUE APPLIQUEE • THE UNIVERSITY OF WESTERN ONTARIO LONDON JUNE 2 JUNE 7 • 2 JUIN 7 JUIN 1985

is manually piloted away from the support ship. The test is executed under computer control. Each thruster is given a step input and the response is monitored by onboard sensors. The control law is calculated from the step responses and the ROV can then be piloted via the velocity controller.

Owens' method has been modified to include gain scheduling for this application. The self-test algorithm calculates a controller at zero-speed, which then brings the vehicle up to a steady forward speed and the test is repeated. This can be done at a range of speeds and the gains expressed as polynomial functions; during operation speed can be monitored and the gains adjusted accordingly.

The self-test method has many advantages. It eliminates expensive hydrodynamic testing and model verification, can easily be adapted to any ROV system and is "adaptive"; when control is degraded by effects such as thruster or umbilical fouling, the self-test can be repeated for the "new" vehicle.

Most of the software for computer simulation of the ROV has now been developed. The equations of motion for an ROV with variable pitch propellers have been subjected to extensive verification. The self-test and velocity controller algorithms have been developed. As figure 1 shows, the velocity controller performs well, displaying fast rise times, small steady state errors and little interaction despite the system nonlinearities.

The controller will be the basis of a hierarchial scheme with a range of task controllers (hovering, following the seabed, moving to a point) at the level next to the operator. The task controller will generate a series of reference signals for a position controller which will ask the velocity controller to calculate the thruster levels.

Methods of obtaining accurate linear position and velocity values will be addressed next. An instrumentation fit will be designed for an existing vehicle, and the controller will be used to demonstrate the improved efficiency of ROV operations.

REFERENCES

1. "Underwater Vehicle Trials, Loche Linnhe 1981/1982", OTP 14, Department of Energy, Offshore Technology Paper.

2. Owens D.H. and Chotai A. "Simple models for robust control of unknown or badly defined multivariable systems" ch.10 Self-tuning and Adaptive Control: Theory and Applications, Harris C.J. and Billings S.A., ed.

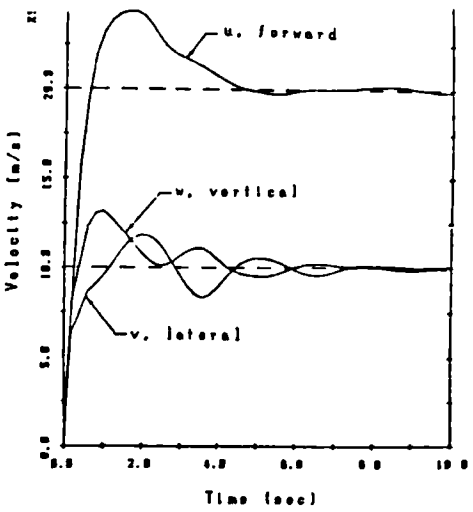

Fig.1 Vehicle response to step change in velocities

Appendix B.2

ROBUST SELF-DESIGNING CONTROLLERS FOR UNDERWATER VEHICLES

K R Goheen E R Jefferys and D R Broome
Department of Mechanical Engineering
University College London
Torrington Place London U K

Abstract

Conventional multivariable and adaptive controllers are hard to design for Remotely Operated Underwater Vehicles (ROVs) because their dynamics are strongly coupled, highly nonlinear and vary according to the vessel's operating configuration. An alternative design procedure which combines some of the ideas of adaptive and robust control is based on a "self-test" which the vehicle can be programmed to execute autonomously. The resulting controller is evaluated by examining its closed-loop poles, responses to step changes in reference inputs and rejection of disturbances caused by turbulence.

1. Introduction

Although remotely operated vehicles (ROVs) have been in widespread use in offshore work for a number of years, the navigational control systems which they employ have many shortcomings. Most ROVs use a human operator in the position control loop. After establishing the position of the vehicle, the operator sets the thruster levels so that the vessel moves towards the desired position and attitude. In strong currents, taking up and holding station relative to the worksite can be very time consuming and mentally exhausting for the operator as he must continuously manipulate thruster levels in order to counteract the turbulence often found around subsea structures. A recent study indicated that during a trial series of typical activities (pipe cutting, plate cleaning, etc), taking up and holding station took up to 35 percent (20 minutes) of the total time required to complete the job [1]. ROVs are expensive to buy and operate so there is a strong incentive to reduce such unproductive time.

A conventional controller is hard to design for a ROV since the linearised equations of motion vary strongly with speed and the relevant coefficients are difficult to determine experimentally. Additionally, the vessel dynamics can be changed significantly by the addition of extra items of equipment. This paper presents a self-test technique which generates a simple vehicle model which is then used in the design of an unique robust decoupling multivariable controller.

The performance of the closed-loop system can be evaluated in the frequency or time domains. A comparison between the achieved closed-loop poles and those specified in the control law provides a non robust measure of the success of the controller design exercise. A simulation of a complex non linear model of the controlled vehicle generates a variety of step responses which demonstrate the transient and steady-state performance, the disturbance rejection properties, the robustness to physical configuration changes and the effect of controller sampling rate. Finally, future work is outlined and conclusions are drawn.

2. Equations of Motion

The equations of motion of a ROV have many similarities with the more familiar models of aircraft or conventional submarines though there are important differences. Aircraft and submarines usually have one axis along which the operating velocity is much greater than the other two and the nonlinear dynamics are conveniently linearised about this condition. ROVs may have comparable velocities along all three axes and this kind of linearisation is not achievable. The factor which sets submarines and ROVs apart from aircraft is the nature of the forces arising from the interaction between the water and the vehicle.

Much of this following development is based upon Lewis, et al [2] but differs significantly in the treatment of the added mass. Figure 1 shows a typical ROV and the axis set which is used to describe it. The equations which describe motion in three local coordinate axes are

$$[\bar{M}]\,[\dot{Q}] = f_d(u, v, w, p, q, r) + \bar{R}(u_r, v_r, w_r, p, q, r) + G(\phi, \theta, \psi) + U + T \qquad (1)$$

Proc. Offshore Mechanics and Arctic Engineering Conference. Tokyo, 1986

where
$\hat{M}$ = mass matrix including hydrodynamic added mass
Q = (u v w p q r)^T
$\hat{F}_d$ = vector of rigid body kinematic forces
$\hat{H}$ = vector of hydrodynamic forces
G = vector of hydrostatic forces
U = vector of forces due to umbilical cable
T = vector of forces due to thrusters

The best way to understand these equations is to first consider an alternative formulation.

$$[M]\ [\dot{Q}] = F_d + \Sigma \text{ (all external forces)} \qquad (2$$

In these equations, [M] does not contain added mass terms. Along with the terms in F_d, it forms the standard equations of motion for any rigid body. These equations are developed in [3].

The summation term represents four external forces:

$$\Sigma \text{ (all external forces)} = \hat{H}\,(u_r, v_r, w_r, p, q, r, \dot{u}_r, \dot{v}_r, \dot{w}_r, \dot{p}, \dot{q}, \dot{r}) + G\,(\phi, \theta, \psi) + U + T \qquad (3)$$

These four terms may be considered in turn.

i) All the forces and moments caused by the relative motion between the water and the vehicle are included in the H term. The standard procedure is to express each force or moment as a function of the relative motion in terms of hydrodynamic derivatives. For example, the fluid moment about the yaw axis caused by acceleration in the x direction is expressed as $N_{\dot{u}}\dot{u}$, where $N_{\dot{u}} = \delta N / \delta \dot{u}$. These hydrodynamic derivatives are derived experimentally and usually lead to very complicated expressions. In this paper, the equations of motion [4] for UMEL's Seapup ROV have been used. A typical term illustrates the complexity:

$$X = 1/2\ \rho L_c^2 U_o^2 [\, X_{|U|U'} + X_{\dot{U}|U|}\dot{U}|U'| + X_{\dot{V}V}\dot{V}V' + X_{\dot{W}|W|}\dot{W}|W'| + X_{\dot{W}W}\dot{W}W' + X_{\beta sgn(\pi-\beta)}|U'| + X_{\dot{r}U}\dot{r}U + X_{\dot{r}r}\dot{r}^2/U' + X_{qq}q^2 + X_{\dot{w}wq}\dot{w}^2\dot{q}/U' + X_{\dot{p}v}\dot{p}v + X_{\dot{p}pv}\dot{p}^2v/U' + X_{pq}pq + X_{rq}rq \,] + X_{\dot{u}}\dot{u} + X_{\dot{r}}\dot{r} \qquad (4)$$

where L_c is a characteristic length, U_o is a reference velocity, ρ is the density of sea water and

$$U' = (u^2 + v^2 + w^2)\ /\ U_o \qquad (5)$$

A prime denotes non-dimensionalisation with respect to the reference velocity, U_o, which is usually the ahead speed of the vehicle. Where the forward speed is near to zero or of the same order as the other translational velocities, a typical operating condition for a ROV, this model is of doubtful validity.

All of these velocities and accelerations are in terms of the relative motion between vehicle and fluid. In this study, it is assumed that the fluid accelerations and angular velocities are negligible which leaves only u, v and w as relative quantities. The last two terms in (4) involve accelerations and it is necessary to include these on the left hand side of (2) in order to solve for these accelerations. With these changes to (2), the equations of motion are now in the form of (1), with hydrodynamic effects included in the mass matrix.

ii) The forces and moments caused by the G term depend upon the values of weight and buoyancy, the positions of the centre of mass and buoyancy and the attitude of the vehicle, defined by its Euler angles, roll (ϕ), pitch (θ) and yaw (ψ).

iii) The umbilical cable, while allowing for the essentially unlimited duration of ROV operations, paradoxically can be the greatest limitation on vehicle performance. The drag, U, produced by the cable depends on its length and thickness, factors involving the cable's surface and the shape it takes up between ROV and support ship. This force has both a steady state and time-varying component. A review of umbilical cable dynamics is given by Dand and Every [5].

iv) Thrusters are strongly nonlinear actuators. They can be either fixed speed, variable pitch or fixed pitch, variable speed. The axial thrust, T, produced is dependent on blade pitch angle, angular speed and inflow conditions, the latter two which are combined in the advance coefficient:

$$J_o = V / nD \qquad (6)$$

where V is the axial speed of the thruster, n is the shaft angular speed and D is the propeller diameter.

For a fixed speed propeller, a typical relationship between thrust, advance coefficient and blade pitch angle is shown in figure 2. This situation is further complicated by the fact that the forces produced by the thruster can have components normal to the axis of the shaft because of momentum drag effects [6].

This section is concluded by noting that equation (1) is given in terms of the rates of change of body-fixed coordinates. In order to carry out a numerical solution of ROV motion it is necessary to change these into rates of change of global coordinates.

3. Controller Structural Philosophy

The control of a ROV is conveniently implemented as a type of hierarchical scheme known as supervisory control [7], higher level controllers direct the action of subordinates by planning the actions they should take, monitoring their performance and trusting them to accomplish the task without continuous assistance. Employed in such devices as deep space probes and manipulator arms, supervisory control may also be applied advantageously to ROVs to achieve faster or better control, to control more degrees of freedom simultaneously than the operator could manage directly and to relieve the operator of tedium.

A hierarchical scheme is attractive because it separates the control problem into a number of levels, each much easier to design and analyse on an individual basis. This division is based on separation of time constants; each level is typified by significantly faster dynamics than the one above it.

The control system for the ROV autopilot will have three levels. A series of task controllers will be next to the operator. He will choose to execute such functions as hovering, following the seabed at a set height and heading or moving to a point. The task controller will generate a series of reference signals for a global position controller which will ask the body-coordinate velocity controller to calculate the

thruster levels.

The design of the higher level controllers becomes manageable if it can be assumed that the vehicle it "sees" has decoupled, well-behaved dynamics. At the lowest level, local velocity, this quality requires the installation of a multivariable controller which either wholly or partially compensates for the coupling and nonlinearities of the vehicle. The closed loop poles of the velocity controller are assigned by the designer according to the vehicle inertia and thruster power. In normal operation, the thrusters must not saturate 'too' often. This assignment then constrains the poles of the higher level position control system.

The rest of this work is concerned with the design of a velocity controller which will manipulate the thrusters to achieve specified translational and yaw angular velocities. A suitable navigation system is assumed. the measurement, filtering and validation of sensor signals involves many issues which cannot be addressed in a brief paper.

4. Velocity Controller Design

The design of a multivariable controller to achieve the decoupled, well-behaved dynamics governing local velocities is a relatively straightforward procedure if a reliable model of the open-loop system is available and if the system is nearly linear. Output or state feedback compensators can be designed and analysed by using various methods, such as Postlethwaite and MacFarlane's multivariable root locus, Rosenbrock's Inverse Nyquist Array or the optimal control techniques [8]. If the system is nonlinear, these linear design methods can be used at a variety of operating points and the gains in the compensators scheduled to change with components of the system state, such as forward speed.

Most of these techniques require a fairly accurate plant model since they are not guaranteed robust with respect to parameter variation and non linearity. Expensive, specialised laboratory facilities and personnel are needed to identify the vehicle and thruster characteristics. The model may be affected by experimental errors so the control engineer must verify that it is sufficiently accurate for design purposes. These activities will add a large amount to the cost of a new or reconfigured ROV.

However, not all of the dynamics affecting the system can be identified prior to the controller design. Operators of ROVs tend to add and remove pieces of equipment such as arms and cameras as the job requires, which can radically alter the dynamics of the vehicle and perhaps make the controller worthless. These unpredictable changes must be dealt with by other techniques which do not involve skilled control engineers in the day to day operation of the vehicle.

One such method is adaptive control which at first sight seems ideal. It would be unaffected by inaccuracies in any model since it would identify the plant parameters on-line. Adaptive control can work for nonlinear plants since they are represented by the "best' instantaneous linear model. However, the dynamics of the plant must not change too quickly if the controller is to adapt as fast as the plant is evolving. Since the eigenvalues which arise from linearised versions of equation (1) are strong functions of the ROV's forward speed, conventional adaptive control methods need substantial modification.

The second method of control system design that can be used when a reliable plant model is not available is one of the robust techniques. A robust control system has fixed gains an maintains acceptable performance when the parameters characterising the plant change within certain bounds. Though a totally accurate model is not required if a robust controller is to be implemented, a nominal model is needed and even robust techniques may not be able to cope with the large changes in the dynamics caused by a configuration change.

Ideally, what is required is a control method which could be developed once and then applied with minimal modifications and expense to any ROV. Such a method should combine the ideas of robust and adaptive control in that it would automatically adapt a fixed gain controller to any ROV and the design of this controller would be immune to changes in the dynamics of that particular vehicle.

5. Robust Control Based on Approximate Models

Owens and Chotai have developed a proportional plus integral (PI) controller based on a low order representation of processes which are very complex or whose models are uncertain [9]. All of the unknown or complicated dynamics is modelled by the multivariable equivalent of the first order lag. This is useful in circumstances where quantitative information is not available but some structural information is, say, from the underlying physical laws. In the case of the ROV, it is known that the velocity degrees of freedom u, v, w and r will behave approximately like first order systems because there is no position restoring force.

The intuitive ideas of this method are best illustrated using the single-input / single-output (SISO) example, shown in figure 3. To avoid confusion between naval architecture and control theory notation which use the same conventional symbols for different variables, all generalised control variables are denoted by capital letters.

A forward loop controller k(s) is to be designed for a real unknown plant G s) with unity negative feedback and the only quantitative information available is the system response Y(t) to a unit step input. The real plant's transfer function can be approximated by a first order lag

$$G(s) = a / (1 + sJ) \qquad (7)$$

where a and J are constructed from the real response Y t as shown in figure 4 along with the response of the approximating system.

A PI controller:

$$K s) = \frac{pJ}{a}\left(1 + \frac{1}{sT}\right) \qquad (8)$$

can be put in the forward path and p and T adjusted so that the desired closed-loop characteristics are obtained. In order to make a prediction about the stability of the real feedback system it is necessary to assume that G s) is minimum phase, which will lead to a root locus of the closed-loop system with one first order asymptote at high gains with the other loci approaching the open-loop zeros figure 5).

This technique can be generalised to the square m x m multi-input / multi-output (MIMO) case by defining the discrete multivariable first order lag (MFOL).

$$G_A^{-1}(z) = (z - 1)\,B_0 + B_1 \quad , \quad |B_0| \neq 0 \qquad (9)$$

The two term controller for this system is:

$$K(z) = B_0^{-1}\,\mathrm{diag}\{(1 - k_j c_j)/(1 - k_j)(1 - c_j)\,z/(z - 1)\}\;B_1 \qquad (10)$$

$$1 \leq j \leq m$$

where m is the number of inputs and outputs.

The closed-loop transfer function is.

$$H_C(z) = I_m + G(z)K(z)^{-1}\,G(z)K(z) \qquad (11)$$

Owens shows that the condition $B_0^{-1}B_1 \neq 0$ can always be achieved for fast sampling rates [10]. For this condition, combining equations 9,10 and 11 yields, after much heavy algebra.

$$H_C(z) = \mathrm{diag}\{(z(2 - k_j - c_j) - (1 - k_j c_j))\,/\,((z - k_j)(z - c_j))\} \qquad (12)$$

$$\text{therefore} \quad H_C(1) = I_m \qquad (13)$$

This indicates that for $B_0^{-1}B_1 = 0$, the jth loop's behaviour will be defined by the choice of the poles k_j and c_j. In addition, the system will have low levels of interaction and (11) shows that reference signals will be tracked with zero steady-state error.

There remains the problem of estimating B_0^{-1} and B_1^{-1}. These matrices can be derived from m open-loop step tests, with input vectors $\underline{U}_1 \ldots \underline{U}_m$ chosen to span the m-dimensional input space. Two pieces of output data are collected from the jth test: the vector of responses at the first sampling period, $\underline{Y}_j^1$ and the vector of steady-state values, $\underline{Y}_j^\infty$. The required model becomes.

$$B_0^{-1} = [\,\underline{Y}_1^1 \;\ldots\; \underline{Y}_m^1][\,\underline{U}_1 \ldots \underline{U}_m]^{-1} \qquad (14)$$

$$B_1^{-1} = [\,\underline{Y}_1^\infty \ldots \underline{Y}_m^\infty][\,\underline{U}_1 \ldots \underline{U}_m]^{-1} \qquad (15)$$

As was the case in the SISO system , stability of the controlled MIMO linearised plant is guaranteed under this scheme if the plant is minimum phase and of full rank and if the sampling rate is "sufficiently fast". So far, no linearised ROV model has violated the requirements.

6. The Self Test

Owens and Chotai's method is now applied to the design of a control system for a ROV. The Seapup has four independently controllable thrusters, so only surge, sway, heave and yaw velocities can be manipulated. Fortunately, roll and pitch are buoyancy stabilised and can be left to regulate themselves.

The self test, which identifies B_0 and B_1 (equations 14,15 ,is executed autonomously under computer control. A batch method identifies the 16 first order transfer functions relating the four inputs to the four outputs. Batch least squares, effectively a smoothing method, was compared to other filtering techniques and found to be much more robust with respect to measurement noise, a major problem in ROV applications.

Before operations begin, the ROV is manually piloted away from the support ship Each thruster in turn is given a step input and the response is monitored by the onboard sensors and logged. The inputs are chosen to be scalar multiples of the unit vectors and so excites a separate column of the matrix of transfer functions; hence each experiment can be analysed separately to yield a channel gain and time constant. When each test is completed, the vehicle is allowed to return to quiescence before the start of the next. At the end of a whole series of tests, the time constants and steady-state gains for each input-output channel, as well as the values of the input which produce zero output, have been calculated. The control law is then calculated from equation 10 and the ROV can then be piloted via the velocity controller

Though this technique is robust with respect to changes in the open-loop plant, it has been modified to include velocity scheduling in this application in an effort to improve step response and pole placement further. After the self-test algorithm has calculated a controller at zero speed, it can bring the vehicle up to a steady forward velocity and repeat the test about this operating point. This can be done at a range of speeds and the gains expressed as polynomial functions, during operation speed can be monitored and the gains adjusted accordingly.

The self-test was evaluated by comparing the time constants and gains it chose during a simulation to those that a human observer of the velocity log would select. The results agreed very closely. The test took 180 seconds and needed a space of sea 33.4 m by 33.0 m in area and 12.0 m deep.

7. System Evaluation

7.1 Eigenvalue Analysis

The stability of a linear system is characterised by its eigenvalues. The ROV system consists of a digital controller, a continuous time, nonlinear plant and a unity negative feedback loop, along with D A and A D converters to interface the digital and analogue components. The converters can be modelled in continuous time by zero order holds (ZOHs) whose Laplace transforms contain transcendental terms. Since this does not occur in the z domain , the eigenvalue analysis uses discrete transforms, after the vehicle's equations have been numerically linearised and converted to an equivalent discrete system.

It was shown in section 5 that this controller has two goals, output decoupling and the assignment of the individual loop dynamics according t the ch ice of the designer. Figure 6 shows the relationship between the desired poles and those actually achieved in the four output loops. Here, the vehicle equations were linearised about 0.0 m/s surge speed. The oscillatory roll and pitch mode eigenvalues are also depicted. Despite the modelling approximations, it is clear that the errors in pole placement are quite small. While the pole positions are not generically robust with respect to parameter variation the nature of the design algorithm gives confidence that the closed loop performance will meet the specification.

7.2 Time Domain Simulation

The method was evaluated by simulation of a complex non linear vehicle model, controlled by the self designing controller. Typical step responses

which are characterised by rise time, settling time, overshoot, steady-state error and degree of output decoupling. The effects of sampling rates, stochastic disturbances and the robustness to physical configuration changes are noted. In all cases, the full nonlinear version of the vehicle equations are controlled.

Figure 7 illustrates the ROV's response to a step input of 0.2 m/s surge, 0.1 m s sway and 0.1 m/s heave speeds, applied to the reference channels simultaneously. A constant gain controller operating at 5 Hz has been used here. All three of these outputs are achieved with very fast rise times and zero steady-state error. The history of thruster commands indicates that it would be very difficult for a pilot to achieve this response manually.

The effect of modifications to the ROV dynamics is illustrated by the addition of a 15 kg camera to the lower edge of the bow of the 115 kg Seapup. A new mass matrix can be calculated assuming the vehicle is in an ideal fluid; the "new" vehicle has considerable differences in its open loop dynamics. Figure 8 shows the result of the same situation as was illustrated in figure 7 with the modified vehicle guided by the original controller. It is clear that response is still very good; the only noticeable difference is slightly larger rise times.

Figure 9 shows the vehicle attempting to hover in a fixed position despite a stochastic current affecting it which varies both in speed and direction. Here, the current model is a first order Gauss-Markov process with the standard deviation of the current speed set to 0.086 m/s and direction to 20 degrees . The controller was switched on only after the first 10 seconds to indicate the improved hovering performance. This same case is illustrated again in figure 10 except that now the controller is operating at 20 Hz. One advantage of the faster sampling rate is apparent; since the system effectively runs open-loop between samples, disturbances will have a greater effect at slower sampling rates and the output variables will tend to stray farther from their references as shown in figures 9 and 10.

8. Conclusions and Future Work

The self-test method of control system design was adopted because of the uncertainty and expense of conventional hydrodynamic testing methods of obtaining an ROV's transfer function. It has been shown to produce a system with minimal computational requirements that has good closed-loop performance and robustness to vehicle configuration changes. There are further advantages, it can be easily implemented in any ROV system and it is "adaptive", although not in the conventional sense; when control is degraded by effects such as thruster or umbilical fouling, the self-test can be repeated for the "new" vehicle.

There are, however, a few areas which require attention. Small limit cycles can occur under certain conditions and the present system is not suitable for roll and pitch control. Both of these problems indicate that a more sophisticated controller designed from a higher order model incorporating second order effects might be required to handle the pitch and roll.

A vehicle will soon become available for an experimental program whose overall goal is to implement and evaluate the self-test controller. Filtering techniques must be developed to combine signals from dissimilar sensors to produce timely and accurate feedback of the linear velocities . System identification methods will be applied to free-running test data in an effort to produce more accurate open-loop models for pilot training and design optimisation.

Future theoretical and practical studies will reconsider the more traditional adaptive control methods so that continuous optimisation of the vehicle performance might be achieved. The system is not continuously excited and the models might have to be scheduled with respect to the forward speed. Work will also begin on the higher levels of control described in section 3.

Acknowledgements

Kevin Goheen is supported by a Commonwealth Scholarship. The Offshore Supplies Office of the UK Department of Energy kindly gave us access to the detailed ROV model.

References

1. "Underwater Vehicle Trials, Loche Linnhe 1981/1982", OTP 14, Department of Energy, Offshore Technology Paper.

2. Lewis D.J., Lipscombe J.M. and Thomasson P.G., "The Simulation of Remotely Operated Underwater Vehicles", Proc. ROV '84, pp 245-252, The Marine Technology Society, San Diego, 1984.

3. Bishop R.E.D. and Parkinson A.G., "Choice of origin for the body axes attached to a rigid vehicle", J. Mech. Engng. Sci., 11, pp 551-555, 1969.

4. Dand I.W., "Some aspects of the hydrodynamics of remotely operated submersibles", Proc. Control 85 (to appear).

5. Dand I.W. and Every M.J., "An overview of the hydrodynamics of umbilical cables and vehicles", Proc. Subtech '83, 1983.

6. Dand I.W. and Every M.J., "Remotely-Operated Vehicle Hydrodynamics", Proc. Subtech '83, Soc. for Underwater Technology, London, 1983.

7. Ferrel W.R. and Sheridan T.B., "Supervisory Control of Remote Manipulation", IEEE Spectrum, Vol.4, No.10, October 1967, pp 81-88.

8. "Design of Modern Control Systems", Bell D.J., Cook P A and Munro N., ed., IEE Control Engineering Series, vol. 20, Peter Peregrinus Ltd., Stevenage, 198..

9. Owens D.H. and Chotai A., "Simple models for robust control of unknown or badly defined multivariable systems" ch.10 Self-tuning and Adaptive Control· Theory and Applications, ed. Harris C.J. and Billings S.A., Peter Peregrinus and the IEE, 1981.

10. Owens D.H. and Chotai A., "Robust control of unknown or large scale systems using transient data only", Research Report No. 134, Dept. Control Engineering, University of Sheffield, UK, 1980.

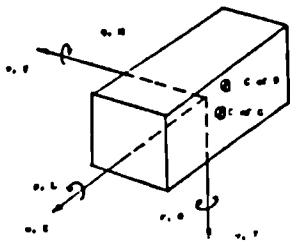

Figure 1: [illegible]

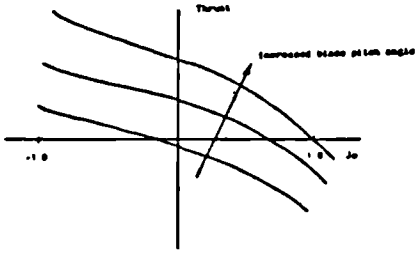

Figure 2: The relationship between axial thrust, blade pitch angle and advance coefficient for a typical thruster

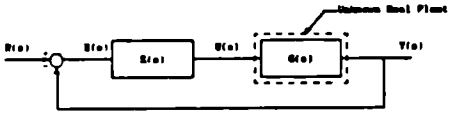

Figure 3. Real feedback system

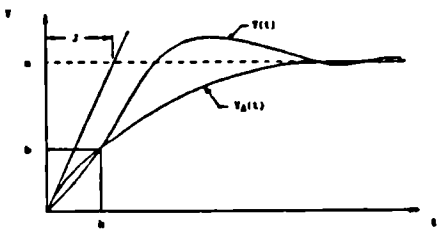

Figure 4. Construction of the approximate plant, G_R

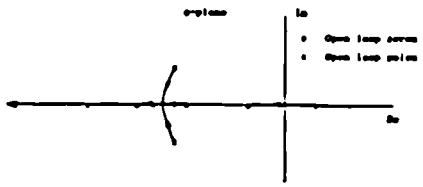

Figure 5. A representative root locus plot

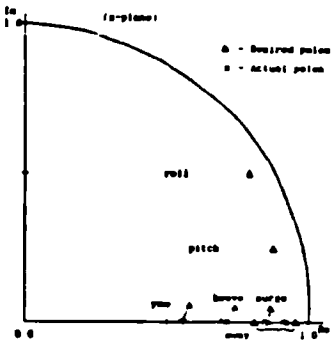

Figure 6: Actual and desired closed loop poles

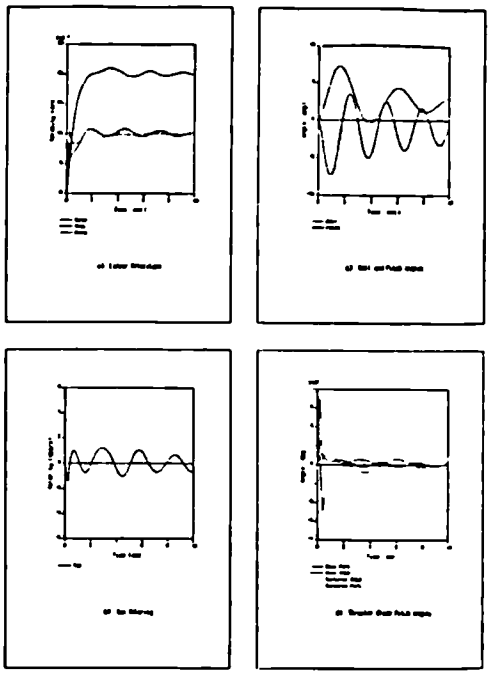

Figure 7 [illegible]

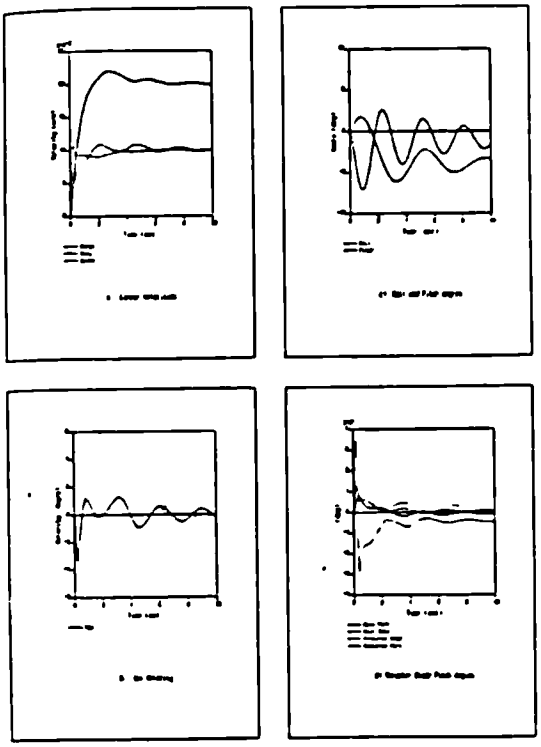

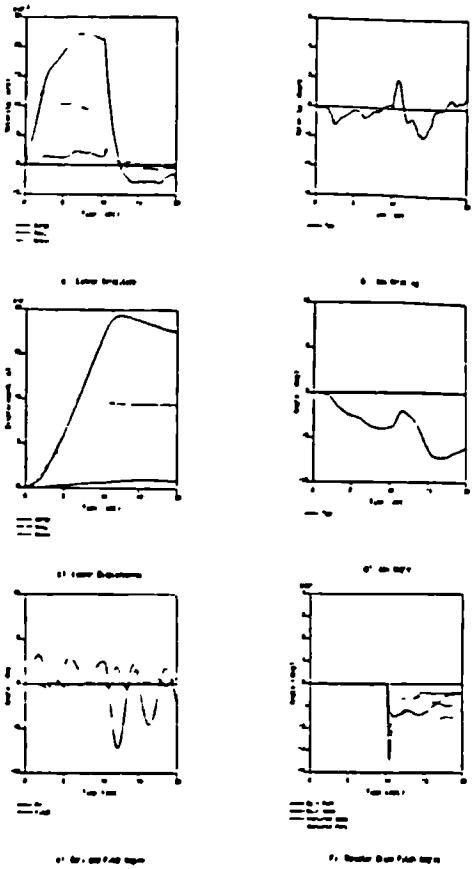

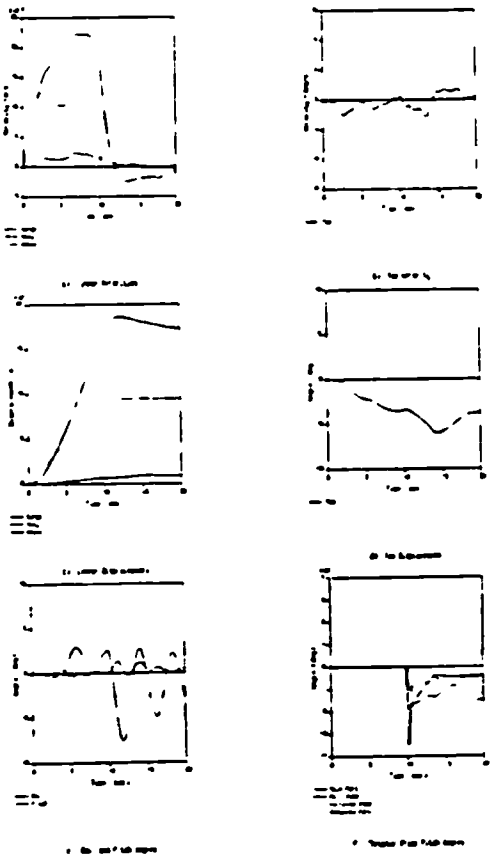

LIST OF REFERENCES

1. Melegari, J.E. "The Evolving Role and Expanding Array of Submersibles and Underwater Vehicles." Proc. Subtech '83, n.pag., Society for Underwater Technology, London, 1983.

2. Brooks, T.L. and Sheridan, T.B. "Superman: A System for Supervising Manipulation and the Study of Human/Computer Interactions." MIT Sea Grant Report No. MITSG 79-20, Cambridge, Mass., 1979.

3. Busby, F.R. "Manned Submersibles." Office of the Oceanographer of the Navy, 1976.

4. Pesch, A.J., Hill, R.G. and Klepser, W.F. "Performance Comparisons of Scuba Divers vs. Submersible Manipulator Controllers in Undersea Work." Proc. Offshore Technology Conference, n.pag., Houston, TX, 1971.

5. Department of Energy Offshore Technology Board. "Underwater Vehicle Trials, Loch Linnhe 1981/82." OTP 14, CIRIA, London, 1983.

6. Westwood, J.D. "Navigation of Underwater Work Systems." Proc. Oceanology International '78, pp 30-34, Society for Underwater Technology, London, 1978.

7. Dunbar, R.M. and Holmes, R.T. "Advances in Remotely Controlled Submersible Research." Proc. Oceanology International '78, pp 13-22, Society for Underwater Technology, London, 1978.

8. Sheridan T.B. and Verplank, W.L. "Human and Computer Control of Undersea Manipulators." Man-Machine Systems Laboratory Report, MIT, Cambridge, Mass., 1978.

9. Yoerger, D.R. and Newman, J.B. "JASON: An Integrated Approach to ROV and Control System Design." Proc. ROV '86, pp 340-353, Society for Underwater Technology, Aberdeen, 1986.

10. Bentoz, K. "New Developments in Undersea Navigation." I.Mech.E. Lecture, 16 October 1985.

11. Kazerooni, H. and Sheridan, T.B. "Computer Simulation and Control of Underwater Vehicles." MIT Sea Grant Report No. MITSG 82-19, Cambridge, Mass., 1982.

12. Fyfe, A.J. and Russell, G.T. "Closed-Loop Control Systems and Hydrodynamics of a Tethered Submersible." Proc. Offshore Technology Conference, n.pag., Houston, TX., 1980.

13. Russell, G.T. and Lane, D.M. "An Intelligent Guidance System for an Autonomous Submersible." Proc. IEE Control '85, pp 162-167, Cambridge, 1985.

14. Fung, P.T.K. and Grimble, M.J. "Self-Tuning Control of Ship Positioning Systems." ch.14 "Self-Tuning and Adaptive Control: Theory and Applications", Ed. Harris C.J. and Billings S.A., Peter Peregrinus Ltd., London, 1983.

15. Goheen, K.R. and Jefferys, E.R. "Underwater Vehicle Controller Design by Self-Test Algorithm." Proc. Canadian Applied Mechanics Conference '85, pp E39-E40, London, Ontario, 1985.

16. Goheen, K.R., Jefferys, E.R. and Broome, D.R. "Robust Self-Designing Controllers for Underwater Vehicles." Proc. Offshore Mechanics and Arctic Engineering Conference, pp 31-38, Tokyo, 1986.

17. Slotine, J.J.E. "Tracking Control of Nonlinear Systems Using Sliding Surfaces." Ph.D. Thesis, MIT Department of Aeronautics and Astronautics, Cambridge, Mass., 1983.

18. Eiken, B. "Dynamics of Atmospheric Flight." John Wiley & Sons Inc., New York, 1972.

19. Clayton, B.R. and Bishop, R.E.D. "Mechanics of Marine Vehicles." E. & F.N. Spon Ltd., London, 1982.

20. Dand, I.W. "Some Aspects of the Hydrodynamics of Remotely Operated Submersibles." Proc. IEE Control '85, pp 156-161, Cambridge, UK, 1985.

21. Dand, I.W. and Every, M.J. "An Overview of the Hydrodynamics of Umbilical Cables and Vehicles, Parts I and II." Proc. Subtech '83, Society for Underwater Technology, n.pag., London, 1983.

22. Jefferys, E.R. and Patel, M.H. "On the Dynamics of Taut Mooring Systems." Engineering Structures, Vol.4, pp 37-43, 1982.

23. Ferriss, D.H. "Approximate Determination of the Configuration of an Underwater Cable Subjected to Steady Hydrodynamic Loading." National Physical Laboratory, Teddington, Middlesex, 1983.

24. Skop, R.A., Griffen, O.M. and Ramsberg, S.E. "Strumming Prediction for the Seacon II Experimental Mooring." Proc. Offshore Technology Conference, OTC 2884, Houston, TX, 1977.

25. Kapensberg, G.K. "A Step Towards the Introduction of Simulation Techniques in the World of Remotely Operated Underwater Vehicles." International Shipbuilding Progress, Vol.32, pp 92-98, 1985.

26. Ferriss, D.H. "Numerical Determination of the Three-Dimensional Equilibrium Configuration of an Underwater Umbilical Subjected to Steady Hydrodynamic Loading." National Physical Laboratory Report DNACS 50/81, 1981.

27. Ferriss, D.H. "Numerical Determination of the Configuration of an Underwater Umbilical Subjected to Steady Hydrodynamic Loading. Part 2: Unsteady Aspects." National Physical Laboratory Report DITC 2/82, 1982.

28. Burns, R.S. "The Automatic Control of Large Ships in Confined Waters." Ph.D. Thesis, Plymouth Polytechnic, 1984.

29. Thomasson, P.G. "Simulators for Use as Design Aids and for Operator Training." Proc. Subtech '83, n.pag., Society for Underwater Technology, London, 1983.

30. James, M.L., Smith, G.M. and Wolford, J.C. "Applied Numerical Methods for Digital Computation with FORTRAN and CSMP." 2nd ed., Harper & Row Inc., New York, 1977.

31. Newman, J.N. "Marine Hydrodynamics." MIT Press, Cambridge, Massachusetts, 1977.

32. Laub, A.J. and Moore, B.C. "Calculation of Transmission Zeros Using QZ Techniques." Automatica, Vol.14, pp 557-566, 1978.

33. MacFarlane, A.G.J. and Karcanius, N. "Poles and Zeros of Linear Multivariable Systems: A Survey of the Algebraic, Geometric and Complex-Variable Theory." International Journal of Control, Vol.24, pp 33-74, 1976.

34. Dand, I.W. Letter to author. 30 November 1984.

35. Singh, M.G. "Dynamical Hierarchial Control." North-Holland Publishing Company, Amsterdam, 1977.

36. Ferrel, W.R. and Sheridan, T.B. "Supervisory Control of Remote Manipulation." IEEE Spectrum, Vol.4, No.10, pp 81-88, 1967.

37. Edmunds, J.M. "Cambridge Linear Analysis and Design Program." Proc. IFAC Symposium on CAD of Control Systems, n.pag., Zurich, Switzerland, 1979.

38. Wonham, W.M. "On Pole-Assignment of Multi-Input Controllable Linear Systems." IEEE Trans. Aut. Contr., AC-12, pp 660-665, 1967.

39. Postlethwaite, I. and MacFarlane, A.G.J. "A Complex Variable Approach to the Analysis of Linear Multivariable Feedback Systems." Lecture Notes in Control and Information Sciences, Vol.12, Springer-Verlag, Berlin, 1979.

40. MacFarlane, A.G.J. "Return-Difference and Return-Ratio Matrices and Their Use in Analysis and Design of Multivariable Feedback Control Systems." Proc. IEE, Vol.117, pp 2037-2049, 1970.

41. Rosenbrock, H.H. "Design of Multivariable Control Systems Using Inverse Nyquist Array." Proc. IEE, Vol.116, pp 1929-1936, 1969.

42. Kalman, R.E. "On the General Theory of Control Systems." Proc. First International Congress of Automatic Control, n.pag., Moscow, 1960.

43. Pontryagin, L.J. "Optimal Control Processes." U.S.P. Mat. Nank Vol.14, No.3, 1959.

44. Bellman, R.E. "Dynamic Programming." Princeton University Press, Princeton, N.J., 1959.

45. Astrom, K.J. "Introduction to Stochastic Control Theory." Academic Press, N.J., 1970.

46. Postlethwaite, I., Edmunds, J.M. and MacFarlane, A.G.J. "Principle Gains and Principle Phases in the Analysis of Linear Multivariable Feedback Systems." IEEE Trans. Aut. Contr., Vol.26, pp 32-46, 1981.

47. Safanov, M.G. "Stability and Robustness of Multivariable Feedback Systems." MIT Press, Cambridge, Mass., 1980.

48. Owens D.H. and Chotai A. "Simple Models for Robust Control of Unknown or Badly Defined Multivariable Systems." ch.10 "Self-Tuning and Adaptive Control: Theory and Applications", Ed. Harris C.J. and Billings S.A., Peter Peregrinus Ltd., London, 1983.

49. Owens D.H. "Multivariable and Optimal Systems." Academic Press Inc., London, 1981.

50. Owens D.H. and Chotai, A. "Robust Control of Unknown or Large Scale Systems Using Transient Data Only." Research Report No. 134, Dept. of Control Engineering, University of Sheffield, UK, 1980.

51. Owens D.H. and Chotai A. "Robust Controller Design for Linear Dynamic Systems Using Approximate Models." Proc. IEE, Vol.130, Pt.D, No.2, March 1983.

52. Hildebrand F.B. "Introduction to Numerical Analysis." 2nd ed., McGraw-Hill Inc., New York, 1974.

53. Franklin G.F. and Powell J.D. "Digital Control of Dynamic Systems." Addison-Wesley Publishing Company, Reading, Massachusetts, 1980.

54. Stengel R.F., Broussard, J.R. and Berry P.W. "Digital Flight Control Design for a Tandem-Rotor Helicopter." Automatica, Vol.14, pp 301-312, 1978.

55. Ljung, L. and Soderstrom, T. "Theory and Practice of Recursive Identification." MIT Press, Cambridge, Mass., 1983.

56. Zadeh, L.A. "From Circuit Theory to System Theory." Proc. IRE, Vol.50, pp 856-865, 1962.

57. Astrom, K.J. and Eykoff, P. "System Identification - A Survey." Automatica, Vol.7, pp 123-162, 1971.

58. Isermann, R., Baur, U., Bamberger, W., Kneppo, P. and Siebert, H. "Comparison of Six On-Line Identification and Parameter Estimation Methods." Automatica, Vol.10, pp 81-103, 1974.

59. Jacobs, O.L.R., Bullingham, R.E.S., Lammer, P., McQuay, H.J., O'Sullivan, G. and Reasbeck, M.P. "Modelling Estimation and Control in the Relief of Post-Operative Pain." Automatica, Vol.21, pp 349-360, 1985.

60. Kucera, V. "Discrete Linear Control." Wiley, Chichester, 1979.

61. Peterka, V. "A Square-Root Filter for Real Time Multivariate Regression." Kybernetika, Vol.11, pp 53-67, 1967.

62. Levenberg, K. "A Method for the Solution of Certain Nonlinear Problems in Least Squares." Quart. Appl. Math., Vol.2, pp 164-168, 1944.

63. Marquardt, D.W. "An Algorithm for Least-Squares Estimation of Non-Linear Parameters." Journal SIAM, Vol.11, pp 431-441, 1963.

64. Tinker, S.J., Bowman, A.R. and Booth, T.B. "Identifying Submersible Dynamics from Free Model Experiments." Proc. RINA, n.v., n.pag., 1979.

65. Freeman, T.G. "Selecting the Best Linear Transfer Function Model." Automatica, Vol.21, pp 361-370, 1985.

66. Soderstrom, T. "On Model Structure Testing in System Identification." International Journal of Control, Vol.26, pp 1-18, 1977.

67. Akaike, H. "Use of an Information Theoretic Quantity for Statistical Model Identification." Proc. 5th Hawaii International Conference on System Science, pp 249-250, 1972.

68. Goodwin, G.C. and Sin, K.S. "Adaptive Filtering Prediction and Control." Prentice-Hall, Inc., N.J., 1984.

69. Deng, Z.L. and Guo, Y.X. "A Multivariable Explicit Self-Designing Controller." Proc. IEE Control '85, pp 23-27, Cambridge, 1985.

70. Isermann, R. "Digital Control Systems." Springer-Verlag, Berlin, 1981.

71. Proc. of the IFAC Conference on System Identification, York, 1-7 July, 1985. Pergammon Press, Oxford, 1985.

72. Kallstrom, C.G. "Identification and Adaptive Control Applied to Ship Steering." Swedish Maritime Research Centre SSPA, publication No.93, Gotenborg, 1982. (reprint of "Teknologie Doktor" thesis, Lund Institute of Technology).

73. Nomoto, K. "Analysis of Kempf's Standard Maneuver Test and Proposed Steering Indices." Proc. 1st Symposium on Ship Maneuverability, Washington (Report 1461, David Taylor Model Basin, Washington), 1960.

74. Jefferys, E.R. and Samra, B.S. "Adaptive Prediction of the Motion of Marine Vehicles." ASME Journal of Energy Resources Technology, Vol.107, No.5, pp 450-454, 1985.

75. Goheen, K.R. and Jefferys, E.R. "Modelling Wavepower Devices by Frequency Response and System Identification Techniques." (in progress), 1986.

76. Robbins, A.J. "Data Decomposition in Structural Identification." Ph.D. Thesis, UMIST, 1980.

77. Jacobs, O.L.R. "Introduction to Adaptive Control." ch.1 "Self-Tuning and Adaptive Control: Theory and Applications", 2nd ed., Ed. Harris C.J. and Billings S.A., Peter Peregrinus Ltd, London, 1985.

78. Aseltine, J.A., Mancini, A.R. and Sarture, C.W. "A Survey of Adaptive Control Systems." IRE Trans. AC, Vol.6, pp 102-108, 1958.

79. Clarke, D.W. "Introduction to Self-Tuning Controllers." ch.2 "Self-Tuning and Adaptive Control: Theory and Applications", 2nd ed., Ed. Harris C.J. and Billings S.A., Peter Peregrinus Ltd., London, 1985.

80. Kalman, R.E. "Design of a Self-Optimising Control System." Transactions ASME, pp 468-478, 1958.

81. Peterka, V. "Adaptive Digital Regulation of Noisy Systems." IFAC Symposium on "Identification and Process Parameter Estimation", n.pag., Prague, 1970.

82. Astrom, K.J. and Wittenmark, B. "On Self-Tuning Regulators." Automatica, Vol.9, pp 185-199, 1973.

83. Osburn, P.V., Whitaker, H.P. and Kezer, A. "New Developments in the Design of Adaptive Control Systems." Inst. Aeronautical Sciences, Paper 61-39, 1961.

84. Wittenmark, B. "Stochastic Adaptive Control Methods - A Survey." International Journal of Control, Vol.21, No.5, pp 705-730, 1975.

85. Astrom, K.J., Borrisson, U., Ljung, L. and Wittenmark, B. "Theory and Applications of Self-Tuning Regulators." Automatica, Vol.13, pp 457-476, 1977.

86. "Control '85", Proc. of IEE Conference, Cambridge, 9-11 July, 1985. IEE, London, 1985.

87. Tugca, A.K. and Reid, R.E. "Adaptive Controller Design for High Speed Containerships." Proc. IEE Control '85, Cambridge, pp 527-532, 1985.

88. Koivo, H.N. "A Multivariable Self-Tuning Controller." Automatica, Vol.16, pp 351-366, 1980.

89. Clarke, D.W. and Gawthrop, P.J. "Self-Tuning Controller." Proc. IEE, Vol.122, pp 929-934, 1975.

90. Borisson, U. "Self-Tuning Regulators - Industrial Applications and Multivariable Theory." Report 7513, Dept. of Automatic Control, Lund Inst. of Tech., Lund, Sweden, 1975.